PASSIVE DETECTION OF PHOSPHORUS IN AGRICULTURAL DRAINAGE WATERS USING REACTIVE HYBRID ANION EXCHANGE RESINS

BY

ZHE LI

DISSERTATION

Submitted in partial fulfillment of the requirements
for the degree of Doctor of Philosophy in Natural Resources and Environmental Sciences
in the Graduate College of the
University of Illinois at Urbana-Champaign, 2020

Urbana, Illinois

Doctoral Committee:

Professor Richard Mulvaney, Chair
Associate Professor Yuji Arai, Director of Research
Assistant Professor Maria Librada Chu
Professor Jianying Shang, China Agriculture University

ABSTRACT

Phosphorus (P) loss from agricultural fields has long been an environmental issue due to its negative impact on aquatic ecosystems such as eutrophication and hypoxia. To reduce agricultural P loss, large-scale P monitoring activities are needed to identify specific fields and or watersheds that are major contributors of P loss. A passive detection technique can be ideal for the monitoring of concentrations and loads of dissolved reactive P (DRP) from a large number of agricultural waterways because of its simplicity and cost effectiveness. The passive detection technique involves the deployment of a reactive adsorbent in water for known periods, and the concentration of P in the adsorbent will be extrapolated to estimate the load of P. Finding an appropriate adsorbent, which has a high affinity for DRP, is critical in developing a successful passive sampling method. Accordingly, polystyrene and polyacrylic anion exchange resins with different functional groups (i.e., strong-base and weak-base) were selected from a large pool of adsorbents (e.g., anion exchange resins, calcium and magnesium oxides, hybrid anion exchange resins, layered double hydroxides, metal oxyhydroxides, zerovalent iron, and zirconium and lanthanum oxides) and evaluated for the use as a P sink. While the pure resins had a non-selective affinity for P, iron (hydr)oxide coated anion exchange resins (hybrid resins) were more selective for phosphate against nitrate and sulfate. Hybrid resins also had high adsorption capacity for DRP (6.33-19.84 mg/g) and high kinetic performance (second-order kinetic rate constant at 0.035-0.127 g/(mg·min)). Furthermore, the hybrid resins was stable and had irreversible characteristics for adsorbed P, making the material suitable for the passive detection method. The passive detection technique with hybrid polystyrene and polyacrylic resins were evaluated to monitor DRP in tile waters during spring storm events. The field-calibrated passive sampling method with hybrid resins produced DRP concentrations of tile waters with no significant difference ($p > 0.05$) with the auto-sampling data, but the technique should be improved to minimize the interference from particulate matter and high flow rate. In conclusion, the passive detection technique with iron oxide coated anion exchange resins is a promising technique to monitor the flux of DRP in eutrophic waters at regional- and watershed-scales.

ACKNOWLEDGMENTS

This study was supported by the National Institute of Food and Agriculture – USDA grant for research funding and China Scholarship Council for living stipend.

I would like to thank everyone who provided help and contributed to my doctoral study. First, I want to express my sincere appreciation to my advisor Dr. Yuji Arai. Thank you for the fundamental contribution to the research, your patience and motivation in the tremendous guidance and advice, and the financial support. In addition, thank you for your exemplary role as an environmental scientist.

I would like to thank the rest of my Ph.D. committee besides my advisor: Dr. Richard Mulvaney, Dr. Ma Librada Chu, and Dr. Jianying Shang for their time and efforts on my proposal defense, preliminary exam and final exam. Thanks for their advice on my research and writings. Special thanks to Dr. Ma Librada Chu for providing the apparatus for the calibration experiment in the passive sampling study.

My thanks also go to the support received from the faculty of the NRES department especially Karen Claus for helping me learn about the department regulations and requirements and related paper works ever since my enrollment. Many thanks also to Lowell Gentry and Corey Mitchell who provided the conditions of the field test in the passive sampling study, and to the staff in MRL research facilities who helped me on material characterization.

I greatly appreciate all the lecturers in the courses I attended at UIUC. Thanks again to Dr. Arai for the teaching on Environmental Soil Chemistry, Dr. Richard Mulvaney on Soil Fertility and Fertilizers, and Dr. Ma Librada Chu on Environmental Soil Physics and NPS Pollution Modeling. These coursework helped me to build the base for my research and guided me to expand my knowledge in this field. I also thank the teachers for my English courses like Eva Miszoglad and Julie Prentice, who patiently corrected my pronunciation and improved my communication skills.

I would like to thank my colleagues and former colleagues: Mary Arenberg, Suwei Xu, Ai Chen, Xiaoqian Jiang, Kai-Yue Chen, Ying Li, Xiaomei Tang, Meijun Yang, and Jienfeng Ning. I appreciate the time we spent together. Special thanks to Suwei Xu and Ying Li for their contribution in the soil desorption study.

Last but not least, I would like to thank my family and friends. Thank you for your suggestions and mental support in my life.

TABLE OF CONTENTS

CHAPTER 1: LITERATURE REVIEW **1**

1.1. Anthropogenic inputs of excess P in the soil-water environment 1

1.2. Environmental impact of excess P in terrestrial and aquatic environment 2

1.2.1. The influence of excessive P in freshwater environments 3

1.2.2. The influence of excessive P in coastal areas 4

1.3. Sources of anthropogenic phosphorus 6

1.3.1. Chemical fertilizers 6

1.3.2. Livestock and poultry manures 7

1.3.3. Municipal sewage and industrial waste 9

1.4. The concentration and speciation of P in agricultural waters 10

1.4.1. The concentration and speciation of P 11

1.4.2. Influencing factors 12

1.5. Reactive adsorbents for dissolved P 15

1.5.1. Metal oxyhydroxides 16

1.5.2. Zero-valent iron 19

1.5.3. Anion exchange and hybrid resins 21

1.5.4. Layered double hydroxides 24

1.5.5. Zirconium and lanthanum oxides 28

1.5.6. Calcium and magnesium oxides 30

1.6. Figures 35

1.7. Tables 40

1.8. References 61

RESEARCH JUSTIFICATION **90**

RESEARCH HYPOTHESES **93**

CHAPTER 2: EVALUATION OF PHOSPHATE REMOVAL PERFORMANCE IN ANION EXCHANGE RESINS AFFECTED BY SURFACE ACIDITY, POLYMER MATRICES AND REACTION CONDITIONS **94**

2.1. Introduction 95

2.2. Materials and Methods 96

2.2.1. Materials 96
2.2.2. Synthesis of iron-loaded hybrid anion exchange resins 97
2.2.3. Characterization of hybrid resins 98
2.2.4. Phosphorus adsorption isotherm in anion exchange resins and hybrid resins 99
2.2.5. Effects of sulfate and nitrate on phosphate adsorption isotherm 100
2.2.6. Phopshate adsorption kinetics in anion exchange resins and hybrid resins 101
2.3. Results and Discussion 103
2.3.1. Material characterization 103
2.3.2. Phosphate adsorption isotherm and effects of co-existing anions 105
2.3.3. Kinetics of P adsorption in pure anion exchange resins and hybrid resins 109
2.4. Conclusions 114
2.5. Figures 115
2.6. Tables 127
2.7. References 132

CHAPTER 3: NOVEL APPLICATION OF HYBRID ANION EXCHANGE RESIN FOR PHOSPHATE DESORPTION KINETICS IN SOILS: MINIMIZING RE-ADSORPTION OF DESORBED IONS 138

3.1. Introduction 139
3.2. Materials and Methods 141
3.2.1. Materials 141
3.2.2. Anion exchange resin and hybrid resin 142
3.2.3. Mineralogical characterization of iron oxide coating of the hybrid resin 143
3.2.4. Physicochemical characterization of soils 144
3.2.5. Total P, inorganic P (IP) and organic P (OP) fractionation of soils 145
3.2.6. Phosphate adsorption isotherm in resins 146
3.2.7. Irreversibility of adsorbed phosphate in resins 147
3.2.8. Phosphate desorption kinetics in soils without P sink 147
3.2.9. Phosphate desorption kinetics in soils using resin bags 148
3.2.10. Stability of Fe oxide coatings in the hybrid resin 150
3.3. Results and Discussion 151
3.3.1. Characterization of soils and resins 151

3.3.2. Phosphate adsorption isotherm in the resins 152
3.3.3. Phosphate irreversibility tests in the resins 153
3.3.4. Phosphate desorption in soils 154
3.4. Conclusions 158
3.5. Figures 160
3.6. Tables 168
3.7. References 172

CHAPTER 4: PASSIVE DETECTION OF PHOSPHORUS IN AGRICULTURAL TILE WATERS USING REACTIVE HYBRID ANION EXCHANGE RESINS 177

4.1. Introduction 178
4.2. Materials and Methods 180
4.2.1. Materials 180
4.2.2. Characterization of the hybrid resins 181
4.2.3. Phosphorus adsorption isotherm in the hybrid resins 182
4.2.4. Phopshate adsorption kinetics in hybrid resins 183
4.2.5. Field deployment of hybrid resin bags 184
4.2.6. Monitoring flow rate, temperature, and DRP concentration of tile water 185
4.2.7. Recovery of passive-sampled P from tile drainage water and its evaluation 185
4.2.8. Calibration of the passive sampling device 186
4.2.9. Stability of the iron coating of hybrid resins 187
4.2.10. Statistical analysis 188
4.3. Results and Discussion 189
4.3.1. Material characterization 189
4.3.2. Batch P adsorption in the hybrid resins 190
4.3.3. Field test of passive sampling of P in tile drainage water using hybrid resins ... 191
4.4. Conclusion 196
4.5. Figures 198
4.6. Tables 208
4.7. References 214

CONCLUSIONS 220

CHAPTER 1: LITERATURE REVIEW

1.1. Anthropogenic inputs of excess P in the soil-water environment

Due to essential functions of phosphorus (P) for organisms and relatively little supply of P through natural weathering and atmospheric deposition, the addition of P to the soil is indispensable for producing today's agricultural harvests. To keep up with increased food demand from rapid population growth, phosphate rocks are extensively excavated and processed into fertilizer and applied to agricultural soils around the world (Gellings and Parmenter, 2004; Cordell et al., 2009). Global P fertilizer use has increased from about 4 Mt in 1950 to 15 Mt in 2000, and will keep increasing as the world population expands (Alexandratos and de Haen, 1995; Zhang et al., 2008). In the 2010/11 fertilizer year, 40.5 Mt of P_2O_5 was consumed for P fertilizer production worldwide, in which China, India, and the USA were the top three countries, accounting for 29.9%, 19.9% and 9.7% of the consumption (Heffer, 2013). According to data from 1994 to 2001, the rate of P fertilizer applied to croplands has already increased beyond 20 kg/ha in Midwest America and East China (Potter et al., 2011). However, the anthropogenic input of P in soils is going beyond crop needs in some agricultural regions. In China, a single country, the estimated P surplus from synthetic fertilizers was estimated to be 4.3 Mt in 2011, which was 50-60 % of Chinese P production and about 20% of global P production that year (Sattari et al., 2014). Inefficient use of P fertilizer not only wastes phosphate rock, a non-renewable resource that may be depleted in 50–100 years (Cordell et al., 2009; Bouwman et al., 2017), but also becomes an environmental concern in many parts of the world.

The negative influence of excess P input to agricultural soil was first studied in what are now developed countries. Eutrophication and its related environmental problems in American water bodies such as the Great Lakes, the Everglades, Chesapeake, and Delaware Bays have been widely studied and were confirmed to be primarily caused or contributed by intensive agricultural P input (Sharpley et al., 1996; Daniel et al., 1998). Eutrophication contributed by high P agricultural drainage has also been prevalent in many lakes and estuaries in Europe (Csathó et al., 2007; Ulen et al., 2007; Withers and Haygarth, 2007). Although the net input of P has been effectively controlled by

regulation and remedial actions in some cases of Europe and the U.S. such as the declined total P input to Lake Erie since the 1970s (Hale et al., 2015; Watson et al., 2016), legacy P in soils and sediments from earlier accumulation may be mobilized and continue to contribute toward water eutrophication. For instance, the export of P from the Maumee Basins has exceeded inputs since the late 1990s. The gross P output of 15-20 kt/yr is one of the primary P sources to Lake Erie, where algal blooms are still reported in recent years (Powers et al., 2016; Watson et al., 2016). In developing countries with the most intensive fertilization such as China and India, the input of P from agricultural activities is mounting sharply and has contributed to environmental water degradation and even municipal water-supply crises (Smil, 2000; Qin et al., 2010; Huang et al., 2017a). Given the challenging situation of environmental P problems, extensive and comprehensive studies should be conducted to make progress on the monitoring and management of P runoff from agricultural soils.

The environmental consequences of excess P input in agricultural soils are multifaceted. Since volatilization seldom occurs toward P in natural conditions (Smil, 2000), the environmental impact of excess P can be divided into the impacts on soil and water and are discussed separately below.

1.2. Environmental impact of excess P in terrestrial and aquatic environment

Although P itself is not toxic to organisms, heavy metals accompanied with phosphate minerals may be introduced to soils with P fertilization. Cadmium is the most common heavy metal element in phosphate rock ore. Its accumulation in soil from heavy P fertilizer application has already been reported by a number of studies (Lagerwerff, 1971; Mortvedt, 1987). Some other toxic elements have also been found in phosphate minerals, such as arsenic, chromium, lead and the radioactive element uranium (Menzel, 1968; Lisk, 1972; Sharpley and Menzel, 1987). Although some researchers reported no significant increase in the uptake of toxic elements when P fertilizers were added at normal dosage, toxic elements supplied by P fertilizers may accumulate in soils in the long run and have potential ecological hazards (Andersson & Mahlin, 1981; Mortvedt, 1987; Sharpley & Menzel, 1987). In addition, when P fertilizers dissolve, P ions released into the soil solution can react with dissolved iron, calcium, and magnesium ions to form

insoluble hydroxy phosphate precipitates that may decrease cation nutrients available for plants (Smil, 2000).

Despite the possible impacts on terrestrial environments, P discharge from agricultural soils becomes an environmental concern mainly because of its role in water eutrophication. Both nitrogen (N) and P substantially runoff from agricultural soils and stimulate the growth of algae (Nixon et al., 1996; Smil, 2000), but P is often the limiting factor responsible for eutrophication since N fluxes to water bodies are relatively large (Liu et al., 2008b). And from the management perspective, it is easier to realize the control of P because of its limited atmospheric exchange compared with N, which highlights the importance of scientific studies on P fluxes from agricultural soils to water bodies (Sharpley and Menzel, 1987). Since the 1970s, P has been recognized as one of the primary controlling nutrients in lakes and other water bodies (Edmondson, 1970; Schindler, 1974). The critical value of total P is considered 0.02 mg/L where eutrophication can be accelerated, which is far lower than P concentrations in soil solution that are required for agricultural plant growth, indicating that agricultural soil can be an important source of P for downstream water bodies (Daniel et al., 1998; Parry, 1998; Huang et al., 2017a). The leaching of P is relatively less serious compared with N fertilizers due to substantial retention by soils. However, discharge of P through surface runoff and tile drainage leads to significantly higher levels of P downstream of agricultural soils (King et al., 2015b; Kleinman et al., 2015). It is estimated that 10.5 Mt P per year is lost from cropland around the world, and its role in eutrophication is expanding due to the increasing input of P associated with agricultural activities (Liu et al., 2008b). In developed countries where point-source P pollution has already been controlled, agricultural soils are often the largest P source for eutrophic water bodies (Dubrovsky et al., 2010; Kleinman et al., 2011).

1.2.1. The influence of excessive P in freshwater environments

The major process of eutrophication caused by excessive P is that the intense anthropogenic input changes P status from a commonly growth-limiting level to mesotrophic or even hypereutrophic level, which stimulates the growth of algae, cyanobacteria, and aquatic macrophytes in water bodies (Correll, 1998; Smil, 2000). In a

laboratory experiment, Boyd and Musig (1981) added 0.3 mg/L soluble P to fish pond water and observed that an average of 41% of the additional P was absorbed within 24 h by planktonic communities in the water samples (Boyd and Musig, 1981). When natural water bodies receive excess P from agricultural drainage water, P is also taken up and stimulates the overgrowth of certain algae species (Edmondson, 1970; Paerl et al., 2011). The bloom and eventual decay of these organisms lead to undesirable environmental consequences.

On the one hand, large amounts of algae reduce water clarity and limit transparency. Thick mats of phytoplankton even block the water surface; on the other hand, the decay of dead plant biomass depletes dissolved oxygen in the water, and releases odorants in water (Pitois et al., 2001; Bryant and Matzinger, 2012; Lee et al., 2017). Some neuro- and hepatotoxins may even be produced when dead algae are decomposed and may pose a serious health hazard to livestock and humans (Lawton and Codd, 1991; Pitois et al., 2001). Thus, eutrophication can change clean lakes and streams into soupy and toxic scum, affecting their recreational functions, and making them unsuitable as drinking water sources. Many countries and cities' drinking water supplies have suffered the threat of water eutrophication, such as the algal blooms in Lake Erie and the Great Lakes in the US, and the cyanobacterial blooms in Lake Taihu and Lake Chaohu in China (Anderson et al., 2002; Paerl et al., 2011; Michalak et al., 2013; Chen and Liu, 2014; Watson et al., 2016; Clark et al., 2017). Besides, the economic value of water bodies is also affected. Fish production and diversity are greatly reduced by algal blooms (Starling, Lazzaro, Cavalcanti, & Moreira, 2002; Seehausen, Alphen, & Witte, 1997).

1.2.2. The influence of excessive P in coastal areas

P used to be considered mainly related to freshwater eutrophication, but now it has also been implicated as a primary or contributing nutrient in coastal eutrophication (Correll, 1998; Kleinman et al., 2011). When rivers carry P into estuaries, similar environmental impacts are also exerted on coastal water systems. Excess P stimulates the growth of algae and zooplankton fed on algae, thus initially increasing the biomass in coastal ecosystems. But when the plankton die and bacteria decompose the residues, the oxidation of organic matter consumes dissolved oxygen, resulting in the formation of the

hypoxic zone. Since oxygen is necessary for all fishes and invertebrates, the waters are depleted of oxygen (hypoxia), resulting in a degraded ecosystem commonly known as "dead zone".

Hypoxic zones occur naturally in many marine environments, but human activities significantly increase their occurrence in coastal areas (Diaz, 2001; Diaz and Rosenberg, 2008). These zones of anthropogenic origin are among the most widespread and serious environmental problems in the current world. Some of the largest ones occur in the northern Gulf of Mexico, the East China Sea and the Baltic Sea (Chen et al., 2007; Conley et al., 2011; White et al., 2014). The occurrence and size of the hypoxic zone depend on weather, hydrological and seasonal factors (Joyce, 2000; Diaz, 2001; Zhu et al., 2016), and thresholds differ at 2~3 mg/L dissolved oxygen (Chen et al., 2007; Diaz and Rosenberg, 2008; Conley et al., 2011). However, it is generally acknowledged that the anthropogenic hypoxia problem is escalating in many coastal areas around the world. Hypoxia was first documented in the northern Gulf of Mexico coast in 1972 (LUMCON 2017), now the largest anthropogenic dead zone in the western hemisphere, where more than 60% of P originates from agricultural soils in the Mississippi-Atchafalaya River Basin (Joyce, 2000; Dodds, 2006; White et al., 2014). The area of the hypoxic zone in the northern Gulf of Mexico was more than 14,500 km^2 in the summers of 2004 through 2013 (Rabotyagov et al., 2014). But the newest study showed that in 2017 summer the hypoxic zone in this area has reached 22,720 km^2, the biggest ever measured (LUMCON 2017). In the East China Sea, coastal hypoxia was first documented in the bottom waters of Yangtze Estuary in August 1981, and the hypoxic area was estimated at more than 12,000 km^2 in 2003. And research in the Baltic Sea covering 115 sites that have experienced hypoxia during the period 1955 - 2009 also reported a significant long-term increase in hypoxic profiles (Conley et al., 2011).

Overall, an anthropogenic hypoxic zone is a global environmental problem that increasingly affects coastal ecosystems and human life. Reduced water quality and declining fishery production and biodiversity are common consequences in hypoxic zones brought about by coastal eutrophication (Ryther and Dunstan, 1971; Jørgensen and Richardson, 1996; Pitois et al., 2001). Benthic fish communities are especially vulnerable to hypoxia (Ryther and Dunstan, 1971; Conley et al., 2011). Toxic substances may also

be released from cyanobacteria and other microorganisms, among which toxin-producing Pfiesteria is a typical case due to its massive fish kills and serious human health impacts (Burkholder and Glasgow, 1997; Grattan et al., 1998).

1.3. Sources of anthropogenic phosphorus

Although excessive P is causing environmental problems in many regions of the world, all P in the biosphere comes from the gradual weathering of phosphate rocks at a low rate in the lithosphere (Chen et al., 2008). Smil (2000) reported that the natural release of P should be about 10 Mt/year globally. Ahl (1988) estimated the virgin atmospheric deposition in the Northern Hemisphere to be less than 5 kg P km^{-2} yr^{-1} (Ahl, 1988). However, human activities have substantially intensified the release of P over the past two centuries. Aside from intensified soil erosion that accelerates lithospheric P mineralization, a number of human activities discharge large quantities of P to soil and waters directly. Fertilizer application to agricultural soils including chemical P fertilizers and livestock manures, as well as the discharge of municipal wastewater, are the major causes of this increase (Liu et al., 2008b; Cooper and Carliell-Marquet, 2013; Li et al., 2016).

1.3.1. Chemical fertilizers

By treating phosphate rocks with acid, modern chemical P fertilizers were produced and applied since the 1840s (Lehr, 1980). A wide variety of highly refined, water-soluble P fertilizers are available today, such as concentrated superphosphate (CSP), monoammonium phosphate (MAP), diammonium phosphate (DAP) and ammonium polyphosphate (APP). Fertilizer consumption data show that DAP has surpassed superphosphate and now ranks as the most popular P fertilizer worldwide, representing than 50% of the market (IFA, 2017). Global consumption of all P fertilizers was more than 1 Mt P yr^{-1} during the late-1930s, exceeded 5 Mt P yr^{-1} by 1960, and reached 15 Mt P yr^{-1} in 2000 (Smil, 2000). Since 2004, the global P fertilizer consumption has been as high as 20.4 Mt P (FAO, 2006), and the increase is expected to continue due to increasing

crop demand from a burgeoning human population (Fixen et al., 2015; Sattari et al., 2014).

Agricultural P input varies widely across the world. Application of P fertilizer is most intensive in the mid-western United States and eastern China (Potter et al., 2010). In the United States, P fertilizer use increased by 3.4 times from 1945 to 1970 and leveled off at 1.8 Mt P yr^{-1} in the 2000s (Yang et al., 2016). Only about 30% of the P from fertilizers is output in agricultural produces, resulting in an average accumulation rate of 22 kg ha^{-1} yr^{-1} for surplus P (Carpenter et al., 1998b). Excess fertilization causes P accumulation in soil. Large quantities of P are also transported to aquatic ecosystems, becoming a major nonpoint source of P input in the United States. The highest P input from chemical fertilizers occurs in mid-west agricultural areas like Iowa, Illinois, and Indiana (Potter et al., 2010). Although total P concentrations have decreased in many water bodies, excessive P is still a primary issue in some regions such as Lake Erie and the Upper Mississippi River Basin (Litke, 1999; Dolan and Chapra, 2012). In China, P fertilizer consumption increased by 3.3 times from 1978 to 2004 and reached 50.9 kg P ha^{-1}, which accounted for 55.8 % of total agricultural input in 2004 (Chen et al., 2008). The P input has already exceeded crop requirement and led to environmental problems in many agricultural areas. It was estimated that average P input and output were 28.9 kg ha^{-1} and 14.2 kg ha^{-1} respectively in China in 2004, leading to an average P surplus of 14.7 kg ha^{-1} (Chen et al., 2008; Li et al., 2016). According to the 1st National census of pollution sources in China, 28.47 Mt P losses from agricultural activities were the dominant contributor to the total P losses in 2007 (MOEP and MOA, 2010). The Yangtze Basin, where net annual P input was estimated to be 9.4 kg ha^{-1} in 2010, received 43% of national P production in China (Powers et al., 2016).

1.3.2. Livestock and poultry manures

Livestock and poultry manure is a traditional source of soil nutrients. Proper application of manure can enhance crop growth, improve soil quality, and reduce the use of chemical fertilizers (Akhtar et al., 2005; Tao and Mancl, 2008). However, improper manure application can also cause a series of environmental problems. Aside from potential heavy metal and antibiotic pollution from manure application, overloaded

macronutrients built up in soils also degrade soil quality and cause aquatic problems (Potter et al., 2010; Ouyang et al., 2013). Modern confinement livestock operations in feedlots accentuate the problem by intensively producing large amounts of manures with high P concentration that exceed the storage capacity of nearby croplands (Carpenter et al., 1998b; Pitois et al., 2001). Globally, P release from manure is basically of the same magnitude as P from inorganic fertilizer. Smil (2000) estimated P release from manures to be 5–10 kg P/ha annually, and Potter et al. (2011) reported the level of over 20 kg/ha manure P in east China, mid-America, and some other agricultural regions. In terms of livestock and poultry species, manure can be classified into cattle manure, swine manure, chicken manure, etc. The content of P varies with different manure sources. Poultry manures usually have higher P content than livestock manure, and swine manure is higher than cattle manure in P content (Akhtar et al., 2005; Ouyang et al., 2013).

In the United States, manures have been similar to chemical fertilizers for agricultural P input since the 1970s. About 112 Mt manures (dry basis) containing 1 Mt P were produced by livestock and poultry in 1974, about half of which was voided by cattle on rangeland (Van Dyne and Gilbertson, 1978). In 2012, manure P was 1.73 Mt P, a 92% increase from 1930 that averaged 2.15 ± 0.36 kg P ha^{-1} yr^{-1} at the national scale. There is extensive spatial variability in the distribution of manure P loads. Most counties with manure P loads of more than 2 kg ha^{-1} yr^{-1} were located in the Upper Mississippi River Basin including southern Minnesota, southern Wisconsin, Iowa, northern Illinois, western Ohio, eastern Nebraska and northern Missouri, and the highest manure P loads exceeded 6.7 kg P ha^{-1} yr^{-1} (Yang et al., 2016). Major manure P sources vary with animal population structures in different counties. Cattle are the primary manure P contributor in most U.S. counties, but swine plays an important role in northeast US and chicken production is the major manure P source in many southeast counties (Dubrovsky et al., 2010; Suh and Yee, 2011; Yang et al., 2016). Different application methods have been developed for manures. Banding application or incorporation into soils can help to reduce manure P runoff (Kleinman et al., 2002; Tarkalson and Mikkelsen, 2004). Solid manures are usually mixed with soils along with tillage, and a number of technologies such as disk injection, aeration infiltration, and pressure injection have also been developed to

incorporate slurry manures in no-till farming systems (Meisinger and Jokela, 2000; Maguire et al., 2011).

In China, along with the fast growth of livestock and poultry husbandry in recent decades, both the production and the P content in manure increased considerably (Van Dyne and Gilbertson, 1978; Li et al., 2016). The total production of manures was 22.1 billion tons in 2003, mainly applied by surface broadcasting with tillage incorporation (Li and Lu, 1991; Li et al. 2009; Shi et al., 2011). According to Li et al. (2009), the average P content was 3.97% in swine manure, 3.53% in chicken manure, 1.49% in cattle manure, which increased by more than 50% compared with the results investigated in the 1990s. Ouyang et al. (2013) reported that swine, chicken, cattle, cow, and sheep contributed 45.6%, 12.8%, 8.9%, and 1.0 % respectively to the total manure P in 2008. Leading livestock species on the contribution of P release were spatially different. Swine was the major source for manure P in southern China, while cattle and sheep play a larger role in the north. The high manure P loads were mainly concentrated in the northeastern provinces of China such as Shandong, Hebei and Hunan province. Hunan province had the top manure P loads along the Yangtze River (Geng et al. 2013; Ouyang et al., 2013).

1.3.3. Municipal sewage and industrial waste

Modern urban residents consume considerable P-containing products. The annual output of P from human waste, detergents and other household cleaning products was estimated to be more than 1 kg per capita, which could transform to hundreds of kg P/ha in some crowded cities. In 2000 the global population of just over 6 billion people released almost 3Mt P in its wastes (Smil, 2000; Parsons and Smith, 2008). Despite the large amount, P input from municipal wastewater is relatively easy to monitor and control due to its concentrated and continuous discharge (Carpenter et al., 1998b; De-Bashan and Bashan, 2004; Bouwman et al., 2009). Chemical precipitation and biological processes can remove more than 90% of all influent P, leaving less than 1 mg L^{-1} P in water after treatment (Parsons and Smith, 2008). In addition, the sludge produced from wastewater treatment contains high concentrations of P, which is a potential source of P in fertilizers (De-Bashan and Bashan, 2004; Egle et al., 2016). In many developed countries and regions, municipal and industrial wastewater contribute only a small portion of total P

input due to the widespread adoption of water treatment practices. For instance, Powers et al. (2016) showed that the P export of the Thames River Basin in the UK declined by 86% during the 2000s in association with a lowered P flux from sewage treatment. According to Cooper and Carliell-Marquet (2013), industrial applications accounted for only 5 % of total P input in the UK. Research on the transport of P in the Midwestern United States also showed that municipal sources contributed about 20% of P loading to Lake Erie during the period 1994-2008, and most of the rest came from the non-point agricultural soils through surface runoff and tile drainage (Dolan and Chapra, 2012; Smith et al., 2015). However, in developing regions where wastewater treatments are still lagging behind, municipal sewage and uncontrolled industrial waste discharge may make a larger contribution to total P loads. In China as of 2003, 91% of industrial wastewater was treated before discharge, as compared to only 32% of urban domestic sewage (National Bureau of Statistics, 2004). Gao et al. (2016) analyzed nutrient release in the Yangtze River Basin around the Three Gorges Reservoir and reported an extremely high value (0.4 mg/L) of total P in Wulong City, which was mainly attributed to the inappropriate mining of phosphate rock resources. However, the export of P in the Yangtze River, which contributed 0.03 Mt P yr^{-1} to the East China Sea, was mainly derived from the increasing use of chemical fertilizers in drainage basins (Yao et al., 2009; Wang et al., 2016).

1.4. The concentration and speciation of P in agricultural waters

P is an essential macro-element for all living organisms, and phosphorus fertilization is a common practice to ensure high production of crops (Bouwman et al. 2017; Lehr, 1980; Suh and Yee, 2011). Although only a small fraction of P in fertilizers would be expected to be lost in drainage waters due to the strong adsorption by soil, particulate and colloidal P can also be transported into downstream waters (Sims et al., 1998; Filippelli, 2008; Suh and Yee, 2011). Increases in the amounts of soluble and particulate P transported in agricultural drainage have been widely observed following the application of P fertilizer, and the release of fertilizer P was especially acute during periods of high rainfall and flood irrigation (Sharpley and Menzel, 1987; Kleinman and Sharpley, 2003; Kleinman et al., 2011).

1.4.1. The concentration and speciation of P

P can be released from agricultural fields via soil erosion, surface runoff and/or tile drainage. Surface runoff was once believe to be the major pathway of P leaching from agricultural soils, but now tile drainage is recognized to be of great importance to agricultural P loss (Smith et al., 2015; Zhang et al., 2015; Van Esbroeck et al., 2016). According to a field study in the Midwestern United States, tile discharge accounted for 48% of total P loss in the field (Smith et al., 2015). A concentrations of P in both surface runoff and tile drainage are highly variable, but can easily exceed the critical levels for accelerated eutrophication (0.02~0.03 mg/L) (King et al., 2015b). A concentration of 20 mg P/L was even recorded in previous studies (Christianson et al., 2016). Numerous studies have been conducted on P loss via runoff and tile drainage with respect to water eutrophication. Many different forms of P were measured in these studies such as total P (TP), particulate P (PP), total dissolved P (DP), dissolved reactive P (DRP), dissolved unreactive P (DURP), etc. TP, PP, and DRP are most commonly collected and used to compare among different studies (Sims et al., 1998; Zhang et al., 2015). Christianson et al. (2016) analyzed drainage P losses from 91 agricultural drainage studies and reported that dissolved forms of P accounted for about 40% of total P load when both DP and TP were reported. Compared with surface runoff water, PP accounted for a larger proportion of TP in tile drainage water, even more than 80% of TP according to some studies (Tan and Zhang, 2011; Zhang et al., 2015). Laubel et al. (1999) reported 0.177~0.876 mg/L of PP loss via subsurface drainage whereas 0.042~0.103 mg/L of DP was lost in a controlled pot experiment. A number of studies reported colloidal P as an important component of P in agricultural runoff but its speciation and transport are still poorly understood. Turner et al. (2004) operationally defined colloidal molybdate-reactive phosphorus (MRP) as MRP associated with particles between 1 nm and 1 μm diameter and determined this component by ultrafiltration. They reported that concentrations of colloidal MRP ranged between 0.16 and 3.07 μM, accounting for 11~56% of the MRP in the 1 μm fraction in surface runoff from three calcareous soils. Heathwaite et al. (2005) evaluated colloidal P loss from agricultural soils and suggested that the mobilization of colloidal P significantly facilitates subsurface P transfer from soil solution and surface-applied fertilizers or manures.

1.4.2. Influencing factors

The reported concentrations of P discharged from agricultural soils varies with a number of factors. The most important influence comes from fertilization events. Zhang et al. (2015) observed 159~444% increases of DRP in the tile drainage water of different cropping systems when comparing treatments with and without P fertilization. Regelink et al. (2013) reported TP lower than 21 μmol/L in drainage water in a field without manure for almost 7 months, and the P was almost evenly distributed among DRP, DUP and PP fractions. When cattle slurry or its solid fraction was applied, the concentrations of TP increased by 60 and 4 times, respectively, and the proportion of DRP increased to no less than 50%. The effect of fertilization on P concentrations in agricultural discharge will gradually decrease due to sorption of P by soil colloids and the decrease of total P from previous runoff (Kleinman and Sharpley, 2003). Gascho et al. (1998) observed more than 5 mg/L DRP in surface runoff after broadcast fertilization with 45 kg P/ha chemical fertilizers, which decreased to less than 1 mg/L after successive rainfall simulations. Daverede et al. (2004) reported average P runoff to be 5.6~10.3 mg DRP/L for simulated rainfall one month after fertilization, and about 1.3 mg DRP/L for six-month rainfall simulation. While the runoff of P from fertilizers gradually declines after application, long-term P fertilization will cause P accumulation in soils, creating a chronic P source to drainage waters (Kleinman et al., 2011). Other factors influencing P loading of agricultural drainage, including the types and amount of P fertilizers applied, and the methods of applications used; the type of vegetation present, drainage management, etc.

1.4.2.1 Types of P fertilizers

P can be introduced to soil either through chemical fertilization or by the application of livestock and poultry manures. Either source can be dominant depending on the countries involved. In general, chemical fertilizer is the major contributor of agricultural P in the developed north and parts of India and China, while manure tends to dominate in the southern hemisphere (Potter et al., 2010). On a global scale, Bouwman et al. (2009) estimated the P supplied by chemical fertilizers and manures to be 13.8 Mt and 17.1 Mt

in 2000, while Potter et al. (2010) estimated that 14.3 Mt yr^{-1} and 24.3 Mt yr^{-1} of P were applied to soil through chemical fertilizers and manures respectively (Potter et al., 2010).

Some studies showed that P from chemical fertilizers has a higher potential for leaching loss than P from manure. Withers et al. (2001) surface-applied triple superphosphate (TSP) and liquid cattle manure both at rates of 60 kg P/ha and determined the P runoff during the first rainfall that occurred 3 weeks after the application. The DRP concentrations were 6.5 mg /L for the TSP treatment and 3.8 mg/L for the manure treatment. Eghball and Gilley (1999) also reported greater P runoff with chemical fertilizer than cattle manure application, but Daverede et al. (2004) observed higher concentrations of DRP in runoff from soils with liquid swine manure application at 33.1-39.4 Mg P/ha than the soils with TSP application at 54 kg P /ha. Bertol et al. (2010) also reported that the application of manure led to a higher rate of P runoff than did mineral fertilization when 21.4 kg P/ha chemical fertilizer and 16.8 kg P/ha liquid swine manure were separately applied. Organic fertilizers from different sources also result in different magnitudes of P loss in runoff (Christianson et al., 2016). Kleinman and Sharpley (2003) observed a significant difference in DRP in the runoff from manured soils that decreased in the order, poultry manure (0.3–32.5 mg DRP/L) > swine manure (0.3–22.7 mg DRP/L) > dairy manure (0.4~2.2 mg/L DRP/L).

1.4.2.2 Application rates and methods of P fertilizers

In addition to the source of P fertilizers, the application rate and application method also affect the concentration of P in agricultural discharge. The positive relation between P loss from agricultural drainage and application rate has been reported for both chemical fertilizers and manures. For instance, Edwards and Daniel (1992) reported the concentrations of DRP in runoff to be 0.8, 16.2, and 34.5 mg/L following broadcast application of poultry manure slurry at 0, 76, and 304 kg P/ha, respectively. However, the rate effect of fertilizers on P loss may not become apparent if P fertilization is not excessive (Izuno et al., 1991; Christianson et al., 2016).

A number of studies also explored the influence of fertilizer application methods. In general, broadcast application leads to a large P load in runoff from agricultural soils (Kleinman and Sharpley, 2003). Daverede et al. (2004) observed greater P runoff from

soils with surface-applied manure than from soils with injected manure during rainfall simulation one month after the manure application, although no significant difference was observed when the rainfall occurred after six months. Christianson et al. (2016) also recommended incorporating manure to disrupt the hydraulic conductivity of soil macro-pores and thereby reduce P loss.

1.4.2.3 Other factors

Fertilization is the major event that influences the load and speciation of P loss from agricultural soils, but P runoff is also affected by some other factors such as agricultural strategies and drainage management (Sims et al., 1998). Zhang et al. (2015) studied P loss in tile drainage water in three different cropping systems (continuous corn, corn–oats–alfalfa– alfalfa rotation, and continuous grass). The concentrations of DRP were 0.105, 0.131, and 0.354 mg/L, respectively. The speciation of P also differed in different cropping systems. Particulate P accounted for 62~72% of TP in tile drainage from cropland under continuous cultivation, reflecting limited labile P in top soils, while dissolved P accounted for 72% of TP in tile drainage from >40 years continuous non-native grass systems. Gaynor and Findlay (1995) compared P loss from surface runoff and tile drainage in a cornfield with different tillage practices (no-till, ridge till, and conventional tillage). They reported that the concentrations of ortho-P were 0.54, 0.34, and 0.24 mg/L, respectively, in tile drainage water, and 1.02, 0.55, and 0.29 mg/L in surface runoff. While conservation tillage can reduce P loss via soil erosion, it significantly increased P loss through runoff as compared with conventional tillage. This trend was also observed by Christianson et al. (2016), based on the findings that no-till caused a significant tripling of the P load in agricultural drainage, relative to the level of 0.04 kg P/ha measured for conventional tillage.

Different concentrations and speciation of P have also been observed in comparing different drainage systems. Valero et al. (2007) reported that drainage water management (DWM) effectively reduced tile drainage volume, but TP concentrations in the drainage water increased by 131% compared to the free drainage. Dissolved reactive P (DRP) concentration (0.053 mg/L) in the tile system was significantly greater than that in the

free drainage system. The overall P load in drainage increased with DWM, and DRP accounted for a larger proportion (~80%) of TP as compared with free drainage (67%).

1.5. Reactive adsorbents for dissolved P

In the last few decades, several methods have been suggested to measure the concentration of P in waters. The most common one is grab sampling, which obtains time-discrete records of the concentration of target substances (Müller et al., 2007; Rozemeijer et al., 2010; Worsfold et al., 2016). The precision and accuracy of grab sampling rely heavily on the sampling frequency, which is limited by manual labor especially for its application in long-term and large-scale monitoring (O'Brien et al., 2009; Knutsson et al., 2013; Edenborn et al., 2017). The minimum detectable concentration is also limited by the volume of sampled water at each time. Other monitoring methods also have their own drawbacks. For example, automatic samplers and analyzers are expensive to purchase and maintain (Rozemeijer et al., 2010); paper-based devices for in-site determination are convenient and cost-efficient, but the detection limit is relatively high and the accuracy is also affected temporal variation of the contaminant concentrations (Jayawardane et al., 2012; Almeida et al., 2018). Since the discharge of DRP from agricultural fields normally occurs at low concentration but can be intensive during heavy precipitation events (Müller et al., 2007; King et al., 2015b; Smith et al., 2015), the above monitoring methods are not ideal for the evaluation of P loss from agricultural fields. Passive sampling techniques rise as a promising alternative in this case. Passive sampling is based on the accumulation of target substances in reactive adsorbents that are deployed on-site. A time-weighted average concentration can be calculated according to the amount of the target substances on adsorbents after a certain period of deployment, which can be several days to months (Ahrens et al., 2015). Thus, the reactivity of adsorbents for P becomes a key factor in the passive detection method. Numerus attempts have been made to measure the concentration of DRP in water bodies using various adsorbents such as metal oxyhydroxides, anion exchange resins, layered double hydroxides, calcium and magnesium oxides, and zirconium and lanthanum oxides. The results of P adsorption capacity and adsorbent characteristics are summarized below.

1.5.1. Metal oxyhydroxides

Metal (oxyhydr)oxides have been widely studied for the removal of phosphate in wastewater, including iron oxides that combine low cost and high efficiency in P removal. The results of P adsorption studies using different Fe-based adsorbents along with their experimental conditions and methods are summarized in Table 1.1.

Since the 1970s, researchers have extensively studied the adsorption of phosphate on a variety of Fe minerals, such as goethite (e.g., Atkinson et al., 1974; Parfitt et al., 1975; Parfitt and Atkinson, 1976; Madrid and Posner, 1979; Parfitt, 1989; Tejedor-Tejedor and Anderson, 1990; Strauss et al., 1997; Ioannou et al., 1998; Antelo et al., 2005; Luengo et al., 2006), hematite (Barron et al., 1988; Elzinga and Sparks, 2007; Huang, 2004; Madrid and de Arambarri, 1985; Parfitt, 1989; Parfitt et al., 1975; Torrent et al., 1994), ferrihydrite (Arai and Sparks, 2001; Parfitt, 1989) and lepidocrocite (Madrid and de Arambarri, 1985; Parfitt et al., 1975) (Table 1.1). These Fe minerals differ in their P adsorption capacities. Parfitt (1989) reported that phosphate retention decreased in the order, ferrihydrite > goethite > hematite. A similar sequence was reported by McLaughlin et al. (1981) and Huang (2004), which was related to the crystallinity and specific surface area of different minerals. McLaughlin et al. (1981) found a positive linear relationship between hydroxyl buffering and P adsorption capacity, suggesting ligand exchange as the mechanism that was also explored in several other studies, especially for the coordination and protonation state of phosphate-iron complexes using infrared analyses and electrophoretic mobility measurements (Arai and Sparks, 2001; Atkinson et al., 1974; Elzinga and Sparks, 2007; Luengo et al., 2006; Parfitt et al., 1975; Parfitt and Atkinson, 1976; Tejedor-Tejedor and Anderson, 1990). For instance, Arai and Sparks (2001) explored the in-situ phosphate adsorption mechanisms at the ferrihydrite–water interface. The results from adsorption envelopes, electrophoretic mobility measurements, and Attenuated Total Reflectance–Fourier Transform Infrared (ATR–FTIR) spectroscopy all supported an inner-sphere adsorption mechanism. Specifically, the complexes were proposed as non-protonated, bidentate binuclear species at pH ≥ 7.5, and protonated species at pH 4-6.

Several studies were later conducted with Fe-bearing materials as adsorbents for P removal from wastewater. For use under field conditions, consideration must be given not

only to adsorption capacity, but also to a material's stability, reusability, and stability under varying conditions. Yoon et al. (2014) studied magnetic iron oxide nanoparticles, which had an advantage for magnetic separation and reuse in water treatment but were relatively low in P sorption capacity (~162.3 mmol/kg). Lalley et al. (2016) tested a goethite-based commercial sorbent, Bayoxide$^{@}$ E33, and three modified adsorbents for P removal from lake water. The maximum sorption capacity (~396.8 mmol /kg) was lower than expected from deionized water-based studies, possibly due to the influence of dissolved organic matter.

To increase P adsorption capacity, Fe and other metals were combined with composite materials. Li et al. (2014) synthesized a Fe-Cu binary oxide with an Fe/Cu molar ratio of 2:1, for which the calculated maximum adsorption capacity was approximately 371.0 mmol/kg at pH 7 and 419.4 mmol/kg at pH 5. Zhang et al. (2009) synthesized an Fe-Mn binary oxide with an Fe/Mn molar ratio of 3:1, which provided an adsorption maximum of 1,161.3 mmol/kg at pH 5.6. The material showed high selectivity for phosphate compared with other common anions and had the advantage of low-cost. Lu et al. (2013) further added aluminum to the Fe-Mn binary oxide and obtained Fe-Al-Mn tri-metal oxide with a Fe: Al: Mn molar ratio of 3:3:1. The sorption capacity for phosphate was ~1,558.1 mmol/kg at 25 ℃, which exceeded that of any single component oxide evaluated.

Aluminum (oxyhydr)oxides are another type of metal oxide that can strongly adsorb phosphate. McLaughlin et al. (1981) examined the adsorption of phosphate by a range of Al-containing components and reported that adsorption capacity decreased in the order of allophane > A1 gel > Fe-coated kaolinite > gibbsite ~ ground kaolinite. Allophane can adsorb phosphate as high as 1,720 mmol/kg from solution with an initial P concentration, 0.1 mM at pH 6.0, which was far greater than P adsorption by other Fe minerals (<100 mmol/kg). Özacar (2003) studied the adsorption of phosphate on alunite, another mineral enriched with aluminum oxides that showed an adsorption maximum of 1,354.8 mmol/kg at pH 5, indicating good potential for economical and efficient P removal in wastewater. Li et al. (2015) studied the effect of Al^{3+} substitution in goethite on P adsorption. The result showed that P adsorption increased with the amount of Al substitution. It was

attributed to the effect of Al incorporation in causing structural defects that inhibited crystallization and increased the surface area and available active sites for P sorption.

In the above laboratory studies of iron and aluminum (oxyhydr)oxides, a biphasic P sorption process was described as fast sorption at first followed by slow sorption before reaching pseudo-equilibrium (Lalley et al., 2016; Lǔ et al., 2013; Luengo et al., 2006). This process was best represented by a pseudo second-order kinetic model (Lalley et al., 2016; Li et al., 2014; L. G. Yan et al., 2010; Yoon et al., 2014; Zhu et al., 2009). Freundlich and Langmuir models have been successfully used to fit P adsorption isotherm data (Barron et al., 1988; Andreas Ioannou et al., 1998; Torrent et al., 1994; Zelmanov and Semiat, 2015; Zhu et al., 2009).

As for the factors affecting P adsorption by the metal (oxyhydr)oxides, pH, ionic strength and coexisting ions were commonly reported in different studies. Although the extent of dependence varies among different minerals, an alkaline pH will significantly suppress P adsorption on variable charge minerals because of stronger electrostatic repulsion from a negatively charged surface (Yan et al., 2010; Zhou et al., 2012). An increase in ionic strength has either no significant influence or a positive effect on phosphate adsorption, which is in agreement with inner-sphere complexation as the dominant mechanism (Antelo et al., 2005; Li et al., 2014; Mallet et al., 2013; Peleka and Deliyanni, 2009). Coexisting cations such as Ca and Mg can enhance phosphate adsorption because they form ion pairs and reduce the electrostatic repulsion between negatively charged groups on the particle surface and phosphate ion in solution (Gao and Mucci, 2003). Common anions such as chloride and nitrate usually have no influence on specific adsorption of phosphate, but carbonate and sulfate can affect P adsorption, depending on the ion concentration, the solution pH, and the composition of adsorbents (Chitrakar et al., 2006a; Li et al., 2014; Lǔ et al., 2013; Mallet et al., 2013). Li et al. (2014) also reported that coexisting silicate and fluoride significantly suppressed phosphate adsorption on Fe-Cu oxide.

Temperature is another important factor influencing phosphate adsorption. According to most thermodynamic studies, P adsorption is an endothermic process that occurs spontaneously and is promoted by an increase in temperature (Li et al., 2014; Yan et al., 2010; Yoon et al., 2014); however, Yoon et al (2014) found that the capacity of

phosphate adsorption for goethite decreased with increasing temperature from 25 to 65 ℃.

To facilitate the practical utilization for wastewater treatment, some studies have combined iron or other metal (oxyhydr)oxide particles with bulk materials such as clay minerals and activated carbon. For instance, Zhou et al. (2012) immobilized nano-particulates of hydrated ferric oxide (HFO) within macroporous activated carbon fibers, producing a hybrid adsorbent with maximum adsorption capacity of 414.8 mmol/kg. Yan et al. (2010) modified bentonite into hydroxy-aluminum, hydroxy-iron, and hydroxy-iron–aluminum pillared bentonites, attaining phosphate adsorption maxima of 409.7, 361.3, and 338.7 mmol/kg, respectively. Structural characterization showed that modification, especially with aluminum, increased the surface area and pore volume of bentonite. Similarly, other studies include montmorillonites and laterites modified with iron or aluminum (oxyhydr)oxides, which are also reported to be promising adsorbents for the removal of phosphate in wastewater (Borgnino et al., 2010, 2009; Huang et al., 2013; Mahardika et al., 2018; Shin et al., 2004; Zhu et al., 2009).

Figure 1.1 shows how P adsorption by metal (oxyhydr)oxides varies as a function of pH. Except for zero-valent iron (ZVI), most of the adsorbents, especially pure iron oxides, show stronger adsorption under acidic conditions, and P adsorption decreases with increasing pH. Considering these adsorbents for P removal at near-neutral pH, some adsorbents performed well. Among pure iron oxides, ferrihydrite and lepidocrocite performed best at near-neutral pH, and some of the composite materials (nanostructured Fe(III)-Cu(II) binary oxides, nanostructured Fe-Al-Mn tri-metal oxide, and a Fe-Mn binary oxide) also removed P effectively at pH~7.

1.5.2. Zero-valent iron

Zero-valent iron (ZVI), which refers to powdered or granulated elemental iron materials, is a well-studied adsorbent for the removal of P in wastewater (e.g., Li et al., 2006; Giasuddin et al., 2007; Allred, 2011). Two mechanisms may account for the removal of P from solution by ZVI: 1) phosphate complexation with ferrous/ferric ion via partial oxidative dissolution and precipitation on the surface of particles due to the low solubility of the compounds, and 2) ligand exchange between phosphate and hydroxyl

functional groups of iron (oxyhydr)oxide minerals formed via surface oxidation of ZVI (Allred, 2012; Almeelbi and Bezbaruah, 2012; Yoshino et al., 2014). Since small particle size provides more surface area, colloidal- and nano-ZVI (NZVI) shows better performance than granular ZVI (Almeelbi and Bezbaruah, 2012; Liu et al., 2013). Nano-ZVI (average particle size <100 nm) has attracted more research attention for its high efficiency of P sorption (Bezbaruah et al., 2009; Giasuddin et al., 2007; Li et al., 2006). Nano-ZVI has a layered structure comprised of an elemental iron core and a shell of iron oxides, which provides both the reductive function of elemental iron and the sorptive characteristics of iron oxides (Sun et al., 2006; W. Yan et al., 2010) combined with a Brunauer–Emmett–Teller (BET) surface area as high as 61 m^2/g (Eljamal et al., 2016). Due to different synthesis conditions and testing environments, the P sorption capacity of ZVI varies from 73 to 7,924 mmol/kg among various studies (Almeelbi and Bezbaruah, 2012; Eljamal et al., 2016; Wen et al., 2014).

The effects of pH, ionic strength, and coexisting ions on P sorption were explored by several researchers (Almeelbi and Bezbaruah, 2012; Eljamal et al., 2016; Sleiman et al., 2017; Wen et al., 2014). Their findings show that the sorption of phosphate by ZVI is negatively influenced by increasing solution pH, but a considerable amount of adsorption capacity still remains at near-neutral pH. Common anions such as sulfate and nitrate generally did not affect the P sorption capacity, but there is divergence on the influence of ionic strength. While Almeelbi and Bezbaruah (2012) and Wen et al. (2014) reported that ionic strength did not have an appreciable effect on P sorption, Sleiman et al. (2017) observed that P sorption capacity increased from 281 to 503 mmol/kg as ionic strength was raided from 1 to 500 mM. Since the point of zero charge of ZVI is 7.5-8.5 (Almeelbi and Bezbaruah, 2012; Lenell and Arai, 2017; Sun et al., 2006; W. Yan et al., 2010), the particle surface is positively charged in acidic and neutral environments. Therefore, electrostatic attraction is also involved in the mechanism of phosphate adsorption by ZVI particles aside from inner-sphere complexation.

Unfortunately, the small particle size of ZVI interferes with the field application by reducing stability, promoting the formation of agglomerates, and impeding separation from the working medium. Modifications of ZVI have therefore been developed, which involve mixing the ZVI with other metals, the use of coating materials or emulsifying

agents or deposition on a solid support (Fu et al., 2014; Jeong et al., 2014; Sleiman et al., 2016). For instance, Khalil et al. (2017) synthesized nano-ZVI supported on treated activated carbon that was effective for P removal from wastewater.

The P adsorption data of three ZVIs are shown in Figure 1.1. The studies by Wen et al. (2014) and Sleiman et al. (2017) showed promising results from using ZVI to remove P at near-neutral pH values, while most of the pure iron oxyhydroxides did not retain P at pH ~7.

1.5.3. Anion exchange and hybrid resins

Anion exchange resin is another important class of material that has been employed for removing P in wastewater (e.g., Yoshida and Galinada, 2002; Anirudhan et al., 2006, Sowmya and Meenakshi, 2014). The results are summarized in Fig. 1.2 and Table 1.2. Anion exchange resins consist of three-dimensional frameworks of macromolecular hydrocarbon chains and have positively charged functional groups such as amino groups (Awual et al., 2011b; Loganathan et al., 2014). Phosphate ions are adsorbed via exchange with chloride or other anions on the surface. However, the non-specific adsorption mechanism often leads to low selectivity between phosphate and anion exchange resins, as reported in early studies. Kunin and Myers (1947) found that several anions, including sulfate and nitrate, had higher exchange potentials than phosphate on a polyamine anion exchange resin, Amberlite IR4B (DuPont Co. Wilmington, DE, USA). Using an anion exchange resin, Dowex 1 x 8-50, Christensen and Posner (1980) reported that selectivity was higher for chloride than for either HPO_4^{2-} or $H_2PO_4^-$. Boari et al. (1976) investigated a series of anion exchange resins for their selectivity for phosphate adsorption and identified hydrostatic interactions as a key factor in determining selectivity in the chloride-phosphate system. Weakly-basic anion exchange resins had a selectivity sequence of $OH^- > [H_{3-n}PO^4]^{-n} \geq C1^-$, whereas strongly-basic anion exchange resins followed the sequence of $[H_{3-n}PO^4]^{-n} \geq C1^- > OH^-$. However, Awual and Jyo (2011) found that selectivity for phosphate was higher for a weakly-basic resin Diaion WA20 (Mitsubishi Chemical, Tokyo, Japan) than that for a strong-base resin Diaion SA10A. The P adsorption capacity of Diaion WA increased from 1,390 to 4,950 mmol/kg with decreasing pH from 7.6 to 2.25, and adsorption was not strongly affected by coexisting

chloride or nitrate. The P adsorption capacity of Diaion SA10A was stable at ~1,600 mmol/kg between pH 3 and 7, but sharply dropped to 390 mmol/kg in the presence of coexisting anions like Cl^-. Awual et al. (2011) concluded that the cross-linked poly(styrene) matrix of many anion exchange resins was disadvantageous to the selective adsorption of phosphate because of its hydrophobic nature. Thus, a new fibrous anion exchanger referred to as FVA was produced, which has primary amino groups that account for the hydrophilic property. Batch experiments showed that P removal by FVA decreased from 6,870 to 2,450 mmol/kg with an increase in pH from 2.3 to 7.1. Chloride and nitrate did not affect the P adsorption, but sulfate decreased P removal at low pH, consistent with preferential retention of ions with higher ionic charge (SO_4^{2-} vs. $H_2PO_4^-$).

The application of anion exchange resins for phosphate removal was also explored for simulated industrial wastewater (Nur et al., 2014; O'Neal and Boyer, 2013; Pan et al., 2009), domestic wastewater (Bottini and Rizzo, 2012; O'Neal and Boyer, 2013; Sendrowski and Boyer, 2013), and stream water (Boyer et al., 2011). Johir et al. (2011) used anion exchange columns containing Purolite A500P and Purolite A520E (Purolite, Bala Cynwyd, PA, USA) as the post-treatment of a membrane bioreactor (MBR) to recover nutrients from wastewater. The MBR effluent contained 3.11-4.18 mg P/L, and 85% of the phosphate was retained by the resin columns. In a subsequent study involving a strong base anion exchange resin (Dowex⁄21K-XLT) (Lenntech USA LLC, Miami Beach, FL, USA) in a membrane adsorption system, Johir et al. (2016) obtained high performance during a secondary P removal treatment. The durability of anion exchange resins and their affinity for phosphate have been utilized in soil testing for bioavailable P. For this purpose, the resin is brought into contact with the soil sample for a predetermined period after being transferred to a nylon bag or impregnated on a membrane. Resin P testing has an important advantage over direct measurements using soil extractions since resins work as dynamic exchangers that continually adsorb P from their vicinity (McGrath et al., 2000; Predotova et al., 2011; Richards et al., 1997; Yavitt and Wright, 1996).

Das Gupta et al. (2012) assembled columns of anion exchange resin, Purolite A500P (Purolite, Bala Cynwyd, PA, USA), which is a macroporous polystyrene cross-linked with divinylbenzene, and hydrous ferric oxide (HFO) in series, and tested the capacity for

removal of nitrate and phosphate from wastewater. The P adsorption capacity of Purolite A500P was ~226 mmol/kg with an initial concentration of 0.5 mM, and the adsorption capacity of HFO was 452 mmol/kg. The concept of a mixed resin and HFO adsorbent was further applied in developing hybrid anion exchangers (HAIX) that consists of HFO-coated anion exchange resins (Blaney et al., 2007; O'Neal and Boyer, 2013; Sendrowski and Boyer, 2013; Sengupta and Pandit, 2011). The use of anion exchange resins for P adsorption could be subject to interference by other anions, but the resin matrix provides an ideal loading space for small particles. Ferrihydrite or HFO can adsorb phosphate with high selectivity and efficiency, but the small size and physical weakness of HFO incur difficulties for application and recovery (Blaney et al., 2007; Johir et al., 2016a; Pan et al., 2009; Sengupta and Pandit, 2011). Thus, hybrid resins, i.e. HFO-loaded anion exchange resins, were proposed for P removal from wastewater.

In the 1970s, Takeshita et al. (1979) investigated the adsorption of phosphate on a Fe(III) oxyhydroxide coated anion exchange resin. They found that the adsorption capacity increased with the content of Fe in the hybrid resin and that the maximum adsorption was ~820 mmol/kg. Yoshida et al. (1984) loaded Fe(III) oxyhydroxide on a resin, Amberlite IRC-50 (DuPont co., Wilmington, DE, USA), and the maximum adsorption capacity was 1,970 mmol/kg. The ligand-exchange reaction between phosphate and coordinated water on the resin-bound iron was considered as the dominant adsorption mechanism. Pan et al. (2009) immobilized nano-sized ferrihydrite within a macroporous anion exchange polystyrene resin D-201 (Sanyi, Anhui, China). The new adsorbent named HFO-201 has a maximum adsorption capacity of 574 mmol/kg, while the adsorption capacity of pure D-201 was 394 mmol/kg. The P removal in the hybrid resin is optimal at pH 6.5-8.0 and is resistant to interference from common monovalent anions. Although the addition of sulfate from 0 to 100 mg/L inhibited the adsorption of phosphate, an increase of sulfate concentration from 100 to even 1,500 mg/L did not lead to further reduction in P adsorption. Blaney et al. (2007) reported a similar result with HAIX composed of HFO impregnated in a strong-base anion exchange resin IRA-900 (DuPont co, Wilmington, DE, USA). The adsorption of phosphate was favored at near-neutral pH and showed relatively high selectivity.

In addition to HFO, other metal oxides have also been evaluated for combined use with anion exchange resins to increase P adsorption. Zhu and Jyo (2005) and Awual et al. (2011a) loaded Zr oxides on anion exchange resins, and the adsorption of phosphate was efficient over a wide pH range in the presence of common anions. Zhang et al. (2016) synthesized a different hybrid anion exchange resin (La-201) using hydrated La oxide within anion exchange resin D-201. The hybrid adsorbent has higher specific surface and smaller pore diameter than the original D-201. Batch adsorption experiments were conducted using La-201, D-201, and HFO-201. The result showed that La-201 had the highest adsorption capacity of 1852 mmol/kg at pH 6-7. The selectivity of P adsorption by La-201 was also better than by HFO-201. The influence of DOC was found to be negligible. Acelas et al. (2015) compared the following three hybrid anion exchange resins. IRA-400 (DuPont Co. Wilmington, DE, USA) loaded with HFO, hydrated zirconium oxide (HZrO) and hydrated copper oxide (HCuO) had the maximum P adsorption of 3584, 2959, and 2389 mmol/kg, respectively. Modeling of kinetic data showed that adsorption was best fitted by the pseudo second-order model, and the rate was limited by intra-particle diffusion.

Figure 1.2 summarizes the P adsorption capacity of resins and hybrid resins as a function of pH. The data did not account for interference from other anions. It is important to note the scale of the y-axis is much greater than that in Figure 1.1, indicating some resin adsorbents showed much greater P adsorption capacity than metal oxyhydroxides and ZVI in Figure 1.1. The pH-dependent adsorption behavior is similar to that of iron oxyhydroxides. However, some metal-loaded resins showed an adsorption capacity of 2,000-3,000 mmol/kg at near-neutral pH values. This is an important property of hybrid resins for application under the field conditions.

1.5.4. Layered double hydroxides

Layered double hydroxides (LDHs), also named as hydrotalcite-like compounds (HTLc), is an anionic clay material that can be represented as $M_{1-x}^{2+}M_{x}^{3+}(OH)_2(A^{n-})_{x/n} \cdot yH_2O$ (Hang-Sik et al., 1996; Ookubo et al., 1993). Layered double hydroxides have a structure of brucite-like hydroxide layers that are positively charged by partial substitution of M^{3+} for M^{2+}. Anions and water molecules are intercalated in the interlayer

space and balance the structural charge (Das et al., 2006; Luengo et al., 2017; Ookubo et al., 1993). The interlayer anions are exchangeable with other anions in water environments, which makes LDH an excellent candidate for the removal of anion pollutants such as phosphate (Ashekuzzaman and Jiang, 2014; Goh et al., 2008). Numerous studies have been conducted to evaluate the P adsorption efficiency by various LDH phases. The efficiencies of selected LDHs are compared in Fig. 1.3 and Table 1.3. Seida and Nakano (2002) synthesized Mg/Fe-LDH, and Ca/Fe LDH, and reported the maximum phosphate adsorption capacity of 500 and 929 mmol/kg, respectively. The removal efficiency was further evaluated using real drain water containing ~0.2 mg/L of P. More than 80 % of phosphate was removed in a column filled with 0.2 g Mg/Fe-LDH. Ashekuzzaman and Jiang (2014) reported the maximum adsorption capacity of 2,287 mmol/kg in Ca/Mg-based LDHs. Several Mg/Al LDHs or LDHs with other metal composition have also been reported to have high P adsorption capacities (> 2,000 mmol/kg) (Hang-Sik et al., 1996; Kuzawa et al., 2006; Luengo et al., 2017; Novillo et al., 2014; Tsuji and Fujii, 2014; Yang et al., 2014).

The high P retention of LDHs is accounted for by the following three adsorption mechanisms; 1) ion exchange process with anions in interlayers, 2) ligand exchange on the surface of metal hydroxide layers, and 3) electrostatic attraction of phosphate on the surface (Badreddine et al., 1999; Khitous et al., 2015; Luengo et al., 2017; Novillo et al., 2014; Ookubo et al., 1993; Yang et al., 2014). For instance, XRD analysis showed that the interlayer distance of Mg/Al-LDH originally loaded with chloride anions increased from 0.30 to 0.37 nm after phosphate adsorption (Ookubo et al., 1993). Novillo et al. (2014) observed the anionic exchange reaction of phosphate with nitrate in the interlayer of Mg/Al-LDH using FTIR analysis. In addition, due to the high PZC of LDHs (~9-12), LDHs are positively charged in water (Goh et al., 2008; He et al., 2010; Novillo et al., 2014; Yang et al., 2014). Thus, electrostatic attraction plays an important role in the initial adsorption process.

Aside from anion exchange, surface complexation, and electrostatic attraction, another mechanism has been proposed when Ca is involved in the composition of LDHs. Zhou et al. (2011) reported P removal of 1,819 mM/kg in Ca/Fe-LDH. X-ray diffraction, XPS, and FTIR analyses showed that the high P sorption capacity of Ca/Fe-LDH is due

to partial dissolution that released Ca ions. Similarly, Tsuji and Fujii (2014) found that the adsorption capacity of Ca/Fe-LDHs was much higher when the Ca:Fe ratio in the adsorbent was increased. The adsorption capacity was more than 2,900 mmol/kg when the Ca:Fe ratio was 3, and it decreased to less than 1,300 mM/kg with a Ca:Fe ratio of 1 because LDH with high Ca:Fe ratio would partially undergo dissolution in aqueous environments with precipitation as hydroxyapatite. The coagulation process helps to remove phosphate in solutions, especially when the reaction is promoted at alkaline pH. Other studies by Seida and Nakano (2002), Ashekuzzaman and Jiang (2014), and Novillo et al. (2014) suggested the phosphate-LDHs interaction as a combination of anion exchange and precipitation processes. A combination of Ca^{2+} and Mg^{2+} as precursors led to new LDH phases that had higher P adsorption capacity than either Ca- or Mg-based LDHs (Ashekuzzaman and Jiang, 2014; Zhou et al., 2011).

The elemental composition of LDHs is one of the major factors that influences their P adsorption capacity. Both the species of metal ions and interlayer anions can affect the interaction of LDHs with phosphate (Cheng et al., 2009; He et al., 2010; Zhou et al., 2011). Das et al. (2006) investigated LDHs with various compositions, including Mg/Al, Zn/Al, Ni/Al, Co/Al, Mg/Fe, Zn/Fe, Ni/Fe and Co/Fe for the adsorption of phosphate. Calcined Mg/Al-LDH was the most effective in removing P with a maximum adsorption capacity of 1,368 mmol/kg, and the adsorption capacity decreased with increasing Mg:Al ratios.

The pH-dependence of P adsorption also varies with the metal composition of LDHs. Ashekuzzaman and Jiang (2014) reported that the extent of P adsorption by a Ca-based LDH could remain steady over a broader pH range as compared to Mg/Fe LDH. Seida and Nakano (2002) observed the opposite pH trend for Mg/Fe LDH and Ca/Fe LDH, in that acidity promoted phosphate adsorption on Mg/Fe LDH, whereas Ca/Fe LDH removed more phosphate under alkaline conditions. In general, alkaline pH is disadvantageous to P adsorption in LDH as well as other adsorbents, due to the deprotonation of functional groups and competition between phosphate and hydroxyl ions (Das et al., 2006). Acidic solutions promote dissolution of LDHs and may thereby reduce their effectiveness for P removal (Luengo et al., 2017; Seida and Nakano, 2002). Several researchers observed a decrease in P adsorption at low pH values (Cheng et al., 2009;

Luengo et al., 2017; Ookubo et al., 1993; Tezuka et al., 2004). However, a few studies reported that dissolved metal ions could react with phosphate at low pH, promoting coagulation. For instance, Novillo et al. (2014) found P adsorption maximized for Mg/Al LDH when the initial pH was 3.0, which is consistent with the previous work by Seida and Nakano (2002) showing a negative correlation between phosphate removal and the initial solution pH. On the contrary, the study of Zn/Al LDH by Cheng et al. (2009) described a sharp decrease in P adsorption at acidic pH due to LDH dissolution.

Despite having a high adsorption capacity, the retention of phosphate by LDHs is generally not highly selective, which can be accounted for by the ion exchange process between phosphate and adsorbed anions on the surface (Drenkova-Tuhtan et al., 2013; He et al., 2010). Hang-Sik et al. (1996) showed that bicarbonate and sulfate significantly reduced P adsorption in Mg/Al LDH. Das et al. (2006) reported that Cl^-, NO_3^-, SO_4^{2-} and SeO_3^{2-} all decreased the efficiency of P removal by calcined Mg-Al, Zn-Al, Ni-Al, Co-Al, Mg-Al, Zn-Fe, Ni-Fe and Co-Fe LDH. Novillo et al. (2014) also observed that the amount of P removal decreased when other anions are present in equal concentrations. Interference was highest by NO_3^-, followed by HCO_3^-, Cl^- and SO_4^{2-}. Other influencing factors, such as temperature have also been explored by previous studies. According to Cheng et al. (2009), the adsorption of phosphate by Zn/Al LDH was an endothermic process, but Das et al. (2006) reported that the adsorption of phosphate by calcined Mg/Al LDH was exothermic in nature. In addition, calcination of LDH was proposed as an effective treatment to enhance the P adsorption because of its structural memory effect (Goh et al., 2008; Hang-Sik et al., 1996; He et al., 2010; Tezuka et al., 2004). For instance, Das et al. (2006) showed higher P adsorption by calcinated Mg/Al LDH (~1,368 mmol/kg) than the uncalcinated material. Cheng et al. (2009) also observed a significant increase in P adsorption capacity after calcinating Zn/Al LDH at 300 ℃ for 4h.

Overall, LDH is a promising adsorbent because of its high capacity to remove P and low cost to manufacture (Luengo et al., 2017; Tsuji and Fujii, 2014; Yang et al., 2014). The field application of LDH, however, is not generally recommended in acidic environments because it is highly soluble at low pH. Therefore, recent studies have been focusing on the reusability of LDH materials to increase their application in water

treatment at near-neutral pH (Drenkova-Tuhtan et al., 2013; Goh et al., 2008; Kuzawa et al., 2006; Luengo et al., 2017).

Figure 1.3 shows the P adsorption capacity of different LDH phases reviewed in this section. The data correspond to P adsorption in the absence of interfering ions. Compared to the limited P adsorption capacity of metal oxyhydroxide and resins (Figures 1.1 and 1.2), many LDHs are promising adsorbents to effectively retain P at pH 6-8.

1.5.5. Zirconium and lanthanum oxides

To improve P removal from wastewater, the adsorption capacity of zirconium (Zr) oxide (Chitrakar et al., 2006b; Huang et al., 2015a; Johir et al., 2016b; Lin et al., 2017; H. Liu et al., 2008; Su et al., 2013), lanthanum (La) oxide (Huang et al., 2015b; Rashidi Nodeh et al., 2017; Xie et al., 2014; Zhang et al., 2012) and lithium (Li) (Wang et al., 2007) oxide have been evaluated in recent years. The P adsorption characteristics of these adsorbents are summarized in Fig. 1.4 and Table 1.4.

Compared with Fe and Al (oxyhydr)oxides, Zr oxides have a higher selectivity for phosphate in the presence of common anions in water (Chitrakar et al., 2006b; Johir et al., 2016b; Su et al., 2013). Su et al. (2013) reported that the P adsorption capacity of amorphous Zr oxide nanoparticles was as high as 1,042 mmol/kg at pH ~6, similar to what was reported by Liu et al. (2008) using mesoporous Zr oxide (~958 mmol/kg). In the study by Chitrakar et al. (2006), amorphous Zr hydroxide retained ~320-550 mmol/kg of P in phosphate-enriched (~0.01 mM phosphate) seawater and synthetic wastewater containing 0.065 mM phosphate.

As for influencing factors such as pH, temperature, ionic strength, and coexisting ions, different studies reported similar results. P adsorption by Zr oxides is generally decreased with increasing pH. For instance, Johir et al. (2016b) reported at P removal by Zr hydroxide decreased from 981 to 597 mmol/kg with increasing pH from 4 to 7. The P adsorption was an endothermic process. Ionic strength had either no significant influence or positive influence on P adsorption. Common anions such as chloride and nitrate did not affect the adsorption, but several studies reported that P removal was deceased by sulfate (Chitrakar et al., 2006b), bicarbonate (Zhang et al., 2017), and acetate (Long et al., 2011). Lin et al. (2017) studied the effect of Ca ions on P adsorption in hydrous

zirconium oxide. The result showed that the maximum adsorption capacity increased from 545 to 1,135 mmol/kg when 1 mM Ca^{2+} was added to the solution. The formation of Zr-P-Ca ternary complexes on the adsorbent surface was suggested as an enhanced adsorption mechanism. Since PZC of Zr oxides/hydroxides is 3-5 (Johir et al., 2016b; Lin et al., 2017; H. Liu et al., 2008), the adsorbent surface is negatively charged in neutral or alkaline solutions. Thus the P adsorption mechanisms in Zr oxides were explained by inner-sphere complexation (Xie et al., 2014; Zhang et al., 2017).

One of the major disadvantages of Zr oxide as a P adsorbent is the cost-efficiency. The cost of Zr hydroxide in technical grade is about 5-20 U.S. dollar per kg (Johir et al., 2016b). Zirconium material is more expensive than Fe or Al materials, but it is cheaper than ion exchange resins, and Zr-adsorbent can be reused since the adsorbed phosphate can be efficiently recovered in alkaline solution (Johir et al., 2016b; Long et al., 2011). In addition, the cost is lower when Zr is made into composite materials with other metals or minerals. Long et al. (2011) synthesized a magnetic Fe–Zr binary oxide, and its maximum adsorption capacity for phosphate was 440 mmol/kg at pH 4. The material was reported to be an excellent adsorbent for phosphate because of good adsorption capacity and ease of recovery due to its magnetic property. Zhang et al. (2017) studied magnetic Fe-Zr oxide nanoparticles with different Fe/Zr molar ratios for their phosphate removal effect. The results showed that specific surface area increased from 124 to 282 m^2/g with increasing Zr content, and the adsorption capacity was maximized when the Zr ratio was high. Huang et al. (2015a) synthesized intercalated Zr ions into the interlayer of montmorillonite. The Zr-pillared montmorillonite had a maximum P adsorption capacity of 555 mmol/kg and showed high selectivity for phosphate in the presence of common anions except for carbonate.

Lanthanum, as a rare earth metal, also attracted research attention for the P removal adsorbent technology due to its ability to form La-phosphate complex even at low P concentrations (i.e., high selectivity for P) (Huang et al., 2017; Xie et al., 2014; Zhang et al., 2016). Common anions such as chloride, nitrate, sulfate, and bicarbonate only have a slight (<5%) influence on phosphate removal. Xie et al. (2014) studied the adsorption of phosphate from wastewater using two kinds of La hydroxides, a commercially available La hydroxide that had a lower P adsorption capacity as compared to the other that was

synthesized (584 and 1,132 mmol/kg). The difference was attributed to a difference in surface area. The commercially available La hydroxide had only 31.1 m^2/g, while the synthesized La hydroxide had 153.3 m^2/g. The most significant advantage of La oxide is that the La hydroxide maintained high adsorption efficiency at acidic to alkaline pH values. It also has excellent recyclability. The adsorbed phosphate is removed by hydrothermal treatment in a NaOH solution. These features make La hydroxide a promising adsorbent for industrial applications.

A representative material is La-modified bentonite (LMB) that was first developed in the 1990s. Haghseresht et al. (2009) reported that the maximum P adsorption capacity of Phoslack, a novel LMB, was 329 mmol/kg. In a field test, four metric tons of Phoslack were put into a reservoir, and the phosphate concentration decreased from 0.98 mg/L to 0.16 mg/L. Another lake-scale test was conducted in Lake De Kuil in the Netherlands where LMB was applied in combination with Fe-flocculant to mitigate cyanobacterial blooms. As a result, the total P concentration in summer decreased from 0.05 mg/L to 0.02 mg/L (Waajen et al., 2016). Other field research on the management of eutrophication using La modified bentonite were reviewed by Copetti et al. (2015). The high efficiency of LMB for P binding was pointed out, although P removal could be suppressed by humic substances and competing oxyanions. Some other La-containing materials such La-doped activated carbon and La-loading silica were also tested, showing good potential for P removal in wastewater (Huang et al., 2015b; Rashidi Nodeh et al., 2017; Zhang et al., 2012).

Figure 1.4 summarizes the P adsorption capacity of various Zr and La oxides. Although they have a good P adsorption capacity at a wide pH range (3-10), the overall P adsorption capacity of Zr oxides and La oxides is less than those in metal oxyhydroxides, ZVI, or resins (Figures 1.1-1.3).

1.5.6. Calcium and magnesium oxides

In addition to metal (oxyhydr)oxides, Ca/Mg-containing materials are also commonly tested for P removal from wastewater. The efficiencies of selected Ca/Mg containing adsorbents for P removal are summarized in Fig. 1.5 and Table 1.5. Due to the

common occurrence of Ca minerals in nature, more studies have utilized natural Ca minerals instead of synthetic products.

Karageorgiou et al. (2007) studied the removal of phosphate using natural calcite (98.2% $CaCO_3$ purity, <0.2 mm fraction). The trend of P removal was pH-dependent. At pH 12, ~40 mg/L phosphate was completely retained within 15 min. Dolomite was also tested by several researchers for P removal efficiency. According to Karaca et al. (2004), 103-558 mmol/kg phosphate was adsorbed by 2 g/L dolomite from solution with 10-60 mg/L initial phosphate concentration. The adsorption data were successfully modeled using pseudo second-order and intraparticle diffusion equations. The reaction was identified as an endothermal process. An increase in the initial solution pH from 1 to 11 slightly enhanced P adsorption. However, Mangwandi et al. (2014) reported that the P adsorption capacity of dolomite considerably decreased with increasing pH from 2 to 10. An increase in ionic strength from 0.05 to 0.3 M NaCl had a positive effect on the P adsorption because of co-adsorption of Na ions that may have reduced the charge repulsion between the phosphate ions and negatively charged mineral surfaces. They also conducted a long-term (7 days) adsorption experiment at high initial P concentrations (100-2,000 mg P/L) at acidic pH and found the monolayer adsorption capacity of 12,187 mmol/kg at pH ~ 2.0. X-ray powder diffraction and FT-IR analyses indicated a formation of $Mg_3(PO_4)_2$ and $Ca_3(PO_4)_2$ through surface precipitation.

Other Ca-containing minerals such as opoka, wollastonite, and limestone were previously evaluated for P removal efficiency (Westholm, 2006; Vohla et al., 2011). Opoka is a kind of silica-calcite sedimentary rock that is enriched in $CaCO_3$ and SiO_2. Jóźwiakowski et al. (2017) conducted column experiments using opoka as a filtration material for P removal from biologically treated domestic wastewater. The removal efficiency was ~97 % after nine weeks of the hydraulic load at 0.72 L/day. Wollastonite is also a Ca-rich metasilicate mineral. Brooks et al. (2000) reported 90 % removal from secondary wastewater after 12 hrs (initial [P]: 10 mg/L, 0.05 mg/L wollastonite). Vohla et al. (2011) conducted a review of adsorbent technology to remove P from wastewater in a constructed wetland. A positive correlation was found between P retention and the content of Ca in natural Ca-containing materials.

Calcination can increase the performance of Ca minerals for P removal since $CaCO_3$ is partially transformed into the more reactive CaO during heating (Vohla et al., 2011). For instance, Brogowski and Renman (2004) conducted P adsorption experiments using opoka (particle size: < 0.25 mm) and reported that the opoka after heating at over 900 ℃ could retain P as high as 1,235 mmol/kg. A commercial P filter material Polonite® is produced from heated opoka (particle size: 2-6 mm), and has been widely tested for the removal of P in different studies. Gustafsson et al. (2008) reported that > 95% of phosphate (~7.39 g P/kg) was removed from synthetic wastewater with an initial P concentration of 0.16 mM. Renman and Renman (2010) proved the long-term (67-92 weeks) effectiveness of P removal in Polonite in column experiments. They suggested that 1-2 kg of the material was needed to treat a $1m^3$ of wastewater with the target of 90% P removal.

It is worth mentioning that apatite, which is characterized by high Ca and P content, has also been proposed as an effective P adsorbent. Song et al. (2007) conducted batch experiments for P recovery from wastewater using a natural apatite (AKA: Jordan phosphate rock, the average particle size of 1.5 mm). Approximately 98% of P was removed after 48 hrs from synthetic hard water containing 0.32 mM phosphate. Other studies also observed that the P recovery process was favored under pH>7, as well as by increased contact time and a high Ca/P molar ratio (Bellier et al., 2006; Chen et al., 2009; Zoltek, 1974). Bellier et al. (2006) modeled the P removal process in apatite at pH 8 using the Langmuir isotherm. The calculated P-retention capacity of apatite was ~10 mmol/kg, but Molle et al. (2005) reported a higher maximum adsorption capacity of 154 mmol/kg for a similar adsorbent. The mechanism of P removal by apatite seems to be different from the removal by other adsorbents (e.g., metal oxyhydroxides) Surface precipitation is an important driving force in addition to adsorption. When a Ca-P solution is metastable, further addition of Ca or P ions does not form bulk precipitates. Instead, precipitation may occur on the surface (Joko, 1984; Molle et al., 2005). The presence of P-crystal in apatite lowers the activation energy between the mineral surfaces and adsorbed phosphate on the surface, facilitating the nucleation of hydroxyapatite on a seed crystal (Bellier et al., 2006; Song et al., 2007; Vohla et al., 2011). In fact, the formation of hydroxyapatite has been commonly observed during P removal at water

treatment plants (Duc et al., 2003; Fernane et al., 2008; Dybowska et al., 2009; Kim and Lee, 2014). Because the point of zero charge for hydroxyapatite is about 7.6-8.6 (Bellier et al., 2006), hydroxyapatite is positively charged at neutral pH and provides sorption sites for phosphate ions. The adsorption and crystallization during the removal of phosphate by apatite are difficult to distinguish. They are considered to be concomitant, and the adsorption process could enhance the crystallization of hydroxyapatite (Molle et al., 2005; Vohla et al., 2011). Troesch et al. (2016) reported a field-scale application of apatite in constructed wetlands and demonstrated efficient P removal from wastewater. However, a limitation was reported that apatite could be partially dissolved and release P under acidic conditions (Molle et al., 2005). Kuo et al. (2009) found that apatite dissolution was a major factor controlling P release from soils in phosphate mine reclamation areas, and stated that natural apatite in soils is a long-term P source instead of a sink for P. In addition to apatite, several other minerals can also serve as a seed for P crystallization (e.g., Zoltek, 1974; Kaneko and Nakajima, 1988; Le Corre et al., 2009; Moriyama et al., 2001). For example, Berg et al. (2006) tested P removal from wastewater using the tobermorite(calcium silica hydrate)-seeded crystallization method. Nearly 100 % of P was removed with the initial phosphate concentration of 25 mg/L. Chen et al. (2009) used xonotlite as a seed crystal and achieved 137 mg/g of P removal under the same reaction condition. Although the P removal capacity is relatively small, the crystallization method was advantageous over chemical precipitation because the need for sludge disposal is eliminated.

In addition to Ca-bearing minerals mentioned above, other minerals such as zeolite, bauxite, and laterite have been tested for P removal (Wood and McAtamney, 1996; Altundoan and Tmen, 2002; Westholm, 2006; Onyango et al., 2007; Karapinar, 2009). Jiang et al. (2013) assessed the P removal efficiency of zeolite (chemical composition: 5% Al_2O_3 and 95% SiO_2, the specific surface area: 500-800 m^2/g). The adsorption capacity calculated from the Langmuir model was approximately 10 mmol/kg. The adsorption was considered to be driven by ion exchange. Chen et al. (2006) synthesized zeolite from industrial fly ash and evaluated its phosphate adsorption capacity. The hydrothermal conversion from fly ash to zeolite increased specific surface area by ~26-90 times and increased the P sorption capacity. Phosphate removal was most efficient at

pH~4, and the maximum sorption capacity varied from 380 to 1,522 mmol/kg with fly ash sources having different chemical compositions. Wu et al. (2006) further enhanced the P sorption capacity of a synthesized zeolite via salt treatments. The original Na-zeolite was converted into Al-, Ca-, Fe-, and Mg-zeolites. Al- and Fe-zeolites were the most effective for P removal. Nearly 100% of phosphate at an initial concentration of 0.8 mM was removed by Al- or Fe-zeolites. In addition, modified zeolite (e.g., chitosan modified, a cationic surfactant named hexadecyltrimethylammonium bromide) is known to have high P adsorption capacity (Bansiwal et al., 2006; Xie et al. 2013).

In summary, dolomite and modified zeolite showed high P adsorption capacity (>1000 mmol/kg) like resins (Figures 1.2 and 1.5) while pure zeolite has low P adsorption capacity (< 700 mmol/kg). These adsorbents did not show pH-dependent P adsorption behavior except for one of the dolomitic materials (Mangwandi et al., 2014).

1.6. Figures

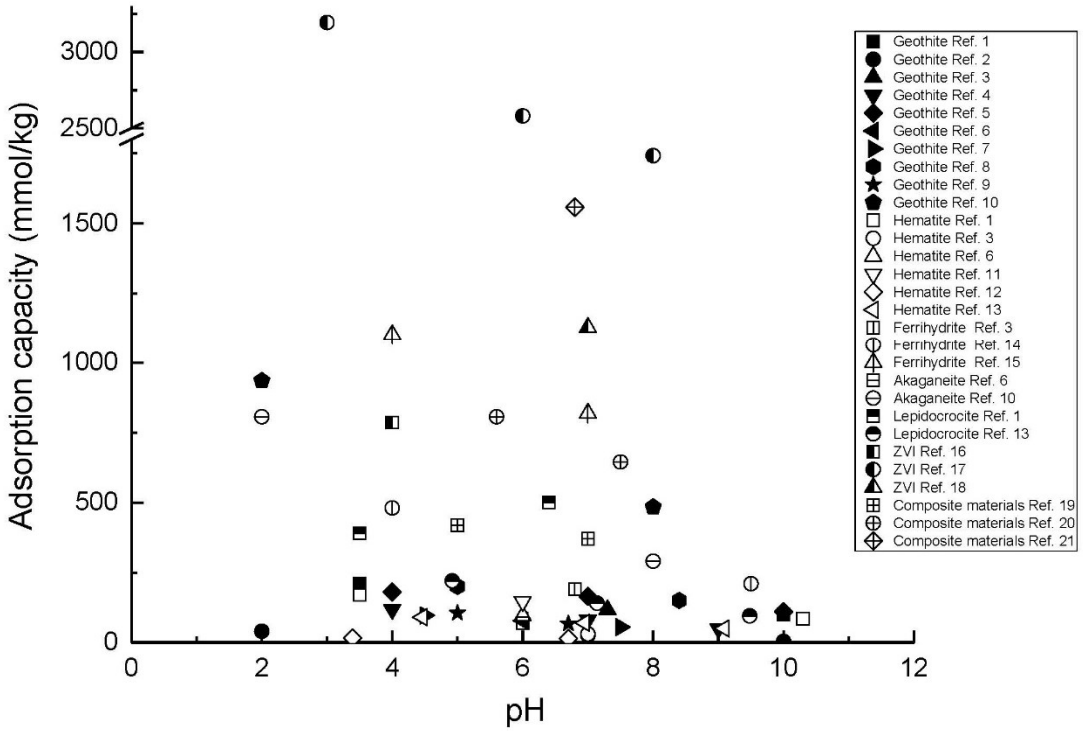

Fig. 1.1. P adsorption capacity of Fe-containing materials with the change of pH in different studies

Note: Ref. 1 Parfitt et al. (1975); Ref. 2 Strauss et al. (1997); Ref. 3 Parfitt (1989); Ref. 4 Ioannou et al. (1998); Ref. 5 Madrid and Posner (1979); Ref. 6 McLaughlin et al. (1981); Ref. 7 Luengo et al. (2006); Ref. 8 Tejedor-Tejedor and Anderson (1990); Ref. 9 Peleka and Deliyanni (2009); Ref. 10 Chitrakar et al. (2006a); Ref. 11 Barron et al. (1988); Ref. 12 Huang (2004); Ref. 13 Madrid and de Arambarri (1985); Ref. 14 Arai and Sparks (2001); Ref. 15 Mallet et al. (2013); Ref. 16 Almeelbi and Bezbaruah (2012); Ref. 17 Wen et al. (2014); Ref. 18 Sleiman et al. (2017); Ref. 19 Li et al. (2014); Ref. 20 Zhang et al. (2009); Ref. 21 Lǔ et al. (2013)

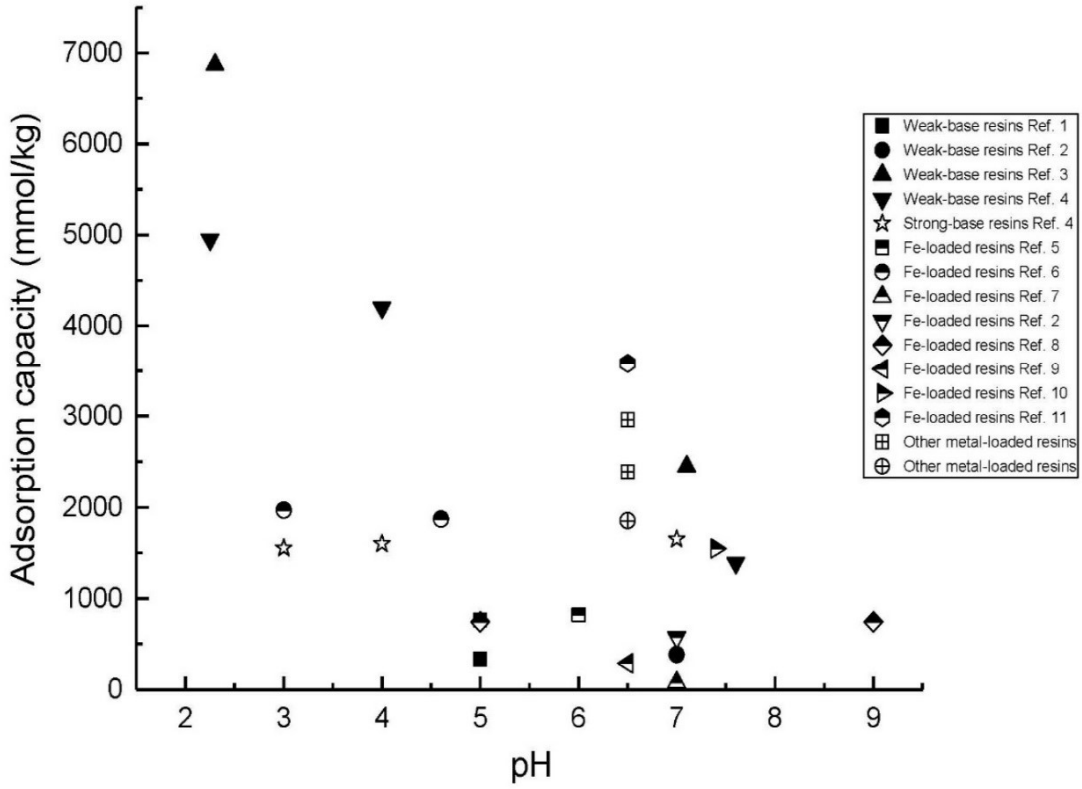

Fig. 1.2. P adsorption capacity of anion exchange resins with the change of pH in different studies

Note: Ref. 1 Anirudhan et al. (2006); Ref. 2 Pan et al. (2009); Ref. 3 Awual et al. (2011b); Ref. 4 Awual and Jyo (2011); Ref. 5 Takeshita et al. (1979); Ref. 6 Yoshida et al. (1984); Ref. 7 Blaney et al. (2007); Ref. 8 Sengupta and Pandit (2011); Ref. 9 O'Neal and Boyer (2013); Ref. 10 Nur et al. (2014); Ref. 11 Acelas et al. (2015); Ref. 12 Zhang et al. (2016)

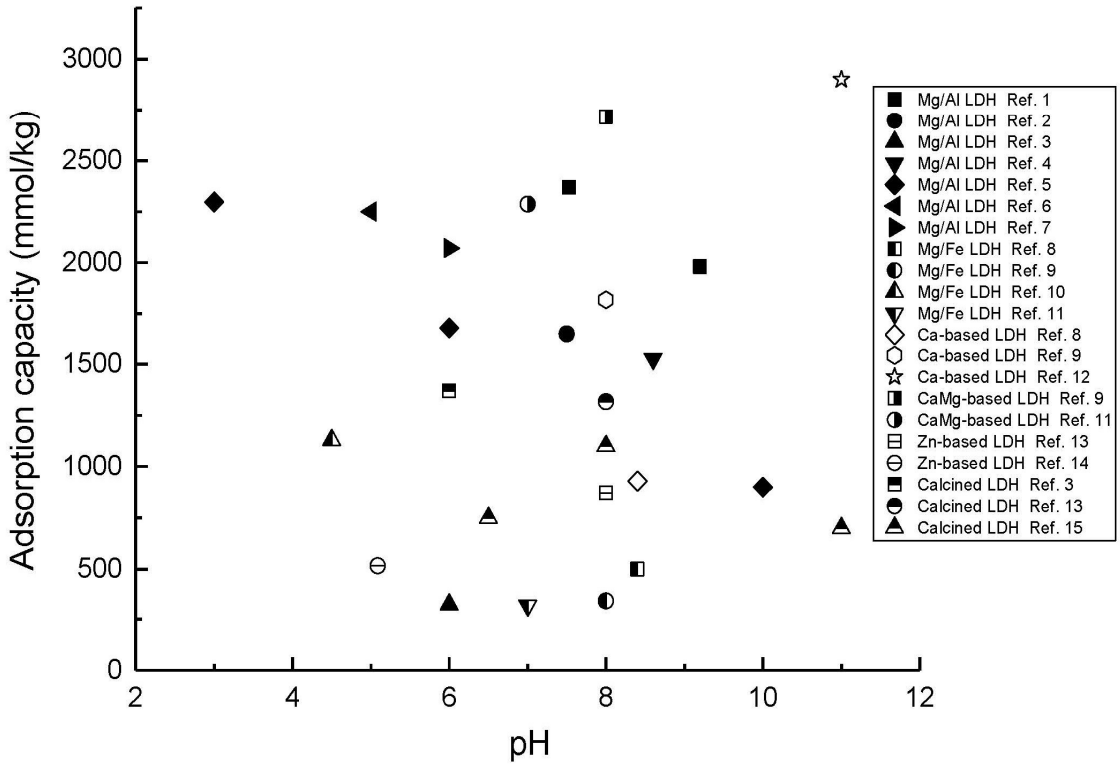

Fig. 1.3. P adsorption capacity of LDHs with the change of pH in different studies

Note: Ref. 1 Ookubo et al. (1993); Ref. 2 Hang-Sik et al. (1996); Ref. 3 Das et al. (2006); Ref. 4 Kuzawa et al. (2006); Ref. 5 Novillo et al. (2014); Ref. 6 Luengo et al. (2017) ; Ref. 7 Khitous et al. (2015); Ref. 8 Seida and Nakano (2002); Ref. 9 Zhou et al. (2011); Ref. 10 Drenkova-Tuhtan et al. (2013); Ref. 11 Ashekuzzaman and Jiang (2014); Ref. 8 Seida and Nakano (2002); Ref. 9 Zhou et al. (2011); Ref. 12 Tsuji and Fujii (2014); Ref. 13 Cheng et al. (2009); Ref. 14 He et al. (2010); Ref. 15 Tezuka et al. (2004)

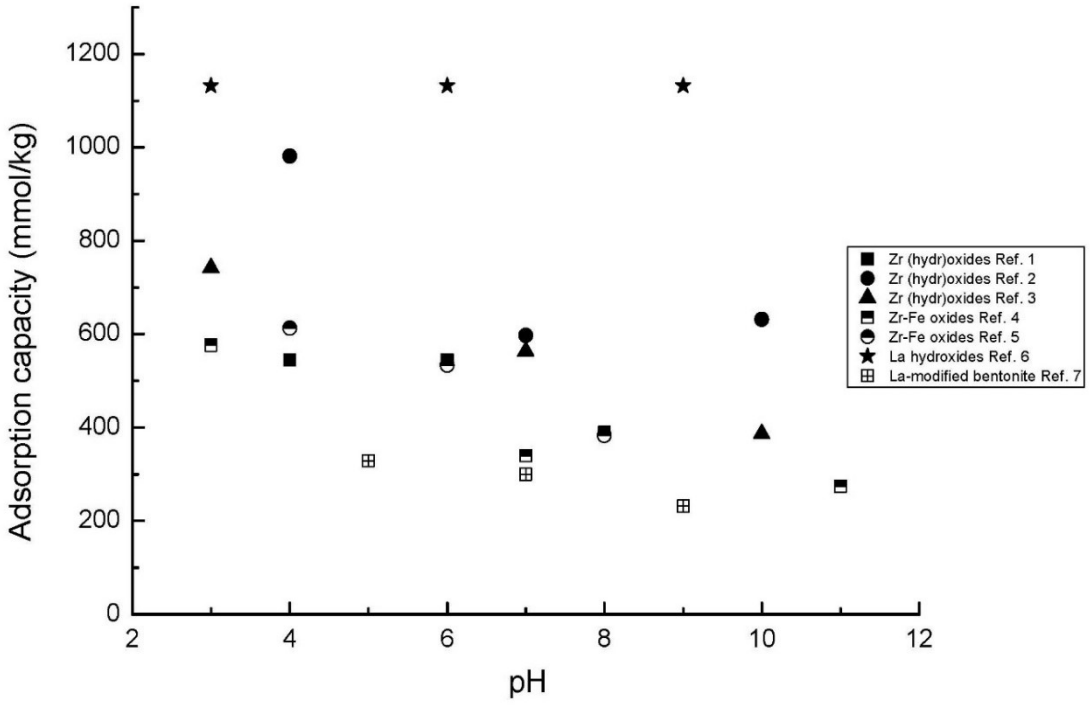

Fig. 1.4. P adsorption capacity of Zr and La-containing materials with the change of pH in different studies

Note: Ref. 1 Lin et al. (2017); Ref. 2 Johir et al. (2016b); Ref. 3 Liu et al. (2008); Ref. 4 Long et al. (2011); Ref. 5 Zhang et al. (2017); Ref. 6 Xie et al. (2014); Ref. 7 Haghseresht et al. (2009)

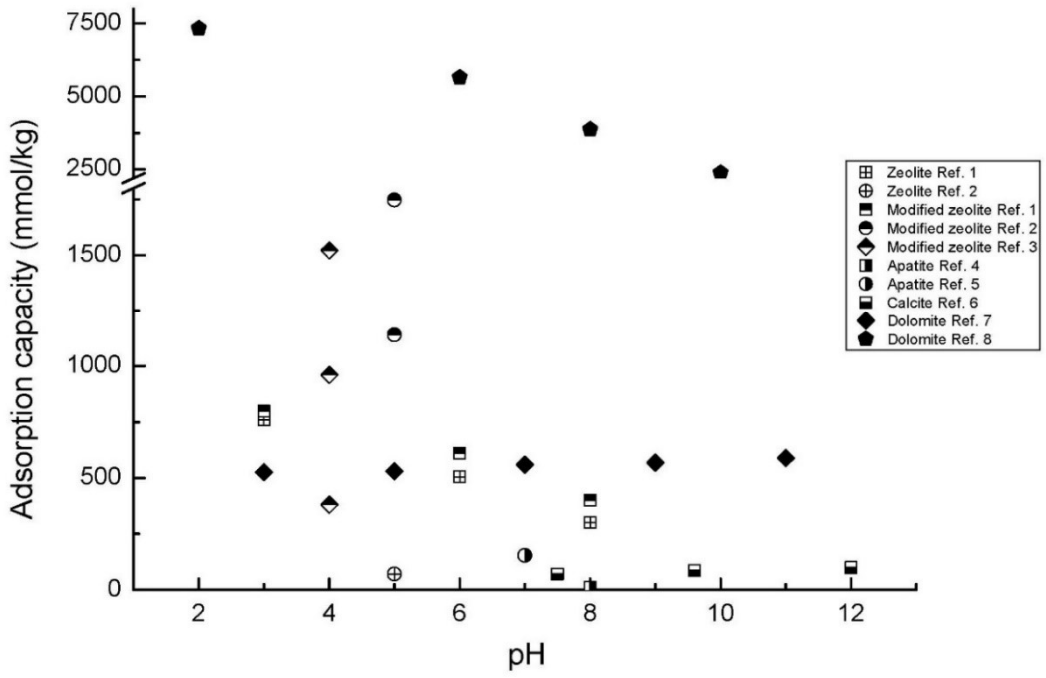

Fig. 1.5. P adsorption capacity of Ca and Mg-containing minerals with the change of pH in different studies

Note: Ref. 1 Onyango et al. (2007); Ref. 2 Wu et al. (2006); Ref. 3 Chen et al. (2006); Ref. 4 Bellier et al. (2006); Ref. 5 Molle et al. (2005); Ref. 6 Karageorgiou et al. (2007); Ref. 7 Karaca et al. (2004); Ref. 8 Mangwandi et al. (2014)

1.7. Tables

Table 1.1. Summary of P adsorption studies on Fe-containing P adsorbents

Reference/adsorbents	Methods	Reaction conditions	Adsorption capacity	Effects of pH and co-existing ions	Mechanism and other findings
Parfitt et al. (1975) Goethite SSA: 80 m2/g Lepidocrocite SSA: 108 m2/g Hematite SSA: 22 m2/g	Adsorption isotherm experiment. Infrared spectroscopic analysis	Background electrolyte: 100 mM KCl pH: 3.5	Goethite: 210 mmol/kg Lepidocrocite: 540 mmol/kg Hematite: 170 mmol/kg	/	The adsorption of P on all of the iron oxides is via a strongly bonded binuclear complex to Fe^{3+} ions in the mineral surface.
Parfitt and Atkinson (1976) Goethite PZC: 8.9 SSA: 80 m2/g	Infrared spectroscopic analysis	pH: 3.6~9.7	197 mmol/kg at pH 3.3	/	Confirmed the formation of a binuclear complex on goethite. Examined the coordination and protonation state of absorbed phosphate.
Madrid and Posner (1979) Goethite PZC: 8 SSA: 84 m2/g	Batch adsorption and desorption experiments with gradient pH, ionic strength and reaction time.	Adsorbent dosage: 2.1 g/L Background electrolyte: 0.01~0.1 M NaCl / LiCl pH: 4~10	180 mmol/kg at pH 4; 165 mmol/kg at pH 7; 110 mmol/kg at pH 10	P adsorption was faster and had higher capacity at lower pH. Increasing the ionic strength depresses the P adsorption when pH<PZC, whereas raising ionic strength enhanced the P adsorption when pH>PZC.	A slow reaction stage followed by rapid initial reactions was observed for both adsorption and desorption processes.
McLaughlin et al. (1981) Hematite SSA: 18 m2/g Goethite SSA: 17 m2/g Akaganeite SSA: 29.4 m2/g Fe gel SSA: 280 m2/g	Batch adsorption experiments with different adsorbents	Initial phosphate concentration: 0.1 mM Adsorbent dosage: 1.875 g/L Background electrolyte: 100 mM NaClO4 pH: 6 Reaction time: 7 days	Hematite: 95 mmol/kg Geothite: 78 mmol/kg Akaganeite: 69 mmol/kg Fe gel: 1130 mmol/kg	/	P sorption capacity of the adsorbents was found linear related ($R^2 = 0.98$) to the amount OH^- sorbed per unit increase in pH value.

Table 1.1. (cont.)

Madrid and de Arambarri (1985) Lepidocrocite SSA: 116 m2/g Hematite SSA: 44 m2/g	Batch adsorption and desorption experiments with gradient pH. Isotopic exchange.	Isotherm experiment with 0~2 mM phosphate Adsorbent dosage: 4 g/L pH: 4~10 Background electrolyte: 0.1 M NaCl Reaction time: 2 days	Lepidocrocite: 220 mmol/kg at pH 4.92; 140 mmol/kg at pH 7.14; 95 mmol/kg at pH 9.48 Hematite: 90 mmol/kg at pH 4.46; 70 mmol/kg at pH 6.95; 50 mmol/kg at pH 9.09	P adsorption decreased with the increase of pH.	P was adsorbed more easily with hematite than with lepidocrocite, as indicated by the different proportions of rapidly and slowly exchangeable P, which could be explained by the different kinds of mesoporosity in the two oxides.
Barron et al. (1988) Aluminous hematite	Batch adsorption experiments with different kinds of hematites.	Isotherm experiments with the equilibrium concentration range 0 to 0.32 mM Adsorbent dosage: 14.3 g/L Background electrolyte: 100 mM KCl pH: 6 Reaction time: 24 h	0.19~3.33 μmol/m2 with different shapes and Al fractions	/	The phosphate adsorption capacities of hematites per unit surface were generally lower than that of goethite.
Parfitt (1989) Hematite Goethite SSA: 310 m2/g Ferrihydrite SSA: 380 m2/g	Batch experiments with different particle size, pH and reaction time.	Initial phosphate concentration: 0~0.08 mM Adsorbent dosage: 28.6 ~57.1 g/L Background electrolyte: 0.002 M CaCl2 pH: ~7 Reaction time: 16 h	Hematite: ~30 mmol/kg	/	The adsorption reactions involved a rapid, strong ligand exchange, followed by weaker ligand exchange, and, probably, by a relatively slow penetration at defect sites and pores. The extent of phosphate uptake during the slow penetration reactions probably depends on the degree of crystallinity or porosity of iron oxides.

Table 1.1. (cont.)

Tejedor-Tejedor and Anderson (1990) Goethite SSA: 81 m2/g	Batch adsorption experiments. CIR-FTIR analysis.	Isotherm experiment with 0~6 mM phosphate. Adsorbent dosage: 30 g/L Background electrolyte: 10 mM NaCl pH: 4~8.4 Reaction time: 20 h	200 mmol/kg at pH 5; 150 mmol/kg at pH 8.4.	/	CIR-FTIR analysis provided evidence for the formation of three different types of complexes: protonated and nonprotonated bridging bidentate and a nonprotonated monodentate. The speciation of these complexes is a function of pH and phosphate surface coverage.
Strauss et al. (1997) Goethite SSA: 18~132 m2/g	Batch experiments with different particle size, pH and reaction time.	Initial phosphate concentration: 0.8 mM Adsorbent dosage: 2 g/L Background electrolyte: 0.01 M NaNO3 pH: 2~11 Reaction time: 0.5 h~6 weeks	45 mmol/kg	P adsorption decreased with the increase of pH.	The crystallinity of the goethite affects the duration and extent of the P adsorption reaction. Phosphate ions were bound on external surface sites first and then penetrated into meso- and micro-pores between the domains of the goethite crystals.
Arai and Sparks (2001) Ferrihydrite SSA: 260 m2/g	Batch experiments with gradient pH and ionic strength. ATR–FTIR analysis.	Initial phosphate concentration: 0.7 mM. Background electrolyte: 10~800 mM NaCl Adsorbent dosage: 2 g/L pH: 3~10 Reaction time: 24 h	480.6 mmol/kg at pH 4; 209.7 mmol/kg at pH 9.5	P adsorption decreased with the increase of pH. The P adsorption was insensitive to changes in ionic strength between pH 3.5 and 7.5, whereas the adsorption increased with increasing ionic strength at pH>7.5.	Inner-sphere adsorption mechanisms. Based on ATR-FTIR analysis, the predominant formation of the nonprotonated bidentate binuclear species at pH>7.5 was proposed. At pH 4–6, protonated inner-sphere complexes were proposed.

Table 1.1. (cont.)

Gao and Mucci (2003) Goethite SSA: 33.5 m2/g	Batch experiments with gradient pH and coexisting anions	Background electrolyte: 700 mM NaCl / artificial sea water Adsorbent dosage: 2.4 g/L pH: 2~10 Reaction time: 1 week	/	P adsorption decreased with the increase of pH in the background 0.7 M NaCl solution. The pH dependence in seawater is different from that in the 0.7 M NaCl solution. Most noteworthy is enhanced adsorption at pH 4.5~6.5. Ca^{2+} and Mg^{2+} increased phosphate adsorption. SO42- decreases phosphate adsorption at pH < 4.5.	Phosphate forms strong ion pairs with Ca^{2+} and Mg^{2+}. The formation of these ion pairs increases phosphate adsorption because of the electrostatic repulsion
Huang (2004) Hematite PZC: 7.3 SSA: 9.12 m2/g	Adsorption isotherm experiments with different pH.	Isotherm experiment with 0.1~0.65 mM phosphate Adsorbent dosage: 20 g/L Background electrolyte: 100 mM NaCl and 60 mM NaAc pH: 3.4~6.7 Reaction time: 3 h	15.8 mmol/kg at pH 3.4; 13.8 mmol/kg at pH 6.7	P adsorption decreased with the increase of pH.	The adsorption isotherms of phosphate on hematite at pH 5.63 and 6.71 intersected those at pH 4.16 and 5.10 because of the changes of protonation state and the electric potential at the surface.
Antelo et al. (2005) Goethite PZC: 9.3 SSA: 70.8 m2/g	Batch experiments with gradient pH and ionic strength.	Isotherm experiment with 0~0.15 mM phosphate Background electrolyte: 10, 100 mM KNO3 pH: 4.5~10 Reaction time: 15~18 h	177 mmol/kg at pH 4.5; 92 mmol/kg at pH 10	P adsorption decreased with the increase of pH. The p adsorption capacity was larger with higher ionic strength.	Postulated three inner-sphere surface complexes (monodentate nonprotonated, bidentate nonprotonated, and bidentate protonated) for phosphate on goethite.

Table 1.1. (cont.)

Chitrakar et al. (2006a) Goethite PZC: 9.5 Akaganeite PZC: 8	Batch experiments with gradient pH and coexisting anions	Adsorption experiments were conducted in 0.01 mM phosphate-enriched sea water and 1.6 mM pure phosphate solution, respectively. Adsorbent dosage: 1 g/L Reaction time: 24 h	Goethite: 320 mmol/kg at pH 7.8 in seawater; 936 mmol/kg at pH 2 in pure phosphate solution. Akaganeite: 270 mmol/kg at pH 7.8 in seawater; 807 mmol/kg at pH 2 in pure phosphate solution	In seawater, the uptake of phosphate increases with the increase of pH to about 7, and then decreases. In pure phosphate solution, the adsorption capacity decreases with the increased pH from 2 to 9. The adsorbents have higher selectivity to phosphate than other common anions except for carbonate.	Electrostatic attraction and the formation of the inner-sphere complex.
Luengo et al. (2006) Goethite SSA: 57 m2/g	Batch experiments with gradient initial phosphate concentration and pH. ATR–IR analysis.	Initial phosphate concentration: 0.0068~0.055 mM Adsorbent dosage: 12.5 g/L Background electrolyte: 100 mM KNO3 pH: 4.5~10.5 Reaction time: 5 h	97 mmol/kg at pH 4.5; 57 mmol/kg at pH 7.5	P adsorption decreased with the increase of pH.	Two surface complexes, the bidentate nonprotonated $(FeO)_2PO_2$ and the bidentate protonated $(FeO)_2(OH)PO$ complexes are formed at the surface at pH 4.5. At pH 7.5 and 9, the dominating surface species is $(FeO)_2PO_2$.
Zhang et al. (2009) Iron-manganese oxide PZC: ~6.6 SSA: 309 m2/g Particle size: 10~30 μm	Batch adsorption experiments with gradient pH, ionic strength and coexisting anions	Isotherm experiment with 0.06~1.3 mM phosphate Adsorbent dosage: 0.2 mg/L pH: 5.6 Background electrolyte: 10 mM NaNO3 Reaction time: 24 h	1161 mmol/kg	P adsorption decreased with the increase of pH from 3 to 10. The adsorption of phosphate was slightly enhanced by the increase of ionic strength from 1 to 100 mM. Anions such as Cl^-, SO_4^{2-}, and CO_3^{2-} had no significant effect on phosphate removal.	The replacement of surface hydroxyl groups by the phosphate species and formation of inner-sphere surface complexes at the water/oxide interface.

Table 1.1. (cont.)

Peleka and Deliyanni (2009) Geothite Particle size: <70 µm SSA: 316 m2/g	Batch experiments with gradient sorbent dosage, pH, ionic strength, and temperature	Isotherm experiment with initial 0~2.1 mM phosphate Adsorbent dosage: 0.1~1 g/L pH: 5, 6.7 Reaction time: 24 h	The calculated maximum capacity was 1516.1 mmol/kg. Actual 105.2 mmol/kg was obtained with an initial 10 mg/L phosphate at pH 5	P adsorption decreased with the increase of pH. The sorption of phosphate increased with increasing ionic strength.	The surface hydroxyl groups play an important role in phosphate adsorption. The sorption of phosphates onto goethite was exothermic.
Almeelbi and Bezbaruah (2012) ZVI Particle size: 0.016 µm PZC: 7.7 SSA: 30~35 m2/g	Batch adsorption experiment with gradient pH, ionic strength and particle size	Initial phosphate concentration: 0.03~0.32 mM Adsorbent dosage: 0.4 g/L Background electrolyte: 0~10 mM CaCl2 pH: ~4 Reaction time: 10~60 min	73 mmol/kg when the initial P concentration was 0.03 mM 786 mmol/kg when the initial P concentration was 0.32 mM	P adsorption decreased with the increase of pH. Sulfate, nitrate, and humic substances showed a statistically significant impact on P removal, but they may not have practical significance in P removal in the field.	Ligand exchange and also electrostatic attraction when pH is less than PZC.
Das Gupta et al. (2012) Hydrous Ferric Oxide Particle size: 177~595 µm	Batch adsorption experiment and column tests	Initial phosphate concentration: 0.5 mM Background electrolyte: 50 mM KNO3 Reaction time: 72 h	451.6 mmol/kg	/	The adsorption of phosphate by HFO was specific adsorption. Both batch and column experiments showed that HFO selectively removed phosphate.
Mallet et al. (2013) Ferrihydrite	Batch experiments with gradient pH, ionic strength and coexisting anions	Initial phosphate concentration: 0.5~5.3 mM Adsorbent dosage: 2 g/L pH: 4 Background electrolyte: 100 mM NaCl Reaction time: 24 h	1103.2 mmol/kg	P adsorption capacity significantly increased with a decrease of pH. Phosphate removal increases with the enhancement of ionic strength. .	Inner-sphere complexes

Table 1.1. (cont.)

Liu et al. (2013) ZVI Particle size: 75~96 μm SSA: 22 m2/g	Batch adsorption experiments with gradient initial P concentration, adsorbent dosage, pH and reaction time	Initial phosphate concentration: 0.16 mM Adsorbent dosage: 0.6 g/L pH: 4~7 Reaction time: 2 h	/	P removal decreased with the increase of pH.	NZVI was oxidized into Fe2+ or Fe3+. Then, P was removed mainly by the formation of FePO4. NZVI had an evident predomination in removing P in oxic solutions than that in anoxic solutions
Lǔ et al. (2013) Iron-aluminum-manganese oxide Isoelectric point: ~9 SSA: 303 m2/g Particle size: 1~20 μm	Batch adsorption experiments with gradient pH, ionic strength and coexisting anions	Isotherm experiment with 0~2.6 mM phosphate Adsorbent dosage: 0.2 mg/L pH: 6.8 Background electrolyte: 10 mM NaCl Reaction time: 24 h	1558 mmol/kg	P adsorption decreased with the increase of pH from 4 to 10.5. In alkaline condition, phosphate removal increased slightly with increasing ionic strength. Sulfate and bicarbonate shows little influence on P removal, but silicate significantly decreased P adsorption	Electrostatic attraction (positively charged when pH<9) and inner-sphere complexation
Wen et al. (2014) ZVI SSA: 27.65 m2/g	Batch adsorption experiments with gradient pH, ionic strength and coexisting anions	Initial phosphate concentration: 0.1~10.5 mM Adsorbent dosage: 1 g/L Background electrolyte: 5~100 mM NaCl pH: 3~12 Reaction time: 2 h	7924 mmol/kg according to the Langmuir model 3194 mmol/kg was actually obtained at pH 3 and about 1740 mmol/kg at pH 8	The P removal efficiency decreased with increasing pH and dropped sharply between 7~8. Ionic strength did not affect phosphate removal. Coexisting chloride, nitrate, and sulfate did not affect phosphate removal, but carbonate significantly impacted the P adsorption.	Phosphate is mainly sequestrated within nZVI by adsorption and co-precipitation
Yoon et al. (2014) Magnetic iron oxide PZC: 7.6 SSA: 82.2 m2/g	Batch experiments with gradient initial P concentration, adsorbent dosage, pH and temperature	Isotherm experiment with initial 0.06~0.6 mM phosphate Adsorbent dosage: 0.6 g/L pH: 2~6 Reaction time: 24 h	162.3 mmol/kg	The phosphate removal was relatively constant at an acidic solution pH, whereas the phosphate removal decreased sharply as the solution pH approached a highly alkaline condition	Ligand exchange process and electrostatic attraction when pH>PZC. The adsorption capacity increased with increasing temperature

Table 1.1. (cont.)

Li et al. (2015) Al-doped goethite SSA: 98 to 279 m2/g with increasing Al content.	Batch adsorption experiments using Al-doped goethite with different Al content.	Initial phosphate concentration: 0.125~0.625 mM Adsorbent dosage: 0.375 g/L Background electrolyte: 37 mM KCl Reaction time: 24 h	The adsorption capacity by pure goethite is 326.8 mmol/kg, which increases sharply to 712 mmol/kg for Al-doped goethite with increasing Al content.	/	Al incorporation causes structural defects in goethite and inhibits the crystal growth of goethite, leading to higher P adsorption capacity.
Eljamal et al. (2016) ZVI Particle size: ~0.04 µm SSA: 61 m2/g	Batch experiments with gradient pH, sorbent dosage and copper chloride concentration	Initial phosphate concentration: 0.53 mM Adsorbent dosage: 1 g/L pH: 2~12	294 mmol/kg with NZVI alone and 526 mmol/kg in the presence of copper chloride	The phosphate removal efficiency decreased with increasing pH. Copper chloride largely promotes the sorption of P by NZVI.	Copper chloride increased iron corrosion, speeding up electron transfer rate and providing iron (hydr)oxide layer which aid in phosphorus adsorption. The recovery of phosphorus from spent NZVI or NZVI/CuCl2 can reach 100% with 1 M NaOH. Aerobic condition accelerated sorption process compared with the anaerobic condition.
Lalley et al. (2016) Goethite-based adsorbent PZC: 9.5 SSA: 140.4 m2/g	Batch adsorption experiment. Column experiment	Adsorption experiments were conducted in lake water containing 0.1 mM phosphate Adsorbent dosage: 1~15 g/L pH: 7 Reaction time: 3 weeks	396.8 mmol/kg	No significant change in phosphate adsorption onto E33 after adding equimolar sulfate or nitrate	Phosphate ion reacts with two singly coordinated Fe–OH groups, forming a bridging, binuclear, bidentate complex.
Sleiman et al. (2017) ZVI Particle size: 250 µm Obtained from Sigma-Aldrich and Jeulin	Batch experiments with gradient aging time, ionic strength, coexisting anions and aging time.	Initial phosphate concentration: 0.1~6.5 mM Adsorbent dosage: 2.5 g/L Background electrolyte: 10 mM NaCl pH: 7.2 Reaction time: 4 h	1129 mmol/kg	The P removal was highly dependent on ionic strength mostly due to chloride, but not dependent on nitrate or sulfate.	ZVI oxides in water and the oxidation products react with phosphate. Aging time significantly affected the P sorption capacity of ZVI and 8h is the best aging time.

Table 1.2. Summary of P adsorption studies on anion exchange resins

Reference/adsorbents	Methods	Reaction conditions	Adsorption capacity	Effects of pH and co-existing ions	Mechanism and other findings
Boari et al. (1976) A series of strong and weak anion exchange resins	Batch adsorption experiments and column study	Initial phosphate concentration: 1~6 mM Adsorbent dosage: 10 g/L pH: 2~11 Background electrolyte: 0.3 M NaCl Reaction time: 48 h	4211 mmol/kg dry resin for Duolite A366 at pH3; 1263 mmol/kg dry resin for Kastel A510 at pH 7	Weak anion resins have high adsorption capacity at acidic condition, but have high selectivity at near neutral condition.	Hydrostatic interactions have great importance in determining resin selectivity in the chloride/phosphate system. A secondary and tertiary amino, porous, 8-10% crosslinked, polyacrylic resin with DETA basic groups would be the best suited for selective phosphate removal from secondary effluents.
Takeshita et al. (1979) Uniselec UR 10 (a Fe(III) complex of chelating resin)	Batch adsorption experiment	Initial phosphate concentration: 0.64~33 mM Adsorbent dosage: 10 g/L pH: 6 Background electrolyte: 0.1~0.2 M NaCl Reaction time: 24 h	820 mmol/kg when Fe content in the resin was 1.34 mmol/g	pH 4~7 was most favorable for the adsorption. The adsorption capacity decreased rapidly after pH 7.	The ligand-exchange reaction of phosphate with coordinated water on the resin-bound iron was the dominant adsorption mechanism. Adsorption capacity increased with the rise in iron content and temperature.
Yoshida et al. (1984) IRC-Fe(III) (a Fe-loaded ion exchange resin) Particle size: 30~50 mesh	Batch adsorption experiment	Initial phosphate concentration: 0.32~32 mM Adsorbent dosage: 10 g/L pH: 3, 4.6 Background electrolyte: 0.3 M NaCl Reaction time: 48 h	1970 mmol/kg at pH 3; 1870 mmol/kg at pH 4.6	The adsorption capacity decreased rapidly with pH rising beyond 4.	The ligand-exchange reaction of phosphate with coordinated water on the resin-bound iron was the dominant adsorption mechanism. Adsorption capacity increased with the rise in iron content.

Table 1.2. (cont.)

Anirudhan et al. (2006) BS-DMAHP (a weak-base anion exchanger produced from banana stem) PZC: 7.8 Surface area: 111.3 m2/g ; Duolite A-7 (a commercial weak base anion exchange resin as reference)	Batch adsorption experiment	Initial phosphate concentration: 0.1~3.2 mM Adsorbent dosage: 2 g/L pH: 2~10 Background electrolyte: 1 M KCl Reaction time: 2 h	BS-DMAHP: 763 mmol/kg at pH 5 Duolite A-7: 334 mmol/kg	The adsorption capacity increased first and then dropped with the increase of pH. Maximum was obtained at pH 5~7.	The adsorption was endothermic process and followed reversible second-order kinetics. The effectiveness of BS- DMAHP was confirmed by treating real phosphate fertilizer industry wastewater collected from a fertilizer industry. The wastewater contained PO4 3- (74.13 mg L-1) and many other ions. 92.5% of the phosphate was removed with 5 g/L adsorbent.
Blaney et al. (2007) HFO-loaded IRA-900 (HAIX, consists of impregnated hydrated ferric oxide nanoparticles with anion-exchange resin)	Batch adsorption experiments and column study	Initial phosphate concentration: 0.008 mM pH: 7~7.5 Background electrolyte: Cl- 90 mg/L, HCO3- 100 mg/L, SO42- 240 mg/L Reaction time: 4~5 days	81 mmol/kg	Doubling concentration of sulfate had practically no effect on the phosphate sorption capacity of HAIX.	Adsorption mechanism includes Lewis acid-base interaction accompanied by the electrostatic attraction. Temperature did not show significant influence on P sorption by HAIX.
Pan et al. (2009) D-201; HFO-201 (HFO-loaded D-201) Particle size: 0.6~1 mm Obtained from Zhengguang Electrical Resin Co. Ltd., Hangzhou, China.	Batch adsorption experiment	Initial phosphate concentration: 0.32 mM Adsorbent dosage: 0.5 g/L pH: 6.5~8 Reaction time: 3 h	D-201: 394 mmol/kg; HFO-201: 574 mmol/kg	The adsorption capacity increased first and then dropped with the increase of pH. Maximum was obtained at pH 7. Sulfate anion strongly competed for ammonium groups, which bind phosphate through electrostatic interaction. However, it does not affect the inner-sphere complexation with HFO.	HFO-201 possesses two types of adsorption sites for phosphate removal: the ammonium groups bound to the D-201 matrix and the loaded HFO nanoparticles. Temperature has a significant effect on outer-sphere interaction and has much less effect on inner-sphere complexation. HFO-201 is easy to regenerate without any significant capacity loss.

Table 1.2. (cont.)

Awual and Jyo (2011) Diaon WA20 (Weak-base anion exchange resin); Diaion SA10A (Strong-base anion exchange resin) Obtained from Mitsubishi Chemical Corporation, Tokyo, Japan.	Batch adsorption experiments and column study	Initial phosphate concentration: 10 mM Adsorbent dosage: 1 g/L pH: 2.25~6.94 Reaction time: 24 h	Diaon WA20: 1390~4950 mmol/kg from pH 7.6 to pH 2.25 Diaion SA10A: 1550~1650 from pH 3 to pH 7	Diaon WA20: P adsorption decreased sharply from pH 2.5 to 7.5. The adsorption process was not strongly affected by chloride and nitrate, but strongly affected by sulfate. Diaion SA10A: P adsorption capacity basically stable between pH 3~7, but the adsorption was markedly affected by chloride, nitrate, and sulfate.	Inner-sphere complexation with amine groups was the dominant mechanism. Different temperatures, namely 10, 20 and 30 °C did not have a significant effect on P adsorption. Weak-base anion exchange resin Diaion WA20 showed higher kinetic performances opposed to Diaion SA10A and was able to use repeatedly for phosphate removal from water for a long time.
Sengupta and Pandit (2011) LayneRT (HAIX) DOW- HFO; DOW-HFO-Cu (Cu(II)-loaded resins) Particle size: 0.3~1.2 mm; Obtained from Solmetex Co.	Batch adsorption experiments and column study	Initial phosphate concentration: 0.16~2.42 mM pH: 5, 9 Reaction time: 24 h	742 mmol/kg at both pH 5 and pH 9	The resins showed high selectivity towards orthophosphate when compared to competing anions, especially sulfate.	Adsorption mechanism includes Lewis acid-base interaction accompanied by the electrostatic attraction. The resins can be efficiently regenerated with 2.5 % sodium chloride and 2.0% sodium hydroxide. Intra-particle diffusion is the rate-limiting step for the phosphorus sorption by HAIX.
Das Gupta et al. (2012) Purolite A500P Particle size: 0.3~0.42 mm	Batch adsorption experiments and column study	Initial phosphate concentration: 0.5 mM Adsorbent dosage: 0.5~10 g/L Background electrolyte: 50 mg/L KNO3 Reaction time: 72 h	226 mmol/kg	/	Purolite A500P has the functional group R-(CH3)3N+ for adsorption of anions. It showed a higher sorption selectivity to nitrate than to phosphate

Table 1.2. (cont.)

O'Neal and Boyer (2013) LayneRT (HAIX) Obtained from Solmetex, Northborough, MA.	Batch adsorption experiment	Initial phosphate concentration: 0~20 mM pH: 6~7 Background solution: Synthetic urine with multiple ions Reaction time: 2 h	291 mmol/kg		/	Adsorption mechanism includes Lewis acid-base interaction accompanied by the electrostatic attraction. HAIX was used for the recovery of P from urine and other wastewater streams. Dilution of urine with tap water decreased the phosphate loading on HAIX resin.
Nur et al. (2014) Purolite FerrIX A33E (a Fe-loaded strong base anion exchange resin) Particle size: 0.3–1.2 mm Obtained from Purolite, U.S.A.	Batch adsorption experiment	Initial phosphate concentration: 0.32 mM Adsorbent dosage: 0.1~10 g/L pH: 7.2~7.6 Reaction time: 72 h	1548 mmol/kg		/	Inner-sphere adsorption by surface complexation on iron oxide as well as outer-sphere adsorption by coulombic forces with the quaternary ammonium functional group. The highly porous nature of the resin bead allows for maximum utilization of the impregnated iron oxide.
Acelas et al. (2015) HFO-loaded resin; HZrO-loaded resin; HCuO-loaded resin (Strong-base anion exchange resin IRA-400, from Amberlite, Dow Chemicals, was utilized as host resin)	Batch adsorption experiment	Initial phosphate concentration: 0.16 mM Adsorbent dosage: 0.2~2 g/L pH: 6~7 Reaction time: 4 h	HFO-loaded resin: 3584 mmol/kg; HZrO-loaded resin: 2959 mmol/kg; HCuO-loaded resin: 2389 mmol/kg	Sulfate reduced P sorption capacity, but HFeO and HZrO were still capable of reducing more than 80% of P in a real wastewater matrix		Electrostatic interactions accompanied by Lewis acid-base interactions (formation of inner-sphere complexes) between phosphate and loaded metals. Chemisorption was the determining step of the adsorption process. The sorption was rate limited by intra-particle diffusion overall.
Zhang et al. (2016) La-201 (Hydrated La(III) oxide-loaded D-201) Particle size: 0.6~0.9 mm	Batch adsorption experiments and column study	Initial phosphate concentration: 1 mM Adsorbent dosage: 0.5 g/L pH: 3~11 Reaction time: 96 h	1852 mmol/kg at pH 6~7	Phosphate adsorption varied insignificantly at acidic pH, and it dropped with pH dropping to alkaline region. With the addition of SO42-, Cl-, NO3-, HCO3-, and SiO32-, the adsorption capacity loss was observed, especially for silicate.		The formation of LaPO4·xH2O was the dominant pathway for selective phosphate adsorption by the immobilized nano-HLO. La-201 exhibited drastically enhanced phosphate removal from synthetic solution as compared to a well recognized Fe(III) oxide nanocomposite HFO-201

Table 1.3. Summary of P adsorption studies on DLHs

Reference/adsorbents	Methods	Reaction conditions	Adsorption capacity	Effects of pH and co-existing ions	Mechanism and other findings
Ookubo et al. (1993) Mg/Al LDH Interlayer Cl-	Batch adsorption experiments	Initial phosphate concentration: 8.7~53 mM; Adsorbent dosage: 10 g/L pH: 7.53 Reaction time: 5 h	2370 mmol/kg	The adsorption capacity was increased with the increase of pH from 1 to 7 then decreased with a further increase of pH up to 9. The significant decrease of phosphate uptake when pH < 5 is due to DLH dissolution.	Ion exchange with interlayer Cl- is the major adsorption mechanism. The ion-exchange properties of hydrotalcite depend strongly on its chemical composition.
Hang-Sik et al. (1996) Mg/Al LDH Interlayer Cl-	Batch adsorption experiments	Initial phosphate concentration: 6.45 mM; Adsorbent dosage: 1 g/L pH: 7.5 Reaction time: 2.5 h	1650 mmol/kg	Nitrate had little influence on phosphate adsorption. Sulfate reduced P adsorption by 12%-13%. Bicarbonate interfered the P adsorption most.	Mg/Al LDH with interlayer Cl- had better P adsorption ability than the LDH with interlayer CO32-. The possibility of LDH's recycle is promising.
Seida and Nakano (2002) (Mg, Ca)/Fe LDH Interlayer CO32-	Batch adsorption experiments and column study	Initial phosphate concentration: 0~48 mM; Adsorbent dosage: 5 g/L pH: 8.4 Reaction time: 24 h	Mg/Fe LDH 500 mmol/kg Ca/Fe LDH 929 mmol/kg	The P adsorption capacity of Mg/Fe LDH decreased with the increase of initial pH, whereas that of Ca/Fe LDH increased with the increase of initial pH.	Adsorption mechanism includes ion exchange between phosphate and interlayer carbonate ions and dissolution–coagulation process. The amount of phosphate removal is considered to depend on both the ion exchange capacity and the buffering property of the compounds.
Das et al. (2006) M2+/M3+ LDH with multiple metal species. Calcined Mg/Al LDH was further studied as the most effective P adsorbent. SSA: 210 m2/g	Batch adsorption experiments	Initial phosphate concentration: 1.6 mM Adsorbent dosage: 0.4 g/L pH: 6 Reaction time: 4 h	Calcined Mg/Al DLH 1368 mmol/kg Uncalcined Mg/Al DLH 323 mmol/kg	The adsorption of phosphate on calcined Mg/Al LDH was promoted with the increase of initial pH from 3 to 5, then steadily decreased with a further increase of pH up to 11. Coexisting Cl-, NO3-, SO42- and SeO32- decreased P adsorption capacity in different degrees. Divalent anions have a stronger interfering effect than monovalent anions.	The percentage of adsorption decreases with increasing Mg-Al molar ratio. Calcination significantly increased the P adsorption ability of Mg/Al LDH. Phosphate adsorption was decreased with increasing temperature from 303 to 333K. Maximum desorption (80%) was achieved using 0.1M NaOH and 4 M NaCl.

Table 1.3. (cont.)

Kuzawa et al. (2006) Mg/Al LDH Interlayer CO32- Obtained from Tomita Pharmaceutical Co. Ltd., Japan Granular particle size: 0.5~1.7 mm	Batch adsorption experiments	Initial phosphate concentration: 6.45 mM; Adsorbent dosage: 1 g/L pH: 8.6 Reaction time: 48 h	1526 mmol/kg	/	The material has high P adsorption capacity even at low phosphate concentration. Adsorbed phosphate could be effectively desorbed with alkaline NaCl solutions and the material was regenerated with 25 w/v% MgCl2 solution.
Cheng et al. (2009) M2+/M3+ LDH with multiple metal species. Zn/Al LDH was further studied as the most effective P adsorbent.	Batch adsorption experiments	Initial phosphate concentration: 0.65 mM; pH: 8 Reaction time: 72 h	Calcined Zn/Al LDH 1315 mmol/kg Uncalcined Zn/Al LDH 871 mmol/kg	An acidic or highly alkaline environment adversely affected phosphate adsorption. The Zn/Al LDH could be an effective adsorbent for phosphate recovery with pH ranging from 5 to 10.	The adsorption of phosphate by Zn/Al LDH is an endothermic process. The absorbed phosphate can be effectively desorbed by a 5 wt% NaOH solution. The regeneration rate of used LDHs was ~60% after six cycles of adsorption-desorption–regeneration.
He et al. (2010) Zn/Al LDH Interlayer Cl-, NO3-, CO32-	Batch adsorption experiments	Initial phosphate concentration: 4 mM Adsorbent dosage: 5 g/L pH: 5.09 Reaction time: 3 days	516 mmol/kg	Zn/Al DLH showed high selectivity toward phosphate, especially when NO3- is the interlayer anion.	Phosphate ions exchange with OH groups and complex with Zn on the surface by outer-sphere complexation or electrostatic attraction. Calcination can increase P adsorption capacity by structural memory effect and brings selectivity.
Zhou et al. (2011) (Mg, Ca)/Fe LDH Interlayer Cl-	Batch adsorption experiments	Initial phosphate concentration: 0~1.45 mM; Adsorbent dosage: 0.2 g/L pH: 8 Reaction time: 24 h	Mg/Fe LDH 339 mmol/kg Ca/Fe LDH 1819 mmol/kg Mg0.5Ca1.5/Fe LDH 2716 mmol/kg	0.1 M NaCl had little effect on the removal of triphosphate by LDHs.	Mg/Fe LDH removed triphosphate mainly by surface adsorption and near-edge intercalation. Ca/Fe LDH removed triphosphate mainly by LDH dissolution and precipitation as Ca-TPP compounds.

Table 1.3. (cont.)

Drenkova-Tuhtan et al. (2013) Mg/Fe-Zr LDH Interlayer NO3-, Cl-	Batch adsorption experiments and pilot-scale test	Initial phosphate concentration: 0.32 mM; Adsorbent dosage: 0.4 g/L pH: 4.5~5 Reaction time: 24 h	1129 mmol/kg	Phosphate adsorption increased with decreasing pH, but in a highly acidic environment (pH < 3) the LDH shell started to dissolve. The affinity for anions of LDHs is decreasing in the order of HCO3-, H2PO4-, NO3-, SO42-.	LDH incorporated with magnetic particles made it easy for separation and recovery of phosphate. Good reusability was obtained for 15 adsorption-desorption cycles on a lab-scale without a significant drop in performance.
Novillo et al. (2014) Mg/Al LDH Interlayer NO3-	Batch adsorption experiments	Initial phosphate concentration: 3.2 mM; Adsorbent dosage: 0.6 g/L pH: 3 Reaction time: 4 h	2297 mmol/kg	The adsorption capacity of the Mg/Al LDH decreased with the increase of initial pH. Coexisting anions inhibited the P adsorption in the order of NO3- < HCO3- < Cl- < SO42-.	Adsorption mechanism includes electrostatic attraction, ion exchange between phosphate and interlayer nitrate and dissolution–coagulation process. Phosphate adsorbed on the LDH can be desorbed at both acid and basic pH values.
Yang et al. (2014) Mg/Al LDH SSA: 104 m2/g PZC: 7.46 Zn/Al LDH SSA: 135 m2/g PZC: 10.26 Interlayer CO32-	Batch adsorption experiments	Phosphate concentration: 0~0.3 mM; Adsorbent dosage: 0.8~6.4 g/L pH: 2~12	Mg/Al LDH 1010 mmol/kg Zn/Al LDH 2206 mmol/kg	The ratio of phosphate changed insignificantly in the pH range of 2–6 for Mg-Al LDH and 2–10 for Zn–Al LDH. With further increase of pH up to 12, there is a drastic decrease.	Adsorption mechanism includes ion exchange between phosphate and interlayer carbonate ions and ligand exchange between phosphate and surface hydroxyl groups.
Tsuji and Fujii (2014) Ca/Fe LDH Interlayer Cl-	Batch adsorption experiments	Initial phosphate concentration: 0.65~3.2 mM; Adsorbent dosage: 0.4 g/L pH: 11 Reaction time: 2 h	2900 mmol/kg when Ca:Fe=3	High pH activates the generation of hydroxyapatite from phosphate and dissolved Ca.	Precipitation reaction between phosphate and dissolved Ca is the major mechanism, and the contribution of ion exchange is weak.

Table 1.3. (cont.)

Ashekuzzaman and Jiang (2014) (Ca, Mg)/(Al, Fe) LDH Interlayer Cl-, NO3-	Batch adsorption experiments	Initial phosphate concentration: 0.32 mM Adsorbent dosage: 0.3 g/L pH: 7 Reaction time: 2 h	Ca1.5Mg0.5/Al (NO3-) LDH 2287 mmol/kg Ca/Al (NO3-) LDH 2152 mmol/kg Mg/Fe (Cl-) LDH 316 mmol/kg	The rate of P adsorption for Ca- and CaMg-based LDHs was almost steady (~98%) in the range of pH between 3.5~10.5, whereas for Mg–Fe(Cl-) LDH, it was at pH between 3~7.5. The P adsorption decreased with further increase in pH up to 12.0.	The P uptake process is expected as a combination of anion exchange and precipitation. Real testing using effluent from a wastewater treatment plant showed good P removal rate (> 90%). Desorption-regeneration performance of Ca-based LDHs was improved when synthesized with both Ca and Mg as divalent precursors.
Luengo et al. (2017) Mg/Al LDH Interlayer Cl-	Batch adsorption experiments	Initial phosphate concentration: 0.056~3.2 mM; Adsorbent dosage: 0.3 g/L pH: 5 Background electrolyte: 0.1M NaCl Reaction time: 4 h	2250 mmol/kg	P adsorption decreased with the increase of initial solution pH from 5 to 9.	Adsorption mechanism includes anion exchange, electrostatic attraction, and surface complexation.

Table 1.4. Summary of P adsorption studies on Zr and La oxides

Reference/adsorbents	Methods	Reaction conditions	Adsorption capacity	Effects of pH and co-existing ions	Mechanism and other findings
Long et al. (2011) Iron-zirconium oxide SSA: 106.2 m2/g	Batch adsorption experiments	Initial phosphate concentration: 0~3.2 mM Adsorbent dosage: 1 g/L pH: 4 Background electrolyte: 1~100 mM NaCl Reaction time: 24 h	440 mmol/kg	P adsorption efficiency decreased with the increased of pH from 1.5 to 10. P adsorption decreased in the presence of nitrate, sulfate, and citrate due to the competition of adsorption sites. Acetic increased P adsorption because it lowered the solution pH.	The adsorption of phosphate was ion exchange reaction. About 86% of P were adsorbed within the first 2 h, followed by a slow stage until the equilibrium state was reached after 24 h. The material was magnetic, easy to separate.
Zhang et al. (2017) Iron-zirconium oxide SSA: 124~282 m2/g with decreasing Fe: Zr ratio from 12:1 to 2:1 PZC: 8~9	Batch adsorption experiments	Initial phosphate concentration: 0.16~3.2 mM Adsorbent dosage: 2 g/L pH: 4 Reaction time: 24 h	377~687 mmol/kg with decreasing Fe:Zr ratio from 12:1 to 2:1	P adsorption decreased with the increase of pH from 1.5 to 10. Phosphate sorption slightly enhanced with the increase of the solution ionic strength. Chloride, sulfate, and nitrate had no obvious impact on P removal. Bicarbonate restrained the phosphate adsorption due to the strong competition for the adsorption sites	Inner-sphere complexation was the dominant adsorption mechanism.
Lin et al. (2017) Hydrous zirconium oxide PZC: 3.3	Batch adsorption experiments	Initial phosphate concentration: 0.05~0.5 mM Adsorbent dosage: 0.4 g/L pH: 7 Reaction time: 24 h	545 mmol/kg	In the absence of Ca^{2+}, P adsorption showed little pH dependence from 4 to 6, but decreased sharply from 6 to 9. In the presence of Ca^{2+}, no significant influence of pH was observed from 4 to 9. Ca^{2+} significantly increased P removal capacity in alkaline solution.	The replacement of the surface chloride and –OH groups by the phosphate species and the formation of inner-sphere phosphate complexes at the solid/solution interface. Most of the adsorbed phosphate could be easily desorbed using the 1.0 M NaOH solution.

Table 1.4. (cont.)

Johir et al. (2016b) Zirconium hydroxide Particle size: 0.1~35 µm	Batch adsorption experiments and lab-scale reactor test	Initial phosphate concentration: 0.32 mM Adsorbent dosage: 0.1~3 g/L pH: 7 Reaction time: 72 h	597 mmol/kg	P adsorption decreased with the increase of pH from 4 to10. The phosphate adsorption capacity slightly decreased in the presence of sulfate but not in the presence of nitrate.	The adsorption was via inner-sphere complexing.
Liu et al. (2008) Mesoporous Zirconium oxide SSA: 232 m2/g Isoelectric point: 4.9	Batch adsorption experiments	Initial phosphate concentration: 0~9.7 mM Adsorbent dosage: 1.2 g/L pH: 6.7~6.9 Background electrolyte: 10 mM KNO3 Reaction time: 24 h	958 mmol/kg	P adsorption decreased with the increase of pH from 3 to11. The P adsorption was slightly affected by ionic strength from 0.001 to 0.1M KNO3.	Inner-sphere complexing was the dominant mechanism. Coulombic attraction was also involved at low pH.
Xie et al. (2014) Lanthanum hydroxides (LH) Amorphous/crystalline SSA: 153.3 m2/g for amorphous LH and 31.1 for crystalline LH	Batch adsorption experiments	Initial phosphate concentration: 0.05~5.3 mM Adsorbent dosage: 2.5 g/L Reaction time: 24 h	Amorphous LH: 1132 mmol/kg Crystalline LH: 584 mmol/kg	The performance for phosphate removal by LHs decreased sharply when pH > 9.0 for crystalline LH and > 12.0 for amorphous LH. The coexistence of chloride, nitrate, sulfate and hydrogen carbonate anions only had slight effect on phosphate removal by LHs.	The adsorption was via ligand exchange mechanism. The amorphous phase and higher specific surface area of synthesized LH resulted in its greater adsorptive capability than commercial LH.
Haghseresht et al. (2009) lanthanum-modified bentonite (Phoslock) Particle size: 22 µm	Batch adsorption experiments and field test	Initial phosphate concentration: 0.32 mM Adsorbent dosage: 0.05~5 g/L Reaction time: 5 h	329 mmol/kg	P adsorption decreased with the increase of pH from 5 to 9. Ionic strength did not have significant influence on the rate of phosphate uptake.	The adsorption was a chemical process. It was an endothermal reaction that the adsorption rate increased at higher temperatures.

Table 1.5. Summary of P adsorption studies on Ca and Si minerals

Reference/adsorbents	Methods	Reaction conditions	Adsorption capacity	Effects of pH and co-existing ions	Mechanism and other findings
Jiang et al. (2013) Zeolite Particle size: 0.85 mm SSA: 500~800 m2/g	Batch experiments and column study	Initial phosphate concentration: 0.1~1.3 mM Adsorbent dosage: 100 g/L Reaction time: 48 h	10 mmol/kg	/	The adsorption was via electrostatic attraction or ion-exchange.
Onyango et al. (2007) Al-activated Zeolite Si/Al ratio: 2.75~3.25 PZC: 7.5 SSA: 642 m2/g	Batch adsorption experiments	Initial phosphate concentration: 0.5~3.2 mM Adsorbent dosage: 1 g/L pH: 4.5 Reaction time: 7 days	806 mmol/kg	The uptake of phosphate decreased with the increase of pH from 2.5 to 10. Nitrate, sulfate, and chloride improved slightly the phosphate removal efficiency while fluoride reduced P removal capacity.	The adsorption was via Coulombic attraction and ligand exchange reaction It was the terminal aluminol sites that were responsible for phosphate sorption.
Wu et al. (2006) Modified zeolite Synthesized from fly ash with Ca, Mg, Al, and Fe salt treatment	Batch adsorption experiments	Initial phosphate concentration: 32.3 mM Adsorbent dosage: 10 g/L pH: ~5 Reaction time: 24 h	1139 mmol/kg	/	The P immobilization was due mainly to ligand exchange by positively charged iron and aluminum phases. The solution pH was lifted during the P sorption. Al3+-ZFA was the best form for phosphate removal at low concentrations
Chen et al. (2006) Modified zeolite Synthesized from different sources of fly ash.	Batch adsorption experiments	Initial phosphate concentration: 32.3 mM Adsorbent dosage: 10 g/L pH: ~4 Reaction time: 24 h	380~1522 mmol/kg	The amount of adsorbed phosphate first increased then dropped with the increase of initial pH. Zeolite with high Ca content have the best performance in P removal when 3.5<pH<9, while the pH range for low Ca zeolite is 3.5<pH<5.5	The mechanism of P removal appears to be the formation of calcium phosphate precipitate and the sorption through ligand exchange. Sorption capacity of all fly ashes increased markedly after the conversion to zeolite because of larger specific surface area and more dissociated Fe2O3.

Table 1.5. (cont.)

Bellier et al. (2006) Apatite Particle size: 2.5~10 mm PZC: 7.6~8.6	Batch experiments and column study	Initial phosphate concentration: 0.16~4.8 mM Adsorbent dosage: 50 g/L pH: 8 Background electrolyte: 1000 µS/cm by adding NaCl Reaction time: 24, 96 h	10 mmol/kg	/	Adsorption occurred almost instantaneously and was rapidly followed by precipitation. Apatite also contributed as a source of Ca, which is essential for Ca–P precipitation
Molle et al. (2005) Apatite Particle size: 0.2~0.9 mm	Batch experiments and column study	Initial phosphate concentration: 16.1 mM Adsorbent dosage: 40 g/L pH: 7 Background electrolyte: 1000 µS/cm by adding NaCl Reaction time: 24 h	154 mmol/kg	The adsorption showed good pH stability.	Adsorption was predominant as long as the surface state was far from a saturated state. Retention in the column study was not governed by adsorption (for long-term removal) but by surface precipitation.
Karageorgiou et al. (2007) Calcite Particle size: < 0.2 mm PZC: 8.2	Batch adsorption experiments	Initial phosphate concentration: 0.63 mM Adsorbent dosage: 1 g/L pH: 12 Background solution: tap water with low hardness	100 mmol/kg	With the pH increased from 7.6, the P uptake increased and became complete in the vicinity of pH 12.	Specific adsorption of orthophosphate species onto the calcite surface seemed to be the driving mechanism.

Table 1.5. (cont.)

Karaca et al. (2004) Dolomite SSA: 0.14 m2/g Composition: $CaMg(CO_3)_2$	Batch adsorption experiments	Initial phosphate concentration: 0.63 mM Adsorbent dosage: 2 g/L pH: 1~11	558 mmol/kg	The amount of phosphate adsorbed increased with increase in pH from 1 to 11.	The P removal was via chemisorption and intraparticle diffusion. The adsorption of phosphate onto dolomite is an exothermically activated process.
Mangwandi et al. (2014) Dolomite Particle size: 0.05~0.1 mm SSA: 0.146 m2/g PZC: 8.55 Composition: $Ca_3(PO_4)_2$ and/or $Mg_3(PO_4)_2$	Batch adsorption experiments	Initial phosphate concentration: 3.2, 64.5 mM Adsorbent dosage: 4 g/L pH: 2 Reaction time: 7 days	7332 mmol/kg	The adsorption capacity decreased considerably with the increase of solution pH from 2 to 10. Adsorption of phosphate increased as the ionic strength increased from 0.05 to 0.3 M NaCl.	Precipitation and ion exchange reaction was the dominant adsorption mechanism.

1.8. References

A-Zarah, A.I. 2015. Drainage Water Quality Evaluation for Irrigation in Al-Ahsa Oasis, Saudi Arabia. Res. J. Environ. Toxicol. 9(2): 90.

Acelas, N.Y., B.D. Martin, D. López, and B. Jefferson. 2015. Selective removal of phosphate from wastewater using hydrated metal oxides dispersed within anionic exchange media. Chemosphere 119: 1353–1360.

Ahl, T. 1988. Background yield of phosphorus from drainage area and atmosphere: An empirical approach. Hydrobiologia 170(1): 35–44.

Ahrens, L., A. Daneshvar, A.E. Lau, and J. Kreuger. 2015. Characterization of five passive sampling devices for monitoring of pesticides in water. J. Chromatogr. A 1405: 1–11.

Akhtar, M., D.L. McCallister, D.D. Francis, and J.S. Schepers. 2005. Manure Source Effects on Soil Phosphorus Fractions and Their Distribution. Soil Sci. 170(3): 183–190.

Alexandratos, N., and H. de Haen. 1995. World consumption of cereals: will it double by 2025? Food Policy 20(4): 359–366.

Allred, B.J. 2011. Laboratory Evaluation of Zero Valent Iron and Sulfur-Modified Iron for Agricultural Drainage Water Treatment. Ground Water Monit. Remediat. 31(3): 82–94.

Allred, B.J. 2012. Laboratory evaluation of porous iron composite for agricultural drainage water filter treatment. Trans. ASABE 55(5): 1683–1697.

Almeelbi, T., and A. Bezbaruah. 2012. Aqueous phosphate removal using nanoscale zero-valent iron. J. Nanoparticle Res. 14(7): 900.

Almeida, M.I.G.S., B.M. Jayawardane, S.D. Kolev, and I.D. McKelvie. 2018. Developments of microfluidic paper-based analytical devices (μPADs) for water analysis: A review. Talanta 177(July 2017): 176–190.

Altundoan, H.S., and F. Tmen. 2002. Removal of phosphates from aqueous solutions by using bauxite. I: Effect of pH on the adsorption of various phosphates. J. Chem. Technol. Biotechnol. 77(1): 77–85.

Anderson, D.M., P.M. Glibert, and J.M. Burkholder. 2002. Harmful algal blooms and eutrophication: Nutrient sources, composition, and consequences. Estuaries 25(4

B): 704–726.

Andersson, A., and M. 1981 Mahlin. 1981. Cadmium effects from phosphorus fertilization in field experiments. Swedish J. Agric. Res. 11: 3–10.

Anirudhan, T.S., B.F. Noeline, and D.M. Manohar. 2006. Phosphate removal from wastewaters using a weak anion exchanger prepared from a lignocellulosic residue. Environ. Sci. Technol. 40(8): 2740–2745.

Antelo, J., M. Avena, S. Fiol, R. López, and F. Arce. 2005. Effects of pH and ionic strength on the adsorption of phosphate and arsenate at the goethite-water interface. J. Colloid Interface Sci. 285(2): 476–486.

Antweiler, R.C., R.L. Smith, M.A. Voytek, J.-K. Böhlke, and K.D. Richards. 2004. Water-quality data from two agricultural drainage basins in Northwestern Indiana and Northeastern Illinois: I. Lagrangian and synoptic data, 1999-2002.

Arai, Y., A. Lanzirotti, S.R. Sutton, M. Newville, J. Dyer, and D.L. Sparks. 2006. Spatial and temporal variability of arsenic solid-state speciation in historically lead arsenate contaminated soils. Environ. Sci. Technol.

Arai, Y., and D.L. Sparks. 2001. ATR-FTIR spectroscopic investigation on phosphate adsorption mechanisms at the ferrihydrite-water interface. J. Colloid Interface Sci. 241(2): 317–326.

Ashekuzzaman, S.M., and J.Q. Jiang. 2014. Study on the sorption-desorption-regeneration performance of Ca-, Mg- and CaMg-based layered double hydroxides for removing phosphate from water. Chem. Eng. J. 246: 97–105.

Atkinson, R.J., R.L. Parfitt, and R.S.C. Smart. 1974. Infra-red study of phosphate adsorption on goethite. J. Chem. Soc. Faraday Trans. 1 Phys. Chem. Condens. Phases 70(2): 1472.

Awual, M.R., S.A. El-Safty, and A. Jyo. 2011a. Removal of trace arsenic(V) and phosphate from water by a highly selective ligand exchange adsorbent. J. Environ. Sci. 23(12): 1947–1954.

Awual, M.R., and A. Jyo. 2011. Assessing of phosphorus removal by polymeric anion exchangers. Desalination 281(1): 111–117.

Awual, M.R., A. Jyo, S.A. El-Safty, M. Tamada, and N. Seko. 2011b. A weak-base fibrous anion exchanger effective for rapid phosphate removal from water. J.

Hazard. Mater. 188(1–3): 164–171.

Badreddine, M., A. Legrouri, A. Barroug, A. De Roy, and J.P. Besse. 1999. Ion exchange of different phosphate ions into the zinc–aluminium–chloride layered double hydroxide. Mater. Lett. 38(6): 391–395.

Baker, L., K.L. Campbell, H.P. Johnson, and J. Hanway. 1976. Nitrate, Phosphorus, and Sulfate in Subsurface Drainage Water. Agriculture 4(3): 406–412.

Bansiwal, A.K., S.S. Rayalu, N.K. Labhasetwar, A.A. Juwarkar, and S. Devotta. 2006. Surfactant-modified zeolite as a slow release fertilizer for phosphorus. J. Agric. Food Chem. 54(13): 4773–4779.

Barron, V., M. Herruzo, and J. Torrent. 1988. Phosphate Adsorption by Aluminous Hematites of Different Shapes. Soil Sci. Soc. Am. J. 52(3): 647.

Bellier, N., F. Chazarenc, and Y. Comeau. 2006. Phosphorus removal from wastewater by mineral apatite. Water Res. 40(15): 2965–2971.

Berg, U., D. Donnert, P.G. Weidler, E. Kaschka, G. Knoll, and R. N??esch. 2006. Phosphorus removal and recovery from wastewater by tobermorite-seeded crystallisation of calcium phosphate. Water Sci. Technol. 53(3): 131–138.

Bertol, O.J., N.E. Rizzi, N. Favaretto, and M.D.C. Lana. 2010. Phosphorus loss by surface runoff in no-till system under mineral and organic fertilization. Sci. Agric. 67(1): 71–77.

Bezbaruah, A.N., S. Krajangpan, B.J. Chisholm, E. Khan, and J.J. Elorza Bermudez. 2009. Entrapment of iron nanoparticles in calcium alginate beads for groundwater remediation applications. J. Hazard. Mater. 166(2–3): 1339–1343.

Blaney, L.M., S. Cinar, and A.K. SenGupta. 2007. Hybrid anion exchanger for trace phosphate removal from water and wastewater. Water Res. 41(7): 1603–1613.

Boari, G., L. Liberti, and R. Passino. 1976. Selective Renovation of Eutrophic Wastes Phosphate Removal. Water Res. 10(5): 421–428.

Booij, K., H.M. Sleiderink, and F. Smedes. 1998. Calibrating the uptake kinetics of semipermeable membrane devices using exposure standards. Environ. Toxicol. Chem. 17(7): 1236–1245.

Borgnino, L., M.J. Avena, and C.P. De Pauli. 2009. Synthesis and characterization of Fe(III)-montmorillonites for phosphate adsorption. Colloids Surfaces A

Physicochem. Eng. Asp. 341(1–3): 46–52.

Borgnino, L., C.E. Giacomelli, M.J. Avena, and C.P. De Pauli. 2010. Phosphate adsorbed on Fe(III) modified montmorillonite: Surface complexation studied by ATR-FTIR spectroscopy. Colloids Surfaces A Physicochem. Eng. Asp. 353(2–3): 238–244.

Bottini, A., and L. Rizzo. 2012. Phosphorus Recovery from Urban Wastewater Treatment Plant Sludge Liquor by Ion Exchange. Sep. Sci. Technol. 47(4): 613–620.

Boujelben, N., J. Bouzid, Z. Elouear, M. Feki, F. Jamoussi, and A. Montiel. 2008. Phosphorus removal from aqueous solution using iron coated natural and engineered sorbents. J. Hazard. Mater. 151(1): 103–110.

Bouwman, A.F., A.H.W. Beusen, and G. Billen. 2009. Human alteration of the global nitrogen and phosphorus soil balances for the period 1970-2050. Global Biogeochem. Cycles 23(4).

Bouwman, A.F., A.H.W. Beusen, L. Lassaletta, D.F. van Apeldoorn, H.J.M. van Grinsven, J. Zhang, and M.K. Ittersum van. 2017. Lessons from temporal and spatial patterns in global use of N and P fertilizer on cropland. Sci. Rep. 7(January): 40366.

Bowman, R.A. 1989. A Sequential Extraction Procedure with Concentrated Sulfuric Acid and Dilute Base for Soil Organic Phosphorus. Soil Sci. Soc. Am. J. 53: 362–366.

Boyd, C.E., and Y. Musig. 1981. Orthophosphate uptake by phytoplankton and sediment. Aquaculture 22(C): 165–173.

Boyer, T.H., A. Persaud, P. Banerjee, and P. Palomino. 2011. Comparison of low-cost and engineered materials for phosphorus removal from organic-rich surface water. Water Res. 45(16): 4803–4814.

Brogowski, Z., and G. Renman. 2004. Characterization of Opoka as a Basis for its Use in Wastewater Wastewater W Treatment Treatment T. Polish J. Environ. Stud. 13(1): 15–20.

Brooks, A.S., M.N. Rozenwald, L.D. Geohring, L.W. Lion, and T.S. Steenhuis. 2000. Phosphorus removal by wollastonite: A constructed wetland substrate. Ecol. Eng. 15(1–2): 121–132.

Bryant, L.D., and A. Matzinger. 2012. Hypolimnetic Oxygen Depletion in Eutrophic Lakes.

Burkholder, J.M., and H.B. Glasgow. 1997. Pfiesteria piscicida and other Pfiesteria-like dinoflagellates: Behavior, impacts, and environmental controls. Limnol. Ocean. 42(5(2)): 1052–1075.

Carpenter, S.R., N.F. Caraco, D.L. Correll, R.W. Howarth, A.N. Sharpley, and V.H. Smith. 1998a. Nonpoint pollution of surface waters with phosphorus and nitrogen. Ecol. Appl. 8: 559–568.

Carpenter, S.R., N.F. Caraco, D.L. Correll, R. W.Howarth, A.N. Sharpley, and V.H. Smith. 1998b. Nonpoint pollution of surface waters with phosphorus and nitrogen. Ecol. Appl. 8(1998): 559–568.

Chen, M., J. Chen, and F. Sun. 2008. Agricultural phosphorus flow and its environmental impacts in China. Sci. Total Environ. 405(1–3): 140–152.

Chen, C.C., G.C. Gong, and F.K. Shiah. 2007. Hypoxia in the East China Sea: One of the largest coastal low-oxygen areas in the world. Mar. Environ. Res. 64(4): 399–408.

Chen, J., H. Kong, D. Wu, Z. Hu, Z. Wang, and Y. Wang. 2006. Removal of phosphate from aqueous solution by zeolite synthesized from fly ash. J. Colloid Interface Sci. 300(2): 491–497.

Chen, X., H. Kong, D. Wu, X. Wang, and Y. Lin. 2009. Phosphate removal and recovery through crystallization of hydroxyapatite using xonotlite as seed crystal. J. Environ. Sci. 21(5): 575–580.

Chen, Y.Y., and Q.Q. Liu. 2014. On the horizontal distribution of algal-bloom in Chaohu Lake and its formation process. Acta Mech. Sin. 30(5): 656–666.

Cheng, X., X. Huang, X. Wang, B. Zhao, A. Chen, and D. Sun. 2009. Phosphate adsorption from sewage sludge filtrate using zinc-aluminum layered double hydroxides. J. Hazard. Mater. 169(1–3): 958–964.

Chitrakar, R., S. Tezuka, A. Sonoda, K. Sakane, K. Ooi, and T. Hirotsu. 2006a. Phosphate adsorption on synthetic goethite and akaganeite. J. Colloid Interface Sci. 298(2): 602–608.

Chitrakar, R., S. Tezuka, A. Sonoda, K. Sakane, K. Ooi, and T. Hirotsu. 2006b. Selective adsorption of phosphate from seawater and wastewater by amorphous zirconium hydroxide. J. Colloid Interface Sci. 297(2): 426–433.

Christensen, H.H., and A.M. Posner. 1980. the Interaction of Phosphate With an Anion

Exchange Resin. J. Soil Sci. 31(3): 447–455.

Christianson, L.E., R.D. Harmel, D. Smith, M.R. Williams, and K. King. 2016. Assessment and Synthesis of 50 Years of Published Drainage Phosphorus Losses. J. Environ. Qual. 45(5): 1467–1477.

Clark, J.M., B.A. Schaeffer, J.A. Darling, E.A. Urquhart, J.M. Johnston, A.R. Ignatius, M.H. Myer, K.A. Loftin, P.J. Werdell, and R.P. Stumpf. 2017. Satellite monitoring of cyanobacterial harmful algal bloom frequency in recreational waters and drinking water sources. Ecol. Indic. 80: 84–95.

Conley, D.J., J. Carstensen, J. Aigars, P. Axe, E. Bonsdorff, T. Eremina, B.M. Haahti, C. Humborg, P. Jonsson, J. Kotta, C. Lännegren, U. Larsson, A. Maximov, M.R. Medina, E. Lysiak-Pastuszak, N. Remeikaitè-Nikienè, J. Walve, S. Wilhelms, and L. Zillén. 2011. Hypoxia is increasing in the coastal zone of the baltic sea. Environ. Sci. Technol. 45(16): 6777–6783.

Cooper, J., and C. Carliell-Marquet. 2013. A substance flow analysis of phosphorus in the UK food production and consumption system. Resour. Conserv. Recycl. 74: 82–100.

Copetti, D., K. Finsterle, L. Marziali, F. Stefani, G. Tartari, G. Douglas, K. Reitzel, B.M. Spears, I.J. Winfield, G. Crosa, P. D'Haese, S. Yasseri, M. Lürling, and M. Lï¿½rling. 2015. Eutrophication management in surface waters using lanthanum modified bentonite: A review. Water Res. 97: 162–174.

Cordell, D., J.O. Drangert, and S. White. 2009. The story of phosphorus: Global food security and food for thought. Glob. Environ. Chang. 19(2): 292–305.

Le Corre, K.S., E. Valsami-Jones, P. Hobbs, and S.A. Parsons. 2009. Phosphorus recovery from wastewater by struvite crystallization: A review.

Correll, D.L. 1998. The Role of Phosphorus in the Eutrophication of Receiving Waters: A Review. J. Environ. Qual. 27(2): 261.

Csathó, P., I. Sisák, L. Radimszky, S. Lushaj, H. Spiegel, M.T. Nikolova, N. Nikolov, P. Čermák, J. Klir, A. Astover, A. Karklins, S. Lazauskas, J. Kopiński, C. Hera, E. Dumitru, M. Manojlovic, D. Bogdanović, S. Torma, M. Leskošek, and A. Khristenko. 2007. Agriculture as a source of phosphorus causing eutrophication in Central and Eastern Europe. Soil Use Manag. 23(SUPPL. 1): 36–56.

Cucarella, V., R. Mazurek, T. Zaleski, M. Kopeć, and G. Renman. 2009. Effect of Polonite used for phosphorus removal from wastewater on soil properties and fertility of a mountain meadow. Environ. Pollut. 157(7): 2147–2152.

Cumbal, L., and A.K. Sengupta. 2005. Arsenic removal using polymer-supported hydrated iron(III) oxide nanoparticles: Role of Donnan membrane effect. Environ. Sci. Technol. 39(17): 6508–6515.

Daniel, T.C., A.N. Sharpley, and J.L. Lemunyon. 1998. Agricultural Phosphorus and Eutrophication: A Symposium Overview. J. Environ. Qual. 27(2): 251.

Das, J., B.S. Patra, N. Baliarsingh, and K.M. Parida. 2006. Adsorption of phosphate by layered double hydroxides in aqueous solutions. Appl. Clay Sci. 32(3–4): 252–260.

Daverede, I.C., a N. Kravchenko, R.G. Hoeft, E.D. Nafziger, D.G. Bullock, J.J. Warren, and L.C. Gonzini. 2004. Phosphorus runoff from incorporated and surface-applied liquid swine manure and phosphorus fertilizer. J. Environ. Qual. 33(4): 1535–1544.

De-Bashan, L.E., and Y. Bashan. 2004. Recent advances in removing phosphorus from wastewater and its future use as fertilizer (1997-2003). Water Res. 38(19): 4222–4246.

Diaz, R.J. 2001. Overview of hypoxia around the world. J. Environ. Qual. 30(2): 275–281.

Diaz, R.J., and R. Rosenberg. 2008. Spreading Dead Zones and Consequences for Marine Ecosystems. Science 321(5891): 926–929.

Dodds, W.K. 2006. Nutrients and the “dead zone”: the link between nutrient ratios and dissolved oxygen in the northern Gulf of Mexico. Front. Ecol. Environ. 4(4): 211–217.

Dolan, D.M., and S.C. Chapra. 2012. Great Lakes total phosphorus revisited: 1. Loading analysis and update (1994-2008). J. Great Lakes Res. 38(4): 730–740.

Drenkova-Tuhtan, A., K. Mandel, A. Paulus, C. Meyer, F. Hutter, C. Gellermann, G. Sextl, M. Franzreb, and H. Steinmetz. 2013. Phosphate recovery from wastewater using engineered superparamagnetic particles modified with layered double hydroxide ion exchangers. Water Res. 47(15): 5670–5677.

Dubrovsky, N.M., K.R. Burow, G.M. Clark, J.M. Gronberg, P.A. Hamilton, K.J. Hitt, D.K. Mueller, M.G.R. M.D. Munn, B.T. Nolan, L.J. Puckett, T.M. Short, N.E.

Spahr, L.A. Sprague, and W.G. Wilber. 2010. The quality of our Nation's waters-Nutrients in the Nation's streams and groundwater, 1992-2004. US Geological Survey.

Duc, M., G. Lefevre, M. Fedoroff, J. Jeanjean, J.C. Rouchaud, F. Monteil-Rivera, J. Dumonceau, and S. Milonjic. 2003. Sorption of selenium anionic species on apatites and iron oxides from aqueous solutions. J. Environ. Radioact. 70(1–2): 61–72.

Dybowska, A., D.A.C. Manning, M.J. Collins, T. Wess, S. Woodgate, and E. Valsami-Jones. 2009. An evaluation of the reactivity of synthetic and natural apatites in the presence of aqueous metals. Sci. Total Environ. 407(8): 2953–2965.

Van Dyne, D.L., and C.B. Gilbertson. 1978. Estimating U.S. Livestock and Poultry Manure and Nutrient Production. Agric. Wastes 1(4): 259–266.

Edenborn, H.M., B.H. Howard, J.I. Sams, D.J. Vesper, and S.L. Edenborn. 2017. Passive detection of Pb in water using rock phosphate agarose beads. J. Hazard. Mater. 336: 240–248.

Edmondson, W.T. 1970. Phosphorus, nitrogen, and algae in Lake Washington after diversion of sewage. Science (80-.). 169(3946): 690–691.

Edwards, D.R., and T.C. Daniel. 1992. Runoff Quality Impacts of Swine Manure Applied to Fescue Plots. Trans. ASAE 35(6): 1827–1832.

Egle, L., H. Rechberger, J. Krampe, and M. Zessner. 2016. Phosphorus recovery from municipal wastewater: An integrated comparative technological, environmental and economic assessment of P recovery technologies. Sci. Total Environ. 571: 522–542.

Ejhieh, A.N., and N. Masoudipour. 2010. Application of a new potentiometric method for determination of phosphate based on a surfactant-modified zeolite carbon-paste electrode (SMZ-CPE). Anal. Chim. Acta 658(1): 68–74.

Eljamal, O., A.M.E. Khalil, Y. Sugihara, and N. Matsunaga. 2016. Phosphorus removal from aqueous solution by nanoscale zero valent iron in the presence of copper chloride. Chem. Eng. J. 293: 225–231.

Elzinga, E.J., and D.L. Sparks. 2007. Phosphate adsorption onto hematite: An in situ ATR-FTIR investigation of the effects of pH and loading level on the mode of phosphate surface complexation. J. Colloid Interface Sci. 308(1): 53–70.

Van Esbroeck, C.J., M.L. Macrae, R.I. Brunke, and K. McKague. 2016. Annual and seasonal phosphorus export in surface runoff and tile drainage from agricultural fields with cold temperate climates. J. Great Lakes Res. 42(6): 1271–1280.

Fernane, F., M.O. Mecherri, P. Sharrock, M. Hadioui, H. Lounici, and M. Fedoroff. 2008. Sorption of cadmium and copper ions on natural and synthetic hydroxylapatite particles. Mater. Charact. 59(5): 554–559.

Filippelli, G.M. 2008. The Global Phosphorus Cycle: Past, Present, and Future. Elements 4(2).

Fixen, P., Brentrup, F., Bruulsema, T., Garcia, F., Norton, R., Zingore, S. 2015. Nutrient/fertilizer use efficiency: measurement, current situation and trends, in: Drechsel, P. et al. (Eds.) Managing water and fertilizer for sustainable agricultural intensification. International Fertilizer Industry Association (IFA), International Water Management Institute (IWMI), International Plant Nutrition Institute (IPNI), and International Potash Institute (IPI). First edition, Paris, France, pp. 8-38.

Fu, F., D.D. Dionysiou, and H. Liu. 2014. The use of zero-valent iron for groundwater remediation and wastewater treatment: A review. J. Hazard. Mater. 267: 194–205.

Funes, A., F.J. Martínez, I. Álvarez-Manzaneda, J.M. Conde-Porcuna, J. de Vicente, F. Guerrero, and I. de Vicente. 2018. Determining major factors controlling phosphorus removal by promising adsorbents used for lake restoration: A linear mixed model approach. Water Res. 141: 377–386.

Gao, Q., Y. Li, Q. Cheng, M. Yu, B. Hu, Z. Wang, and Z. Yu. 2016. Analysis and assessment of the nutrients, biochemical indexes and heavy metals in the Three Gorges Reservoir, China, from 2008 to 2013. Water Res. 92: 262–274.

Gao, Y., and A. Mucci. 2003. Individual and competitive adsorption of phosphate and arsenate on goethite in artificial seawater. Chem. Geol. 199(1–2): 91–109.

Gascho, G.J., R.D. Wauchope, J.G. Davis, C.C. Truman, C.C. Dowler, J.E. Hook, H.R. Sumner, and A.W. Johnson. 1998. Nitrate-nitrogen, soluble, and bioavailable phosphorus runoff from simulated rainfall after fertilizer application. Soil Sci. Soc. Am. J. 62(6): 1711–1718.

Gaynor, J.D., and W.I. Findlay. 1995. Soil and Phosphorus Loss from Conservation and Conventional Tillage in Corn Production. J. Environ. Qual. 24(4): 734.

Gellings, C., and K. Parmenter. 2004. Energy efficiency in fertilizer production and use. Effic. use Conserv. energy. Encycl. Life Support Syst.: 1–15.

Gentry, L.E., M.B. David, T. V. Royer, C.A. Mitchell, and K.M. Starks. 2007. Phosphorus Transport Pathways to Streams in Tile-Drained Agricultural Watersheds. J. Environ. Qual. 36: 408–415.

Giasuddin, A.B.M., S.R. Kanel, and H. Choi. 2007. Adsorption of humic acid onto nanoscale zerovalent iron and its effect on arsenic removal. Environ. Sci. Technol. 41(6): 2022–2027.

Goh, K.H., T.T. Lim, and Z. Dong. 2008. Application of layered double hydroxides for removal of oxyanions: A review. Water Res. 42(6–7): 1343–1368.

Gong, X., K. Li, C. Wu, L. Wang, and H. Sun. 2018. Passive sampling for monitoring polar organic pollutants in water by three typical samplers. Trends Environ. Anal. Chem. 17(January): 23–33.

Grattan, L.M., D. Oldach, T.M. Perl, M.H. Lowitt, D.L. Matuszak, C. Dickson, C. Parrott, R.C. Shoemaker, C.L. Kauffman, M.P. Wasserman, J.R. Hebel, P. Charache, and J.G. Morris. 1998. Learning and memory difficulties after environmental exposure to waterways containing toxin-producing Pfiesteria or Pfiesteria-like dinoflagellates. Lancet 352(9127): 532–539.

Gunold, R., R.B. Schäfer, A. Paschke, G. Schüürmann, and M. Liess. 2008. Calibration of the Chemcatcher®passive sampler for monitoring selected polar and semi-polar pesticides in surface water. Environ. Pollut. 155(1): 52–60.

Das Gupta, M., P. Loganathan, and S. Vigneswaran. 2012. Adsorptive Removal of Nitrate and Phosphate from Water by a Purolite Ion Exchange Resin and Hydrous Ferric Oxide Columns in Series. Sep. Sci. Technol. 47(12): 1785–1792.

Gustafsson, J.P., A. Renman, G. Renman, and K. Poll. 2008. Phosphate removal by mineral-based sorbents used in filters for small-scale wastewater treatment. Water Res. 42(1–2): 189–197.

Haerifar, M., and S. Azizian. 2013. Mixed surface reaction and diffusion-controlled kinetic model for adsorption at the solid/solution interface. J. Phys. Chem. C 117(16): 8310–8317.

Haghseresht, F., S. Wang, and D.D. Do. 2009. A novel lanthanum-modified bentonite,

Phoslock, for phosphate removal from wastewaters. Appl. Clay Sci. 46(4): 369–375.

Hale, R.L., N.B. Grimm, C.J. Vörösmarty, and B. Fekete. 2015. Nitrogen and phosphorus fluxes from watersheds of the northeast U.S. from 1930 to 2000: Role of anthropogenic nutrient inputs, infrastructure, and runoff. Global Biogeochem. Cycles 29: 341–356.

Hang-Sik, S., K. Mi-Joo, N. Se-Yong, and M. Hi-Chung. 1996. Phosphorus removal by hydrotalcite-like compounds (HTLcs). Water Sci. Technol. 34(1–2): 161–168.

He, H., H. Kang, S. Ma, Y. Bai, and X. Yang. 2010. High adsorption selectivity of ZnAl layered double hydroxides and the calcined materials toward phosphate. J. Colloid Interface Sci. 343(1): 225–231.

Heathwaite, L., P. Haygarth, R. Matthews, N. Preedy, and P. Butler. 2005. Evaluating Colloidal Phosphorus Delivery to Surface Waters from Diffuse Agricultural Sources. J. Environ. Qual. 31(4): 287–298.

Heffer, P. 2013. Assessment of Fertilizer Use by Crop at the Global Level. Paris.

Ho, Y.S., and G. McKay. 1999. The sorption of lead(II) ions on peat. Water Res. 33(2): 578–584.

Ho, Y.S., and G. McKay. 2000. The kinetics of sorption of divalent metal ions onto sphagnum moss peat. Water Res. 34(3): 735–742.

Huang, X. 2004. Intersection of isotherms for phosphate adsorption on hematite. J. Colloid Interface Sci. 271(2): 296–307.

Huang, W., J. Chen, F. He, J. Tang, D. Li, Y. Zhu, and Y. Zhang. 2015a. Effective phosphate adsorption by Zr/Al-pillared montmorillonite: Insight into equilibrium, kinetics and thermodynamics. Appl. Clay Sci. 104: 252–260.

Huang, J., C. chun Xu, B.G. Ridoutt, X. chun Wang, and P. an Ren. 2017a. Nitrogen and phosphorus losses and eutrophication potential associated with fertilizer application to cropland in China. J. Clean. Prod. 159: 171–179.

Huang, W., X. Yu, J. Tang, Y. Zhu, Y. Zhang, and D. Li. 2015b. Enhanced adsorption of phosphate by flower-like mesoporous silica spheres loaded with lanthanum. Microporous Mesoporous Mater. 217: 225–232.

Huang, W., Y. Zhang, and D. Li. 2017b. Adsorptive removal of phosphate from water

using mesoporous materials: A review. J. Environ. Manage. 193: 470–482.

Huang, W.Y., R.H. Zhu, F. He, D. Li, Y. Zhu, and Y.M. Zhang. 2013. Enhanced phosphate removal from aqueous solution by ferric-modified laterites: Equilibrium, kinetics and thermodynamic studies. Chem. Eng. J. 228: 679–687.

Ioannou, A., A. Dimirkou, and P. Papadopoulos. 1998. Phosphate sorption by goethite and kaolinite-goethite system as described by isotherms. Commun. Soil Sci. Plant Anal. 29: 2175–2190.

Izuno, F.T., C.A. Sanchez, F.J. Coale, A.B. Bottcher, and D.B. Jones. 1991. Phosphorus Concentrations in Drainage Water in the Everglades Agricultural Area. J. Environ. Qual. 20(3): 608.

Jayawardane, B.M., I.D. McKelvie, and S.D. Kolev. 2012. A paper-based device for measurement of reactive phosphate in water. Talanta 100: 454–460.

Jeong, J.-Y., B.-M. Ahn, Y.-J. Kim, and J.-Y. Park. 2014. Continuous phosphorus removal from water by physicochemical method using zero valent iron packed column. Water Sci. Technol. 70(5): 895.

Jiang, C., L. Jia, Y. He, B. Zhang, G. Kirumba, and J. Xie. 2013. Adsorptive removal of phosphorus from aqueous solution using sponge iron and zeolite. J. Colloid Interface Sci. 402: 246–252.

Johir, M.A.H., J. George, S. Vigneswaran, J. Kandasamy, and A. Grasmick. 2011. Removal and recovery of nutrients by ion exchange from high rate membrane bio-reactor (MBR) effluent. Desalination 275(1–3): 197–202.

Johir, M.A.H., T.T. Nguyen, K. Mahatheva, M. Pradhan, H.H. Ngo, W. Guo, and S. Vigneswaran. 2016a. Removal of phosphorus by a high rate membrane adsorption hybrid system. Bioresour. Technol. 201: 365–369.

Johir, M.A.H., M. Pradhan, P. Loganathan, J. Kandasamy, and S. Vigneswaran. 2016b. Phosphate adsorption from wastewater using zirconium (IV) hydroxide: Kinetics, thermodynamics and membrane filtration adsorption hybrid system studies. J. Environ. Manage. 167(3): 167–174.

De Jonge, H., and G. Rothenberg. 2005. New device and method for flux-proportional sampling of mobile solutes in soil and groundwater. Environ. Sci. Technol. 39(1): 274–282.

Jørgensen, B.B., and K. Richardson. 1996. Eutrophication in Coastal Marine Ecosystems. Coast. Estuar. Stud. 52: 273.

Joyce, S. 2000. The dead zones: oxygen-starved coastal waters. Environ. Health Perspect. 108(3).

Jóźwiakowski, K., M. Gajewska, A. Pytka, M. Marzec, M. Gizińska-Górna, A. Jucherski, A. Walczowski, M. Nastawny, A. Kamińska, and S. Baran. 2017. Influence of the particle size of carbonate-siliceous rock on the efficiency of phosphorous removal from domestic wastewater. Ecol. Eng. 98: 290–296.

Kaneko, S., and K. Nakajima. 1988. Phosphorus Removal by Crystallization Using a Granular Activated Magnesia Clinker. Source J. (Water Pollut. Control Fed. 60(7): 1239–1244.

Karaca, S., A. Gürses, M. Ejder, and M. Açikyildiz. 2004. Kinetic modeling of liquid-phase adsorption of phosphate on dolomite. J. Colloid Interface Sci. 277(2): 257–263.

Karageorgiou, K., M. Paschalis, and G.N. Anastassakis. 2007. Removal of phosphate species from solution by adsorption onto calcite used as natural adsorbent. J. Hazard. Mater. 139(3): 447–452.

Karapinar, N. 2009. Application of natural zeolite for phosphorus and ammonium removal from aqueous solutions. J. Hazard. Mater. 170(2–3): 1186–1191.

Khalil, A.M.E., O. Eljamal, T.W.M. Amen, Y. Sugihara, and N. Matsunaga. 2017. Optimized nano-scale zero-valent iron supported on treated activated carbon for enhanced nitrate and phosphate removal from water. Chem. Eng. J. 309: 349–365.

Khitous, M., Z. Salem, and D. Halliche. 2015. Removal of phosphate from industrial wastewater using uncalcined MgAl-NO3 layered double hydroxide: batch study and modeling. Desalin. Water Treat. 3994(3): Ahead of Print.

Kim, Y.J., and Y.J. Lee. 2014. Characterization of mercury sorption on hydroxylapatite: Batch studies and microscopic evidence for adsorption. J. Colloid Interface Sci. 430: 193–199.

King, K., M. Williams, and N. Fausey. 2015a. Contributions of Systematic Tile Drainage to Watershed-Scale Phosphorus Transport. J. Environ. Qual. 44(2): 486–494.

King, K.W., M.R. Williams, M.L. Macrae, N.R. Fausey, J. Frankenberger, D.R. Smith,

P.J.A. Kleinman, L.C. Brown, N.R. Fausey, L.C. Brown, P.J.A. Kleinman, and L.C. Brown. 2015b. Phosphorus Transport in Agricultural Subsurface Drainage: A Review. J. Environ. Qual. 44(2): 467.

Kingston, J.K., R. Greenwood, G.A. Mills, G.M. Morrison, and L.B. Persson. 2000. Development of a novel passive sampling system for the time-averaged measurement of a range of organic pollutants in aquatic environments. J. Environ. Monit. 2(5): 487–495.

Kleinman, P.J. a, and A.N. Sharpley. 2003. Effect of Broadcast Manure on Runoff Phosphorus Concentrations over Successive Rainfall Events. J. Environ. Qual. 32(3): 1072–1081.

Kleinman, P.J.A.A., A.N. Sharpley, R.W. McDowell, D.N. Flaten, A.R. Buda, L. Tao, L. Bergstrom, Q. Zhu, A.R. Buda, L. Tao, L. Bergstrom, and Q. Zhu. 2011. Managing agricultural phosphorus for water quality protection: Principles for progress. Plant Soil 349(1–2): 169–182.

Kleinman, P.J. a, A.N. Sharpley, B.G. Moyer, and G.F. Elwinger. 2002. Effect of mineral and manure phosphorus sources on runoff phosphorus. J. Environ. Qual. 31(6): 2026–2033.

Kleinman, P.J.A., D.R. Smith, C.H. Bolster, and Z.M. Easton. 2015. Phosphorus Fate, Management, and Modeling in Artificially Drained Systems. J. Environ. Qual. 44(2): 460–466.

Knutsson, J., S. Rauch, and G.M. Morrison. 2013. Performance of a passive sampler for the determination of time averaged concentrations of nitrate and phosphate in water. Environ. Sci. Process. Impacts 15(5): 955–962.

Kunin, R., and R.J. Myers. 1947. The anion exchange equilibria in an anion exchange resin. J. Am. Chem. Soc. 69(11): 2874–8.

Kuo, Y.M., W.G. Harris, R. Muñoz-Carpena, R.D. Rhue, and Y. Li. 2009. Apatite control of phosphorus release to runoff from soils of phosphate mine reclamation areas. Water. Air. Soil Pollut. 202(1–4): 189–198.

Kuzawa, K., Y.J. Jung, Y. Kiso, T. Yamada, M. Nagai, and T.G. Lee. 2006. Phosphate removal and recovery with a synthetic hydrotalcite as an adsorbent. Chemosphere 62(1): 45–52.

Lagerwerff, J. 1971. Uptake of cadmium, lead and zinc by radish from soil and air. Soil Sci. 111(2): 129–133.

Lakshminarayana, J.S., H.J. O'Neill, S.D. Jonnavithula, D.A. Léger, and P.H. Milburn. 1992. Impact of atrazine-bearing agricultural tile drainage discharge on planktonic drift of a natural stream. Environ. Pollut. 76(3): 201–210.

Lalley, J., C. Han, X. Li, D.D. Dionysiou, and M.N. Nadagouda. 2016. Phosphate adsorption using modified iron oxide-based sorbents in lake water: Kinetics, equilibrium, and column tests. Chem. Eng. J. 284: 1386–1396.

Laubel, A.L., O.H. Jacobsen, B. Kronvang, A. Grant, and H.E. Anderson. 1999. Subsurface drainage loss of particulate phosphorus from field plot experiments and a tile drained catchment. J. Environ. Qual. 28: 576–584.

Lawton, L.A., and G.A. Codd. 1991. Cyanobacterial (Blue-Green Algal) Toxins and their Significance in UK and European Waters. Water Environ. J. 5(4): 460–465.

Lee, J., P.K. Rai, Y.J. Jeon, K.-H. Kim, and E.E. Kwon. 2017. The role of algae and cyanobacteria in the production and release of odorants in water. Environ. Pollut. 227: 252–262.

Lehr, J.R. 1980. Phosphate raw materials and fertilizers: Part I - A look ahead.

Lenell, B.A., and Y. Arai. 2017. Perrhenate sorption kinetics in zerovalent iron in high pH and nitrate media. J. Hazard. Mater. 321: 335–343.

Li, X., D.W. Elliott, and W. Zhang. 2006. Zero-Valent Iron Nanoparticles for Abatement of Environmental Pollutants: Materials and Engineering Aspects. Crit. Rev. Solid State Mater. Sci. 31(4): 111–122.

Li, G., S. Gao, G. Zhang, and X. Zhang. 2014. Enhanced adsorption of phosphate from aqueous solution by nanostructured iron(III)-copper(II) binary oxides. Chem. Eng. J. 235: 124–131.

Li, G., M.K. van Ittersum, P.A. Leffelaar, S.Z. Sattari, H. Li, G. Huang, and F. Zhang. 2016. A multi-level analysis of China's phosphorus flows to identify options for improved management in agriculture. Agric. Syst. 144: 87–100.

Li, W., L. Wang, F. Liu, X. Liang, X. Feng, W. Tan, L. Zheng, and H. Yin. 2015. Effects of Al3 +doping on the structure and properties of goethite and its adsorption behavior towards phosphate. J. Environ. Sci. (China) 45: 18–27.

Lin, J., Y. Zhan, H. Wang, M. Chu, C. Wang, Y. He, and X. Wang. 2017. Effect of calcium ion on phosphate adsorption onto hydrous zirconium oxide. Chem. Eng. J. 309: 118–129.

Lisk, D.J. 1972. Trace Metals in Soils, Plants, and Animals. Adv. Agron. 24(C): 267–325.

Litke, D.W. 1999. Review of Phosphorus Control Measures in the United States and Their Effects on Water Quality. Water-Resources Investig. Rep. 99-4007: 1–38.

Liu, H., T. Chen, X. Zou, Q. Xie, C. Qing, D. Chen, and R.L. Frost. 2013. Removal of phosphorus using NZVI derived from reducing natural goethite. Chem. Eng. J. 234: 80–87.

Liu, H., X. Sun, C. Yin, and C. Hu. 2008a. Removal of phosphate by mesoporous ZrO2. J. Hazard. Mater. 151(2–3): 616–622.

Liu, Y., G. Villalba, R.U. Ayres, and H. Schroder. 2008b. Global Phosphorus Flows and Environmental Impacts from a Consumption Perspective. J. Ind. Ecol. 12(2): 229–247.

Liu, C., Q. Wang, F. Huang, and J. Zhang. 2016. Removal of phosphorus from anaerobic membrane bioreactor effluent by ion exchange resin. Sep. Sci. Technol. 51(17): 2833–2843.

Loganathan, P., S. Vigneswaran, J. Kandasamy, and N.S. Bolan. 2014. Removal and recovery of phosphate from water using sorption. Crit. Rev. Environ. Sci. Technol. 44(8): 847–907.

Long, F., J.L. Gong, G.M. Zeng, L. Chen, X.Y. Wang, J.H. Deng, Q.Y. Niu, H.Y. Zhang, and X.R. Zhang. 2011. Removal of phosphate from aqueous solution by magnetic Fe-Zr binary oxide. Chem. Eng. J. 171(2): 448–455.

Low, M.J.D. 1960. Kinetics of chemisorption of gases on solids. Chem. Rev. 60(3): 267–312.

Lǔ, J., H. Liu, R. Liu, X. Zhao, L. Sun, and J. Qu. 2013. Adsorptive removal of phosphate by a nanostructured Fe-Al-Mn trimetal oxide adsorbent. Powder Technol. 233: 146–154.

Luengo, C., M. Brigante, J. Antelo, and M. Avena. 2006. Kinetics of phosphate adsorption on goethite: Comparing batch adsorption and ATR-IR measurements. J.

Colloid Interface Sci. 300(2): 511–518.

Luengo, C. V., M.A. Volpe, and M.J. Avena. 2017. High sorption of phosphate on Mg-Al layered double hydroxides: Kinetics and equilibrium. J. Environ. Chem. Eng. 5(5): 4656–4662.

Madrid, L., and P. de Arambarri. 1985. Adsorption of phosphate by two iron oxides in relation to their porosity. J. Soil Sci. 36(4): 523–530.

Madrid, L., and A.M. Posner. 1979. Desorption of phosphate from goethite. Eur. J. Soil Sci. 30(4): 697–707.

Maguire, R.O., P.J.A. Kleinman, C.J. Dell, D.B. Beegle, R.C. Brandt, J.M. McGrath, and Q.M. Ketterings. 2011. Manure Application Technology in Reduced Tillage and Forage Systems: A Review. J. Environ. Qual. 40(2): 292.

Mahardika, D., H.-S. Park, and K.-H. Choo. 2018. Ferrihydrite-impregnated granular activated carbon (FH@GAC) for efficient phosphorus removal from wastewater secondary effluent. Chemosphere 207: 527–533.

Mallet, M., K. Barthélémy, C. Ruby, A. Renard, and S. Naille. 2013. Investigation of phosphate adsorption onto ferrihydrite by X-ray Photoelectron Spectroscopy. J. Colloid Interface Sci. 407: 95–101.

Mangwandi, C., A.B. Albadarin, Y. Glocheux, and G.M. Walker. 2014. Removal of ortho-phosphate from aqueous solution by adsorption onto dolomite. J. Environ. Chem. Eng. 2(2): 1123–1130.

McGrath, D.A., N.B. Comerford, and M.L. Duryea. 2000. Litter dynamics and monthly fluctuations in soil phosphorus availability in an Amazonian agroforest. For. Ecol. Manage. 131(1–3): 167–181.

McLaughlin, J.R., J.C. Ryden, and J.K. Syers. 1981. Sorption of Inorganic Phosphate By Iron- and Aluminium- Containing Components. J. Soil Sci. 32(3): 365–378.

Meisinger, J., and W. Jokela. 2000. Ammonia volatilization from dairy and poultry manure. Manag. Nutr. Pathog. from Anim. Agric. (January 2000): 1–21.

Menzel, R.G. 1968. Uranium, Radium, and Thorium Content in Phosphate Rocks and Their Possible Radiation Hazard. J. Agric. Food Chem. 16(2): 231–234.

Michalak, A.M., E.J. Anderson, D. Beletsky, S. Boland, N.S. Bosch, T.B. Bridgeman, J.D. Chaffin, K. Cho, R. Confesor, I. Daloglu, J. V. DePinto, M.A. Evans, G.L.

Fahnenstiel, L. He, J.C. Ho, L. Jenkins, T.H. Johengen, K.C. Kuo, E. LaPorte, X. Liu, M.R. McWilliams, M.R. Moore, D.J. Posselt, R.P. Richards, D. Scavia, A.L. Steiner, E. Verhamme, D.M. Wright, and M.A. Zagorski. 2013. Record-setting algal bloom in Lake Erie caused by agricultural and meteorological trends consistent with expected future conditions. Proc. Natl. Acad. Sci. 110(16): 6448–6452.

Molle, P., A. Liénard, A. Grasmick, A. Iwema, and A. Kabbabi. 2005. Apatite as an interesting seed to remove phosphorus from wastewater in constructed wetlands. Water Sci. Technol. 51(9): 193–203.

Moriyama, K., T. Kojima, Y. Minawa, S. Matsumoto, and K. Nakamachi. 2001. Development of artificial seed crystal for crystallization of calcium phosphate. Environ. Technol. (United Kingdom) 22(11): 1245–1252.

Mortvedt, J.J. 1987. Cadmium Levels in Soils and Plants From Some Long-term Soil Fertility Experiments in the United States of America1. J. Environ. Qual. 16(2): 137.

Müller, B., A. Stöckli, R. Stierli, E. Butscher, and R. Gächter. 2007. A low cost method to estimate dissolved reactive phosphorus loads of rivers and streams. J. Environ. Monit. 9(1): 82–86.

Murphy, J., and J.P. Riley. 1962. A modified single solution method for the determination of phosphate in natural waters. Anal. Chim. Acta 27: 31–36.

Nixon, S.W., J.W. Ammerman, L.P. Atkinson, V.M. Berounsky, G. Billen, W.C. Boicourt, W.R. Boynton, T.M. Church, D.M. Ditoro, R. Elmgren, J.H. Garber, a E. Giblin, R. a Jahnke, N.J.P. Owens, M.E.Q. Pilson, and S.P. Seitzinger. 1996. The fate of nitrogen and phosphorus at the land sea margin of the North Atlantic Ocean. Biogeochemistry 35(1): 141–180.

NOAA, N.O. and A.A. 2017. Gulf of Mexico “dead zone” is the largest ever measured.

Novillo, C., D. Guaya, A. Allen-Perkins Avendaño, C. Armijos, J.L. Cortina, and I. Cota. 2014. Evaluation of phosphate removal capacity of Mg/Al layered double hydroxides from aqueous solutions. Fuel 138: 72–79.

Nur, T., M.A.H. Johir, P. Loganathan, T. Nguyen, S. Vigneswaran, and J. Kandasamy. 2014. Phosphate removal from water using an iron oxide impregnated strong base

anion exchange resin. J. Ind. Eng. Chem. 20(4): 1301–1307.

O'Brien, D.S., K. Booij, D.W. Hawker, and J.F. Mueller. 2011. Method for the in situ calibration of a passive phosphate sampler in estuarine and marine waters. Environ. Sci. Technol. 45(7): 2871–2877.

O'Brien, D.S., B. Chiswell, and J.F. Mueller. 2009. A novel method for the in situ calibration of flow effects on a phosphate passive sampler. J. Environ. Monit. 11(1): 212–219.

O'Neal, J.A., and T.H. Boyer. 2013. Phosphate recovery using hybrid anion exchange: Applications to source-separated urine and combined wastewater streams. Water Res. 47(14): 5003–5017.

Ödemiş, B., S. Bozkurt, N. Ağca, and M. Yalçin. 2006. Quality of shallow groundwater and drainage water in irrigated agricultural lands in a mediterranean coastal region of Turkey. Environ. Monit. Assess. 115(1–3): 361–379.

Onyango, M.S., D. Kuchar, M. Kubota, and H. Matsuda. 2007. Adsorptive removal of phosphate ions from aqueous solution using synthetic zeolite. Ind. Eng. Chem. Res. 46(3): 894–900.

Ookubo, A., K. Ooi, and H. Hayashi. 1993. Preparation and Phosphate Ion-Exchange Properties of a Hydrotalcite-like Compound. Langmuir 9(5): 1418–1422.

Ouyang, W., F. Hao, X. Wei, and H. Huang. 2013. Spatial and temporal trend of Chinese manure nutrient pollution and assimilation capacity of cropland and grassland. Environ. Sci. Pollut. Res. 20(7): 5036–5046.

Özacar, M. 2003. Equilibrium and kinetic modelling of adsorption of phosphorus on calcined alunite. Adsorption 9(2): 125–132.

Paerl, H.W., H. Xu, M.J. McCarthy, G. Zhu, B. Qin, Y. Li, and W.S. Gardner. 2011. Controlling harmful cyanobacterial blooms in a hyper-eutrophic lake (Lake Taihu, China): The need for a dual nutrient (N & P) management strategy. Water Res. 45(5): 1973–1983.

Pan, B., J. Wu, B. Pan, L. Lv, W. Zhang, L. Xiao, X. Wang, X. Tao, and S. Zheng. 2009. Development of polymer-based nanosized hydrated ferric oxides (HFOs) for enhanced phosphate removal from waste effluents. Water Res. 43(17): 4421–4429.

Parfitt, R.L. 1989. Phosphate reactions with natural allophane, ferrihydrite and goethite.

J. Soil Sci. 40(2): 359–369.

Parfitt, R.L., and R.J. Atkinson. 1976. Phosphate adsorption on goethite (a-FeOOOH). Nature 264: 740–742.

Parfitt, R.L., R.J. Atkinson, and R.S.C. Smart. 1975. The Mechanism of Phosphate Fixation by Iron Oxides1. Soil Sci. Soc. Am. J. 39(5): 837.

Parry, R. 1998. Agricultural Phosphorus and Water Quality: A U.S. Environmental Protection Agency Perspective. J. Environ. Qual. 27(2): 258.

Parsons, S.A., and J.A. Smith. 2008. Phosphorus Removal and Recovery from Municipal Wastewater. Elements 4(2): 109–112.

Peleka, E.N., and E.A. Deliyanni. 2009. Adsorptive removal of phosphates from aqueous solutions. Desalination 245(1–3): 357–371.

Pitois, S., M.H. Jackson, and B.J. Wood. 2001. Sources of the eutrophication problems associated with toxic algae: an overview. J. Environ. Health 64(5): 25–32.

Potter, P., N. Ramankutty, E.M. Bennett, and S.D. Donner. 2010. Characterizing the spatial patterns of global fertilizer application and manure production. Earth Interact. 14(2).

Powers, S.M., T.W. Bruulsema, T.P. Burt, N.I. Chan, J.J. Elser, P.M. Haygarth, N.J.K. Howden, H.P. Jarvie, Y. Lyu, H.M. Peterson, A.N. Sharpley, J. Shen, F. Worrall, and F. Zhang. 2016. Long-term accumulation and transport of anthropogenic phosphorus in three river basins. Nat. Geosci. 9(5): 353–356.

Predotova, M., W.A. Bischoff, and A. Buerkert. 2011. Mineral-nitrogen and phosphorus leaching from vegetable gardens in Niamey, Niger. J. Plant Nutr. Soil Sci. 174(1): 47–55.

Qin, B., G. Zhu, G. Gao, Y. Zhang, W. Li, H.W. Paerl, and W.W. Carmichael. 2010. A drinking water crisis in Lake Taihu, China: Linkage to climatic variability and lake management. Environ. Manage. 45(1): 105–112.

Rabalais, N.N., R.J. Díaz, L.A. Levin, R.E. Turner, D. Gilbert, and J. Zhang. 2010. Dynamics and distribution of natural and human-caused hypoxia. Biogeosciences 7(2): 585–619.

Rabotyagov, S.S., T.D. Campbell, M. White, J.G. Arnold, J. Atwood, M.L. Norfleet, C.L. Kling, P.W. Gassman, A. Valcu, J. Richardson, R.E. Turner, and N.N. Rabalais.

2014. Cost-effective targeting of conservation investments to reduce the northern Gulf of Mexico hypoxic zone. Proc. Natl. Acad. Sci. 111(52): 18530–18535.

Rashidi Nodeh, H., H. Sereshti, E. Zamiri Afsharian, and N. Nouri. 2017. Enhanced removal of phosphate and nitrate ions from aqueous media using nanosized lanthanum hydrous doped on magnetic graphene nanocomposite. J. Environ. Manage. 197: 265–274.

Raveendran, E., and I.M. Madany. 1991. Characteristics of agricultural drainage water in Bahrain. Sci. Total Environ. 104(3): 239–247.

Redfield, A.C. 1958. The Biological Control of Chemical Factors in the Environment. Am. Sci. 46(3): 205–221.

Regelink, I.C., G.F. Koopmans, C. van der Salm, L. Weng, and W.H. van Riemsdijk. 2013. Characterization of Colloidal Phosphorus Species in Drainage Waters from a Clay Soil Using Asymmetric Flow Field-Flow Fractionation. J. Environ. Qual. 42(2): 464.

Renman, A., and G. Renman. 2010. Long-term phosphate removal by the calcium-silicate material Polonite in wastewater filtration systems. Chemosphere 79(6): 659–664.

Richards, M.B., R.M. Cowling, and W.D. Stock. 1997. Soil nutrient dynamics and community boundaries in the Fynbos vegetation of South Africa. Plant Ecol. 130(2): 143–153.

Roll, I.B., and R.U. Halden. 2016. Critical review of factors governing data quality of integrative samplers employed in environmental water monitoring. Water Res. 94: 200–207.

Royer, T. V., J.L. Tank, and M.B. David. 2004. Transport and Fate of Nitrate in Headwater Agricultural Streams in Illinois. J. Environ. Qual. 33(4): 1296.

Rozemeijer, J., Y. van der Velde, H. de Jonge, F. van Geer, H.P. Broers, and M. Bierkens. 2010. Application and Evaluation of a New Passive Sampler for Measuring Average Solute Concentrations in a Catchment Scale Water Quality Monitoring Study. Environ. Sci. Technol. 44(4): 1353–1359.

Ryther, J.H., and W.M. Dunstan. 1971. Nitrogen , Phosphorus , and Eutrophication in the Coastal Marine Environment. Science (80-.). 171(3975): 1008–1013.

Sattari, S.Z., M.K. van Ittersum, K.E. Giller, F. Zhang, and A.F. Bouwman. 2014. Key

role of China and its agriculture in global sustainable phosphorus management. Environ. Res. Lett. 9(5): 054003.

Schäfer, R.B., A. Paschke, B. Vrana, R. Mueller, and M. Liess. 2008. Performance of the Chemcatcher® passive sampler when used to monitor 10 polar and semi-polar pesticides in 16 Central European streams, and comparison with two other sampling methods. Water Res. 42(10–11): 2707–2717.

Schindler, D.W. 1974. Eutrophication and recovery in experimental lakes: implications for lake management. Science (80-.). 184(4139): 897–899.

Seida, Y., and Y. Nakano. 2002. Removal of phosphate by layered double hydroxides containing iron. Water Res. 36(5): 1306–1312.

Sendrowski, A., and T.H. Boyer. 2013. Phosphate removal from urine using hybrid anion exchange resin. Desalination 322: 104–112.

Sengupta, S., and A. Pandit. 2011. Selective removal of phosphorus from wastewater combined with its recovery as a solid-phase fertilizer. Water Res. 45(11): 3318–3330.

Sharpley, A.N., S.C. Chapra, R. Wedepohl, J.T. Sims, T.C. Daniel, and K.R. Reddy. 1994. Managing Agricultural Phosphorus for Protection of Surface Waters: Issues and Options. J. Environ. Qual. 23: 437–451.

Sharpley, A.N., and R.G. Menzel. 1987. The Impact of Soil and Fertilizer Phosphorus on the Environment. Adv. Agron. 41: 297–324.

Sharpley, A., T.C. Daniel, J.T. Sims, and D.H. Pote. 1996. Determining environmentally sound soil phosphorus levels. J. Soil Water Conserv. 51(2): 160–166.

Shi, J., X. Yu, M. Zhang, S. Lu, W. Wu, J. Wu, and J. Xu. 2011. Potential Risks of Copper, Zinc, and Cadmium Pollution due to Pig Manure Application in a Soil–Rice System under Intensive Farming: A Case Study of Nanhu, China. J. Environ. Qual. 40(6): 1695.

Shin, E.W., J.S. Han, M. Jang, S.H. Min, J.K. Park, and R.M. Rowell. 2004. Phosphate Adsorption on Aluminum-Impregnated Mesoporous Silicates: Surface Structure and Behavior of Adsorbents. Environ. Sci. Technol. 38(3): 912–917.

Sims, J.T., R.R. Simard, and B.C. Joern. 1998. Phosphorus Loss in Agricultural Drainage: Historical Perspective and Current Research. J. Environ. Qual. 27(2):

277.

Sleiman, N., V. Deluchat, M. Wazne, M. Mallet, A. Courtin-Nomade, V. Kazpard, and M. Baudu. 2016. Phosphate removal from aqueous solution using ZVI/sand bed reactor: Behavior and mechanism. Water Res. 99: 56–65.

Sleiman, N., V. Deluchat, M. Wazne, M. Mallet, A. Courtin-Nomade, V. Kazpard, and M. Baudu. 2017. Phosphate removal from aqueous solutions using zero valent iron (ZVI): Influence of solution composition and ZVI aging. Colloids Surfaces A Physicochem. Eng. Asp. 514: 1–10.

Smil, V. 2000. Phosphorus in the environment: natural flows and human interferences. Annu. Rev. energy Environ. 25(1): 53–88.

Smith, D.R., K.W. King, L. Johnson, W. Francesconi, P. Richards, D. Baker, and A.N. Sharpley. 2015. Surface Runoff and Tile Drainage Transport of Phosphorus in the Midwestern United States. J. Environ. Qual. 44(2): 495.

Song, Y.H., D. Donnert, U. Berg, P.G. Weidler, and R. Nueesch. 2007. Seed selections for crystallization of calcium phosphate for phosphorus recovery. J. Environ. Sci. 19(5): 591–595.

Sowmya, A., and S. Meenakshi. 2014. A novel quaternized chitosan-melamine-glutaraldehyde resin for the removal of nitrate and phosphate anions. Int. J. Biol. Macromol. 64: 224–232.

Starling, F., X. Lazzaro, C. Cavalcanti, and R. Moreira. 2002. Contribution of omnivorous tilapia to eutrophication of a shallow tropical reservoir: evidence from a fish kill. Freshw. Biol. 47(12): 2443–2452.

Strauss, R., G.W. Brümmer, and N.J. Barrow. 1997. Effects of crystallinity of goethite: II. Rates of sorption and desorption of phosphate. Eur. J. Soil Sci. 48(1): 101–114.

Su, Y., H. Cui, Q. Li, S. Gao, and J.K. Shang. 2013. Strong adsorption of phosphate by amorphous zirconium oxide nanoparticles. Water Res. 47(14): 5018–5026.

Suh, S., and S. Yee. 2011. Phosphorus use-efficiency of agriculture and food system in the US. Chemosphere 84(6): 806–813.

Sun, Y.-P., X. Li, J. Cao, W. Zhang, and H.P. Wang. 2006. Characterization of zero-valent iron nanoparticles. Adv. Colloid Interface Sci. 120(1–3): 47–56.

Sylvester, P., P. Westerhoff, T. Möller, M. Badruzzaman, and O. Boyd. 2007. A Hybrid

Sorbent Utilizing Nanoparticles of Hydrous Iron Oxide for Arsenic Removal from Drinking Water. Environ. Eng. Sci. 24(1): 104–112.

Tahovská, K., P. Čapek, H. Šantrůčková, J. Kaňa, and J. Kopáček. 2016. Measurement of in situ Phosphorus Availability in Acidified Soils using Iron-Infused Resin. Commun. Soil Sci. Plant Anal. 47(4): 487–494.

Takeshita, R., I. Yoshida, and K. Ueno. 1979. Adsorption behaviour of phosphate ion on the iron (III) compleks of a chelating Resin. Bul. Chem. Soc. Japan 52 (9): 2577–2580.

Tan, C.S., and T.Q.Q. Zhang. 2011. Surface runoff and sub-surface drainage phosphorus losses under regular free drainage and controlled drainage with sub-irrigation systems in southern Ontario. Can. J. Soil Sci. 91(3): 349–359.

Tao, J., and K. Mancl. 2008. Estimating Manure Production, Storage Size, and Land Application Area. Agric. Nat. Resour. Fact Sheet.

Tarkalson, D.D., and R.L. Mikkelsen. 2004. Runoff Phosphorus Losses as Related to Phosphorus Source, Application Method, and Application Rate on a Piedmont Soil. J. Environ. Qual. 1430(14122): 1424–1430.

Tejedor-Tejedor, M.I., and M.A. Anderson. 1990. Protonation of Phosphate on the Surface of Goethite As Studied by CIR-FTIR and Electrophoretic Mobility. Langmuir 6(3): 602–611.

Tezuka, S., R. Chitrakar, K. Sakane, A. Sonoda, K. Ooi, and T. Tomida. 2004. The synthesis and phosphate adsorptive properties of Mg(II)-Mn(III) layered double hydroxides and their heat-treated materials. Bull. Chem. Soc. Jpn. 77(11): 2101–2107.

Torrent, J., U. Schwertmann, and V. Barrón. 1994. Phosphate sorption by natural hematites. Eur. J. Soil Sci. 45(1): 45–51.

Tran, A.T.K., R. V Hyne, and P. Doble. 2007. Determination of commonly used polar herbicides in agricultural drainage waters in Australia by HPLC. Chemosphere 67(5): 944–953.

Troesch, S., D. Esser, and P. Molle. 2016. Natural Rock Phosphate: A Sustainable Solution for Phosphorous Removal from Wastewater. Procedia Eng. 138: 119–126.

Tsuji, H., and S. Fujii. 2014. Phosphate recovery by generating hydroxyapatite via

reaction of calcium eluted from layered double hydroxides. Appl. Clay Sci. 99: 261–265.

Turner, B.L., M.A. Kay, and D.T. Westermann. 2004. Colloidal Phosphorus in Surface Runoff and Water Extracts from Semiarid Soils of the Western United States. J. Environ. Qual. 33(4): 1464.

Ulen, B., J. Folster, M. Bechmann, H.P. Jarvie, and H. Tunney. 2007. Agriculture as a phosphorus source for eutrophication in the north-west European countries, Norway, Sweden, United Kingdom and Ireland: a review. (Special issue: Agriculture, Phosphorus, Eutrophication: a European Perspective.). Soil Use Manag. 23: 5–15.

Valero, C.S., C.A. Madramootoo, and N. Stämpfli. 2007. Water table management impacts on phosphorus loads in tile drainage. Agric. Water Manag. 89(1–2): 71–80.

Vohla, C., M. Kõiv, H.J. Bavor, F. Chazarenc, and Ü. Mander. 2011. Filter materials for phosphorus removal from wastewater in treatment wetlands-A review. Ecol. Eng. 37(1): 70–89.

Vrana, B., I.J. Allan, R. Greenwood, G.A. Mills, E. Dominiak, K. Svensson, J. Knutsson, and G. Morrison. 2005. Passive sampling techniques for monitoring pollutants in water. TrAC - Trends Anal. Chem. 24(10): 845–868.

Waajen, G., F. van Oosterhout, G. Douglas, and M. Lürling. 2016. Management of eutrophication in Lake De Kuil (The Netherlands) using combined flocculant – Lanthanum modified bentonite treatment. Water Res. 97: 83–95.

Wang, S.L., C.Y. Cheng, Y.M. Tzou, R.B. Liaw, T.W. Chang, and J.H. Chen. 2007. Phosphate removal from water using lithium intercalated gibbsite. J. Hazard. Mater. 147(1–2): 205–212.

Wang, H., M. Dai, J. Liu, S.J. Kao, C. Zhang, W.J. Cai, G. Wang, W. Qian, M. Zhao, and Z. Sun. 2016. Eutrophication-Driven Hypoxia in the East China Sea off the Changjiang Estuary. Environ. Sci. Technol. 50(5): 2255–2263.

Watson, S.B., C. Miller, G. Arhonditsis, G.L. Boyer, W. Carmichael, M.N. Charlton, R. Confesor, D.C. Depew, T.O. Höök, S.A. Ludsin, G. Matisoff, S.P. McElmurry, M.W. Murray, R. Peter Richards, Y.R. Rao, M.M. Steffen, and S.W. Wilhelm. 2016. The re-eutrophication of Lake Erie: Harmful algal blooms and hypoxia.

Harmful Algae 56: 44–66.

Weber, W., and J. Morris. 1963. Kinetics of adsorption on carbon from solution. J. Sanit. Eng. Div. 89(2): 31–60.

Wen, Z., Y. Zhang, and C. Dai. 2014. Removal of phosphate from aqueous solution using nanoscale zerovalent iron (nZVI). Colloids Surfaces A Physicochem. Eng. Asp. 457(1): 433–440.

Westholm, L.J. 2006. Substrates for phosphorus removal - Potential benefits for on-site wastewater treatment? Water Res. 40(1): 23–36.

White, M.J., C. Santhi, N. Kannan, J.G. Arnold, D. Harmel, L. Norfleet, P. Allen, M. DiLuzio, X. Wang, J. Atwood, E. Haney, and M. V. Johnson. 2014. Nutrient delivery from the Mississippi River to the Gulf of Mexico and effects of cropland conservation. J. Soil Water Conserv. 69(1): 26–40.

Whittig, L.D., and W.R. Allardice. 1986. X-ray diffraction techniques. p. 331–362. *In* Methods of soil analysis. Part 1. Physical and mineralogical methods.

Williams, M.R., K.W. King, and N.R. Fausey. 2015. Drainage water management effects on tile discharge and water quality. Agric. Water Manag. 148: 43–51.

Withers, P.J.A., and P.M. Haygarth. 2007. Agriculture, phosphorus and eutrophication: A European perspective. Soil Use Manag. 23(SUPPL. 1): 1–4.

Wood, R.B., and C.F. McAtamney. 1996. Constructed wetlands for waste water treatment: The use of laterite in the bed medium in phosphorus and heavy metal removal. Hydrobiologia 340(1–3): 323–331.

Worsfold, P., I. McKelvie, and P. Monbet. 2016. Determination of phosphorus in natural waters: A historical review. Anal. Chim. Acta 918: 8–20.

Wu, D., B. Zhang, C. Li, Z. Zhang, and H. Kong. 2006. Simultaneous removal of ammonium and phosphate by zeolite synthesized from fly ash as influenced by salt treatment. J. Colloid Interface Sci. 304(2): 300–306.

Xi, Y., M. Mallavarapu, and R. Naidu. 2010. Reduction and adsorption of Pb2+in aqueous solution by nano-zero-valent iron - A SEM, TEM and XPS study. Mater. Res. Bull. 45(10): 1361–1367.

Xie, J., C. Li, L. Chi, and D. Wu. 2013. Chitosan modified zeolite as a versatile adsorbent for the removal of different pollutants from water. Fuel 103: 480–485.

Xie, J., Z. Wang, S. Lu, D. Wu, Z. Zhang, and H. Kong. 2014. Removal and recovery of phosphate from water by lanthanum hydroxide materials. Chem. Eng. J. 254: 163–170.

Xu, X., B. Gao, Q. Yue, and Q. Zhong. 2011. Bioresource Technology Sorption of phosphate onto giant reed based adsorbent : FTIR , Raman spectrum analysis and dynamic sorption / desorption properties in filter bed. Bioresour. Technol. 102(9): 5278–5282.

Yan, W., A.A. Herzing, C.J. Kiely, and W.X. Zhang. 2010a. Nanoscale zero-valent iron (nZVI): Aspects of the core-shell structure and reactions with inorganic species in water. J. Contam. Hydrol. 118(3–4): 96–104.

Yan, L.G., Y.Y. Xu, H.Q. Yu, X.D. Xin, Q. Wei, and B. Du. 2010b. Adsorption of phosphate from aqueous solution by hydroxy-aluminum, hydroxy-iron and hydroxy-iron-aluminum pillared bentonites. J. Hazard. Mater. 179(1–3): 244–250.

Yang, Q., H. Tian, X. Li, W. Ren, B. Zhang, X. Zhang, and J. Wolf. 2016. Spatiotemporal patterns of livestock manure nutrient production in the conterminous United States from 1930 to 2012. Sci. Total Environ. 541: 1592–1602.

Yang, K., L.G. Yan, Y.M. Yang, S.J. Yu, R.R. Shan, H.Q. Yu, B.C. Zhu, and B. Du. 2014. Adsorptive removal of phosphate by Mg-Al and Zn-Al layered double hydroxides: Kinetics, isotherms and mechanisms. Sep. Purif. Technol. 124: 36–42.

Yao, Q.Z., Z.G. Yu, H.T. Chen, P.X. Liu, and T.Z. Mi. 2009. Phosphorus transport and speciation in the Changjiang (Yangtze River) system. Appl. Geochemistry 24(11): 2186–2194.

Yavitt, J.B., and S.J. Wright. 1996. Temporal patterns of soil nutrients in a Panamanian moist forest revealed by ion-exchange resin and experimental irrigation. Plant Soil 183(1): 117–129.

Yoon, S.Y., C.G. Lee, J.A. Park, J.H. Kim, S.B. Kim, S.H. Lee, and J.W. Choi. 2014. Kinetic, equilibrium and thermodynamic studies for phosphate adsorption to magnetic iron oxide nanoparticles. Chem. Eng. J. 236: 341–347.

Yoshida, H., and W.A. Galinada. 2002. Equilibria for adsorption of phosphates on OH-type strongly basic ion exchanger. AIChE J. 48(10): 2193–2202.

Yoshida, I., R. Takeshita, and K. Ueno. 1984. Studies of the Selective Adsorption of Anions by Metal Ion Loaded Ion-exchange Resin. VI. The Adsorption Behavior of the Phosphate Ion on the Iron (III) Loaded Ion-exchange Resin. Bull. Chem. Soc. Jpn. 57(1): 54–57.

Yoshino, H., M. Tokumura, and Y. Kawase. 2014. Simultaneous removal of nitrate, hydrogen peroxide and phosphate in semiconductor acidic wastewater by zero-valent iron. J. Environ. Sci. Heal. - Part A Toxic/Hazardous Subst. Environ. Eng. 49(9): 998–1006.

Zhang, H., W. Davison, R. Gadi, and T. Kobayashi. 1998. In situ measurement of dissolved phosphorus in natural waters using DGT. Anal. Chim. Acta 370: 29–38.

Zhang, C., Y. Li, F. Wang, Z. Yu, J. Wei, Z. Yang, C. Ma, Z. Li, Z.Y. Xu, and G. Zeng. 2017. Performance of magnetic zirconium-iron oxide nanoparticle in the removal of phosphate from aqueous solution. Appl. Surf. Sci. 396: 1783–1792.

Zhang, G., H. Liu, R. Liu, and J. Qu. 2009. Removal of phosphate from water by a Fe-Mn binary oxide adsorbent. J. Colloid Interface Sci. 335(2): 168–174.

Zhang, L., J. Liu, L. Wan, Q. Zhou, and X. Wang. 2012. Batch and Fixed-Bed column performance of phosphate adsorption by lanthanum-doped activated carbon fiber. Water. Air. Soil Pollut. 223(9): 5893–5902.

Zhang, W., W. Ma, Y. Ji, M. Fan, O. Oenema, and F. Zhang. 2008. Efficiency, economics, and environmental implications of phosphorus resource use and the fertilizer industry in China. Nutr. Cycl. Agroecosystems.

Zhang, Y., B. Pan, C. Shan, and X. Gao. 2016. Enhanced Phosphate Removal by Nanosized Hydrated La(III) Oxide Confined in Cross-linked Polystyrene Networks. Environ. Sci. Technol. 50(3): 1447–1454.

Zhang, T.Q., C.S. Tan, Z.M. Zheng, and C.F. Drury. 2015. Tile Drainage Phosphorus Loss with Long-Term Consistent Cropping Systems and Fertilization. J. Environ. Qual. 44(2): 503–511.

Zhou, Q., X. Wang, J. Liu, and L. Zhang. 2012. Phosphorus removal from wastewater using nano-particulates of hydrated ferric oxide doped activated carbon fiber prepared by Sol-Gel method. Chem. Eng. J. 200–202: 619–626.

Zhou, J., Z.P. Xu, S. Qiao, Q. Liu, Y. Xu, and G. Qian. 2011. Enhanced removal of triphosphate by MgCaFe-Cl-LDH: Synergism of precipitation with intercalation

and surface uptake. J. Hazard. Mater. 189(1–2): 586–594.

Zhu, M.X., K.Y. Ding, S.H. Xu, and X. Jiang. 2009. Adsorption of phosphate on hydroxyaluminum- and hydroxyiron-montmorillonite complexes. J. Hazard. Mater. 165(1–3): 645–651.

Zhu, X., and A. Jyo. 2005. Column-mode phosphate removal by a novel highly selective adsorbent. Water Res. 39(11): 2301–2308.

Zhu, J., Z. Zhu, J. Lin, H. Wu, and J. Zhang. 2016. Distribution of hypoxia and pycnocline off the Changjiang Estuary, China. J. Mar. Syst. 154: 28–40.

Zoltek, J. 1974. Phosphorus nucleation removal by orthophosphate. Water Pollut. Control Fed. 46(11): 2498–2520.

RESEARCH JUSTIFICATION

Phosphorus (P) loss from agricultural fields has long been an environmental issue due to its negative impact on aquatic ecosystems such as eutrophication and hypoxia (Sharpley et al., 1994; Carpenter et al., 1998). Compared to nitrogen, little P is typically lost from fields (Gentry et al., 2007). Larger amounts of P can be lost during major erosion events, and recently dissolved reactive P (DRP) losses at high concentrations have been reported through tile drainage in the Lake Erie watersheds of northwestern Ohio (King et al., 2015a). Concentrations of DRP can range from just detectable to many tenths of a mg L^{-1} in tile lines, and can be many mg L^{-1} in surface runoff (King et al., 2015a). These concentrations and loads of DRP are more than enough to lead to eutrophication in downstream water bodies. For the control of P loss from agricultural fields, it is a prerequisite to monitor the loads of P from a large number of agricultural waterways and identify the major pathways of P loss in each field. However, it is not feasible to install large numbers of automated samplers in agricultural drainage ditches and tile lines throughout the United States agricultural lands because of the cost. A more practical alternative would be a quick, easy, and economical technique that can be used to monitor the P concentrations in eutrophic waters during critical wet seasons when a large quantity of P is discharged from agricultural fields.

Several methods have been suggested to monitor the concentration of P in waters. The most common one is grab sampling, which obtains time-discrete records of the concentration of target substances (Müller et al., 2007; Rozemeijer et al., 2010; Worsfold et al., 2016). The precision and accuracy of grab sampling rely heavily on the sampling frequency, which is limited by manual labor especially for its application in long-term and large-scale monitoring (O'Brien et al., 2009; Knutsson et al., 2013; Edenborn et al., 2017). The minimum detectable concentration is also limited by the volume of sampled water at each time. Another disadvantage is that the discrete (i.e., snapshot) measurement may miss specific discharge events (Vrana et al., 2005; Ahrens et al., 2015). Other monitoring methods also have their own drawbacks. For example, automatic samplers and analyzers are expensive to purchase and maintain (Rozemeijer et al., 2010); paper-based devices for in-site determination are convenient and cost-efficient, but the detection

limit is relatively high and the accuracy is also affected temporal variation of the contaminant concentrations (Jayawardane et al., 2012; Almeida et al., 2018). Since the discharge of DRP in agricultural fields has been reported to be usually at low concentration but occurs during heavy precipitation events (Müller et al., 2007; King et al., 2015b; Smith et al., 2015), the above monitoring methods are not ideal for the evaluation of P loss from agricultural fields. A passive sampling technique rises as a promising alternative in this case. It is based on the accumulation of target substances in adsorbents in a permeable containment like mesh bags that are deployed on-site. A time-weighted average concentration can be calculated according to the amount of the target substances on adsorbents after a certain period of deployment, which can be several days to months (Ahrens et al., 2015).

As reviewed above, different adsorbents exhibit various P adsorption capacities. The retention of P in these adsorbents is affected by the physical and chemical conditions of wastewater. However, it is safe to say that some adsorbents are reactive enough (e.g., hybrid anion exchange resins and alkaline earth-based materials) that they have potential to be used in the passive detection method to monitor P in agricultural drainage water. In contrast to the water treatment facilities, temporal variations exist in agricultural drainage water. The variations in environmentally relevant conditions such as P concentration, interfering ions, and flow rate should be accounted for when a proper adsorbent is selected. Eutrophic waters in agricultural systems are generally at near-neutral pH, and this makes the removal of P via adsorption difficult because P adsorption capacity for most inorganic adsorbents at near-neutral pH is lower than under acidic pH. Adsorbent specific selectivity for P in the presence of interfering ions at neutral pH values should be prioritized. The stability of adsorbents also becomes important for field application. The adsorbents must be large enough to be entrapped in mesh bags and should withstand seasonally fluctuating flow rate and temperature without sacrificing P removal efficiency. For the passive detection technique, adsorbent materials should be economical and provide maximal for ease of recovery. Considering all criteria, reactive hybrid anion exchange resins have the greatest potential for the use in passive sampling techniques to monitor P flux in agricultural wastewaters. The objective of this study was to evaluate the

passive detection technique with reactive hybrid anion exchange resins to monitor P in agricultural tile waters.

RESEARCH HYPOTHESES

Based on the research justification above, the following three hypotheses were developed.

1. The concentration of P and common anions (e.g., sulfate and nitrate) affect the maximum P retention capacity of reactive (hybrid) anion exchange resins.

2. Iron hydroxide-loaded anion exchange resins is a reactive adsorbent that can adsorb phosphate efficiently and irreversibly.

3. The passive detection technique with reactive hybrid anion exchange resins can be used to monitor dissolved P in agricultural tile waters.

To test these three hypotheses, the work reported in the following three research chapters was conducted.

CHAPTER 2: EVALUATION OF PHOSPHATE REMOVAL PERFORMANCE IN ANION EXCHANGE RESINS AFFECTED BY SURFACE ACIDITY, POLYMER MATRICES AND REACTION CONDITIONS

Abstract

Anion exchange resins have been widely used for the removal of anionic pollutants from wastewaters. However, the effects of resin types and surface properties on the removal of phosphate (P) from water have not been clearly understood. In this study, three anion exchange resins with different polymer matrices (polystyrene and polyacrylic) and resin functional groups (strong-base and weak-base) were used in batch P adsorption experiments to explore the P adsorption capacity in the presence of common surface water anions such as nitrate and sulfate. And the effect of surface modification with iron hydroxides (i.e., hybrid resin) on P adsorption was studied. Results showed that the P adsorption capacity of the strong-base polystyrene resin, the weak-base polystyrene resin and the weak-base polyacrylic resin was 13.16, 5.17 and 21.19 mg/g, respectively. The hybrid resins loaded with iron hydroxides showed better resistance to the influence of co-existing nitrate and sulfate in the P adsorption process than the resins without iron hydroxides-coating. The decrease of P adsorption capacity caused by the presence of nitrate reduced from 0.8-6.4 % to 0.4-2.3 %. The kinetic processes of P adsorption by both pure resins and hybrid resins were successfully modeled using the pseudo-second-order equation. Overall, the iron-loaded hybrid resins showed higher affinity for phosphate compared with the respective pure resins, suggesting that hybrid resins can be promising adsorbents for the removal of P in aquatic environments.

2.1. Introduction

Anion exchange resin is an important class of adsorbent material applied for the removal of phosphate from wastewater. Anion exchange resins is composed of covalently cross-linked frameworks of macromolecular hydrocarbon chains and have positively charged functional groups (Awual et al., 2011; Loganathan et al., 2014). There are different types of anion exchange resin matrix, among which are polystyrene resins that the most common type in practical applications because of good resistance to physical and chemical stresses (Boari et al., 1976; Zagorodni, 2006). However, the hydrophobic property of the polymer matrix could have a negative effect on the interaction with hydrated polar compounds (Awual et al., 2011). Polyacrylic resins are another important type of anion exchange resin for environmental research. Polyacrylic resins are made from alkyl acrylates and methacrylates as polymers, which could provide better hydrophilic properties than polystyrene resins. They have the advantages of easier regeneration and a better resistance to organic fouling (Zagorodni, 2006; Pan et al., 2009a). The hydrophilic nature of polyacrylic resins could provide a better affinity for phosphate than polystyrene resins, which could make polyacrylic resins more suitable as the adsorbents for the removal of phosphate from water, but this needs laboratory verification and comprehensive comparison with other resins. Anion exchange resins can also be categorized by the surface functional group, such as strong-base and weak-base. The former contains quaternary amine as the functional group, while tertiary (or secondary or primary) amine is present in the latter. Weak-base anion exchange resins usually have higher exchange capacity and regeneration efficiency than strong-base anion exchange resins (Zagorodni, 2006; Awual and Jyo, 2011).

Anion exchange resins can serve as a sorbent for phosphate in wastewater because phosphate ions can be exchanged with chloride or other anions that are pre-loaded on the resin surfaces. But, due to the non-specific adsorption mechanism of anion exchange resins, P removal is subject to interference by other environmental prevalent anions like sulfate in environments. In general, oxyanions with higher charges would have stronger competition with phosphate for the adsorption sites (Das et al., 2006; Awual and Jyo, 2011). With a few exceptions (Boari et al., 1976; Awual and Jyo, 2011), there is little

comparative study of different types of anion exchange resins for resistance to the interference by common oxyanions on P removal effect

To improve P adsorption specificity, the surface matrix of resins has often been modified with secondary coating materials. Hydrated ferric oxides (HFO) are one of the most extensively studied loading materials for the synthesis of hybrid anion exchanger (HAIX) to remove anionic pollutants. Iron (hydr)oxides as Lewis acids can form inner-sphere complexation with phosphate as a Lewis base, thus phosphate can be adsorbed with high affinity and efficiency. However, the small size and physical weakness of HFO incur difficulties for application and recovery (Blaney et al., 2007; Pan et al., 2009b; Sengupta and Pandit, 2011; Johir et al., 2016). Anion exchange resins loaded with HFO are expected to combine the advantages of both materials to enhance the removal of phosphate from wastewater (Sengupta and Pandit, 2011; O'Neal and Boyer, 2013; Sendrowski and Boyer, 2013), but the most efficient combination of resin type and surface loading to optimize P removal is not clearly understood.

Based on previous investigations, there are several knowledge gaps that need to be addressed to optimize P removal efficiency: 1) effects of resin matrix (polystyrene and polyacrylic) including functional groups (strong-base and weak-base), 2) effects of interfering anions, and 3) effects of surface modification of resin to form hybrid resins. Accordingly, the objective of this study is to compare the three (hybrid) anion exchange resins for P removal, relative to differences in surface acidity, polymer matrix, and reaction conditions (e.g., interfering anions).

2.2. Materials and Methods

2.2.1. Materials

All chemicals were ACS-reagent grade, and ultra-pure water (18.2 MΩ) was used unless otherwise stated.

Three anion exchange resins were tested in this study, among which were a strong-base polystyrene-DVB resin AMBERLITE™ HPR9200, a weak-base polystyrene-DVB resin AMBERLITE™ HPR9600, and a weak-base polyacrylic resin AMBERLITE™ IRA67, (Du Pont Co., Wilmington, USA). Resins were cleaned using the following acid-

base treatments. For all resins, 100 g moist resin was added in a 1-L polypropylene bottle containing 1.0 L of 1 M HCl. The bottle was agitated on an orbital shaker at 80 rpm for 24 h. After washing three times with water, the resin was treated with 1-L of 1 M NaOH in the bottle, and then shaken on an orbital shaker at 80 rpm for 24 h. Washing with water was subsequently repeated, followed by air-drying and storage of the resin at room temperature. The appearance of the anion exchange resins are shown in Fig. 2.1 and the physicochemical characteristics of the three anion exchange resins are summarized in Table 2.1, as provided by (Staicu et al., 2017; Dupont, 2019; Purolite, 2019).

A commercially available product - FerrIX™A33E (Purolite, USA), which is an iron-loaded strong-base polystyrene-DVB hybrid resin, was also used. The basic physicochemical properties are present in Table 2.1.

2.2.2. Synthesis of iron-loaded hybrid anion exchange resins

The synthesis of iron-loaded hybrid resins principally consists of 1) the loading of ferric ions and 2) the precipitation and transformation of iron hydroxide. The detailed protocol is as follows. Firstly, 20 g of parent resin was weighted into a 500-mL polypropylene bottle, treated with 250 mL of 1 M HNO_3 then shaken on an orbital shaker at 75 rpm for 1 hr. After washing three times with DI water, the resin was treated with 100 mL of 0.5 M $Fe(NO_3)_3$ and shaken at 75 rpm for 1 hr.; secondly, 90 mL of 5 M NaOH was added to the bottle, immediately followed by adding ultra-pure water to dilute the suspension to 500 mL; finally, the resin was heated in an oven at 70 °C for 60 hrs to convert the loaded iron into goethite. After the incubation, the hybrid resin was rinsed twice with ultra-pure water. The resin was treated with 250 mL of 0.5 M $NaHCO_3$ solution and shaken at 75 rpm for 2 hrs, followed by a treatment with 250 mL of 0.5 M NaCl and shaken for 2 hr, to exchange the hydroxyl ion on the resin surface. After the final washing with ultra-pure water, the hybrid resin was air-dried and stored at room temperature for future use.

2.2.3. Characterization of hybrid resins

The content and the mineralogical information of the iron loaded on hybrid resins was studied after the synthesis of the hybrid resins.

The total iron content of the hybrid resins was determined after acid digestion. To be specific, 0.1 g of the hybrid resin was added into a 125-mL screw-capped polypropylene bottle with 100 mL of 5% hydroxylamine and 5 M HCl for the digestion of iron in the hybrid resin (Upping et al., 1986; Sager, 1992). The mixture was shaken in an ultrasonic bath (Bransoic, CPX2800) for 5 min and then with an orbital shaker at 80 rpm for 48 hr. The digest was filtered with Whatman No.2 filter paper and the total iron concentration in the filtrate was measured in triplicate by a spectrophotometric method using 1, 10-phenanthroline (Tamura et al., 1974).

The mineralogy of the iron loaded on hybrid resins was analyzed using Fe K-edge X-ray absorption spectroscopy (XAS) at ID12 at Advanced Photon Source (Argonne, IL, USA). A monochromator consisting of a double-crystal Si (220) at Phi=0o was used. An incident beam of X-ray energy was calibrated using Fe foil at the first inflection point (7112 eV) and detuned 50% at 7770eV. Beam size was 2mm in width x 1mm in height. The calibration energy was monitored using Fe foil during the scan. The transmission measurements were performed in air at room temperature. Spectra were recorded with three regions: 10 eV steps from 6880 to 7090 eV with 1sec. dwell, 0.25 eV steps over the pre-edge from 7090 to 7140eV with 1sec. dwell, and 0.25 eV steps from k of 1.62 to 14 Å-1 with 1sec. dwell. Three spectra were recorded. Acquiring multiple spectra across time allows us to quantitative evaluation of reproducibility. Reference spectra of synthetic pure ferrihydrite, goethite, hematite, and lepidocrocite were also collected. Spectra were normalized with standard features of the ATHENA software package (Ravel and Newville, 2005), and a linear combination of XAS reference spectra fit analysis was conducted.

The iron (oxyhydr)oxide mineralogical analysis of hybrid resins was also conducted using X-ray diffraction methodology. The resin powder was placed in the 25-stage sample holder provided on the instrument (Bruker D-5000 XRD) and positioned the goniometer was positioned to start its angular scan at 45 kV and 30 mA. The lower limit

for 2θ was set to 5° and the upper limit to 80°. The scanning rate was set at 2.0°/min. The value for 2θ was calculated using Bragg's Law ($2d\sin\theta = n\lambda$).

In addition, the surface area of the hybrid resins as well as the pure anion exchange resins was measured using ethylene glycol monoethyl ether (EGME) method (Klute et al., 1986). Resins were first dried in an oven at 40 ℃. About 0.5 g of dried resin samples were then placed in petri dishes, and transferred to a vacuum desiccator with another petri dished containing 10 mL of EGME. The desiccator was connected to laboratory vacuum and evacuated for 10 minutes, and the samples were subsequently left in the isolated desiccator overnight before re-weighing. The evacuation-stabilization-weighting cycle was repeated until the weights were relatively constant. At this point, monolayer coverage is assumed and the specific surface area was calculated using the equation (Klute et al., 1986):

$$A = W_g/(W_s \cdot 0.000286)$$

where A = specific surface (m^2/g), W_g = difference of weight of resin before and after EGME equilibration (g), and W_s = weight of the dried resin (g); 0.000286 is the mass of EGME required to form a monolayer on 1 m^2 of surface.

2.2.4. Phosphorus adsorption isotherm in anion exchange resins and hybrid resins

To compare maximum P adsorption capacities of the anion exchange resins with different resin matrix, functional groups and surface modifications, P adsorption isotherm experiments were conducted.

A 100 mg /L phosphate stock solution was prepared by dissolving disodium phosphate in 10 mM NaCl. Then the stock solution was diluted to 3, 10, 20, 30, 40, 50 mg/L for the isotherm experiment. Duplicate resin samples (0.1 g) were added to a 50-mL Nalgene high-speed centrifugation tube treated with 30 mL of phosphate solution and then mixed on an orbital shaker at 80 rpm for 24 hrs. After 24 hrs, the suspensions were sampled and filtered using a 0.45 μm syringe filter. Aliquots were analyzed for P concentration colorimetrically (He et al., 1998). The solution pH was kept at 7.5 by manually adding diluted HCl or NaOH and the temperature was maintained at 21℃ throughout the experiment.

Isotherm data of the adsorption experiments was fitted by the Freundlich and Langmuir model.

For the Freundlich model

$$q = K_f \cdot C^{1/n}$$

where q is the amount of phosphate adsorbed (mg P/g) ; C is the final equilibrium concentration of phosphate (mg P/L) ; K_f is a parameter related to the adsorption capacity; and n is a parameter related to the intensity of adsorption.

For the Langmuir model

$$\frac{C}{q} = \frac{1}{Q_m \cdot K_m} + \frac{C}{Q_m}$$

where q is the amount of P adsorbed (mg P/g); C is the final equilibrium concentration of phosphate (mg P/L); Q_m represents the maximum adsorption capacity (mg P/g); and K_m is a parameter related to the bonding strength (L/mg).

2.2.5. Effects of sulfate and nitrate on phosphate adsorption isotherm

To study the interference of coexisting anions on P adsorption in (hybrid) resins, the adsorption isotherm experiments were also conducted in the presence of sulfate and nitrate.

Sulfate and nitrate were added as sodium nitrate and sodium sulfate at the concentration of 1 mM during the preparation of phosphate solution. The following steps of the isotherm experiment were same with Section 2.3 and the P concentration was measured colorimetrically (He et al., 1998). In addition, the nitrate concentration after adsorption was also measured colorimetrically (Collos et al., 1999; Patey et al., 2008), and the sulfate concentration was tracked using ion chromatographic analysis (Mulik et al., 1976; Tabatabai and Dick, 1983).

2.2.6. Phopshate adsorption kinetics in anion exchange resins and hybrid resins

Kinetic experiments were conducted as described below using the three anion exchange resins (Pan et al., 2009b; Sengupta and Pandit, 2011) and three respective hybrid resins. Two P stock solutions at the concentration of 10 and 20 mg/L were prepared by dissolving disodium phosphate in 0.01M NaCl solution. The solution pH was adjusted to 7.5 by adding diluted HNO_3 or NaOH, which were buffered by 10 mM 3-(N-morpholino) propanesulfonic acid (MOPS). The temperature was maintained at 21°C throughout the experiment.

The hybrid resin (0.1 g) was added to 30 mL of phosphate solution in a 50-mL centrifugation tube. It was stirrer on an orbital shaker at 80 rpm for different periods (3 min, 10 min, 30 min, 1 hr., 4 hrs, 8 hrs, 16 hrs, and 24 hrs). After shaking, the supernatant was quickly sampled and filtered through a 0.45 μm syringe filter. The phosphate concentrations in the samples were determined colorimetrically (He et al., 1998).

The data from kinetic experiments were fitted to pseudo-first order model (Ho and McKay, 1999), pseudo-second order model (Ho and McKay, 2000), Elovich model (Low, 1960), and intra-particle diffusion model (Weber and Morris, 1963).

For the Pseudo-first order model, the following equation will be used.

$$q_t = q_e(1 - e^{-k_1 t})$$

which can be expressed in linear form:

$$\ln(q_t - q_e) = \ln(q_e) - k_1 t$$

where q_t is the amount of phosphate adsorbed per unit weight of adsorbents (mg P g^{-1}) at time t (hr). q_e is the adsorption capacity of the adsorbent (mg P/g) at equilibrium, and k_1 (g/mg/hr) is the first order rate constant. The terms q_e and k_1 were calculated by linear regression of $\ln(q_t - q_e)$ vs. t.

For the Pseudo-second order model, the following equation was used.

$$\frac{t}{q_t} = \frac{1}{k_2 {q_e}^2} + \frac{1}{q_e} t$$

where q_t is the amount of phosphate adsorbed per unit weight of adsorbent (mg P/g) at time t (hr), q_e is the adsorption capacity of adsorbents (mg P/g) at equilibrium, and k_2 (g/mg/hr) is the second order rate constant. The terms q_e and k_2 were calculated by the linear regression of $\frac{t}{q_t}$ vs. t where the slope and intercept correspond to $\frac{1}{q_e}$ and $\frac{1}{k_2 {q_e}^2}$, respectively.

For the Elovich model, the following equation was used.

$$q_t = \frac{\ln(\alpha\beta)}{\beta} + \frac{1}{\beta}\ln(t)$$

where q_t is the amount of phosphate adsorbed per unit weight of adsorbent (mg P/g) at time t (hr), α (mg/mL/min) is the initial adsorption rate constant, and the parameter b (mL/mg) is related to the extent of surface coverage and activation energy for chemisorption. The terms α and β were calculated by linear regression of q_t vs. $\ln(t)$ where the slope and intercept correspond to $\frac{1}{\beta}$ and $\frac{\ln(\alpha\beta)}{\beta}$, respectively.

For the intra-particle diffusion model, the following equation was used.

$$q_t = k_d t^{1/2} + C$$

where q_t is the amount of phosphate adsorbed per unit weight of adsorbent (mg P/g) at time t (min). k_d is the intra-particle diffusion constant, and C is a parameter related to the thickness of the boundary layer, which were calculated by linear regression of q_t vs.$t^{1/2}$.

2.3. Results and Discussion

2.3.1. Material characterization

2.3.1.1. Physical and chemical properties of pure anion exchange resins and hybrid resins

To compare the influence of physicochemical properties of resins on P adsorption capacity, the following three anion exchange resins were chosen. AMBERLITE™ HPR9200 is a strong-base polystyrene-DVB resin, representing the most common type of polymeric adsorbent in environmental applications. The macroporous structure is featured by relatively high mechanical stability and opaque appearance. AMBERLITE™ HPR9600 is a weak-base polystyrene-DVB resin with macroporous structure. Another anion exchange resin tested in this study was AMBERLITE™ IRA67, which is a weak-base polyacrylic resin. Because of the polar and hydrophilic characteristics from acrylic ester groups, this type of resin has been successfully applied for wastewater removal of highly water-soluble compounds in wastewater such as reactive and sulfonated compounds (Boari et al., 1976; Zagorodni, 2006; Pan et al., 2009a). Within the same weak-base resin group, P adsorption capacity of the polyacrylic resin, IRA67, was compared with that of the polystyrene-DVB based resin, HPR9600.

To improve P adsorption capacity, hybrid resins (i.e., iron oxide coated resins) were prepared by loading the pure anion exchange resins with iron hydroxides. FerrIX™A33E is a commercially available hybrid resin that is produced from a strong-base polystyrene-DVB resin, HPR9200. Although the particle size of FerrIX™A33E varies, the average particle size of all three hybrid resins (i.e., FerrIX™A33E, Hybrid HPR9600 and hybrid IRA7) is similar. The P adsorption capacity of resins was compared before and after the surface modification (i.e. iron loading).

Total surface area (TSA) of the three anion exchange resins varies substantially despite the similar particle sizes (Table 2.1). It is important to note that EGME-based TSA gives much larger surface area than the BET-based specific surface area. Because of the temperature-sensitive stability of polymer resins, the BET method, which requires heating at >90^{o}C to remove moisture before the N_2 adsorption analysis, was not a suitable method for polymer resins with limited thermal stability. The weak-base polyacrylic resin, IRA67, has the highest surface area at 3515 ± 21 m^2/g, followed by HPR9200 at

1625 ± 21 m^2/g, and HPR9600 at 672 ± 40 m^2/g. The TSA of hybrid HPR9600 is similar to that of its parent resin, which makes sense because of the lowest loading level of iron oxides on the resin (~5.5 mg/g). The total surface area of FerrIX™A33E (i.e., hybrid HPR9200) was found to be significantly lower than that of HPR9200, which could be explained by a decrease in microporosity as a result of the penetration of small goethite particles in the porous structure. However, the iron loading treatment in IRA67 increased its TSA from 2084 ± 7 m^2/g to 3515 ± 21 m^2/g. The effects of surface modification on the surface area of the resin are highly debated. Zhang et al. (2016) showed that the specific surface area of an anion exchange resin increased from 10.5 to 27.5 m^2/g after iron loading. The influence of iron loading/coating on the surface area of anion exchange resins is related to specific interactions between the iron oxide coating and the gel-type resin matrix. In the case of the iron loaded IRA67, polyacrylic properties were interacting with ferric ions within the surface porous structure during the synthesis, increasing iron-loading level.

2.3.1.2. Iron content in hybrid resins

As shown in Table 2.1, the total iron content of the commercially available product - FerrIX™A33E was 196.0 ± 3.0 mg Fe/g resin, while the iron loading levels of the two synthesized hybrid resins, hybrid HPR9600 and hybrid IRA67, were 5.5 ± 0.4 and 13.4 ± 0.8 mg/g, respectively. Although the resin matrix is polystyrene-DVB in both FerrIX™A33E and the hybrid HPR9600, the parent resins have different functional groups (strong-base vs. weak-base). These functional groups played a critical role in the coating process of iron oxides.

On the other hand, the comparison between hybrid HPR9600 and hybrid IRA67 clearly showed that IRA67 was a better parent resin in terms of iron loading. Although both were weak-base resins, the polyacrylic resin retained more iron oxides than the polystyrene-DVB resin. The better iron loading result could be explained by the hydrophilic property of polyacrylic resins. Hydrated ferric ions could be relatively easier to diffuse into the polyacrylic structure compared with polystyrenes, thus more iron oxides were fixed at the porous structure of the resin. Most of the research published on iron-loaded hybrid resins used polystyrene-DVB resins as the parent matrix since it is the

most common type of anion exchange resin (Cumbal and SenGupta, 2005; Pan et al., 2009b; Sarkar et al., 2011; Acelas et al., 2015). Our result showed that polyacrylic resins could be adopted to improve the effect of iron loading on hybrid resins.

2.3.1.3. Mineralogy of iron in hybrid resins

The result of iron oxide mineralogic analysis of hybrid resins is shown in Fig. 2.2 and Table 2.2. FerrIX™A33E contains goethite. This result was also confirmed by a conventional powder X-ray diffraction analysis. The subsequent XAS analysis confirmed that goethite is the dominant species in hybrid HPR9600 and hybrid IRA67.

2.3.2. Phosphate adsorption isotherm and effects of co-existing anions

2.3.2.1. P adsorption isotherm of pure anion exchange resins and hybrid resins

2.3.2.1.1. Comparison among pure anion exchange resins

The P adsorption isotherms obtained for anion exchange resins are shown in Fig. 2.3. Comparing the isotherm curves of the three pure resins, it is shown that the P adsorption capacity follows the order of IRA67 > HPR9200 > HPR9600. Both the three isotherm curves were fitted well by the Freundlich model ($R^2 > 0.98$) and the Langmuir model ($R^2 > 0.97$) (Table 2.3, Figs. 3 and 4). The maximum P adsorption capacity parameter (Qm) derived from the Langmuir model was 21.19, 13.16, 5.17 mg/g of resin for IRA67, HPR9200, HPR9600, respectively. The order follows the total surface area of the three resins. The highest TSA of IRA (10.17 m^2/g) adsorbed P most and followed by HPR9200 (8.09 m^2/g), and HPR9600 (7.69 m^2/g).

Since HPR9200 and HPR9600 are both polystyrene-DVB resins, the comparison of the two resins indicates that strong-base resin functional groups (quaternary ammonium) could provide a stronger P adsorption ability than weak-base resin functional groups (tertiary or secondary amine). A similar result was reported in Awual and Jyo (2011), where a strong-base resin Diaion SA10A showed a slightly higher P adsorption at pH ~7 than a weak-base resin Diaon WA20. The weak-base polyacrylic resin IRA67 showed the highest P adsorption ability among the three anion exchange resins, indicating polyacrylic resins are a better material than polystyrene-DVB resins in terms of P adsorption. Anion

exchange resins have already attracted research attention as a possible adsorbent for P removal in wastewater treatment since phosphate can be attracted by the positively charged resin functional groups and trapped through ion exchange with other anions loaded on the resins (Awual et al., 2011; Loganathan et al., 2014). Several studies have already shown anion exchange resins to be effective for P removal from wastewaters (Yoshida and Galinada, 2002; Anirudhan et al., 2006; Sowmya and Meenakshi, 2014). Resin performance varies in different studies and cannot readily be compared because of different experimental conditions. Boari et al. (1976) compared the P adsorption performance of 30 types of anion exchange resins with different properties and reported that polyacrylic resins are best suited for phosphate removal because of their hydrophilic properties.

2.3.2.1.2. Comparison between pure resins and their respective hybrid resins

In contrast to our common expectation that iron oxide coating enhances P adsorption, the hybrid resins did not show a greater P adsorption as compared to their respective pure resins. The performance of each pair is discussed below.

The P adsorption isotherm curves of HPR9200 and FerrIX™A33E (i.e., Hybrid HPR9200) crossed at the point with C_{eq} at ~13 mg/L (Fig. 2.3a). The hybrid resin adsorbed more P than the pure resin at low initial P concentrations, but its P adsorption became less than that of the pure resin at C_{eq} higher than 13 mg/L. The P adsorption capacity of FerrIX™A33E in the Langmuir model was 7.69 mg/g, which is lower than that of HPR9200 (Table 2.3, Figs. 3 and 4).

Fig. 2.3b shows the isotherm curves of HPR9600 and the respective hybrid resin. The P adsorption of Hybrid HPR9600 was lower than its parent resin at each initial P concentration (Fig. 2.3b). Although the maximum adsorption capacity of the hybrid resin calculated from the Langmuir model was greater than HPR9600 (6.33 mg/g vs. 5.17 mg/g), R^2 of the Langmuir model fit for the data of hybrid HPR9600 is relatively low (R^2 = 0.90), making the comparison less convincing. For the polyacrylic resin IRA67, the effect of iron loading on P adsorption performance was relatively small. The P adsorbed by Hybrid IRA67 was slightly greater for IRA67 in the range of P concentrations. But the Langmuir maximum adsorption capacity of the hybrid resin was lower than its parent

resin (19.84 mg/g, $R^2 = 0.98$). A similar trend was also observed in the comparison between HPR9200 and the respective hybrid resin.

The synthesis of hybrid resins by loading iron oxide on anion exchange resins has already been used for industrial applications (Blaney et al., 2007; Sengupta and Pandit, 2011; O'Neal and Boyer, 2013; Sendrowski and Boyer, 2013; Nur et al., 2014). Several studies compared the P adsorption of newly synthesized hybrid resins with their parent resins. They reported that P adsorption increased after the parent materials were loaded with iron oxide (Takeshita et al., 1979; Pan et al., 2009b; Acelas et al., 2015). However, the hybrid resins did not show a greater P adsorption capacity in this study. This difference could be explained by the difference in the mineralogy of the loaded iron oxide in the hybrid resins. In this study, the synthesis of hybrid resin included a heating procedure at 70 °C for 60hr after the iron loading, to convert amorphous iron oxyhydroxide into goethite. Previous studies usually did not include thermal treatment. In several cases the loading process produced amorphous iron hydroxides that were nano-sized which could provide a higher reactivity (Sengupta and Cumbal, 2007; Pan et al., 2009b; Ren et al., 2012; You et al., 2016). Although goethite is more stable and could be more strongly attached to the resin particles, it should be less reactive and, therefore may not provide a significant increase in P adsorption capacity. The goethite coating could also block the micropores of resins, reducing the reactive surface area. The total surface area of FerrIX™A33E was measured to be only half of that for HPR9200. After converting the P adsorption capacity into the mass of P per area of resins, a higher capacity was obtained for the hybrid resin (9.49 g/m^2) than the pure resin (8.09 g/m^2).

Nevertheless, although the iron loading showed a different influence on the P adsorption of the resins, the P adsorption ability of the three hybrid resins still followed the order of hybrid IRA67 > hybrid HPR9200 > hybrid HPR9600. The same order was observed in their respective pure resins, indicating that the properties of parent resin itself had a greater influence on the P adsorption ability than did the iron-loading treatment evaluated in this study.

2.3.2.2. Effect of nitrate and sulfate on P adsorption

The P adsorption isotherm of the resins were repeated in the presence of interfering ions. The initial concentration of nitrate and sulfate was 1 mM, which is just above the common range of nitrate and sulfate concentration in agricultural drainage water in the Midwestern U.S. (Baker et al., 1975; Ahiablame et al., 2011; Zimmerman, 2016).

The isotherm curves from the above isotherm experiments are shown in Fig. 2.4. It can be seen that for all resins, the addition of sulfate significantly lowered the amount of P adsorbed, while nitrate had a much smaller effect or no influence on P adsorption. To accurately assess the influence of interfering ions on P adsorption in different resins, % P adsorption by the six resins at each initial P concentration was compared (Table 2.4). The percentage of the P adsorbed decreased with increasing the initial P concentration for almost every resin. On average, the addition of nitrate led to a decrease in P adsorption by 5.3%, 6.4%, and 0.8% for HPR9200, HPR9600 and IRA67, respectively, while the addition of sulfate led to a decrease by 12.3%, 32.4%, and 5.4%, respectively. Therefore, IRA67 has the most resistance to the influence of co-existing ions among the three resins. HPR9600 not only has the lowest P adsorption capacity, but also has a low affinity for P since it is easily interfered by other anions.

For hybrid resins, the addition of nitrate led to a decrease in P adsorption by 2.3%, 1.8%, and 0.4% for FerrIX™A33E, Hybrid HPR9600 and Hybrid IRA67, respectively, while the addition of sulfate led to a decrease in P adsorption by 4.2%, 30.0%, and 5.3%, respectively. Compared with their respective pure resins, the iron-loading process significantly reduced the influence of nitrate on P adsorption. For HPR9200 and its respective hybrid resin FerrIX™A33E, the influence of sulfate also reduced from 12.3% to 4.2%. The other two pairs did not show a significant influence of the iron-loading on the resistance of co-existing sulfate, possibly because the loaded iron content was too low.

The result of the interference effect of nitrate and sulfate on P adsorption in this study is in accordance with the previous research. It is generally known that anion exchange resin could not have a very high affinity for a specific anion due to the non-specific adsorption mechanism. Kunin and Myers (1947) found that several anions, including nitrate and sulfate, had higher exchange potentials than phosphate on a

polyamine anion exchange resin, Amberlite IR4B. Other studies like Christensen and Posner (1980) and Kunin and Myers (1947) also showed a similar result with greater retention of other anions over phosphate. Boari et al. (1976) investigated a series of anion exchangers for their selectivity for P adsorption and concluded that hydrostatic interactions had great importance in determining resin adsorption selectivity. They found a direct correlation between resin basicity and P affinity, where weak-base resins had a higher affinity for P than did strong-base resins.

An increase in the affinity for P after iron-loading is also observed in other hybrid resin studies. For example, Blaney et al. (2007) synthesized a hybrid anion exchanger by impregnating iron oxides in a strong-base anion exchange resin IRA-900. The hybrid resin showed a high affinity for P in the presence of other commonly encountered anions like chloride and bicarbonate. The P uptake was also not noticeably influenced by competing sulfate ions. Pan et al. (2009) reported a similar result that an iron-loaded hybrid resin was resistant to interference by common monovalent anions. Although the addition of sulfate from 0 to 100 mg/L inhibited P adsorption, the further increase in sulfate concentration from 100 to even 1,500 mg/L did not lead to a further negative influence. Since the mechanism of P adsorption on hybrid resins is a combination of electrostatic interactions of the functional groups of resins and P inner-sphere complexation in loaded iron hydroxides, it is reasonable to say that the iron-loading treatment provides a higher preference for P adsorption in the resin and better resistance to interference by other co-existing anions (Cumbal and SenGupta, 2005; Sengupta and Pandit, 2011; O'Neal and Boyer, 2013; Acelas et al., 2015).

2.3.3. Kinetics of P adsorption in pure anion exchange resins and hybrid resins

2.3.3.1. Kinetics of P adsorption in pure anion exchange resins

For all three resins, the P adsorption was shown as a biphasic process. P adsorption increased with time in the first 240 minutes as shown in Fig. 2.5 and Fig. 2.6, after which an equilibrium reached as indicated by a flatted kinetic curve (not shown in the figures). The kinetic data of the P adsorption were fitted with different kinetic models, including the pseudo-first-order model (Ho and McKay, 1999), pseudo-second-order model (Ho

and McKay, 2000), Elovich model (Low, 1960), and intra-particle diffusion model (Weber and Morris, 1963). The linear fitting plot of each model is shown in Fig. 2.11-14 (a-c). The parameters of these kinetic models are summarized in Table 2.5.

(1) Pseudo-first-order model and pseudo-second-order model

The Pseudo-first-order model (also known as the Lagergren rate equation) is the most widely used rate equation for the sorption of a solute from a liquid solution (Ho et al., 2000). The model describes non-reversible sorption processes governed by the first-order rate equation, assuming that the rate of chemisorption controls the overall sorption kinetics, sorption only occurs on a monolayer localized sites, and the sorbed ions do not interact with each other (Largitte and Pasquier, 2016). The pseudo-second-order model describes sorption processes governed by the second-order rate equation.

For all three anion exchange resins, the pseudo-first-order model did not fit well with the kinetic data (Fig. 2.11, $R^2 < 0.5$ for both HPR9200 and IRA67) except for HPR9600 at 20 mg/L initial P concentration ($R^2 = 0.926$). However, the pseudo-second-order model showed a very high R^2 for the kinetic data obtained with all the three resins (Fig. 2.12, $R^2 > 0.999$). In addition, the term $k_2 {q_e}^2$ from the pseudo-second-order model is considered to be an indication of the initial rate of a sorption process (Lalley et al., 2016). While the rate constant k_2 decreased when the initial P concentration increases from 10 mg/L to 20 mg/L, the initial sorption rate increased from 1.11, 0.17, 0.97 mg/(g min) to 2.55, 0.253, 3.628 mg/(g min) for HPR9200, HPR9600 and IRA67, respectively. Therefore, the initial sorption increased with the higher initial P concentration in solution, and the sequence of initial sorption rates among the three resins is consistent with their phosphate adsorption capacities.

(2) Elovich model and intra-particle diffusion model

The Elovich model, first proposed by Roginsky and Zeldovich in 1934, is another common kinetic model that describes chemisorption well. The model assumes that there are interactions between the sorbed ions and the energy of adsorption increases linearly with the surface coverage (Haerifar and Azizian, 2013; Largitte and Pasquier, 2016).

The Elovich model did not fit well for HPR9200 and IRA67 with either 10 or 20 mg/L initial P concentration (Fig. 2.13, $R^2 < 0.652$), and relatively better for HPR9600 ($R^2 = 0.861, 0.879$ for the initial 10 and 20 mg P/L). The R^2 value of the Elovich model was greater than that of the pseudo-first-order model except for the data of HPR9600 at initial 20 mg P/L, but it was not as good as the fitting results of the pseudo-second-order model. However, a much better fitting by the Elovich model could be obtained ($R^2 > 0.807$) when the fitting is conducted only for the first 60 minutes. It also indirectly indicates a rapid chemisorption mechanism of the P adsorption process.

In addition to the adsorption process within the adsorptive and the external surface of a sorbent, an overall sorption process also includes the mass transfer of solutes from the bulk solution to the sorbent surface (film diffusion) and the internal diffusion of the adsorptive to the sorption sites (pore diffusion). Due to the operation of rapid mixing, the film diffusion process tends not to become the rate-limiting step in a batch experimental system (Assumptions, 1971; Ho et al., 2000; Tan and Hameed, 2017). To further evaluate the diffusion process, the kinetic sorption data of this experiment were also modeled using the intra-particle diffusion model (Weber and Morris, 1963).

The intra-particle diffusion model did not fit well with the kinetic data in this experiment as shown in Fig. 2.13. However, the fitting curves showed an apparent biphasic feature, indicating that two steps occurred during the sorption process. A good fitting was obtained ($R^2 > 0.807$) when the model fitting is conducted using only the data of first 60 minutes. It indicated that the rate of initial sorption process is controlled by pore diffusion. The subsequent flatted phase in the kinetic curves reflects a slower diffusion into micropores and the final equilibrium stage.

Overall, the modeling of the kinetic data provided meaningful information about the controlling mechanism of the sorption of phosphate in anion exchange resins. Different initial P concentrations did not have a strong influence on the R^2 values of different models. No matter at 10 or 20 mg/L initial P concentration, the kinetic data of the three resins were best fitted by the pseudo-second-order model. This fitting result indirectly suggests that the mechanism of phosphate adsorption by anion exchange resins is primary chemisorption, which is in agreement with the rapid removal of water pollutants by ion exchangers in previous studies (Ho et al., 2000; Paul Chen et al., 2002; Awual and Jyo,

2011; Awual et al., 2011). As for the comparison of kinetic performance between the three kinds of resins, no large difference was found in this study, since the adsorption of P by all three resins was fast even at high initial P concentration. The second-order rate constant of the strong-base polystyrene resin HPR9200 (0.136 g/(mg min)) was relatively higher than for the weak-base polyacrylic resin IRA67 (0.111 g/(mg min)) or the weak-base polystyrene resin HPR9600 (0.106 g/(mg min)). For comparison, it was reported in previous studies that polyacrylic resins could have faster kinetics on P adsorption due to its hydrophilic property (Boari et al., 1976), and Awual and Jyo (2011) demonstrated a higher kinetic performance of a weak-base resin Diaion WA20 than a strong-base resin Diaion SA10A.

2.3.3.2. Kinetics of P adsorption in hybrid resins

The kinetic data of P adsorption in the three hybrid resins with initial P concentrations at 10 and 20 mg/L are shown in Fig. 2.9 and Fig. 2.10. The results are similar to those in their respective pure resins (Fig. 2.7 and Fig. 2.8). The P adsorption process was biphasic. The kinetics of the adsorption process was also studied by fitting the four kinetic models: pseudo-first-order model, pseudo-second-order model, Elovich model, and intra-particle diffusion model. The linear fitting plot of each model is shown in Fig. 2.11-14 (d-f). The parameters of these kinetic models are summarized in Table 2.6.

Judging from R^2 of the fitting with different models, the kinetic data of the hybrid resins were also best fitted by the pseudo-second-order model ($R^2 > 0.999$), followed by the Elovich model and the pseudo-first-order model ($0.412 < R^2 < 0.887$), and least fitted by the intra-particle diffusion model ($R^2 < 0.578$), regardless of whether the initial P concentration was 10 or 20 mg/L. Therefore, P adsorption in hybrid resins is also dominantly a chemisorption process. Other conclusions drawn from the kinetic models were also similar to that of pure resins. For example, the higher $k_2 {q_e}^2$ of the pseudo-second-order model at 20 mg/L initial P concentration indicated a stronger initial sorption than for the 10 mg/L group. The two-phase linearity correlation in the fitting plot of the intra-particle diffusion model indicated a fast diffusion process in the initial stage of P adsorption.

The iron-loading treatment increased the kinetic performance of HPR9600 since the second-order rate constant (k_2) increased from 0.106 to 0.127 g/(mg min) and from 0.050 to 0.067 g/(mg min) at the initial P concentration of 10 and 20 mg/L, respectively. However, Hybrid HPR9200 and Hybrid IRA67 showed decreased kinetic rates in both P concentration groups compared with their respective pure resins. The k_2 of Hybrid HPR9200 was 0.080 g/(mg min) while that of HPR9200 was 0.136 g/(mg min) at the initial P concentration of 10 mg/L. The k_2 of Hybrid IRA67 was 0.066 g/(mg min) while that of IRA67 was 0.104 g/(mg min) at the initial P concentration of 20 mg/L. The adsorption of phosphate ions could be slowed if the reactive sites of resins are partly blocked by iron oxide coatings.

Although there was little comparative study of the kinetics of P adsorption before and after metal oxide-loading treatment in previous research, several studies have been reported involving kinetic analysis of the P adsorption of hybrid resins. For instance, Ding et al. (2012) conducted P adsorption experiments with an iron oxide-loaded polyacrylic resin. They reported a sharp increase of P adsorption in the first 10 minutes and then a slight increase after 30 minutes, which was similar to the kinetic data in this study. The kinetic data were also fitted well with the pseudo-second-order model. Likewise, Sendrowski and Boyer (2013) also reported a rapid initial P adsorption and the best fitting of the pseudo-second-order kinetic model in the study of phosphate removal from urine using a hybrid anion exchange resin. Acelas et al. (2015) modified an anion exchange resin with three kinds of metal loading - hydrated ferric oxide, hydrated zirconium oxide, and hydrated copper oxide. The kinetic performance of the three hybrid resins were both fitted well in the pseudo-second-order model, indicating the chemisorption mechanism. And their linear fitting of the intra-particle diffusion model also showed multi-linearity as observed in this study. Overall, hybrid resins can maintain highly efficient performances of P removal, demonstrating that they can be a promising adsorbent for the removal of P in aquatic environments.

2.4. Conclusions

This study showed that the type of resin matrix, resin functional groups, and iron-loading treatment influence the P adsorption performance of anion exchange resins.

The polyacrylic resin had the highest P adsorption capacity among the three tested anion exchange resins. It also had a higher affinity with phosphate compared with the polystyrene resins, which was reflected by the better resistance to the interference of co-existing nitrate and sulfate ions. Polyacrylic resins were also a better parent material to synthesize hybrid resin since iron loading was greater than with polystyrene resins under a same synthesis condition. The comparison between a strong-base resin and a weak-base resin indicated that the former could provide a higher P adsorption capacity and affinity.

The effects of iron oxide-loading treatment on P adsorption performance were similar in all three resins. The P adsorption capacity was slightly decreased because goethite particles blocked the micropores of parent resins, resulting in a decrease in total surface area. But hybrid resins showed better resistance to the interference of co-existing nitrate and sulfate than did respective pure resins.

The P adsorption kinetics in the pure resins and the hybrid resins are biphasic, characterized by fast adsorption during the first 30 minutes followed by slow adsorption with increasing time. Regardless of initial P concentration and resin types, the kinetics of P adsorption were best fitted by the pseudo-second-order model.

Overall, polyacrylic matrix, strong-base resin functional groups, and iron oxide-loading treatment are properties of anion exchange resins to increase P adsorption. The iron oxide loading treatment might be one of the best surface modifications to enhance the P adsorption process, suggesting potential application for P removal in aquatic environments.

2.5. Figures

Fig. 2.1. Photo of anion exchange resins. First row (left to right): HPR9200; HPR9600; and IRA67. Second row (left to right): hybrid HPR9200; hybrid HPR9600; and hybrid IRA67.

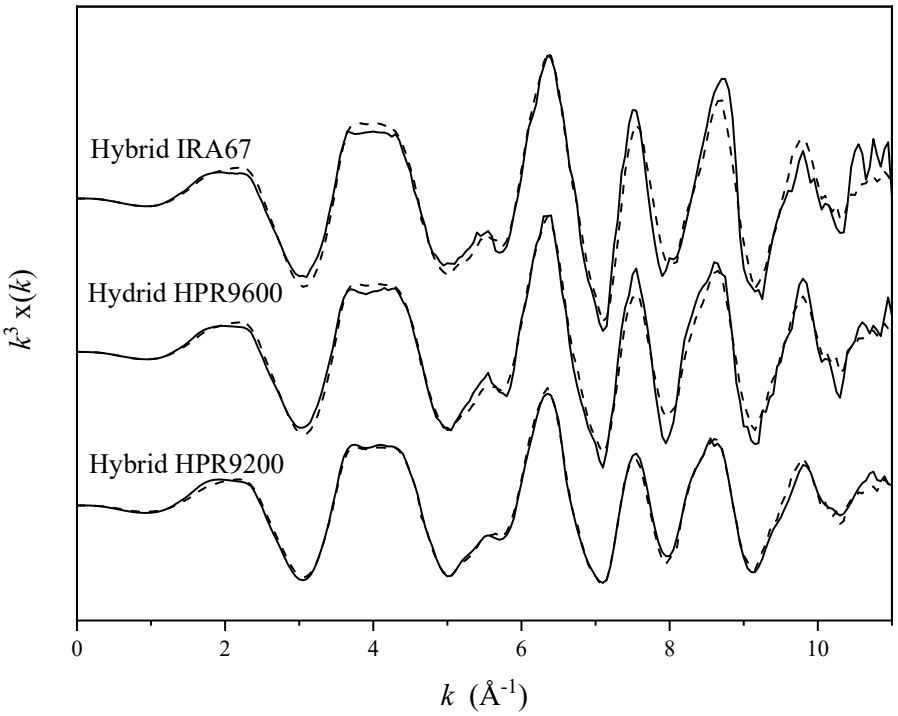

Fig. 2.2. Results of linear combination of reference compound X-ray absorption spectroscopy (XAS) spectra fit of hybrid HPR9200 (i.e., FerrIX™A33E), hybrid HPR9600, and hybrid IRA67. Black solid line and dashed line represent the normalized k3 weighted XAS spectra and fit, respectively. The parameters of the fit are shown in Table 2.

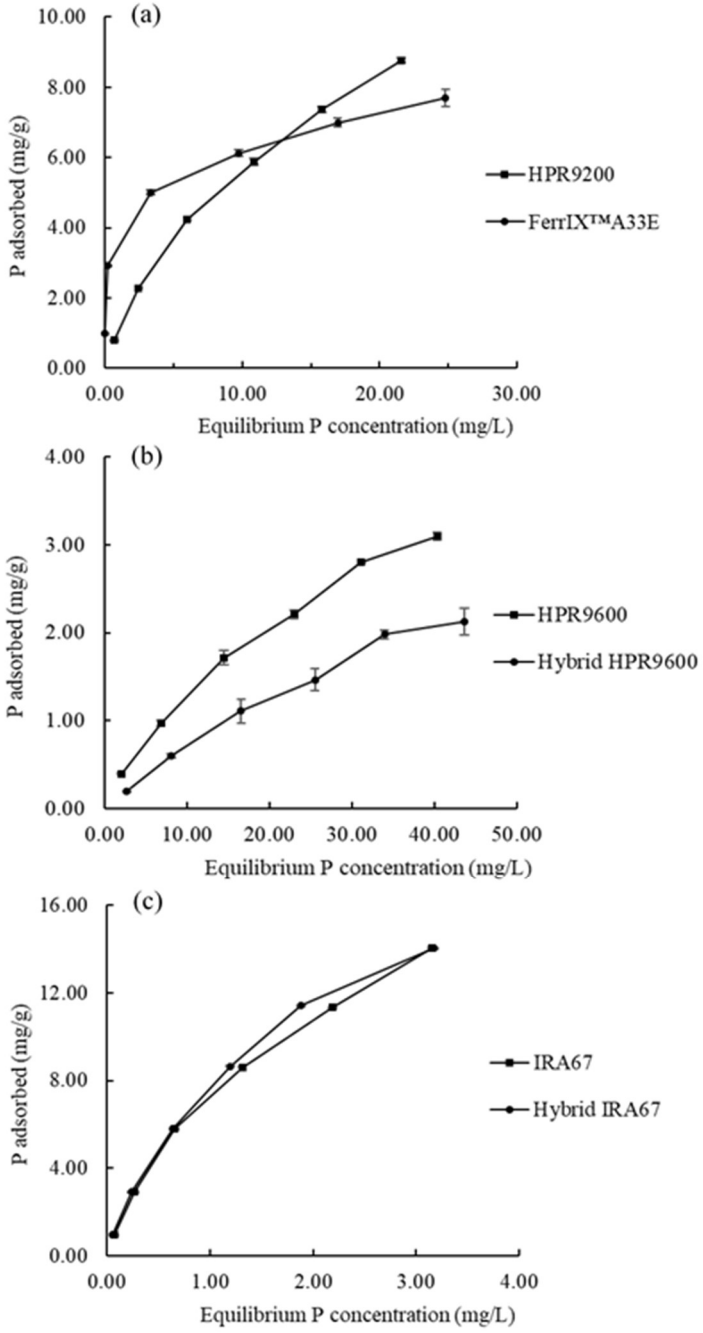

Fig. 2.3. Phosphate adsorption isotherms at pH 7.5 for anion exchange resins and respective hybrid resins: (a) HPR9200 and FerrIX™A33E (i.e., hybrid HPR9200), (b) HPR9600 and Hybrid HPR9600, and (c) IRA67 and Hybrid IRA67.

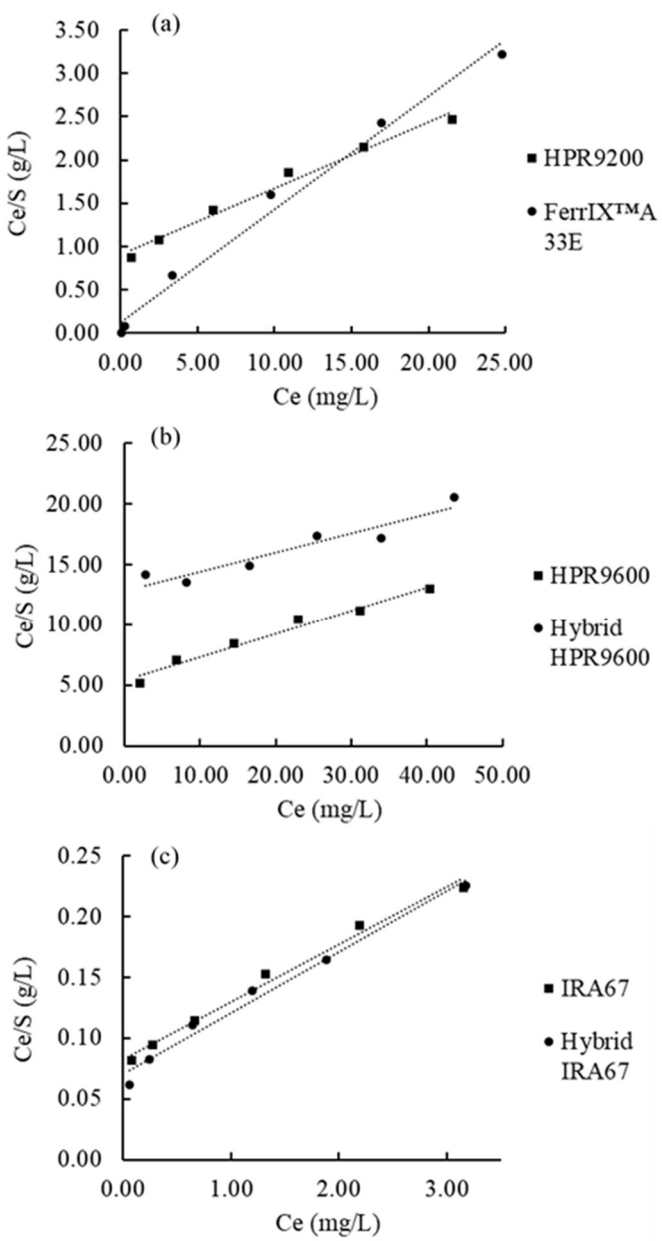

Fig. 2.4. Linear fitting plot of Langmuir model for the isotherm data shown in Fig. 2.3. (a) HPR9200 and FerrIX™A33E (i.e., hybrid HPR9200), (b) HPR9600 and Hybrid HPR9600, and (c) IRA67 and Hybrid IRA67.

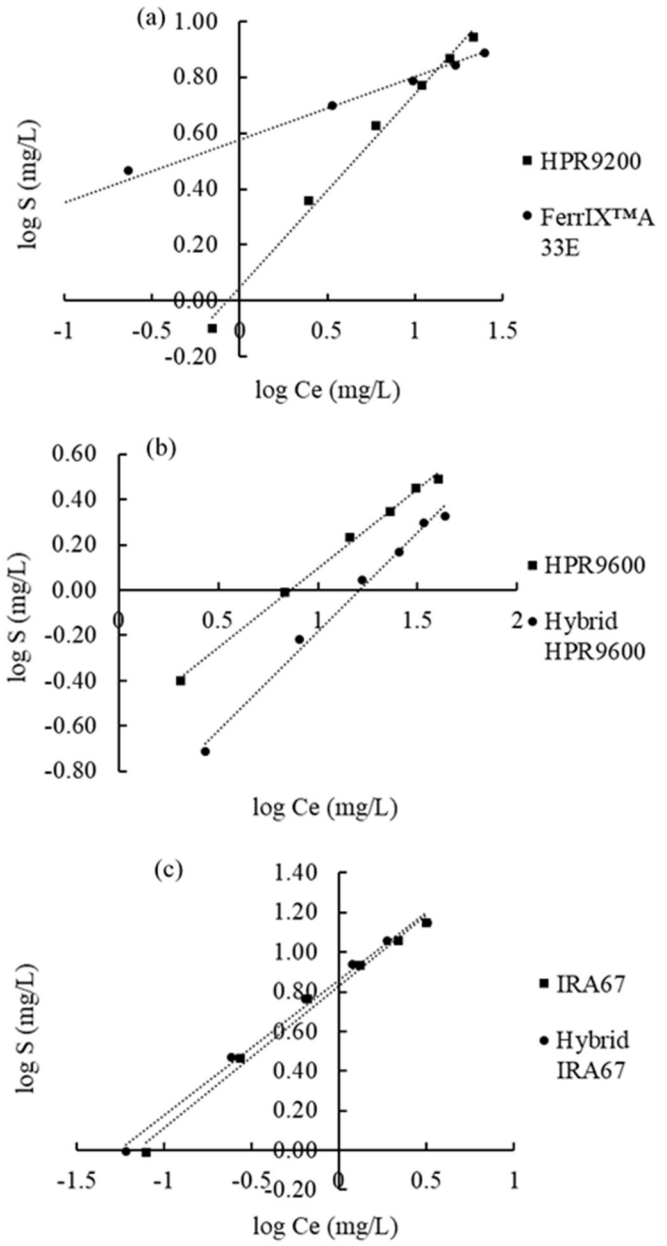

Fig. 2.5. Linear fitting plot of Freundlich model for the isotherm data shown in Fig. 2.3 (a) HPR9200 and FerrIX™A33E (i.e., hybrid HPR9200), (b) HPR9600 and Hybrid HPR9600, and (c) IRA67 and Hybrid IRA67.

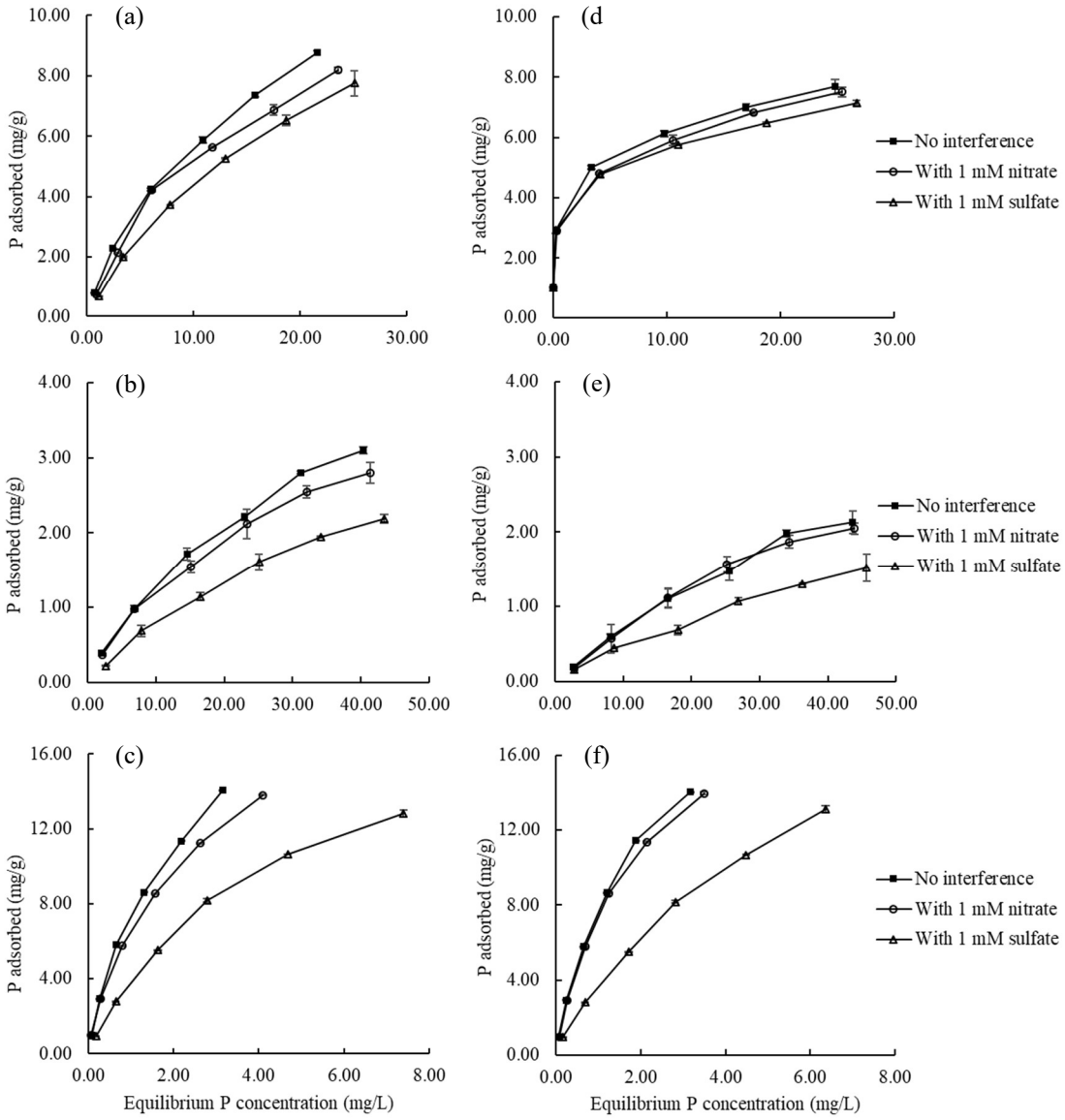

Fig. 2.6. Phosphate adsorption isotherm in anion exchange resins and respective hybrid resins in the presence of interfering ions (nitrate and sulfate). (a) HPR9200, (b) HPR9600, (c) IRA67; and their corresponding hybrid resins (d) FerrIX™A33E (i.e., hybrid HPR9200), (e) Hybrid HPR9600, (f) Hybrid IRA67.

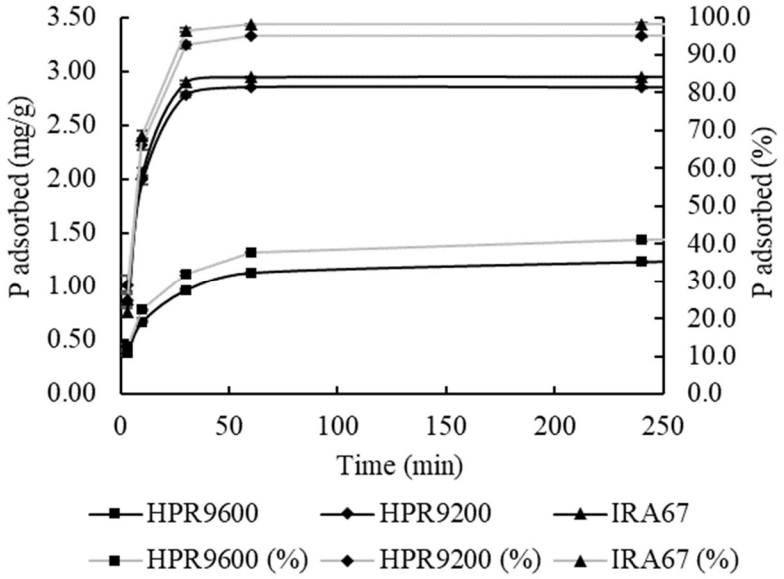

Fig. 2.7. Phosphate adsorption kinetics in anion exchange resins under initial P concentration of 10 mg/L. The curves are presented for the first 240 minutes, after which the adsorption reached equilibrium as indicated by flatted curves.

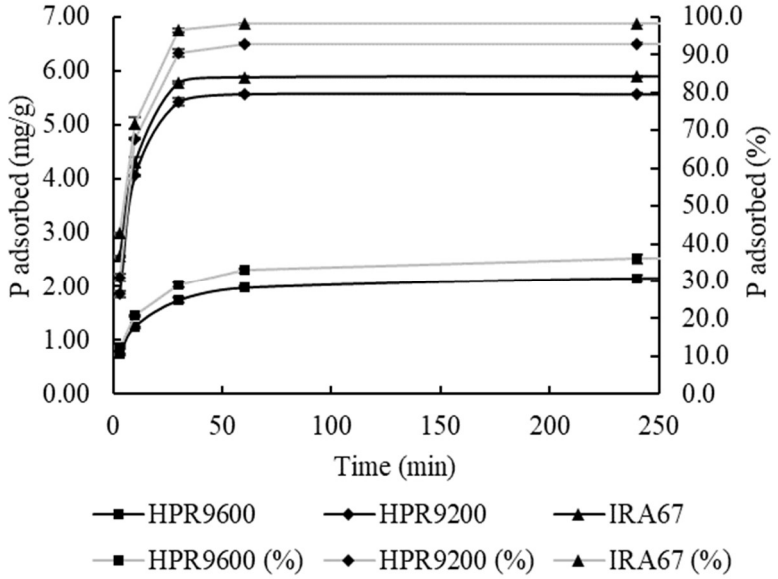

Fig. 2.8. Phosphate adsorption kinetics in anion exchange resins under the initial P concentration at 20 mg/L. The curves are presented for the first 240 minutes, after which the adsorption reached equilibrium as indicated by flatted curves.

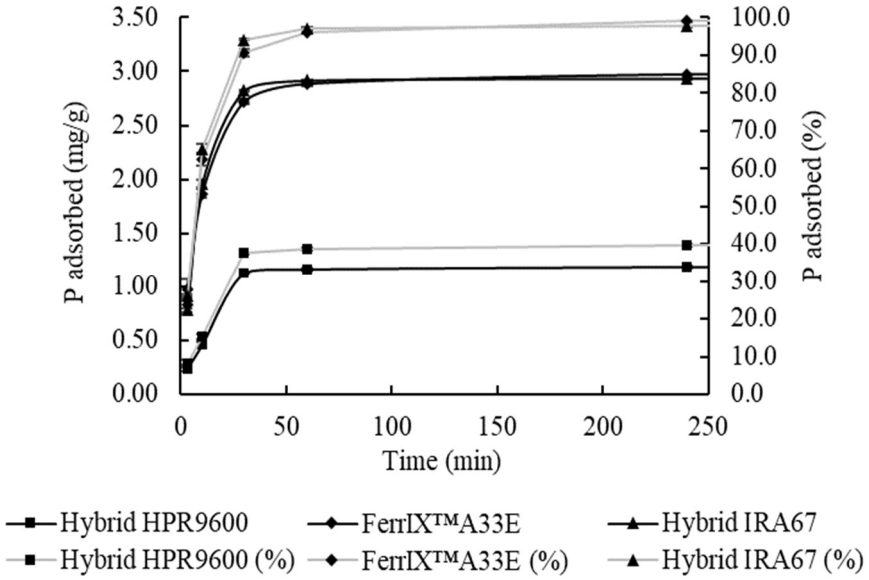

Fig. 2.9. Phosphate adsorption kinetics in hybrid resins under the initial P concentration at 10 mg/L. The curves are presented for the first 240 minutes, after which the adsorption reached equilibrium as indicated by flatted curves.

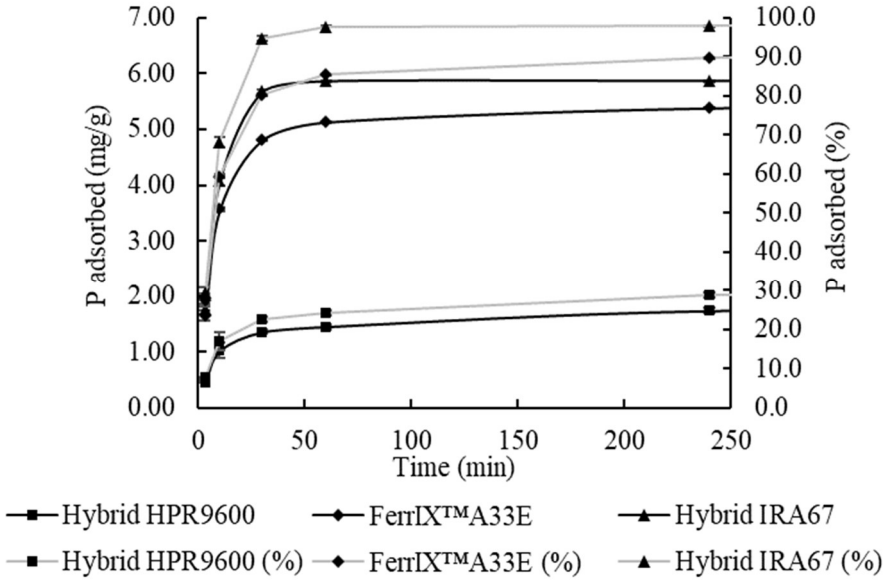

Fig. 2.10. Phosphate adsorption kinetics in hybrid resins under the initial P concentration at 20 mg/L. Kinetic curves are presented for the first 240 minutes, after which the adsorption reached equilibrium as indicated by a flatted phase.

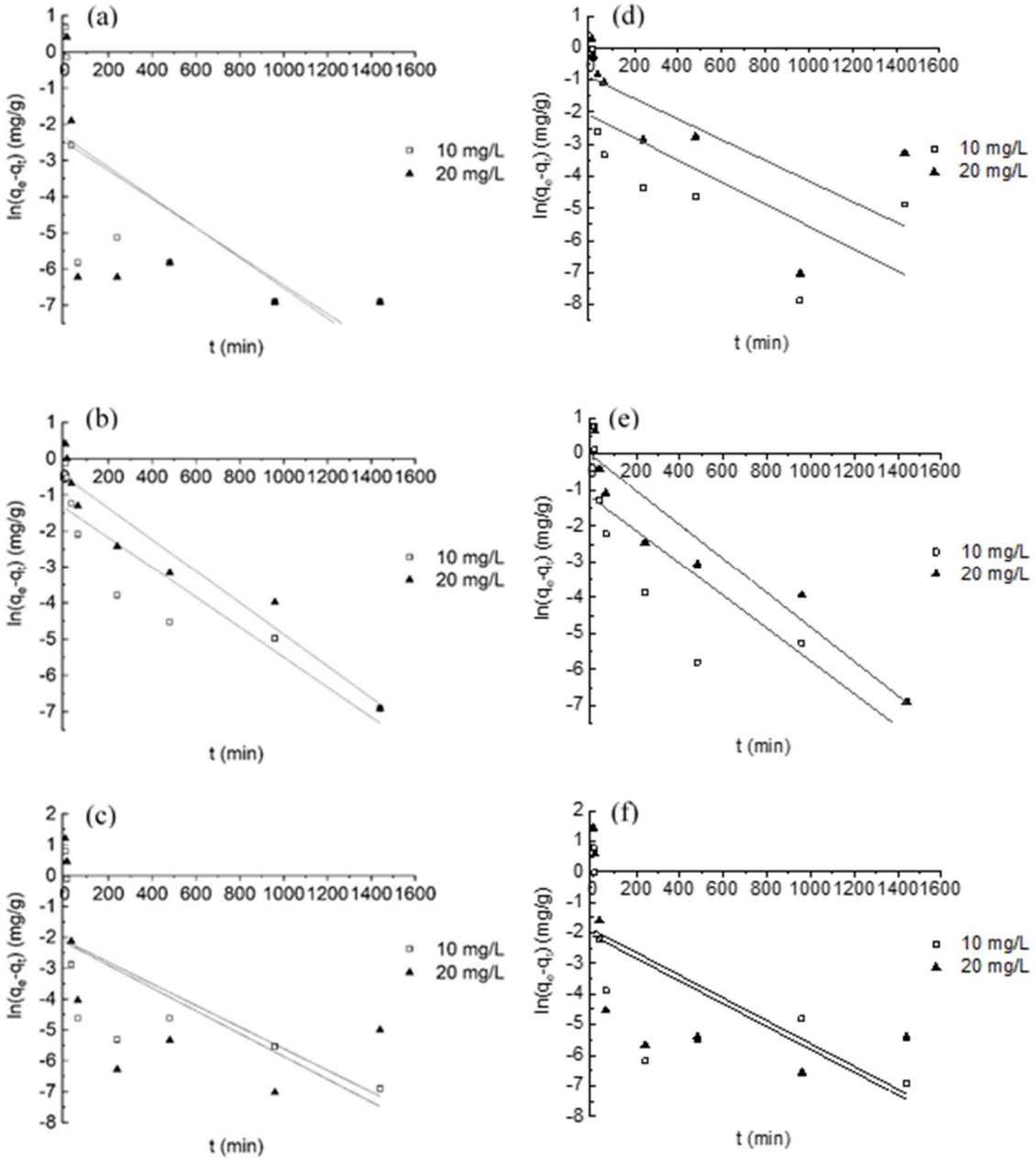

Fig. 2.11. Pseudo first-order model fit of kinetic data of P adsorption in (a) HPR9200, (b) HPR9600, (c) IRA67, (d) FerrIX™A33E, (e) Hybrid HPR9600, and (f) Hybrid IRA67. The fitness and model parameters are summarized in Table 2.5 and Table 2.6.

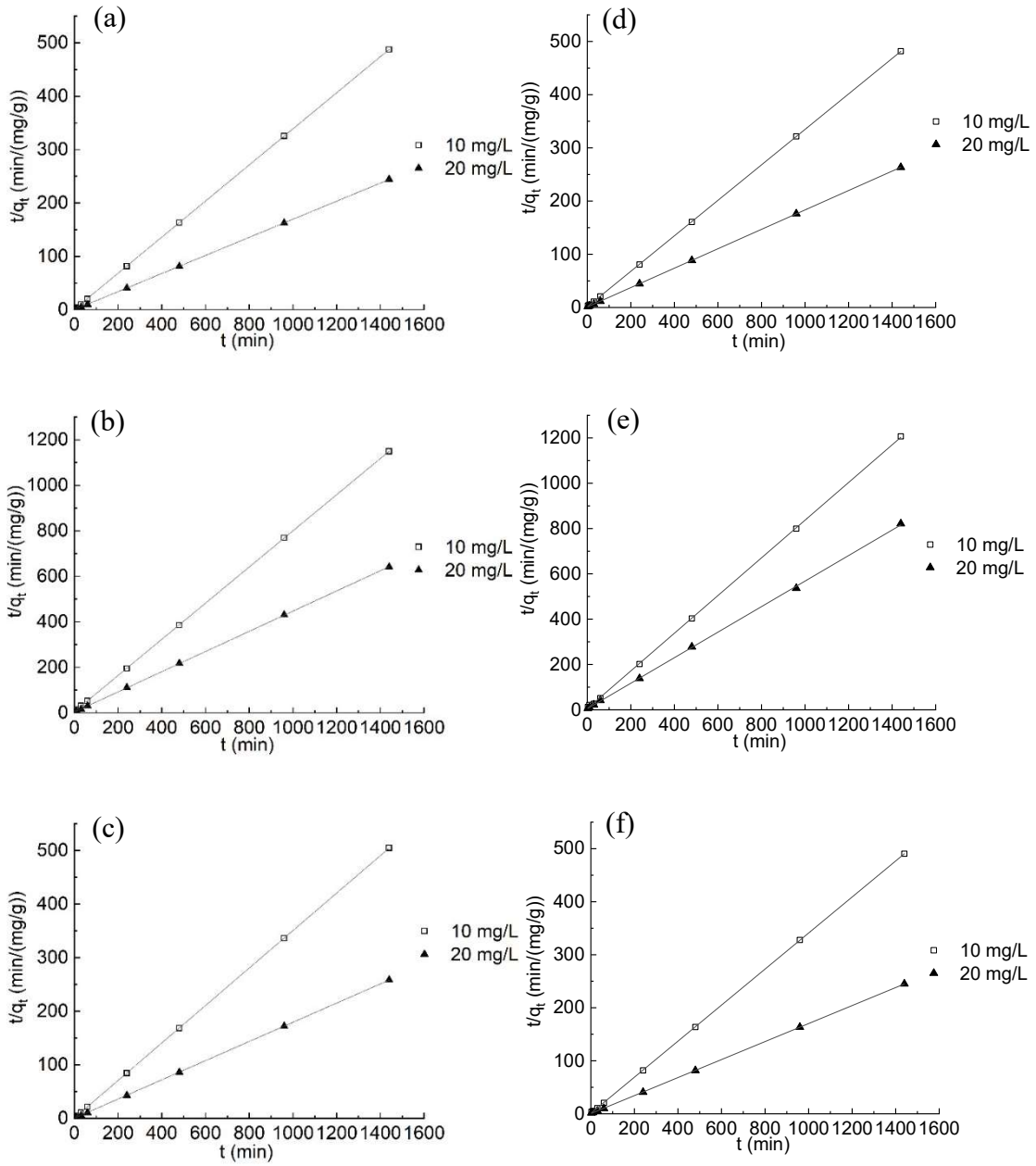

Fig. 2.12. Pseudo second-order model fit of kinetic data of P adsorption in (a) HPR9200, (b) HPR9600, (c) IRA67, (d) FerrIX™A33E, (e) Hybrid HPR9600, and (f) Hybrid IRA67. The fitness and model parameters are summarized in Table 2.5 and Table 2.6.

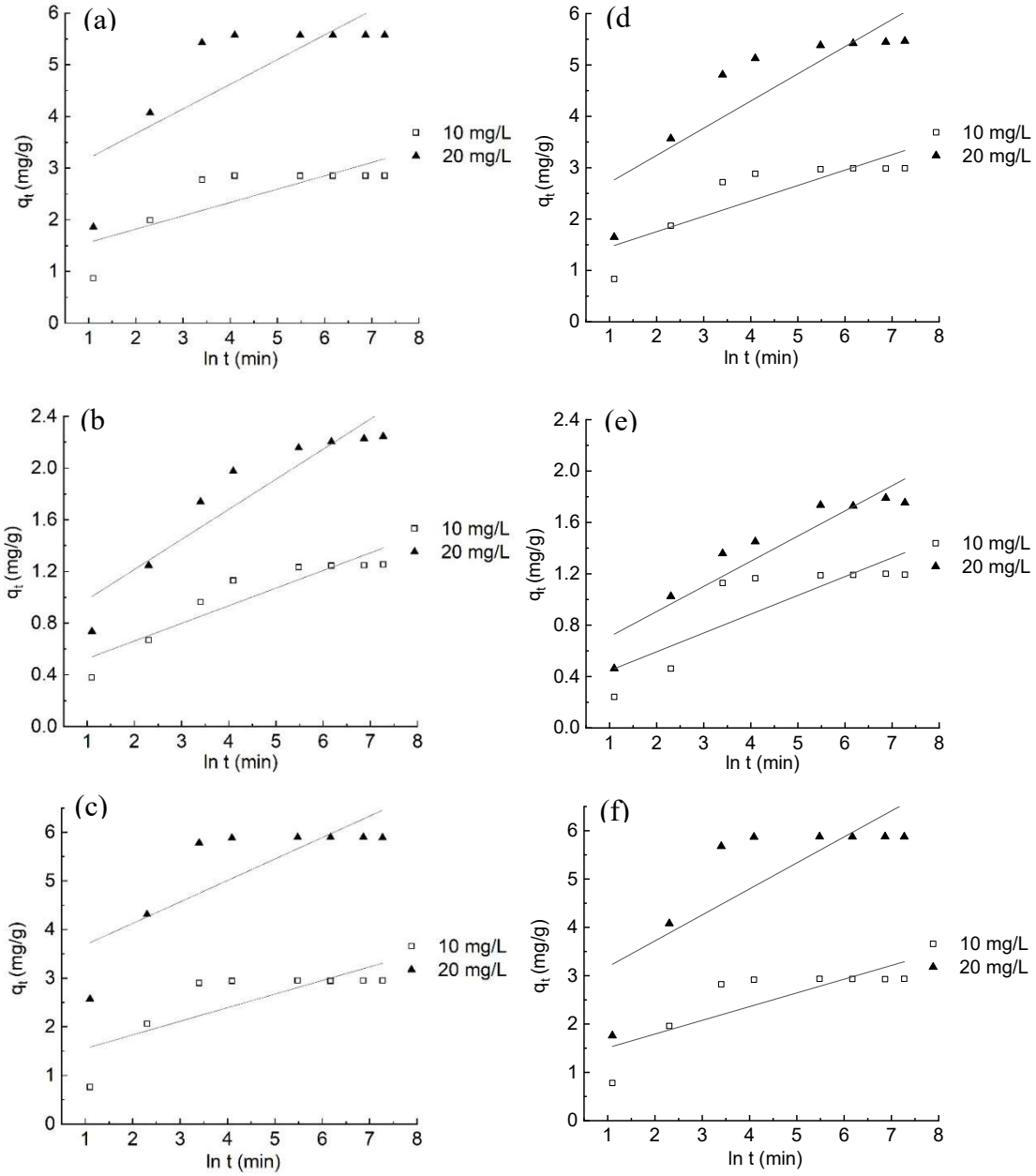

Fig. 2.13. Elovich model fit of kinetic data of P adsorption in (a) HPR9200, (b) HPR9600, (c) IRA67, (d) FerrIX™A33E, (e) Hybrid HPR9600, and (f) Hybrid IRA67. The fitness and model parameters are summarized in Table 2.5 and Table 2.6.

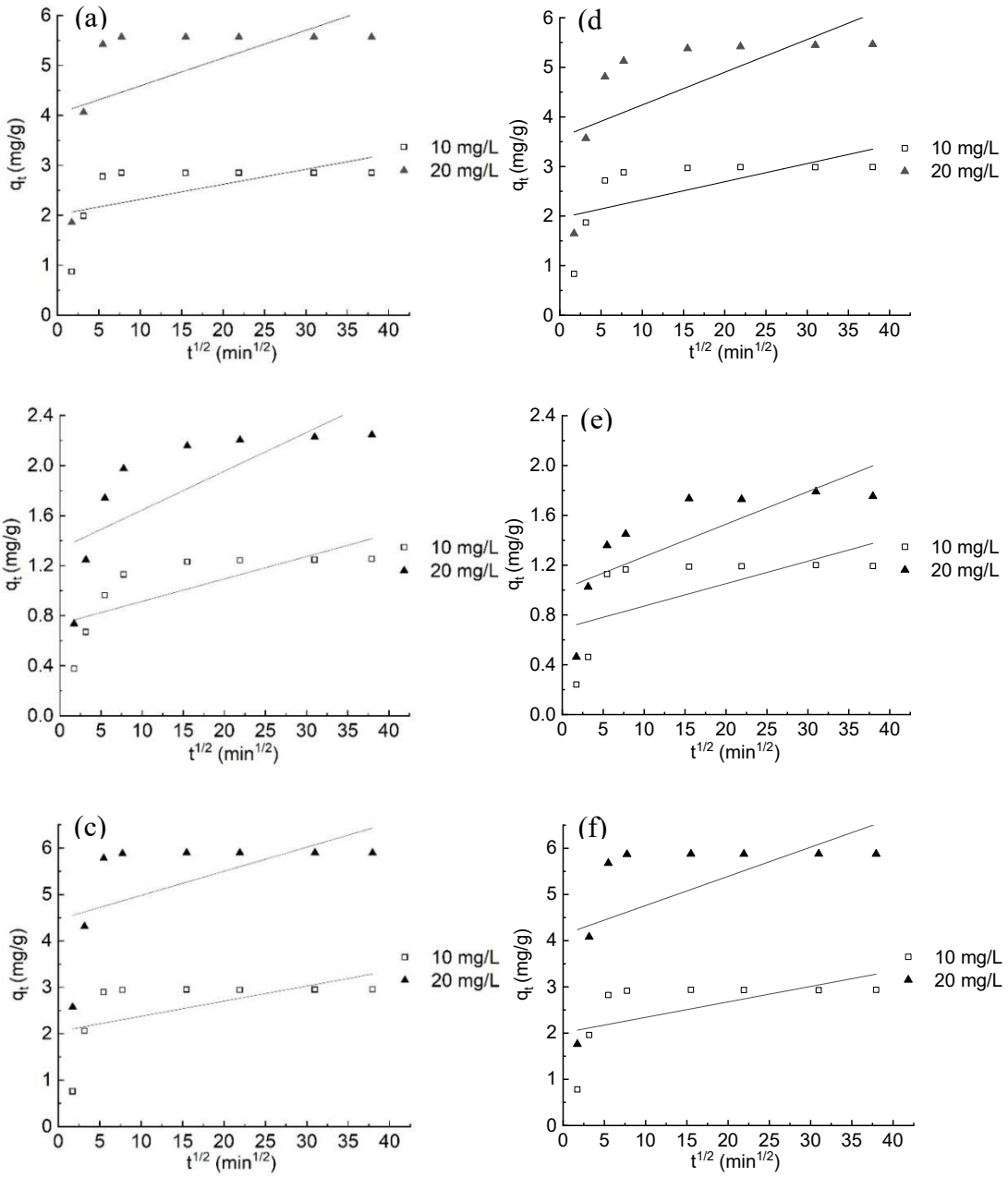

Fig. 2.14. Intra-particle diffusion model fit of kinetic data of P adsorption in (a) HPR9200, (b) HPR9600, (c) IRA67, (d) FerrIX™A33E, (e) Hybrid HPR9600, and (f) Hybrid IRA67. The fitness and model parameters are summarized in Table 2.5 and Table 2.6.

2.6. Tables

Table 2.1. General characteristics of anion exchange resins and their respective hybrid resins used in this study.

Resin	Matrix	Structure type	Type of functional groups	Physical form	Particle size (μm)	Iron content (mg/g)	Total surface area (m^2/g)
AMBERLITE™ HPR 9200	Polystyrene-DVB	Macroporous	Strong-base	White, opaque, spherical beads	640 ± 50	0	1625 ± 21
FerrIX™A33E (Hybrid HPR 9200)	Polystyrene-DVB	Macroporous	Strong-base	Brown, opaque, spherical beads	750 ± 450	196.0 ± 3.0	810 ± 38
AMBERLITE™ HPR 9600	Polystyrene-DVB	Macroporous	Weak-base	Cream, opaque, spherical beads	550 ± 50	0	672 ± 40
Hybrid HPR9600	Polystyrene-DVB	Macroporous	Weak-base	Reddish cream, spherical beads	550 ± 50	5.5 ± 0.4	668 ± 14
AMBERLITE™ IRA67	Polyacrylic	Gel	Weak-base	White, translucent, spherical beads	625 ± 125	0	2084 ± 7
Hybrid IRA67	Polyacrylic	Gel	Weak-base	Reddish brown, spherical beads	625 ± 125	13.4 ± 0.8	3515 ± 21

Table 2.2. Linear combination reference compound fit of Fe K-edge XAS spectra of hybrid resins.

Samples	Goethite	Hematite	*R*-factor
FerrIX™A33E (Hybrid HPR9200)	1.00 (0)	---	0.010
Hybrid HPR9600	0.94 (0)	0.06 (0)	0.036
Hybrid IRA67	0.82 (4)	0.18 (2)	0.060

Table 2.3. Parameters of isotherm models in phosphate adsorption by resins. Qm and Km represent the maximum adsorption (mg P/g) and a parameter related to the bonding strength (L/mg) in the Langmuir model, respectively. Kf and n are a parameter related to the adsorption capacity and a parameter related to the intensity of adsorption in the Freundlich model, respectively.

Resin	Langmuir model			Freundlich model		
	Q_m (mg/g)	K_m (L/mg)	R^2	n	K_f ($mg^{1-1/n}$ $L^{1/n}/g$)	R^2
HPR9200	13.158	0.083	0.983	1.442	1.117	0.993
HPR9600	5.173	0.036	0.976	1.429	0.248	0.997
IRA67	21.186	0.570	0.988	1.392	6.790	0.989
FerrIX™A33E	7.686	0.948	0.983	4.435	3.759	0.983
Hybrid HPR9600	6.329	0.012	0.897	1.142	0.087	0.991
Hybrid IRA67	19.841	0.719	0.983	1.467	7.263	0.993

Table 2.4. Percentage P adsorption in anion exchange resins and respective hybrid resins as a function of initial P concentrations. The experiments were conducted in 10 mM NaCl with or without 1 mM $NaNO_3$/Na_2SO_4.

Resin	Interference ions	Initial P concentration (mg/L)					
		3.33	10	20	30	40	50
HPR9200	Control	79.74	75.93	70.69	65.27	61.41	58.45
	With 1 mM nitrate	73.60	71.47	70.19	62.48	57.23	54.70
	With 1 mM sulfate	67.17	66.62	61.89	58.55	54.32	51.71
HPR9600	Control	39.55	32.49	28.59	24.56	23.36	20.66
	With 1 mM nitrate	37.31	32.69	25.66	23.57	21.22	18.66
	With 1 mM sulfate	22.17	22.93	19.03	17.85	16.21	14.58
IRA67	Control	97.66	97.30	96.75	95.69	94.62	93.80
	With 1 mM nitrate	97.93	97.17	96.08	94.82	93.53	91.96
	With 1 mM sulfate	94.59	93.59	91.98	90.88	88.51	85.46
FerrIX™A33E (Hybrid HPR9200)	Control	99.90	97.70	83.47	68.03	58.32	51.26
	With 1 mM nitrate	99.32	97.01	80.26	65.53	56.78	50.09
	With 1 mM sulfate	99.80	97.72	79.81	63.91	53.96	47.56
Hybrid HPR9600	Control	19.31	20.08	18.51	16.31	16.52	14.19
	With 1 mM nitrate	18.75	19.03	18.54	17.37	15.58	13.65
	With 1 mM sulfate	15.63	14.74	11.42	11.89	10.84	10.15
Hybrid IRA67	Control	98.22	97.63	96.83	96.08	95.37	93.76
	With 1 mM nitrate	97.56	97.50	96.65	95.90	94.73	93.15
	With 1 mM sulfate	95.12	93.27	91.59	90.79	88.98	87.49

Table 2.5. Parameters of various kinetic equations to model the P adsorption kinetic data in pure anion exchange resins.

Resin		HPR9200		HPR9600		IRA67	
Initial P concentration (mg/L)		10	20	10	20	10	20
Pseudo-first order model	k_1 (1/min)	0.004	0.004	0.004	0.004	0.004	0.004
	q_e (mg/g)	0.084	0.095	0.257	0.610	0.115	0.122
	R^2	0.491	0.420	0.843	0.926	0.526	0.371
Pseudo-second order model	k_2 (g/(mg min))	0.136	0.082	0.106	0.050	0.111	0.104
	q_e (mg/g)	2.860	5.587	1.259	2.255	2.960	5.907
	$k_2q_e^2$ (mg/(g min))	1.113	2.551	0.169	0.253	0.973	3.628
	R^2	1.000	1.000	1.000	1.000	1.000	1.000
Elovich model	α (mg/(L min))	40.679	141.776	2.363	5.821	26.531	683.708
	β (L/mg)	3.879	2.097	7.331	4.296	3.573	2.264
	R^2	0.641	0.633	0.861	0.879	0.625	0.652
Intra-particle diffusion model	k_d (mg/(g $min^{1/2}$))	0.030	0.056	0.018	0.031	0.033	0.052
	C	2.018	4.038	0.736	1.335	2.051	4.461
	R^2	0.325	0.318	0.551	0.578	0.313	0.334

Table 2.6. Parameters of various kinetic equations to model the P adsorption kinetic data in hybrid resins.

Resin		FerrIX™A33E (Hybrid HPR9200)		Hybrid HPR9600		Hybrid IRA67	
Initial P concentration (mg/L)		10	20	10	20	10	20
Pseudo-first order model	k_1 (1/min)	0.045	0.005	0.003	0.003	0.004	0.004
	q_e (mg/g)	0.291	0.929	0.120	0.391	0.124	0.150
	R^2	0.726	0.887	0.510	0.535	0.487	0.412
Pseudo-second order model	k_2 (g/(mg min))	0.080	0.035	0.127	0.067	0.108	0.066
	q_e (mg/g)	3.000	5.482	1.203	1.775	2.943	5.889
	$k_2q_e^2$ (mg/(g min))	0.719	1.056	0.184	0.212	0.934	2.300
	R^2	1.000	1.000	1.000	1.000	1.000	1.000
Elovich model	α (mg/(L min))	14.185	32.626	1.137	2.708	21.200	73.344
	β (L/mg)	3.337	1.890	6.831	5.105	3.522	1.859
	R^2	0.727	0.758	0.709	0.878	0.656	0.648
Intra-particle diffusion model	k_d (mg/(g $min^{1/2}$))	0.037	0.066	0.018	0.026	0.034	0.063
	C	1.960	3.582	0.691	1.006	2.006	4.130
	R^2	0.403	0.436	0.398	0.578	0.337	0.330

2.7. References

Acelas, N.Y., B.D. Martin, D. López, and B. Jefferson. 2015. Selective removal of phosphate from wastewater using hydrated metal oxides dispersed within anionic exchange media. Chemosphere 119: 1353–1360.

Ahiablame, L.M., I. Chaubey, D.R. Smith, and B.A. Engel. 2011. Effect of tile effluent on nutrient concentration and retention efficiency in agricultural drainage ditches. Agric. Water Manag. 98(8): 1271–1279.

Allen, S.J., G. McKay, and K.Y.H. Khader. 1989. Intraparticle diffusion of a basic dye during adsorption onto sphagnum peat. Environ. Pollut. 56(1): 39–50.

Anirudhan, T.S., B.F. Noeline, and D.M. Manohar. 2006. Phosphate removal from wastewaters using a weak anion exchanger prepared from a lignocellulosic residue. Environ. Sci. Technol. 40(8): 2740–2745.

Assumptions, B. 1971. Diffusion-Kinetic Model. Physical Chemistry. p. 171–190

Awual, M.R., and A. Jyo. 2011. Assessing of phosphorus removal by polymeric anion exchangers. Desalination 281(1): 111–117.

Awual, M.R., A. Jyo, S.A. El-Safty, M. Tamada, and N. Seko. 2011. A weak-base fibrous anion exchanger effective for rapid phosphate removal from water. J. Hazard. Mater. 188(1–3): 164–171.

Baker, L., K.L. Campbell, H.P. Johnson, and J. Hanway. 1975. Nitrate, Phosphorus, and Sulfate in Subsurface Drainage Wate. J. Environ. Qual. 4(3): 406–412.

Blaney, L.M., S. Cinar, and A.K. SenGupta. 2007. Hybrid anion exchanger for trace phosphate removal from water and wastewater. Water Res. 41(7): 1603–1613.

Boari, G., L. Liberti, and R. Passino. 1976. Selective Renovation of Eutrophic Wastes Phosphate Removal. Water Res. 10(5): 421–428.

Chabani, M., and A. Bensmaili. 2005. Kinetic modelling of the retention of nitrates by Amberlite IRA 410. Desalination 185(1–3): 509–515.

Christensen, H.H., and A.M. Posner. 1980. The interaction of phosphate with an anion exchange resin. J. Soil Sci. 31(3): 447–455.

Collos, Y., F. Mornet, A. Sciandra, N. Waser, A. Larson, et al. 1999. An optical method for the rapid measurement of micromolar concentratrions of nitrate in marine phytoplankton cultures. J. Appl. Phycol. 11(2): 179–184.

Cumbal, L., and A.K. SenGupta. 2005. Arsenic removal using polymer-supported hydrated iron(III) oxide nanoparticles: Role of Donnan membrane effect. Environ. Sci. Technol. 39(17): 6508–6515.

Das, J., B.S. Patra, N. Baliarsingh, and K.M. Parida. 2006. Adsorption of phosphate by layered double hydroxides in aqueous solutions. Appl. Clay Sci. 32(3–4): 252–260.

Ding, L., C. Wu, H. Deng, and X. Zhang. 2012. Adsorptive characteristics of perchlorate from aqueous solutions by MIEX resin. J. Colloid Interface Sci. 376(1): 224–232.

Dupont. 2019. https://www.dupont.com/water/amberlite-data-sheets.html.

Fierro, V., V. Torné-Fernández, D. Montané, and A. Celzard. 2008. Adsorption of phenol onto activated carbons having different textural and surface properties. Microporous Mesoporous Mater. 111(1–3): 276–284.

Haerifar, M., and S. Azizian. 2013. Mixed surface reaction and diffusion-controlled kinetic model for adsorption at the solid/solution interface. J. Phys. Chem. C 117(16): 8310–8317.

He, Z., V. Baligar, K. Ritchey, and D. Martens. 1998. Determination of Soluble Phosphorus in the Presence of Organic Ligands or Fluoride. Soil Sci. Soc. Am. J. 62(6): 1538–1541.

Ho, Y.S., and G. McKay. 1999. The sorption of lead(II) ions on peat. Water Res. 33(2): 578–584.

Ho, Y.S., and G. McKay. 2000. The kinetics of sorption of divalent metal ions onto sphagnum moss peat. Water Res. 34(3): 735–742.

Ho, Y.S., J.C.Y. Ng, and G. McKay. 2000. Kinetics of pollutant sorption by biosorbents: Review. Sep. Purif. Methods 29(2): 189–232.

Johir, M.A.H., T.T. Nguyen, K. Mahatheva, M. Pradhan, H.H. Ngo, et al. 2016. Removal of phosphorus by a high rate membrane adsorption hybrid system. Bioresour. Technol. 201: 365–369.

Klute, A., D.L. Carter, M.M. Mortland, and W.D. Kemper. 1986. Specific Surface. John Wiley & Sons, Ltd. p. 413–423

Kunin, R., and R.J. Myers. 1947. The anion exchange equilibria in an anion exchange resin. J. Am. Chem. Soc. 69(11): 2874–2878.

Lalley, J., C. Han, X. Li, D.D. Dionysiou, and M.N. Nadagouda. 2016. Phosphate adsorption using modified iron oxide-based sorbents in lake water: Kinetics, equilibrium, and column tests. Chem. Eng. J. 284: 1386–1396.

Largitte, L., and R. Pasquier. 2016. A review of the kinetics adsorption models and their application to the adsorption of lead by an activated carbon. Chem. Eng. Res. Des. 109: 495–504.

Loganathan, P., S. Vigneswaran, J. Kandasamy, and N.S. Bolan. 2014. Removal and recovery of phosphate from water using sorption. Crit. Rev. Environ. Sci. Technol. 44(8): 847–907.

Low, M.J.D. 1960. Kinetics of chemisorption of gases on solids. Chem. Rev. 60(3): 267–312.

Mulik, J., R. Puckett, D. Williams, and E. Sawicki. 1976. Ion Chromatographic Analysis Of Sulfate And Nitrate In Ambient Aerosols. Anal. Lett. 9(7): 653–663.

Nur, T., M.A.H. Johir, P. Loganathan, T. Nguyen, S. Vigneswaran, et al. 2014. Phosphate removal from water using an iron oxide impregnated strong base anion exchange resin. J. Ind. Eng. Chem. 20(4): 1301–1307.

O'Neal, J.A., and T.H. Boyer. 2013. Phosphate recovery using hybrid anion exchange: Applications to source-separated urine and combined wastewater streams. Water Res. 47(14): 5003–5017.

Pan, B., B. Pan, W. Zhang, L. Lv, Q. Zhang, et al. 2009a. Development of polymeric and polymer-based hybrid adsorbents for pollutants removal from waters. Chem. Eng. J. 151(1–3): 19–29.

Pan, B., J. Wu, B. Pan, L. Lv, W. Zhang, et al. 2009b. Development of polymer-based nanosized hydrated ferric oxides (HFOs) for enhanced phosphate removal from waste effluents. Water Res. 43(17): 4421–4429.

Patey, M.D., M.J.A. Rijkenberg, P.J. Statham, M.C. Stinchcombe, E.P. Achterberg, et al. 2008. Determination of nitrate and phosphate in seawater at nanomolar concentrations. TrAC - Trends Anal. Chem. 27(2): 169–182.

Paul Chen, J., M.L. Chua, and B. Zhang. 2002. Effects of competitive ions, humic acid, and pH on removal of ammonium and phosphorous from the synthetic industrial effluent by ion exchange resins. Waste Manag. 22(7): 711–719.

Purolite. 2019. https://www.purolite.com/product/ferrixa33e.

Ren, J., N. Li, and L. Zhao. 2012. Adsorptive Removal of Cr (VI) from Water by Anion Exchanger Based Nanosized Ferric Oxyhydroxide Hybrid Adsorbent. Chem. Biochem. Eng. Q. 26(2): 111–118.

Sager, M. 1992. Chemical speciation and environmental mobility of heavy metals in sediments and soils. Tech. Instrum. Anal. Chem. 12(C): 133–175.

Sarkar, S., P.K. Chatterjee, L.H. Cumbal, and A.K. SenGupta. 2011. Hybrid ion exchanger supported nanocomposites: Sorption and sensing for environmental applications. Chem. Eng. J. 166(3): 923–931.

Sendrowski, A., and T.H. Boyer. 2013. Phosphate removal from urine using hybrid anion exchange resin. Desalination 322: 104–112.

Sengupta, A.K., and L.H. Cumbal. 2007. Hybrid anion exchanger for selective removal of contaminating ligands from fluids and method of manufacture thereof. : U.S. Patent 7,291,578.

Sengupta, S., and A. Pandit. 2011. Selective removal of phosphorus from wastewater combined with its recovery as a solid-phase fertilizer. Water Res. 45(11): 3318–3330.

Sowmya, A., and S. Meenakshi. 2014. A novel quaternized chitosan-melamine-glutaraldehyde resin for the removal of nitrate and phosphate anions. Int. J. Biol. Macromol. 64: 224–232.

Staicu, L.C., N. Morin-Crini, and G. Crini. 2017. Desulfurization: Critical step towards enhanced selenium removal from industrial effluents. Chemosphere 172(2017): 111–119.

Tabatabai, M.A., and W.A. Dick. 1983. Simultaneous Determination of Nitrate, Chloride, Sulfate, and Phosphate in Natural Waters by Ion Chromatography1. J. Environ. Qual. 12(2): 209–213.

Takeshita, R., I. Yoshida, and K. Ueno. 1979. Adsorption behaviour of phosphate ion on the iron (III) compleks of a chelating Resin. Bul. Chem. Soc. Japan 52(9): 2577–2580.

Tamura, H., K. Goto, T. Yotsuyanagi, and M. Nagayama. 1974. Spectrophotometric determination of iron(II) with 1,10-phenanthroline in the presence of large amounts of iron(III). Talanta 21(4): 314–318.

Tan, K.L., and B.H. Hameed. 2017. Insight into the adsorption kinetics models for the removal of contaminants from aqueous solutions. J. Taiwan Inst. Chem. Eng. 74: 25–48.

Upping, E., D.W. Thompson, M. Ohnstad, and N.B. Hetherington. 1986. Effects of ph on the release of metals from naturally-occurring oxides of mn and fe. Environ. Technol. Lett. 7(1–12): 109–114.

Weber, W., and J. Morris. 1963. Kinetics of adsorption on carbon from solution. J. Sanit. Eng. Div. 89(2): 31–60.

Yoshida, H., and W.A. Galinada. 2002. Equilibria for adsorption of phosphates on OH-type strongly basic ion exchanger. AIChE J. 48(10): 2193–2202.

You, X., D. Guaya, A. Farran, C. Valderrama, and J.L. Cortina. 2016. Phosphate removal from aqueous solution using a hybrid impregnated polymeric sorbent containing hydrated ferric oxide (HFO). J. Chem. Technol. Biotechnol. 91(3): 693–704.

Zagorodni, A.A. 2006. Ion exchange materials: properties and applications. First edit. Elsevier.

Zhang, Y., B. Pan, C. Shan, and X. Gao. 2016. Enhanced Phosphate Removal by Nanosized Hydrated La(III) Oxide Confined in Cross-linked Polystyrene Networks. Environ. Sci. Technol. 50(3): 1447–1454.

Zimmerman, B. 2016. Exploration of Ion Species in Agricultural Subsurface Drainage Waters. Iowa state university.

CHAPTER 3: NOVEL APPLICATION OF HYBRID ANION EXCHANGE RESIN FOR PHOSPHATE DESORPTION KINETICS IN SOILS: MINIMIZING RE-ADSORPTION OF DESORBED IONS

Abstract

The process of phosphate desorption from soils is difficult to measure using stirred batch techniques because of accumulation of desorbed ions in a bathing solution. To accurately measure the apparent rate coefficient of phosphate, desorption from soils, it is necessary to remove the desorbed ions. In this study, a novel hybrid (i.e., iron oxide coated) anion exchange resin was used as a sink to study long-term (7days) P desorption kinetics in intensively managed agricultural soils in the Midwestern U.S. (total phosphorus (TP): 196-419 mg/kg). The phosphate desorption kinetics in the hybrid anion exchange resin method were compared with those in the other conventional batch desorption method with pure anion exchange resins or without any sink. The extent of P desorption in the hybrid resin methods was >50% of total desorbed phosphate in the other methods. The initial kinetic rate estimated in the pseudo-second order kinetic model was also highest (3.03 to 31.35 mg/(g·hr)) in the hybrid resin method when the same soil system was compared. This is because adsorbed P in the hybrid resins was nearly irreversible. The hybrid anion exchange resin might be a new and ideal sink in measuring the P desorption process in soils and sediments.

3.1. Introduction

The desorption process of ions is one of the most important soil chemical processes influencing the availability of inorganic pollutants in soil. Along with the solid-state speciation of contaminants, the rate of release, including desorption and dissolution is critical to environmental risk assessment.

The kinetic rate is often evaluated using stirred batch desorption techniques, bathing soil particles in a solution without a sink. However, such methods have a major experimental problem, re-adsorption of desorbed ions to soils (i.e., backward reaction) and or accumulation of desorbed ions in a bathing solution. Therefore, the rate does not represent the actual apparent rate coefficient of the desorption process in soils. To overcome the problem, the stirred flow method is often used in soil chemistry and geochemistry experiments (Sparks, 1989). This method traps soil particles in a stirred-flow chamber, and a continuous flow of influent is pumped into the chamber, resulting in continuous removal of desorbed ions from the soil particles. This process will eliminate the accumulation of desorbed ions and minimize the backward reactions. This method works well in fine slit and clay fractions of soils, but it is not suited for natural soils that have sand and coarse silt fractions. In a reaction chamber, soil particles were continuously mixed using a magnetic stir bar. While fine fractions are mixed well in a chamber, coarse fractions (i.e., sand and coarse silt) settle at the bottom of the chamber where the magnetic stir bar is rotating. This will abrade coatings of sand and silt particles and or break micro-aggregates. In natural soils, coarse particles often have reactive coatings. Therefore, the coarse fraction can interact with ions like phosphate in the environment (Hendershot and Lavkulich, 1983; Harris et al., 1996; Arai and Livi, 2013). Destruction of the natural integrity of soil particles is a major experimental flaw.

To avoid the abrasion of particle coatings and micro aggregates, the overhead mixing method is often suggested. However, a well-homogenized state is difficult to achieve because coarse fractions tend to settle at the bottom of a reaction vessel. Variable

soil/solution ratios in a water column become an issue when the soil suspension at the constant soil/solution ratio needs to be sampled during the kinetic experiments (Zasoski and Burau, 1978). Therefore, this overhead mixing method is not ideal to study the ion desorption in soils.

To accurately measure the desorption rate of natural soils, one must overcome these technical issues in the stirred batch methods and the stirred flow method. If possible, it is ideal to provide a sink to remove desorbed ions from a bathing solution. Anion exchange resins have been widely used to remove phosphate from wastewater through the ion exchange process (Zhao and Sengupta, 1998; Awual and Jyo, 2011; Das Gupta et al., 2012; Liu et al., 2016). The matrix of ion exchange resins provides good adsorption sites for desorbed ions, but they predominantly removed desorbed ions via ion exchange reaction and are not selective toward a specific anion of interest, phosphate (van Raij et al., 1986; Somasiri and Edwards, 1992; Awual and Jyo, 2011). The modification of anion exchange resins by coating with other materials can improve their performance as a sink (Pan et al., 2009a; Sengupta and Pandit, 2011; Sendrowski and Boyer, 2013; You et al., 2016).

Iron (oxyhydr)oxide is one of the most extensively studied adsorbents to remove anionic pollutants. A Lewis base like phosphate can form inner-sphere complexes on the iron (oxyhydr)oxide surface (Tejedor-Tejedor and Anderson, 1990; Arai and Sparks, 2001; Elzinga and Sparks, 2007). Thus, their high affinity for anions makes it an efficient adsorbent. However, its small particle size and high reactivity make it difficult to apply for the soil desorption experiments because iron oxides particles cannot be easily separated from bulk soils (Blaney et al., 2007; Pan et al., 2009b; Sengupta and Pandit, 2011; Johir et al., 2016). Anion exchange resins coated with iron (oxyhydr)oxide, hybrid resin, are larger and easier to handle and expected to be a promising sink for the removal of phosphate from water and soil solutions (Sengupta and Pandit, 2011; O'Neal and

Boyer, 2013; Sendrowski and Boyer, 2013). Resins are more robust materials than filter papers, so they withstand the mixing action more than iron oxide impregnated papers.

Several researchers have shown the high affinity of iron (oxyhydr)oxide loaded resins for anionic pollutants like phosphate, arsenate, and selenate from wastewaters (Boyer et al., 2011; Bottini and Rizzo, 2012; Sendrowski and Boyer, 2013; Nur et al., 2014). However, the use of hybrid anion exchange resin as a sink in soil desorption kinetic experiments has rarely been evaluated in soil science. It was hypothesized that hybrid anion exchange resin is an ideal sink for P to measure the P desorption rate. In this study, a commercially available hybrid anion exchange resin was used in a mesh bag to evaluate phosphate desorption kinetics from agricultural soils in the Midwestern U.S., and the results of kinetic rates were compared with the rates in a respective pure anions exchange resin and in a conventional batch desorption method without a sink. To assure the hybrid resins is an ideal sink for phosphate; the hybrid resin was tested for the maximum phosphate retention capacity and irreversibility. Its performance as a P sink was evaluated in long-term soil desorption experiments.

3.2. Materials and Methods

3.2.1. Materials

The soil samples were collected at the depth of 0-18, 72-90 and 162-180 cm in an intensively managed agricultural land in Douglas County in east-central Illinois, hereinafter referred to as S_18, S_90 and S_180, respectively. The major soil series at the site is Milford silty clay loam (fine, mixed, superactive, mesic Typic Endoaquolls). The field received no-till and strip-till practices and has been used to grow corn and soybeans. Soils in this area are poorly drained dark-colored mollisols according to the U.S. Department of Agriculture (USDA) soil taxonomy (USDA Soil Survey, 2006). All chemicals (Sigma-Aldrich, St. Louis, MO) used in this study are ACS grade unless otherwise specified. Ultrapure water (18.2 MΩ·cm) was used to make all solutions.

3.2.2. Anion exchange resin and hybrid resin

A pure anion exchange resin and an iron oxide-loaded hybrid resin were used as P sinks in the desorption experiments. A pure anion exchange resin AMBERLITE™ HPR 9200 (DuPont Company, Wilmington, USA) was chosen because of its wide application in environmental research. A commercially available product, FerrIX™A33E (Purolite, PA, USA), was used as a hybrid resin. It shares the same properties of the parent anion exchange resin with AMBERLITE™ HPR 9200. The choice of a commercial hybrid resin is to provide easier access of the adsorbent to scientists who are interested in reproducing similar desorption experiments in different soils.

The total surface area of resins was analyzed using the ethylene glycol monoethyl ether (EGME) method. The resins were first dried in an oven at 40 ℃ for the hybrid resins and 70 ℃ for pure resins until they reached constant weight. 40 ℃ was chosen for the hybrid resin so as to prevent conversion of iron oxide coating to hematite. Approximately 0.5g of dried resin samples were weighed and then placed in Petri dishes. The dish was placed in a vacuum desiccator with another Petri dish filled with a 10 mL EGME solution (Sigma-Aldrich, St. Louis, MO). The evacuation-stabilization-weighting cycle was repeated until the weights were constant. It took about six days. Assuming monolayer coverage, the specific surface area was calculated using the equation (Klute et al., 1986):

$$A = W_g/(W_s \cdot 0.000286)$$

where A = specific surface (m^2/g), W_g = weight of EGME retained by the sample after monolayer equilibration (g), and W_s = weight of the dried resin (g); 0.000286 is the mass of EGME required to form a monolayer on 1 m^2 of the surface.

Before the soil desorption experiment, the functional group of the pure resin HPR 9200 was saturated with bicarbonate. Twenty grams of resin were shaken in a 1-L

polypropylene bottle filled with a 0.5 M $NaHCO_3$ solution for 1 hr. This treatment was followed by washing with de-ionized water twice. The resins were air-dried.

In order to effectively separate resins from soils during the desorption experiments, 6.5 cm × 4.5 cm polyester monofilament mesh bags with 150 μm mesh size were used to enclose the resin beads (Universal Filters, Inc., Asbury Park, NJ). The mesh size is large enough to prevent the diffusion-limited reaction through the bag but small enough not to leach hybrid resin beads. Each bag was filled with 1 g of resin beads and then sewn up to seal the opening. Staples were not used to seal the bag to avoid metal contamination in the system.

3.2.3. Mineralogical characterization of iron oxide coating of the hybrid resin

The mineralogical analysis of the hybrid resin, FerrIX™A33E, was conducted using an X-ray diffraction method. The finely ground resin powder was placed in the 25-stage sample holder on the instrument, Bruker D-5000 XRD unit (Bruker Corporation, Billerica, MA, USA), and positioned the goniometer to start its angular scan at 45 kV and 30 mA. The lower limit for 2θ was set to 5° and the upper limit to 80°. The scanning rate was set at 2.0°/min. The 2θ was calculated using Bragg's Law ($2d\sin\theta = n\lambda$), and the 2θ-intensity XRD pattern was plotted. Peak assignment and mineral identification were performed using the ICDD database (Powder Diffraction File 4, PDF-4+) with the 2theta position and intensity ratio of each peak.

The Fe mineralogy was also analyzed using Fe K-edge X-ray absorption spectroscopy (XAS) at ID12 at Advanced Photon Source (Argonne, IL, USA). Because XAS is more sensitive to pick up residual amorphous phases like ferrihydrite. A monochromator consisting of a double-crystal Si (220) at Phi=0° was used. An incident beam of X-ray energy was calibrated at the first inflection point (7112 eV) of a Fe foil spectrum and detuned 50% at ~7770eV. Beam size was 2 mm in width x 1mm in height. The calibration energy was monitored using a Fe foil during the scan. The transmission

measurements were performed in air at room temperature. Spectra were recorded with three regions: 10 eV steps from 6880 to 7090 eV with 1sec. dwell, 0.25 eV steps over the pre-edge from 7090 to 7140eV with 1sec. dwell, and 0.25 eV steps from k of 1.62 to 14 $Å^{-1}$ with 1sec. dwell. Three spectra were recorded. Acquiring multiple spectra across time allows us to quantitatively evaluation of reproducibility. Reference spectra of synthetic ferrihydrite, goethite, hematite, and lepidocrocite were also collected. These minerals were synthesized according to the methods described by Schwertmann and Cornell (2008). All mineral samples were diluted in boron nitride (Sigma-Aldrich, St. Lois, MO) except for the hybrid resin sample. The finely ground hybrid resins were packed in a polycarbonate holder and directly measured. Because of polymer background, the dilution with BN was not necessary. Spectra were normalized using standard features of the ATHENA software package (Ravel and Newville, 2005), and linear combination of XAS reference spectra fit analysis was conducted at a *k* range of 2-11 $Å^{-1}$.

3.2.4. Physicochemical characterization of soils

Physicochemical properties of soils were measured using the following standard soil science methods. Soil pH was measured at a soil/water ratio of 1:2 in ultrapure water (McLean, 1982; Thomas, 1996). Organic matter content was measured using a loss-on-ignition method (Schulte and Hopkins, 1996). A hydrometer method was used to determine soil texture (Gee and Bauder, 1986). Cation exchange capacity was measured using an ammonium acetate (NH4OAc) method at pH 7 (Ross and Ketterings, 1995). The concentration of extractable P in soils was measured using the Mehlich 3 method (Mehlich, 1984) and the Bray I method (Bray and Kurtz, 1945). The molybdenum blue method with excess ammonium molybdenum (He et al., 1998) was used to determine P concentration in extracted solutions.

3.2.5. Total P, inorganic P (IP) and organic P (OP) fractionation of soils

Total IP and OP were measured in the soils in duplicates using the sequential extraction method described by Kuo (1996). It uses concentrated sulfuric acid (Thermo Fisher Scientific, Waltham, MA) and dilute NaOH solutions. Approximately 1.0 g air-dried soil sample was mixed with 1.5 mL of concentrated H_2SO_4 in a 50 mL volumetric flask. After mixing, 2 mL of deionized water was added in 0.5 mL increments while mixing vigorously for 10 sec after each addition. 21.5 mL of deionized water was added after cooling to room temperature, and then the sample was filtered through Whatman No.2 filter papers (GE Healthcare, Chicago, IL). The filtrate was saved in a 50 mL centrifuge tube for "acid extracted phosphate" determination using the molybdenum blue method (He et al., 1998). The soil residue and filter paper were then placed in a 125 mL Erlenmeyer flask, followed by addition of 49 mL of 0.5 M NaOH solution, shaking for 2 h at 80 rpm, and then filtered the soil suspension through Whatman No.2 filter papers. The filtrate was analyzed for "base extracted phosphate" using the same colorimetric method. The concentration of total IP in the soil was calculated by summing the P concentration in the acid (P_i^a) or base (P_i^b) extracts.

For total P (TP) determination, a 2 mL aliquot from the acid or base extract was pipetted into a 50 mL volumetric flask. 0.5 g of $K_2S_2O_8$ (Sigma-Aldrich, St. Louis, MO) and 2 mL of 5.5 M H_2SO_4 solution were added and digested on a hot plate at 150°C for 30 min. After cooling, five drops of *p*-nitrophenol were added. pH was adjusted with 1-10 M NaOH solutions until the color changed to yellow. The P concentration was then determined using the molybdenum blue method (He et al., 1998). The concentration of TP was calculated by summing the P concentration in acid (TP^a) and base (TP^b).

Accordingly, total OP fraction in the initial soil sample was calculated using the following equation (Kuo, 1996).

$$P_o = TP^a + TP^b - P_i^a - P_i^b$$

3.2.6. Phosphate adsorption isotherm in resins

To design desorption kinetic experiments with a sink, it is important not to exceed the maximum phosphate retention capacity of the sink during desorption experiments. To understand the maximum phosphate adsorption capacity of the pure resin and the hybrid resin, P adsorption isotherm experiments with these resins were conducted at 21 ± 0.5℃.

A 100 mg /L phosphate stock solution was prepared by dissolving disodium phosphate in 10 mM NaCl. Approximately 0.1 g pure resin AMBERLITE™ HPR 9200 or hybrid resin FerrIX™A33E were added into a 50 mL Nalgene high-speed centrifugation tube. Appropriate amounts of the phosphate solution were added to make the initial phosphate concentrations of 3, 10, 20, 30, 40, and 50 mg/L. During the first several hours, pH was manually adjusted with 0.01-0.1M HCl or NaOH. The tubes were mixed on an orbital shaker at 80 rpm for 24 hrs. The experiments were conducted in duplicate. After 24 hrs, the resin suspensions were sampled and filtered using a 0.45 μm polyvinylidene fluoride (PVDF) syringe filter. Aliquots were colorimetrically analyzed for the concentration of phosphate (He et al., 1998).

Isotherm data were modeled using Freundlich and Langmuir equations.

For the Freundlich model

$$q = K_f \cdot C^{1/n}$$

where q is the amount of phosphate adsorbed (mg /g); C is the final equilibrium concentration of phosphate (mg/L); K_f is a parameter related to the adsorption capacity; n is a parameter related to the intensity of adsorption.

For the Langmuir model

$$\frac{C}{q} = \frac{1}{Q_m \cdot K_m} + \frac{C}{Q_m}$$

where q is the amount of phosphate adsorbed (mg /g); C is the final equilibrium concentration of phosphate (mg /L); Q_m represents the maximum adsorption capacity (mg/g); and K_m is a parameter related to the bonding strength (L/mg).

To account for the phosphate adsorption capacity of the mesh bag during the soil desorption experiment (i.e., background P adsorption), a P adsorption isotherm experiment was repeated using blank mesh bags. The mesh bags were cut into strips and 0.5 g of the strip was put into Nalgene 50 mL centrifugation tubes. Different concentrations (1, 2, 3, 4, and 5 mg/L) of phosphate solutions at pH 7.5 in 10 mM NaCl were added. After shaking the tubes on an orbital shaker at 80 rpm for 24 hr, aliquots were colorimetrically analyzed for the P concentration (He et al., 1998).

3.2.7. Irreversibility of adsorbed phosphate in resins

The pure resins or the hybrid resins as a sink should be evaluated for the irreversibility (i.e., desorption of adsorbed phosphate from resins). The irreversibility of adsorbed phosphate was tested in duplicate. Resins were first reacted with phosphate by mixing 0.1 g of resin and 20 mL of a 10 mg /L sodium phosphate solution in 50 mL centrifugation tubes. After shaking the mixture on an orbital shaker at 85 rpm for 24 hrs, an aliquot was carefully decanted. The mass of wet resins and the entrained solution was recorded. To start the irreversibility test of adsorbed phosphate, 20 mL of P-free solution containing 10 mM NaCl and 5 mM 3-(N-morpholino) propanesulfonic acid (MOPS) (Sigma-Aldrich, St. Louis, MO) at pH 7.5 was introduced to the tubes, and the tubes were shaken on an orbital shaker at 85 rpm. After 1, 8, 16 hrs, 1, 2, 3, 5, and 7 days, the concentration of desorbed phosphate was measured by sacrificing each tube. The P concentration was determined colorimetrically (He et al., 1998).

3.2.8. Phosphate desorption kinetics in soils without P sink

To evaluate the hybrid resin-based phosphate desorption method, the following three systems are compared: 1) desorption without a sink, 2) desorption using the hybrid resin, and 3) desorption using a respective anion exchange resin.

First, a soil phosphate desorption experiment was conducted without a sink. Approximately 5.00-10 g of air-dried soils were added into 125 mL polypropylene bottles containing 100 mL of ultra-pure water. In this experiment, pH remained at near soil pH. The bottles were gently shaken on a reciprocal shaker at 80 rpm. Because soil suspensions were gently agitated, grinding of coating materials, sample alternation, was not an issue in this desorption method. After 2, 4, 8, 16 hrs, 1, 2, 3, 5, and 7 days, suspensions were sampled and filtered through 0.45 μm PVDF syringe filters. The aliquot was colorimetrically analyzed for the P concentrations (He et al., 1998).

3.2.9. Phosphate desorption kinetics in soils using resin bags

A phosphate desorption kinetic experiment was conducted using mesh bags filled with either FerrIX™A33E or AMBERLITE™ HPR 9200. The resins used were first hydrated in a 10 mM NaCl solution and pH was adjusted to the corresponding soil pH with 0.001-0.1M HCl or NaOH solution. Approximately 5 g of air-dried soil [10 g of soil S_180 that was much lower in TP (see section 3.1)]. sample was added into a 125 mL polypropylene bottles that were filled with 100 mL of ultra-pure water. A resin-filled mesh bag was placed in each bottle. The bottles were shaken on an orbital shaker at 80 rpm.

After shaking for 2, 4, 8, 16 hrs, 1, 2, 3, 5, and 7 days, the resin bag was removed carefully from each bottle and rinsed once with 20 mL of de-ionized water. Then, the resin was dried in a convection oven at 37 ℃ for 5 hrs. When resins were recovered from a reaction vessel, the mesh bag containment made an easy separation of resin beads from soil suspensions. Soil particles were not found inside a mesh bag, probably because the mesh bags remained in the top layer of soil solution during shaking whereas soil suspensions largely remained at the bottom of the reaction vessel during the gentle agitation. To recover adsorbed P from the resins, ~0.5 g of the dried resins were treated with 30 mL of 0.5 M NaOH + 0.5 M Na_2SO_4. The chemical composition of this

extractant was tested to assure 100% P recovery under the reaction condition of this experiment. The tube was shaken on an orbital shaker at 80 rpm for 24 hrs. The solution was passed through a 0.45 μm PVDF syringe filter and neutralized with 0.5 M HCl. The P concentration was colorimetrically determined (He et al., 1998). The experiment was conducted in duplicate.

To understand how the mass of the hybrid resin affects the kinetic rate, the experiments were repeated using 0.5 g, 1 g, and 2 g of the hybrid resin in a mesh bag under the same experimental condition. The soil used in this test is S_18.

Data from the kinetic experiments were evaluated using the pseudo-first order equation (Ho and McKay, 1999), a pseudo-second order equation (Ho and McKay, 2000), Elovich equation (Low, 1960), and an intra-particle diffusion model (Weber and Morris, 1963).

The pseudo-first order equation,

$$q_t = q_e(1 - e^{-k_1 t}),$$

can be expressed in linear form as:

$$\ln(q_e - q_t) = \ln(q_e) - k_1 t$$

where q_t is the amount of phosphate adsorbed on unit weight of adsorbent (mg·g^{-1}) at time t (hr). q_e is the adsorption capacity of adsorbents (mg/g) at equilibrium, and the term k_1 (g/mg/hr) is the first order rate constant. The terms, q_e and k_1, can be calculated by linear regression of $\ln(q_t - q_e)$ vs. t.

The pseudo-second order equation follows the form,

$$\frac{t}{q_t} = \frac{1}{k_2 {q_e}^2} + \frac{1}{q_e} t,$$

where q_t is the amount of phosphate adsorbed on a unit weight of adsorbent (mg/g) at time t (hr), q_e is the adsorption capacity of adsorbents (mg P/g) at equilibrium, and k_2

(g/mg/hr) is the second order rate constant. The terms, q_e and k_2, can be calculated by linear regression of $\frac{t}{q_t}$ vs. t where the slope and intercept correspond to $\frac{1}{q_e}$ and $\frac{1}{k_2 {q_e}^2}$, respectively.

The Elovich equation is given by,

$$q_t = \frac{\ln(\alpha\beta)}{\beta} + \frac{1}{\beta}\ln(t),$$

where q_t is the amount of phosphate adsorbed per unit weight of adsorbents (mg/g) at time t (hr). α (mg/mL/min) is the initial adsorption rate constant, and the parameter b (mL/mg) is related to the extent of surface coverage and activation energy for chemisorptions. The α and β terms were obtained calculated by regressing q_t vs. $\ln(t)$ where the slope and intercept correspond to $\frac{1}{\beta}$ and $\frac{\ln(\alpha\beta)}{\beta}$, respectively.

The intra-particle diffusion model is based on the equation,

$$q_t = k_3 t^{1/2},$$

where q_t is the amount of phosphate adsorbed on unit weight of adsorbent (mg/g) at time t (hr), and k_3 is the intra-particle diffusion constant that can be calculated by regressing q_t vs.$t^{1/2}$ where the slope corresponds to k_3.

3.2.10. Stability of Fe oxide coatings in the hybrid resin

To test the stability of Fe coatings of the hybrid resin during desorption experiments, the total iron content of the hybrid resin in a mesh bag was monitored during the same desorption experiment. A mesh bag containing ~1 g of the hybrid resin was added into triplicate 125 mL polypropylene bottles that were filled with 100 mL of 10 mM NaCl solution at pH 7. The bottles were shaken at an orbital shaker on 80 rpm. After 7 days, the hybrid resins were removed from the mesh bag, and air-dried. Approximately 0.1 g of the hybrid resin was placed in a clean polypropylene bottle to react with a 100 mL of extractant solution containing 5% hydroxylamine and 5 M HCl (Upping et al., 1986;

Sager, 1992). The mixture was placed in an ultrasonic bath (Bransoic, CPX2800) for 5 min and then shaken on an orbital shaker at 80 rpm for 48 hrs. The beads were separated by filtrating through Whatman No.2 filter papers, and the total Fe concentration in the filtrate was measured using the spectrophotometric method with 1, 10-phenanthroline (Sigma-Aldrich, St. Louis, MO) (Tamura et al., 1974). The total Fe concentration in these hybrid resins was compared with that of the material before the desorption experiments.

3.3. Results and Discussion

3.3.1. Characterization of soils and resins

The physicochemical properties of the soil samples are summarized in Table 3.1. While OC decreases with increasing depth, IC increases at the lower depth. This is due to the presence of carbonates in subsoils (Xu et al., 2020). Soil pH increases with increasing depth from 18 to 180cm. Weakly acidic pKa of carboxylic acids in organic matter buffer at near neutral at the surface. Slightly alkaline pH in subsoils at the depth of 90-180 cm is controlled by calcite and dolomitic materials (Xu et al., 2020). Because of near neutral to slightly alkaline pH, CEC is high (23-29 $cmol_c/kg$) throughout the profile. % base saturation is ~96% in all samples.

In soil S_18, the results of agronomic soil P tests are 10-14.5 mg/kg which is lower than the recommended level for corn, according to the Illinois Agronomy Handbook (Fernández and Hoeft, 2009). However, the total P in the soils is high (~390 mg/kg) for the surface soil. The majority of P is in the inorganic form, and the OP fraction is ~140 mg/kg in S_18. The content of OP decreases from 140 to 7 mg/kg with increasing depth from 18 to180 cm. However, the IP fraction remains high (~360 mg/kg) up to 90 cm. The S_180 sample contains ~190 mg/kg of IP.

The properties of resins used in this study are shown in Table 3.2. Both the pure resin AMBERLITE™ HPR9200 and the hybrid resin FerrIX™A33E have polystyrene-

DVB as their polymeric matrix. The structure and resin functional groups are same. The particle size of the pure resin and the hybrid resin is ~640 μm and ~750 μm. The mineralogy of iron oxides in the hybrid resin is predominantly goethite (Fig. 3.2). The XAS analysis also shows the same results.

The total surface area of FerrIX™A33E (i.e., hybrid HPR9200), 810.4 ± 38.2 m^2/g, is significantly lower than that of HPR9200 (1625.1 ± 20.9 m^2/g), which could be explained by the surface coverage of small goethite particles over the porous structure of pure anion exchange resin.

The stability of Fe oxide coating on FerrIX™A33E was tested in a control system without soils. At t = 0, the iron content of the hybrid resin is 196 ± 3 mg Fe/g (Table 3.2). After shaking a mesh bag containing FerrIX™A33E in a 10 mM NaCl solution for 7 days, there was a negligible change in total Fe in FerrIX™A33E. The iron content was 194 ± 2 mg Fe/g. This suggests that the Fe oxide coating of the hybrid resin remains stable during the desorption experiment. The Fe coatings did not leach outside of the mesh bag during the desorption experiments.

3.3.2. Phosphate adsorption isotherm in the resins

The results of the adsorption isotherm experiment show a typical L-shape curve for both resins, indicating that the adsorbates have high affinity at low surface coverage (Fig. 3.3a). When the initial P concentration was at 10 mg/L, ~76 % of P was adsorbed by the pure resin, while ~98 % was adsorbed by the hybrid resin. Interestingly, the hybrid resin showed a greater affinity for P at the C_{eq}: 0-15 mg/L, and the pure resin had a greater affinity for P at C_{eq} >15 mg/L. It is important to note that the adsorption isotherm data in Fig. 3.3a were corrected for the residual P adsorption in mesh bags. Phosphate adsorption by a blank polyester mesh bag was < 0.04 mg/g (Fig. 3.3b).

To compare the affinity of these adsorbents, adsorption isotherm data for the pure resin were modeled using Freundlich and Langmuir equations. The results are

summarized in Table 3.3. The model fit in both resins shows an excellent fit. Although these models do not describe the adsorption mechanisms, model parameters can be used to compare the P adsorption capacity of different adsorbents. In the Langmuir model, the maximum adsorption (mg P/g), Q_m, indicates that the pure resin has greater adsorption than the hybrid resin. This was observed in Fig. 3.3a. However, in the Freundlich model, the adsorption capacity (K_f) of the hybrid resin is much greater than that in the pure resin. Each adsorbent seems to have different properties for P.

Using the isotherm data of these resins, it was assured that P adsorption capacity of the two resins is more than enough to be a P sink during the desorption experiments, even 100 % of TP (TP< 0.5 mg P/g) is released from the soils. It was determined the ideal soil:resin ratio to be 5-10 g of soil:1 g of resin.

3.3.3. Phosphate irreversibility tests in the resins

To evaluate potential release of P adsorbed by the resins, the desorption of P from P adsorbed resins was tested. The result of the irreversibility test shows a major difference between the pure resin and the hybrid resin serving as P sinks (Fig. 3.4). After providing the total P loading level of 2 mg/g, the resins were shaken in a P-free solution up to 7 days. The cumulative percentage of desorbed P is shown in Fig. 3.4. Approximately 13.3 % of the adsorbed P in the pure resin was released into solution after 7 days, and 12.9 % of the P already desorbed within 1 hr. It is clear that the pure anions exchange resin is a good sink for the P desorption experiment. In contrast, less than 0.3% of adsorbed P was desorbed from the hybrid resin, which should be accounted for by the inner-sphere complexation of phosphate on the iron oxide coating in the hybrid resins (Arai and Sparks, 2001; Hongshao and Stanforth, 2001). The irreversibility test indicates that the hybrid resin had a near negligible backward reaction (i.e., desorption). The hybrid resin is a better P sink in soil desorption studies.

3.3.4. Phosphate desorption in soils

3.3.4.1. The extent of P desorption from soils

The result of P desorption is shown in Fig. 3.5 and Table 3.4. The amount of P desorbed varies among the three soil samples. With or without a P sink, the extent of P desorption after 168 hrs (7 days) follows the order of S_18 > S_90 > S_180. This was not surprising because the soils at 0-90cm contained more TP than subsoils (Table 3.1). The extent of P desorption was vastly different among the different desorption methods. For each soil, the largest P desorption after 7 days is always found in the hybrid resin system, followed by the pure resin system and the system without a P sink. It is important to note that under the fixed mass of adsorbents, the total surface area of pure anion exchange resin, 1625.1 ± 20.9 m^2/g, is two times greater than that of the hybrid resin, FerrIX™A33E (i.e., 810.4 ± 38.2 m^2/g). This suggests that a difference in surface area was not the controlling factor for removing P from the bathing solution in this experiment.

To be specific, the topsoil S_18 released 1.32 mg P/g soil without sink after 7 days, which was 0.34 % of its total P (Fig. 3.5a and Table 3.1). In the presence of the pure anion exchange resin, the extent of P desorption increased to 9.50 mg P/g (~2.43 % of TP). In the case of the hybrid resin, it was even greater. Approximately 17mg/kg (~4.35% of TP) was desorbed after 7days. The same trend was also observed in the other two subsoils. The soil S_90 released only 0.53 mg/kg (~0.13 % of TP) without any sink, but the total desorbed P increased to 7.90 mg P/g (~1.88 % of TP) with the hybrid resin as a sink. The pure resin was not as effective as the hybrid resin. In the case of soil S_180, which contains the lowest TP, the efficiency in removing desorbed P was best in the hybrid resin. Only the hybrid resin was able to desorb appreciate amounts of P (~3.45 mg P/g), but no more than 0.67mg P/g (~ 0.3 % of TP) was desorbed with the pure resin or without any sink.

In summary, the hybrid resin performed best in soils that have a wide range of total desorbable P, the extent of P desorption. Unfortunately, the traditional batch method without any sink or the use of pure anion exchange resin did not produce good results. The backward reaction or accumulation of desorption ions is likely the reason. In the batch system re-adsorption of desorbed phosphate was readily occurring. In the anion exchange pure resin system, the sink did not behave like a finite sink. As reported in the irreversibility test section, adsorbed P in the pure resin seems to desorb back into the bathing solution. To further validate the hybrid resin based- desorption method, P desorption kinetics in three desorption methods were evaluated using several different models.

3.3.4.2. Phosphate desorption kinetics

As shown in Fig. 3.5, soil P desorption in all desorption methods shows fast desorption within 24 hr and then gradually reaching the steady-state in the next several days. The P desorption kinetics were evaluated using different kinetic models. They are pseudo-first-order model (Ho and McKay, 1999), pseudo-second-order model (Ho and McKay, 2000), Elovich model (Low, 1960), and intra-particle diffusion model (Weber and Morris, 1963). Overall, the pseudo-second-order model fits best for the P desorption data in different desorption methods (Table 3.5). Fig. 3.6 shows the results of linear fitting of these models to the data in each case. Based on the goodness of it, the pseudo-second-order model fit best and other models did not fit the data well. The parameters of these kinetic models for the P desorption process are discussed below.

(1) Pseudo-first-order model and pseudo-second-order model

For three soils, the pseudo-first-order model does not fit well with the kinetic data ($R^2 < 0.8$) (Table 3.5). There is no clear trend in the rate constant among different desorption conditions or different soil samples. However, the pseudo-second-order model

fit resulted in very high R^2 values for the kinetic data of all soils, especially for the batch with hybrid resins ($R^2 > 0.999$). The hybrid resin systems also have a larger rate constant (k_2) and the adsorption capacity of adsorbents at equilibrium (q_e) than the pure resin systems. The batch without any sink had the smallest q_e among three systems, but the rate constant did not show this trend. It should be noted that R^2 of these models becomes low in the system without resins because of a large standard deviation within the small signal (Fig. 3.5c). The term $k_2 {q_e}^2$ from the pseudo-second-order model can be used as an indication of the initial rate of a desorption process (Lalley et al., 2016). As shown in Table 3.5, the initial rate of P desorption follows the trend of hybrid resin > pure resin > no resin. However, among the three soil samples, S_90 has a higher initial P desorption rate than the topsoil S_18, which could be due to the different P speciation in the soils. Inorganic P made up a much higher composition of total P in S_90 than in S_18. It is the fact that S_90 desorbed P faster at the beginning but slower at the end of experiments.

(2) Elovich model and Intra-particle diffusion model

Judging from the R^2 values, the Elovich model and the intra-particle diffusion model have a good fit for the desorption data when the resins are present as a P sink. The goodness of fit in the Elovich model ($0.82 < R^2 < 0.98$) is greater than that of the pseudo-first-order model, but not as good as that of the pseudo-second-order model. The Elovich model does not fit well to describe the data of the system without resins. The R^2 of the intra-particle model is slightly lower than that of the Elovich model. The intra-particle model works better in the resin systems than in the system without resins. The diffusion rate constant (K_d) was always highest when the hybrid resin was present as P sink for the three soils, possibly suggesting the diffusion-limited P exchange process in the hybrid resins.

In summary, soils could desorb more P when anion exchange resins are present in a reaction vessel. However, the hybrid resins work better than the pure resin for removing

P from bathing solutions (i.e., the extent of P desorption) than the pure resins do due to minimized backward reaction during the desorption experiment. In term of kinetic model fit, the pseudo-second-order model was the best, and the parameter, $k_2 {q_e}^2$, can be used to describe the initial rate of a desorption process.

3.3.4.3. Phosphate desorption kinetic rate affected by the mass of resin

The desorption experiments were repeated in the soil S-18 using different amounts of the hybrid resin to evaluate the effects of resin mass on the kinetic rate. The results are summarized in Fig. 3.7 and Tables 3.5. The biphasic desorption kinetic process was observed in all three systems. A fast P release was followed by a slow desorption process. The extent of total desorbed P is similar (i.e., within error bars of each data point at the same sampling time) in these soils. After 168hrs, ~16.3 mg/kg of P was release in all systems.

Fig. 3.8 shows the linear plots of the pseudo-first-order model, the pseudo second-order model, the Elovich model, and the intra-particle diffusion model for the P desorption kinetic data shown in Fig. 3.7. The fitting parameters associated with these models are summarized in Table 3.5 with the R^2 values. As previously discussed, the pseudo-second-order model provides the best fit in modeling the P desorption kinetic data (i.e., $R^2 = 1$).

To assess how the mass of hybrid resin affects the kinetic rate, the same model was used to estimate the initial kinetic rate, $k_2 {q_e}^2$ from the pseudo-second-order model. The rate increased from ~8.8 to 11.8 mg/ g·hr by increasing the mass of hybrid resin from 0.5 to 2 g. This suggests that the experimental design, the mass of the resin in the desorption system, can influence the rate of P release and is critical in evaluating the kinetic process.

3.4. Conclusions

This study shows one of the best batch P desorption methods available in the field. The use of the hybrid anion exchange resins as a P sink was very efficient in removing desorbed P from agricultural soils. Overall, the iron oxide-coated hybrid resins were a better P sink than the respective pure anion exchange resins. The results of the hybrid resin system showed that the extent of P desorption and the initial kinetic rate, $k_2 {q_e}^2$, were greater than those in the conventional batch methods with and without pure anion exchange resins. This is because adsorbed P in the hybrid resin was nearly irreversible whereas the pure anion exchange resin released ~13% of adsorbed P. This indicates the backward reaction (i.e., re-adsorption) in the hybrid resin system was minimized. The pseudo-second order model was successfully used in evaluating the P desorption kinetic data in the hybrid resin.

There are several key points when the hybrid resin-based desorption method is adapted. The maximum adsorption capacity of the hybrid resin sink should be tested to assess a proper soil/resin ratio in the experiment. pH should be maintained or adjusted at the relevant soil pH values during the experiments. The irreversibility test of P from P adsorbed hybrid resins should also be tested under the specific reaction conditions. Minimizing the backward reaction (i.e., re-adsorption) is key for desorption kinetic experiments to be successful using a hybrid resin as a sink. When evaluating the kinetic rate of multiple soil samples, the amount of resin in a mesh bag should be consistent since it could influence the initial kinetic rate.

The implication of this study includes that the hybrid anion exchange resin method can be applied to the soil desorption kinetic study of other anions like arsenate in coarse-textured soils and sediments. It is highly recommended to assess the P desorption behavior in sandy soils and vadose zone sediments that cannot be stirred in a reactor to retain the natural integrity of mineral coatings and aggregates. One could also consider the use of different hybrid ion exchange resins. The different type of hybrid ion exchange

resins should be further evaluated for the assessment of desorption behavior of other inorganic contaminants (e.g., oxyanions, metal(loid)s, oxocations) in soils and sediments.

3.5. Figures

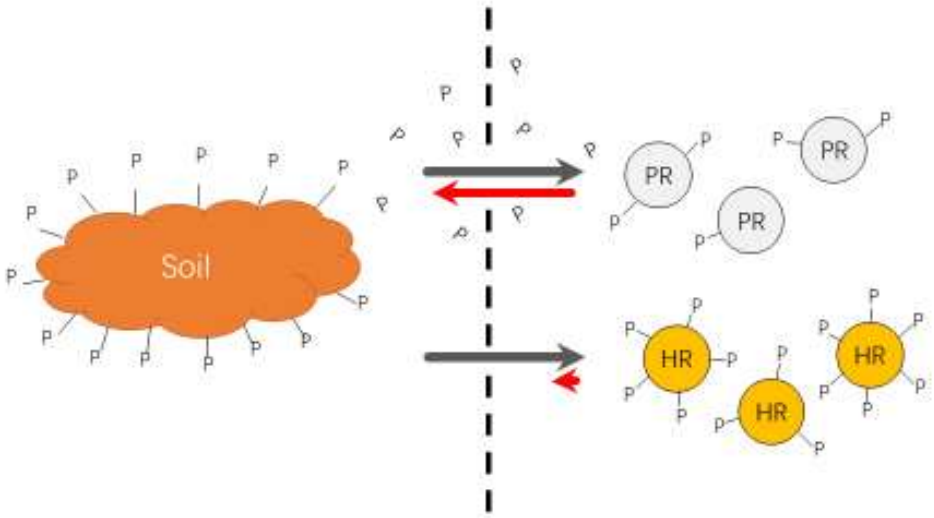

Fig. 3.1. A schematic illustration of phosphate(P) desorption systems using pure resins (PR) and hybrid resins (HR) as a P sink. Forward and backward reactions are shown in black and red arrows, respectively. A vertical dotted line indicates a boundary between a mesh bag and a soil solution. Note that 1) more P is retained in HR because of a small backward reaction (i.e., P release) from HR compared to that from PR.

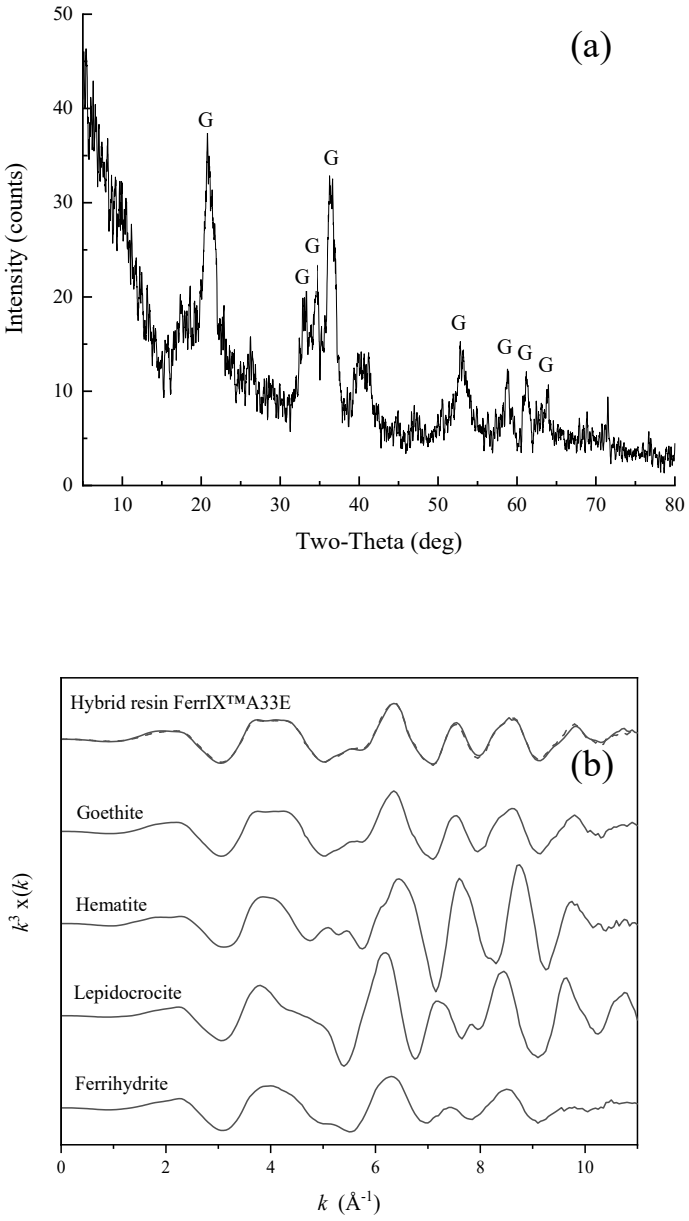

Fig. 3.2. (a) XRD pattern of the ground hybrid resin FerrIX™A33E. Identified peaks correspond to goethite (G), and (b) Linear combination fit of reference compound fit of a normalized k^3 weighted spectrum of the hybrid resin. Dotted line indicates fit. The fit results show the Fe oxide mineralogy of the hybrid resin is 100±0% goethite with r-factor of 0.01.

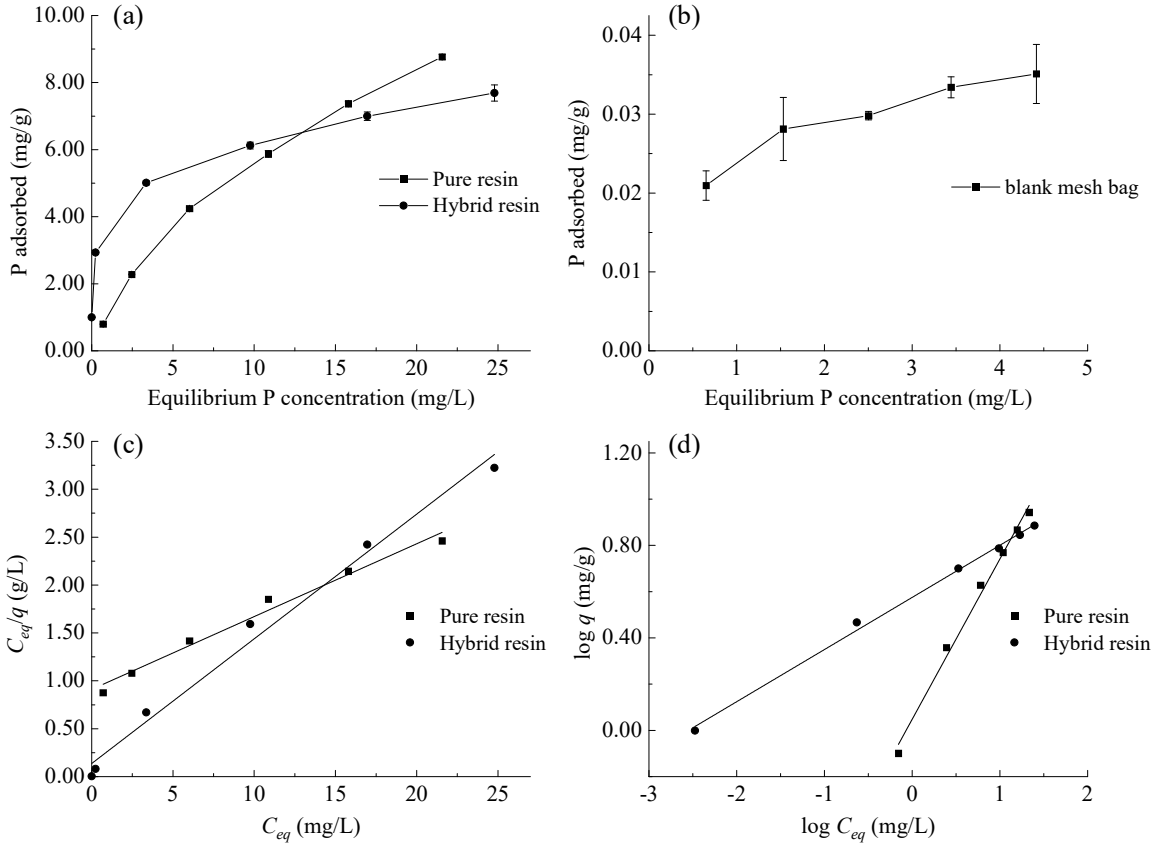

Fig. 3.3. (a) Phosphate adsorption isotherm at pH 7.5 in the pure anion exchange resin and the hybrid resin. (b) phosphate adsorption isotherm at pH 7.5 in a blank mesh bag. (c) Langmuir model of the isotherm data in Fig. 3a and (d) Freundlich model of the isotherm data in Fig. 3b.

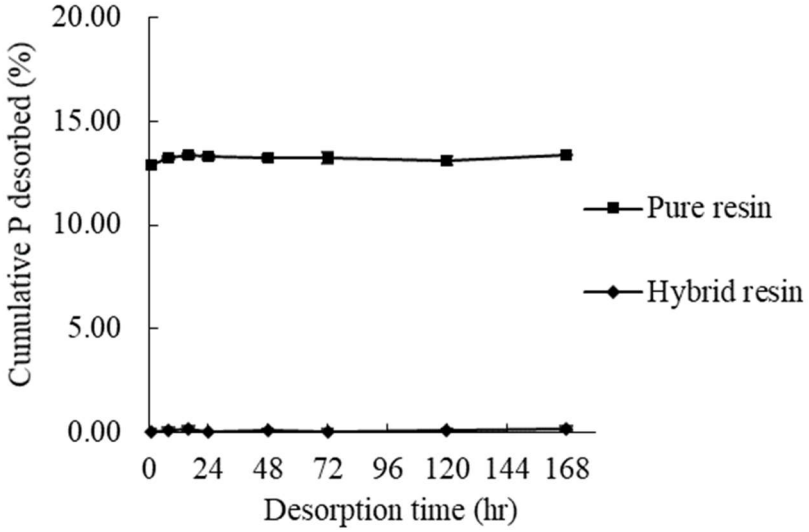

Fig. 3.4. Phosphate release from a phosphate adsorbed pure resin and a phosphate adsorbed hybrid resin up to 7 days. The initial phosphate loading level in both resins is at 2 mg /g.

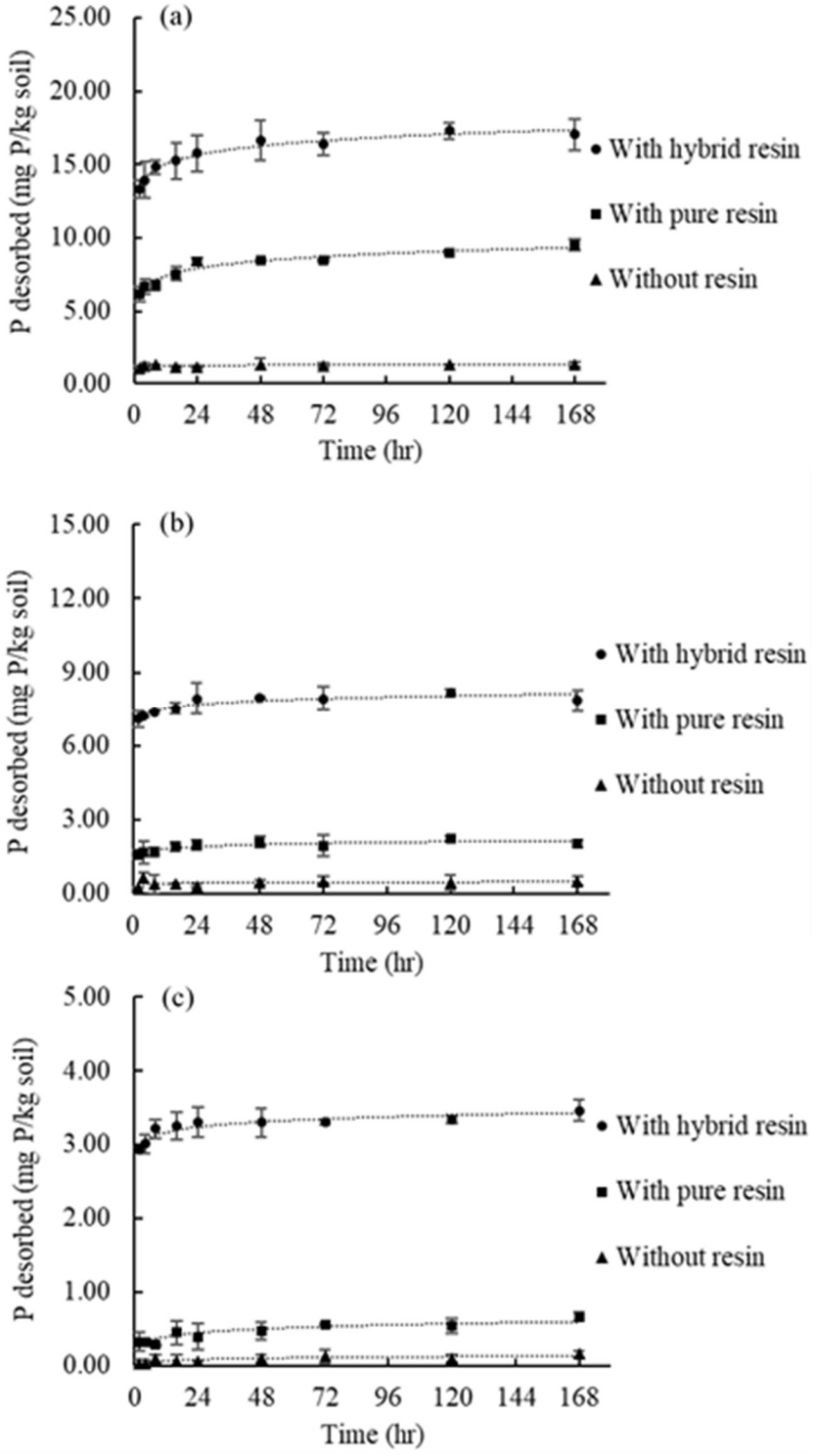

Fig. 3.5. Phosphate desorption kinetics from soils (a) S_18, (b) S_90, and (c) S_180 in different desorption systems.

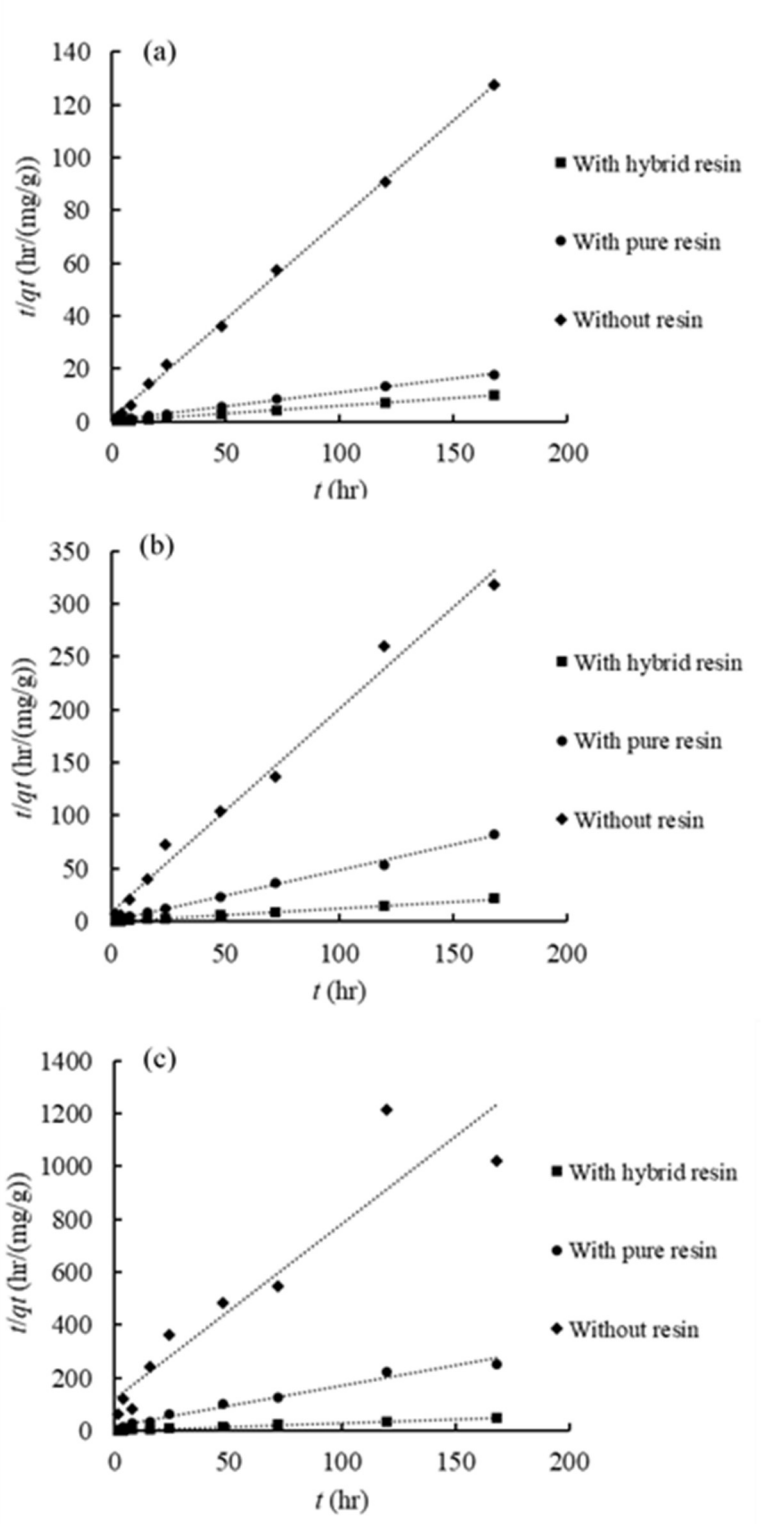

Fig. 3.6. Linear plot of pseudo-second-order model for the phosphate desorption data shown in Figure 5 (a) S_18, (b) S_90, (c) S_180.

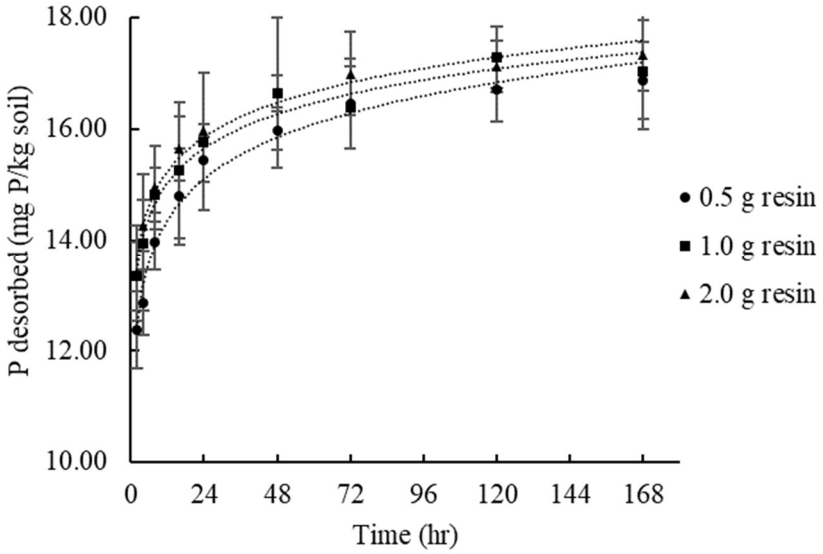

Fig. 3.7. Phosphate desorption kinetics in soil S_18 as a function of the hybrid resin mass (0.5-2g).

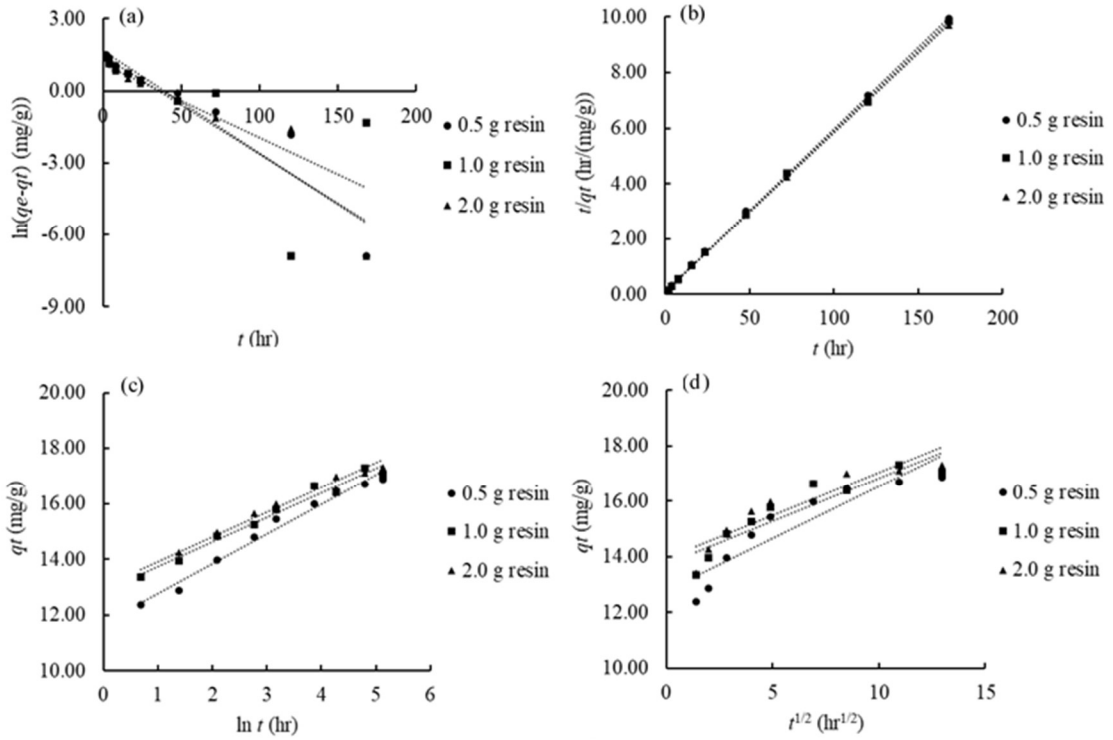

Fig. 3.8 Linear plot of (a) Pseudo first-order model, (b) Pseudo second-order model, (c) Elovich model, (d) Intra-particle diffusion model for the P desorption kinetic data shown in Fig. 3.7.

3.6. Tables

Table 3.1. Selected physicochemical properties and P concentrations of Douglas County soils.

Soil sample ID	Depth	pH	%IC†	%OC†	CEC†	%base†	M3P†	B1P†	OM†	Texture	TIP†	TOP†	TP†
	cm		------% by wt.------		$cmol_c/kg$	%	-------mg/kg-------		%		----------mg/kg----------		
S_18	0-18	6.95	0.11 (±0.03)‡	2.25 (±0.01)	26.72 (±2.86)	95.69 (±0.01)	14.50 (±0.71)	10.00 (±1.41)	4.27 (±0.02)	SC§	251.90 (±0.18)	139.79 (±17.98)	391.69 (±18.16)
S_90	72-90	8.03	0.27 (±0.06)	0.80 (±0.01)	23.23 (±0.46)	96.05 (±0.31)	5.00 (±0.00)	2.00 (±0.00)	2.12 (±0.02)	SCL§	363.74 (±11.38)	54.77 (±16.30)	418.51 (±4.91)
S_180	162-180	8.20	2.18 (±0.11)	0.54 (±0.02)	28.80 (±1.19)	96.37 (±0.03)	1.00 (±0.00)	<1	1.39 (±0.01)	SC	189.35 (±7.17)	7.05 (±1.11)	196.41 (±8.28)

† %IC = Inorganic carbon content; % OC = Organic carbon content; CEC = Cation exchange capacity; %base = Percent base saturation; M3P = Mehlich III extractable phosphorus; B1P = Bray I phosphorus; OM = Organic matter content; TIP = Total inorganic phosphorus; TOP = Total organic phosphorus; TP = Total phosphorus.

‡ Values in the parentheses are the standard deviations.

§ SC = Silty clay; SCL = Silty clay loam.

Table 3.2. General characteristics of the pure resin and the hybrid resin used in this study. Total Fe content of FerrIX™A33E.

Resin	Matrix	Structure type	Type of resin functional groups	Physical form	Particle size (μm)	Iron content (mg/g)	Specific surface areas (m^2/g)
AMBERLITE™ HPR9200, pure anion exchange resin	Polystyrene-DVB	Macroporous	Strong-base	White, spherical beads	640 ± 50	0	1625.1 ± 20.9
FerrIX™A33E, hybrid resin	Polystyrene-DVB	Macroporous	Strong-base	Brown, spherical beads	750±150	196.0±3.0	810.4 ± 38.2

Table 3.3. Parameters of isotherm models in phosphate adsorption by resins. Q_m and K_m represent the maximum adsorption (mg P/g) and a parameter related to the bonding strength (L/mg) in the Langmuir model, respectively. K_f and n are a parameter related to the adsorption capacity and a parameter related to the intensity of adsorption in the Freundlich model, respectively.

Resin	Langmuir model			Freundlich model		
	Q_m (mg/g)	K_m (L/g)	R^2	n	K_f	R^2
AMBERLITE™ HPR9200 (Pure resin)	13.16	1.10	0.983	1.44	1.12	0.993
FerrIX™A33E (Hybrid HPR9200)	7.69	7.29	0.989	4.43	3.76	0.997

Table 3.4. Phosphate desorption from P rich soils in different desorption systems. The total desorbed P is described in mg/kg, and the values in parentheses represent percentage of total desorbed P with respect to total P in each soil.

Soil sample ID	Desorption systems	Time (hr)								
		2	4	8	16	24	48	72	120	168
S_18	1g of hybrid resin	13.34 (3.4)	13.95 (3.6)	14.82 (3.8)	15.25 (3.9)	15.77 (4)	16.64 (4.2)	16.38 (4.2)	17.29 (4.4)	17.03 (4.3)
	1g of pure resin	6.15 (1.6)	6.67 (1.7)	6.75 (1.7)	7.56 (1.9)	8.37 (2.1)	8.46 (2.2)	8.46 (2.2)	8.98 (2.3)	9.5 (2.4)
	No resin	1.06 (0.3)	1.25 (0.3)	1.32 (0.3)	1.12 (0.3)	1.12 (0.3)	1.32 (0.3)	1.25 (0.3)	1.32 (0.3)	1.32 (0.3)
	0.5 g hybrid resin	12.38 (3.2)	12.87 (3.3)	13.97 (3.6)	14.79 (3.8)	15.44 (3.9)	15.97 (4.1)	16.46 (4.2)	16.71 (4.3)	16.87 (4.3)
	2 g of hybrid resin	13.40 (3.4)	14.26 (3.6)	14.95 (3.8)	15.65 (4.0)	15.97 (4.1)	16.67 (4.3)	16.99 (4.3)	17.12 (4.4)	17.32 (4.4)
S_90	1g of hybrid resin	7.09 (1.7)	7.19 (1.7)	7.37 (1.8)	7.53 (1.8)	7.94 (1.9)	7.95 (1.9)	7.93 (1.9)	8.15 (1.9)	7.85 (1.9)
	1g of pure resin	1.6 (0.4)	1.66 (0.4)	1.69 (0.4)	1.91 (0.5)	1.99 (0.5)	2.1 (0.5)	1.96 (0.5)	2.24 (0.5)	2.03 (0.5)
	No resin	0.26 (0.1)	0.66 (0.2)	0.4 (0.1)	0.4 (0.1)	0.33 (0.1)	0.46 (0.1)	0.53 (0.1)	0.46 (0.1)	0.53 (0.1)
S_180	1g of hybrid resin	2.93 (1.5)	3 (1.5)	3.21 (1.6)	3.24 (1.7)	3.29 (1.7)	3.29 (1.7)	3.29 (1.7)	3.33 (1.7)	3.45 (1.8)
	1g of pure resin	0.33 (0.2)	0.32 (0.2)	0.29 (0.1)	0.46 (0.2)	0.4 (0.2)	0.48 (0.2)	0.56 (0.3)	0.54 (0.3)	0.67 (0.3)
	No resin	0.03 (0)	0.03 (0)	0.1 (0)	0.07 (0)	0.07 (0)	0.1 (0)	0.13 (0.1)	0.1 (0)	0.16 (0.1)

Table 3.5. Parameters of kinetic models in the phosphate desorption data shown in Table 3.4.

Soil sample ID	Desorption systems	Pseudo-first order model			Pseudo-second order model				Elovich model			Intra-particle diffusion model		
		k_1 (1/hr)	q_e (mg/g)	R^2	k_2 (g/(mg hr))	q_e (mg/g)	k_2qe^2 (mg/(g hr))	R^2	α (mg/(L hr))	β (L/mg)	R^2	k_d (mg/(g $hr^{1/2}$))	C	R^2
S_18	1g of hybrid resin	0.031	3.014	0.482	0.037	17.241	11.099	1.000	1.72E+06	1.128	0.972	0.311	13.726	0.844
	1g of pure resin	0.038	4.734	0.763	0.029	9.461	2.601	0.998	1.45E+03	1.360	0.957	0.266	6.269	0.882
	No resin	0.026	0.059	0.342	0.466	1.328	0.821	1.000	5.93E+10	25.316	0.338	0.015	1.141	0.335
	0.5 g resin	0.043	5.362	0.905	0.031	17.007	8.873	1.000	5.59E+04	0.929	0.982	0.376	12.778	0.843
	2.0 g resin	0.041	4.278	0.883	0.039	17.391	11.848	1.000	2.08E+06	1.125	0.982	0.309	13.946	0.834
S_90	1g of hybrid resin	0.021	0.659	0.326	0.495	7.962	31.348	1.000	3.73E+12	4.376	0.845	0.076	7.206	0.660
	1g of pure resin	0.019	0.461	0.316	0.443	2.097	1.949	0.996	1.74E+04	7.837	0.821	0.044	1.644	0.675
	No resin	0.031	0.272	0.581	0.429	0.520	0.116	0.988	3.01E+05	43.668	0.089	0.009	0.391	0.103
S_180	1g of hybrid resin	0.027	0.502	0.729	0.258	3.423	3.029	0.999	5.08E+11	10.040	0.879	0.034	3.020	0.727
	1g of pure resin	0.028	0.506	0.753	0.158	0.651	0.067	0.979	1.201	13.158	0.831	0.030	0.268	0.889
	No resin	0.022	0.152	0.700	0.367	0.151	0.008	0.882	0.040	41.322	0.724	0.009	0.032	0.733

3.7. References

Arai, Y., and K.J. Livi. 2013. Underassessed phosphorus fixation mechanisms in soil sand fraction. Geoderma 192(1): 422–429.

Arai, Y., and D.L. Sparks. 2001. ATR-FTIR spectroscopic investigation on phosphate adsorption mechanisms at the ferrihydrite-water interface. J. Colloid Interface Sci. 241(2): 317–326.

Awual, M.R., and A. Jyo. 2011. Assessing of phosphorus removal by polymeric anion exchangers. Desalination 281(1): 111–117.

Barrow, N.J. 1984. Modeling the effects of pH on phosphate sorption by soils. J. Soil Sci. 35(2): 283–297.

Blaney, L.M., S. Cinar, and A.K. SenGupta. 2007. Hybrid anion exchanger for trace phosphate removal from water and wastewater. Water Res. 41(7): 1603–1613.

Bottini, A., and L. Rizzo. 2012. Phosphorus Recovery from Urban Wastewater Treatment Plant Sludge Liquor by Ion Exchange. Sep. Sci. Technol. 47(4): 613–620.

Boyer, T.H., A. Persaud, P. Banerjee, and P. Palomino. 2011. Comparison of low-cost and engineered materials for phosphorus removal from organic-rich surface water. Water Res. 45(16): 4803–4814.

Bray, R.H.., and L.T. Kurtz. 1945. Determination of total, organic, and available forms of phosphorus in soils. Soil Sci. 59(1): 39–46.

Elzinga, E.J., and D.L. Sparks. 2007. Phosphate adsorption onto hematite: An in situ ATR-FTIR investigation of the effects of pH and loading level on the mode of phosphate surface complexation. J. Colloid Interface Sci. 308(1): 53–70.

Fernández, F., and R. Hoeft. 2009. Managing soil pH and crop nutrients. Illinois Agronomy Handbook. p. 91–112

Gee, G.W., and J.W. Bauder. 1986. Particle Size Analysis. Methods Soil Anal. Part 1—Physical Mineral. Methods 9(9): 901–926.

Das Gupta, M., P. Loganathan, and S. Vigneswaran. 2012. Adsorptive Removal of Nitrate and Phosphate from Water by a Purolite Ion Exchange Resin and Hydrous Ferric Oxide Columns in Series. Sep. Sci. Technol. 47(12): 1785–1792.

Harris, W.G., R.D. Rhue, G. Kidder, R.B. Brown, and R. Littell. 1996. Phosphorus retention as related to morphology of sandy coastal plain soil materials. Soil Sci. Soc. Am. J. 60(5): 1513–1521.

He, Z., V. Baligar, K. Ritchey, and D. Martens. 1998. Determination of Soluble Phosphorus in the Presence of Organic Ligands or Fluoride. Soil Sci. Soc. Am. J. 62(6): 1538–1541.

Hendershot, W.H., and L.M. Lavkulich. 1983. Effect of sesquioxide coatings on surface charge of standard mineral and soil samples. Soil Sci. Soc. Am. J. 47(6): 1252–1260.

Ho, Y.S., and G. McKay. 1999. The sorption of lead(II) ions on peat. Water Res. 33(2): 578–584.

Ho, Y.S., and G. McKay. 2000. The kinetics of sorption of divalent metal ions onto sphagnum moss peat. Water Res. 34(3): 735–742.

Hongshao, Z., and R. Stanforth. 2001. Competitive adsorption of phosphate and arsenate on goethite. Environ. Sci. Technol. 35(24): 4753–4757.

Johir, M.A.H., T.T. Nguyen, K. Mahatheva, M. Pradhan, H.H. Ngo, et al. 2016. Removal of phosphorus by a high rate membrane adsorption hybrid system. Bioresour. Technol. 201: 365–369.

Klute, A., D.L. Carter, M.M. Mortland, and W.D. Kemper. 1986. Specific Surface. John Wiley & Sons, Ltd. p. 413–423

Kuo, S. 1996. Phosphorus, in: Sparks, D.L. et al. (Eds.), Methods of Soil Analysis. Part 3. Chemical Method. Soil Science Society of America, Inc; American Society of Agronomy, Inc., Madison, pp. 869–919

Lalley, J., C. Han, X. Li, D.D. Dionysiou, and M.N. Nadagouda. 2016. Phosphate adsorption using modified iron oxide-based sorbents in lake water: Kinetics, equilibrium, and column tests. Chem. Eng. J. 284: 1386–1396.

Liu, C., Q. Wang, F. Huang, and J. Zhang. 2016. Removal of phosphorus from anaerobic membrane bioreactor effluent by ion exchange resin. Sep. Sci. Technol. 51(17): 2833–2843.

Low, M.J.D. 1960. Kinetics of chemisorption of gases on solids. Chem. Rev. 60(3): 267–312.

McLean, E.O. 1982. Soil pH and Lime Requirement Determination. Methods of Soil Analysis. Part 2. Chemical and Microbiological Properties. p. 199–224

Mehlich, A. 1984. Mehlich 3 Soil Test Extractant: A Modification of Mehlich 2 Extractant. Commun. Soil Sci. Plant Anal. 15(12): 1409–1416.

Nur, T., M.A.H. Johir, P. Loganathan, T. Nguyen, S. Vigneswaran, et al. 2014. Phosphate removal from water using an iron oxide impregnated strong base anion exchange resin. J. Ind. Eng. Chem. 20(4): 1301–1307.

O'Neal, J.A., and T.H. Boyer. 2013. Phosphate recovery using hybrid anion exchange: Applications to source-separated urine and combined wastewater streams. Water Res. 47(14): 5003–5017.

Pan, B., B. Pan, W. Zhang, L. Lv, Q. Zhang, et al. 2009a. Development of polymeric and polymer-based hybrid adsorbents for pollutants removal from waters. Chem. Eng. J. 151(1–3): 19–29.

Pan, B., J. Wu, B. Pan, L. Lv, W. Zhang, et al. 2009b. Development of polymer-based nanosized hydrated ferric oxides (HFOs) for enhanced phosphate removal from waste effluents. Water Res. 43(17): 4421–4429.

van Raij, B., J.A. Quaggio, and N.M. da Silva. 1986. Extraction of phosphorus, potassium, calcium, and magnesium from soils by an ion-exchange resin procedure. Commun. Soil Sci. Plant Anal. 17(5): 547–566.

Ravel, B., and M. Newville. 2005. ATHENA, ARTEMIS, HEPHAESTUS: Data analysis for X-ray absorption spectroscopy using IFEFFIT. J. Synchrotron Radiat. 12(4): 537–541.

Ross, D.S., and Q. Ketterings. 1995. Recommended Methods for Determining Soil Cation Exchange Capacity. In: J.T. Sims and A. Wolf (eds.) Recommended soil testing procedures for the northeastern United States. Northeast Regional Bulletin. pp. 62–69

Sager, M. 1992. Chemical speciation and environmental mobility of heavy metals in sediments and soils. Tech. Instrum. Anal. Chem. 12(C): 133–175.

Schulte, E.E., and B.G. Hopkins. 1996. Estimation of Soil Organic Matter by Weight Loss-On-Ignition, in: Magdoff, F.R. et al. (Eds.), Soil Organic Matter: Analysis and Interpretation, Soil Science Society of America. Inc., Madison, pp. 21–31

Schwertmann, U., and R.M. Cornell. 2008. Iron oxides in the laboratory: preparation and characterization. John Wiley & Sons.

Sendrowski, A., and T.H. Boyer. 2013. Phosphate removal from urine using hybrid anion exchange resin. Desalination 322: 104–112.

Sengupta, S., and A. Pandit. 2011. Selective removal of phosphorus from wastewater combined with its recovery as a solid-phase fertilizer. Water Res. 45(11): 3318–3330.

Somasiri, L.L.W., and A.C. Edwards. 1992. An Ion Exchange Resin Method for Nutrient Extraction of Agricultural Advisory Soil Samples. Commun. Soil Sci. Plant Anal. 23(7–8): 645–657.

Sparks, D.L. 1989. Kinetics of soil chemical processes. ACADEMIC PRESS, INC., San Diego, the United States.

Tamura, H., K. Goto, T. Yotsuyanagi, and M. Nagayama. 1974. Spectrophotometric determination of iron(II) with 1,10-phenanthroline in the presence of large amounts of iron(III). Talanta 21(4): 314–318.

Tejedor-Tejedor, M.I., and M.A. Anderson. 1990. Protonation of Phosphate on the Surface of Goethite As Studied by CIR-FTIR and Electrophoretic Mobility. Langmuir 6(3): 602–611.

Thomas, G.W. 1996. Soil pH and soil acidity. Methods soil Anal. Part 3 - Chem. methods. (5): 475–490.

Upping, E., D.W. Thompson, M. Ohnstad, and N.B. Hetherington. 1986. Effects of ph on the release of metals from naturally-occurring oxides of mn and fe. Environ. Technol. Lett. 7(1–12): 109–114.

USDA Soil Survey. 2006. Soil Survey of Douglas County, Illinois.

Weber, W., and J. Morris. 1963. Kinetics of adsorption on carbon from solution. J. Sanit. Eng. Div. 89(2): 31–60.

Xu, S., L. Gentry, K. Chen, and Y. Arai. 2020. Intensive agricultural management induced subsurface accumulation of labile phosphorus in tile line dominated Midwestern agricultural soils. Soil Sci. Soc. Am. J. (In press).

You, X., D. Guaya, A. Farran, C. Valderrama, and J.L. Cortina. 2016. Phosphate removal from aqueous solution using a hybrid impregnated polymeric sorbent containing hydrated ferric oxide (HFO). J. Chem. Technol. Biotechnol. 91(3): 693–704.

Zasoski, R.J., and R.G. Burau. 1978. A technique for studying the kinetics of adsorption in suspensions. Soil Sci. Soc. Am. J. 42(2): 372–374.

Zhao, D., and A.K. Sengupta. 1998. Ultimate removal of phosphate from wastewater using a new class of polymeric ion exchangers. Water Res. 32(5): 1613–1625.

CHAPTER 4: PASSIVE DETECTION OF PHOSPHORUS IN AGRICULTURAL TILE WATERS USING REACTIVE HYBRID ANION EXCHANGE RESINS

Abstract

Tile drainage waters carry considerable loads of phosphorus (P) from agricultural fields to rivers and streams in the Midwestern U.S. An innovative and economical approach to monitor dissolved reactive P (DRP) flux in tile waters is needed to understand the extent of P loss in field-scale. In this study, a passive sampling technique was evaluated in laboratory and field-scale experiments. Iron oxide-coated polyacrylic/polystyrene anion exchange resins (hybrid resins) in mesh bags were used as a P sink. Laboratory batch adsorption isotherm and kinetic experiments indicated that the hybrid polyacrylic and polystyrene resins had high P adsorption capacity (7.69 and 19.84 mg/g, respectively), but the second-order rate constant was slightly greater for the hybrid polyacrylic resin (0.108 g/(mg·min)) than for the polystyrene resins (0.080 g/(mg·min)). The passive sampling method with field-calibrated hybrid polyacrylic resin and hybrid polystyrene resins (sampling rate: 0.1351 and 0.0763 L/h, respectively) predicted the average DRP concentrations of 0.006-0.020 mg/L, which corresponded to loads of P loss at 0.10-0.33 g/ha/day. The method also produced DRP concentrations of tile waters that did not differ significantly ($p > 0.05$) from the auto-sampling data. A rapid increase in DRP concentration during storm events and subsequent flooding events was also predicted well. In conclusion, a passive detection method using iron oxide coated hybrid resins can be recommended for monitoring seasonally fluctuating DRP flux in agricultural waters as long as the hybrid resins are well calibrated under specific field conditions (e.g., flow rate and concentration range).

4.1. Introduction

Phosphorus (P) loss from agricultural fields has long been an environmental issue due to its negative impacts on aquatic ecosystems such as eutrophication and hypoxia (Carpenter et al., 1998; Sharpley et al., 1994). Compared to nitrogen, little P is typically lost from fields from surface runoff (Gentry et al., 2007a). However, larger amounts of P can be lost during major erosion events and through subsurface tile drains. In fact, recently dissolved reactive P (DRP) losses at high concentrations have been reported through tile drainage in the Lake Erie watersheds of northwestern Ohio (K. King et al., 2015). Concentrations of DRP can range from <0.005 mg/L to many tenths of a mg L^{-1} in tile lines, and can be many mg L^{-1} in surface runoff (K. King et al., 2015). These concentrations and loads of DRP are more than enough to lead to eutrophication in downstream water bodies. To better understand and control P loss from agricultural watersheds, extensive monitoring is required to identify the major pathways of P loss in each field. However, due to the high cost of flow monitoring equipment and intensive sample analysis, it is not feasible to comprehensively assess P loads in agricultural drainage ditches and tile lines throughout the Midwestern United States (Rozemeijer et al., 2010) because of the cost. Therefore, it is ideal to develop a quick, easy, and inexpensive technique that could be used to monitor the P concentrations in agricultural waters during critical wet seasons when a large quantity of P is discharged from agricultural fields.

Several methods have been suggested to monitor the concentration of contaminants and nutrients in waters. The most common one is grab sampling, which obtains time-discrete records of the concentration of target substances (Müller et al., 2007; Rozemeijer et al., 2010; Worsfold et al., 2016). The precision and accuracy of grab sampling rely heavily on the sampling frequency, which is limited by manual labor especially for its application in long-term and large-scale monitoring (O'Brien et al., 2009; Knutsson et al., 2013;Edenborn et al., 2017). The minimum detectable concentration is also limited by the volume of water sampled at each time. Another disadvantage is that the discrete (i.e., snapshot) measurement may miss specific discharge events that happen during extreme rainfall (Ahrens et al., 2015; Vrana et al., 2005). Paper-based devices for in-site determination have also been suggested and are convenient and cost-efficient, but the

detection limit is relatively high and the accuracy is also affected by temporal variation of the contaminant concentrations (Jayawardane et al., 2012;Almeida et al., 2018). Transport of DRP in agricultural drainage water has generally been reported to be at low concentration; however, concentration quickly increases with tile flow immediately following heavy precipitation events (Müller et al., 2007; King et al., 2015b; Smith et al., 2015). Thus, the above monitoring methods are not ideal for the evaluation of P loss from agricultural fields. Passive sampling techniques offer a promising alternative for this purpose

Passive sampling is based on the accumulation of target substances in adsorbents that are deployed on-site. A time-weighted average concentration can be calculated according to the amount of the target substances on adsorbents after a certain period of deployment, which can be several days to months (Ahrens et al., 2015). As a time-integrated monitoring method, passive sampling is ideal for the detection of contaminants or nutrients that are in low concentration and with discrete discharge (Ahrens et al., 2015; Edenborn et al., 2017; Roll and Halden, 2016; Vrana et al., 2005). Use of passive samplers for the monitoring of aquatic contaminants started in the 1980s (Vrana et al., 2005). As of today it has been extensively utilized for the detection of organic pollutants and metals using several commercially available samplers (Gong et al., 2018; Gunold et al., 2008; Kingston et al., 2000; Schäfer et al., 2008). But its application for the monitoring of nutrients in agricultural waters has not been extensively tested.

To design a successful passive sampler, choosing a proper adsorbent is one of the most important steps. The uptake of target compounds by the sorbent material should be kinetically fast and have a large sorption capacity, and it would be preferable if the sorption is compound-specific (Ahrens et al., 2015; Edenborn et al., 2017; Vrana et al., 2005). The material should also allow the free passage of pore water and enable the recovery of the sorbed substances (De Jonge and Rothenberg, 2005). For the monitoring of DRP in agricultural waters using the passive sampling method, iron (oxyhydr)oxide coated anion exchange resin is an ideal adsorbent (O'Neal and Boyer, 2013; Sendrowski and Boyer, 2013; Sengupta and Pandit, 2011) since iron (oxyhydr)oxides can selectively and rapidly adsorb phosphate via inner-sphere complexation (Chitrakar et al., 2006; Funes et al., 2018; Luengo et al., 2006). The objective of this study was to evaluate the

passive sampling method using hybrid anion exchange resin bags to monitor the DRP loss in agricultural tile drainage water. Specifically, this study was aimed to evaluate: 1) P adsorption capacity of hybrid anion exchange resins in laboratory experiments, 2) its performance as a P sink in passive detection technique in field experiments, and 3) the prediction of DRP in the passive detection technology.

4.2. Materials and Methods

4.2.1. Materials

Two kinds of hybrid resins were selected in this study. A commercially available product - FerrIX™A33E (Purolite, King of Prussia, USA), which is an iron-loaded strong-base polystyrene-DVB hybrid resin, was chosen. Hereafter it is referred to as HR1. The second hybrid resin, designated as HR2, was synthesized via coprecipitation of iron oxides with weak-base polyacrylic resin, IRA67 (DuPont company, Wilmington, USA).

The preparation of HR2 was accomplished following two steps: 1) loading of ferric ions and 2) precipitation and transformation of iron (oxyhydr)oxide. Approximately 20 g of IRA67 resin and 250 mL of 1 M HNO_3 were placed in a 500 mL polypropylene bottle. The mixture was shaken on an orbital shaker at 75 rpm for 1 hr. After sedimentation for a few hours, the acidic solution was decanted and the resin was rinsed with ultrapure water. The acid washed resins were then mixed with 100 ml of 0.5 M $Fe(NO_3)_3$ and the mixture was shaken on an orbital shaker at 75 rpm for 1 hr. The mixture was titrated with 90 mL of 5 M NaOH, and its volume was adjusted to 500 mL. The bottles were shaken at 75 rpm for 3 hrs. Finally, the mixtures were placed in a convection oven at 70 °C for 60 hr. After the incubation, the hybrid resin was rinsed twice with ultrapure water. To exchange the hydroxide ion on the hybrid resin surface, resins were treated with 250 mL of 0.5 M $NaHCO_3$ for 2 hr, and then shaken with 250 mL of 0.5 M NaCl for 2 hr. After the final washing the resins with ultra-pure water, the hybrid resin was air-dried and stored for future use. This step helps to buffer the resin suspension at near neutral pH.

All reagents were prepared using ultrapure water (18.2 MΩ-cm), and ACS grade chemicals were used unless otherwise mentioned in text. All experiments were conducted at 21±0.8°C.

4.2.2. Characterization of the hybrid resins

The total Fe content and the mineralogical information of the iron loaded on hybrid resins were studied. The total iron content of the hybrid resins was determined after acid digestion. To dissolve iron in the hybrid resin, approximately 0.1 g of the hybrid resin was transferred into a 125 mL screw-capped polypropylene bottle that was filled with 100 mL of 5% hydroxylamine and 5 M HCl (Sager, 1992; Upping et al., 1986). The mixture was shaken in ultrasonic bath (Bransoic, CPX2800) for 5 min and then shaken at an orbital shaker at 80 rpm for 48 hrs., and the following filtration through Whatman No.2 filter paper the total iron concentration in the filtrate was measured in triplicate by a spectrophotometric method using 1, 10-phenanthroline (Tamura et al., 1974).

The mineralogy was assessed using Fe K-edge X-ray absorption spectroscopy (XAS) at ID12 at Advanced Photon Source, Argonne, IL, USA. A monochromator consisting of a double-crystal Si (220) was used. An incident beam of X-ray energy was calibrated using a Fe foil at the first inflection point (7112 eV) and detuned 50% at 7770eV. The beam size used was 2 mm in width x 1 mm in height. The calibration energy was monitored using a Fe foil during the scan. The transmission measurements were performed in air at room temperature. Spectra were recorded with three regions: 10 eV steps from 6880 to 7090 eV with 1 sec. dwell, 0.25 eV steps over the pre-edge from 7090 to 7140eV with 1 sec. dwell, and 0.25 eV steps from k of 1.62 to 14 $Å^{-1}$ with 1 sec. dwell. Three spectra were recorded. Acquiring multiple spectra across time allows us quantitative evaluation of reproducibility. Reference spectra of synthetic pure ferrihydrite, goethite, hematite, and lepidocrocite were also collected. These minerals were synthesized according to the methods described by Schwertmann and Cornell (Schwertmann and Cornell, 1991). Spectra were normalized with standard features of the ATHENA software package (Ravel and Newville, 2005), and linear combination of XAS reference spectra fit analysis was conducted.

The total surface area of the hybrid resins was measured using the ethylene glycol monoethyl ether (EGME) method (Klute et al., 1986). Approximately 0.5 g of oven-dried resins was placed in petri dishes and then in a vacuum desiccator with another petri dished filled with 10 mL EGME. The desiccator was connected to laboratory vacuum and evacuated for 10 minutes. The samples were then left in the desiccator overnight before re-weighing. The evacuation-stabilization-weighting cycle was repeated until the weights were constant.

4.2.3. Phosphorus adsorption isotherm in the hybrid resins

To characterize the maximum P adsorption capacity of the hybrid resins, P adsorption isotherm experiments were conducted. The results were used to design the field deployment experiments so that each resin bag does not exceed the maximum adsorption capacity of the resin.

A 100 mg/L phosphate stock solution was prepared in 10 mM NaCl, and then the stock solution was diluted to 3, 10, 20, 30, 40, and 50 mg/L for the isotherm experiment. Approximately 0.1 g of resin samples were added in a 50 mL Nalgene high speed centrifuge tube. A 30 mL phosphate solution was added and mixed with the resin on an end-over shaker at 30 rpm for 24 hr. The experiments were conducted in duplicate. After 24 hr, the suspensions were sampled and filtered through a 0.45 μm polyvinylidene difluoride (PVDF) filter. Aliquots were analyzed for phosphate concentration colorimetrically (He et al., 1998). The solution pH was kept at 7.5 using 0.01-0.1M HCl or NaOH.

Adsorption isotherm data were fitted to the Freundlich and Langmuir models.

For the Freundlich model

$$q = K_f \cdot C^{1/n} \text{ (Eq. 1)}$$

where q is the amount of phosphate adsorbed (mg P/g) ; C is the final equilibrium concentration of phosphate (mg P/L) ; K_f is a parameter related to the adsorption capacity; and n is a parameter related to the intensity of adsorption.

For the Langmuir model

$$\frac{C}{q} = \frac{1}{Q_m \cdot K_m} + \frac{C}{Q_m} \text{ (Eq. 2)}$$

where q is the amount of P adsorbed (mg P/g); C is the final equilibrium concentration of phosphate (mg P/L); Q_m represents the maximum adsorption capacity (mg P/g); and K_m is a parameter related to the bonding strength (L/mg).

4.2.4. Phopshate adsorption kinetics in hybrid resins

Phosphate adsorption kinetics were studied in the hybrid resins. 10mg/L of a P stock solution was prepared in 0.01 M NaCl solution. The solution pH was adjusted to 7.5 using 0.01-0.1M HNO_3 or NaOH with buffering from the use of 10 mM 3-(N-morpholino) propanesulfonic acid (MOPS) organic buffer.

Approximately 0.1 g of the hybrid resins was added to 30 mL of phosphate solution in centrifuge tubes. It was mixed on an orbital shaker at 80 rpm. After different sampling periods (3 min, 10 min, 30 min, 1 hr, 4 hr, 8 hr, 16 hr, and 24 hr), the supernatant was passed through a 0.45 μm PVDF filter. The phosphate concentrations in the samples were determined colorimetrically (He et al., 1998).

The data from kinetic experiments were fitted using a pseudo-first order model (Ho and McKay, 1999) and a pseudo-second order model (Ho and McKay, 2000).

For the pseudo-first order model

$$q_t = q_e(1 - e^{-k_1 t}) \text{ (Eq. 3)}$$

where q_t is the amount of phosphate adsorbed per unit weight of adsorbent (mg P g^{-1}) at time t (hr), q_e is the adsorption capacity of adsorbents (mg P/g) at equilibrium, k_1 (g/mg/hr) is the first order rate constant, and the terms, q_e and k_1, were calculated by linear regression of $\ln(q_t - q_e)$ vs. t.

For the pseudo-second order model

$$\frac{t}{q_t} = \frac{1}{k_2 {q_e}^2} + \frac{1}{q_e} t \text{ (Eq. 4)}$$

where q_t is the amount of phosphate adsorbed per unit weight of adsorbent (mg P/g) at time t (hr), q_e is the adsorption capacity of the adsorbents (mg P/g) at equilibrium, and k_2 (g/mg/hr) is the second order rate constant. The terms, q_e and k_2, were calculated by linear regression of plotting $\frac{t}{q_t}$ vs. t , where the slope and intercept correspond to $\frac{1}{q_e}$ and $\frac{1}{k_2 {q_e}^2}$, respectively.

4.2.5. Field deployment of hybrid resin bags

To deploy the hybrid resins in tile drainage water, the flow-through bag method was used to enclose the resin beads (Edenborn et al., 2017). To be specific, ~1 g of resin beads were enclosed in a polyester monofilament mesh bag (5 cm diameter × 5 cm height, 150 μm mesh size) (Universal Filters, Inc. Asbury Park, NJ).

The study site is located in Douglas County in east-central Illinois (Fig. 4.1) where a replicated tile drainage study based on timing of fertilizer N application was being conducted (Xu et al., 2020). The field is under no-till and strip-till practices and has been used to grow corn and soybeans in simple rotation. To demonstrate there were no statistically significant responses resulting from the N treatment or crop phase on DRP concentration, DRP loads, or tile discharge, an analysis of variance was performed using linear mixed models with N treatment as the fixed effect and block as the random effect (data not shown). Tile lines #4, #7 and #46 were selected for monitoring P loss. The three tiles drain 1.95, 1.86 and 1.63 hectares, respectively. To facilitate the drainage of soils for crop growth, the construction of drainage ditches and tile pipes started from 1878 (USDA Soil Survey, 2006). The sites received diammonium phosphate (18-46-0) at the rate of 22.4 g/m^2 every other year following soybean until 2016; however, no P fertilizer was applied from 2017 through 2020. Anhydrous ammonia was applied to corn at the rate of 20.2 g/m^2 in spring 2020.

From March 12th to April 23rd in 2020, mesh bags with FerrIX™A33E (HR1) and Hybrid IRA67(HR2) were deployed in duplicate for each tile line. The resin mesh bags were retrieved and replaced with new ones every 3 to 4 days. The collected hybrid resins were gently rinsed in ultrapure water and oven-dried at 40 ℃.

4.2.6. Monitoring flow rate, temperature, and DRP concentration of tile water

Each tile was fitted with an inline water level control structure containing a stoplog with a 45º V-notch weir (Agri Drain Corporation., Adair, IA). Water depth and temperature were recorded every 15 minutes using a Water Level Datalogger Model 3001 (Solinst, Ontario, Canada). Flow rates were determined using a discharge equation for inline water level control structures described by Chun and Cooke (2008). Approximately 50 mm of rain on April 19-20 caused flooding in the receiving agricultural ditch, which submerged all tiles and elevated water height by more than 1 m in each water level control structure. To be conservative, flow rate was adjusted to 0 L/s immediately following water heights that generate the maximum tile flow for each tile (approximately 2.5 L/s). When the water level in each water control structures began to decline, flow was assumed to resume until the height returned to the maximum discharge rate.

Water samples from the three tiles were collected every 3 to 5 days using ISCO 3700 automatic water samplers (Teledyne, Lincoln NE 68504, USA). Samples were passed through a 0.45 μm PVDF filters, and the filtrates were analyzed for DRP using a colorimetric method (He et al., 1998).

4.2.7. Recovery of passive-sampled P from tile drainage water and its evaluation

Adsorbed P from recovered hybrid resins was extracted in a 0.5 M NaOH and 0.5 M Na_2SO_4 solution. Recovered resins were briefly rinsed in ultrapure water to remove entrained tile water, and air-dried for 2 days. Approximately 0.5 g dry hybrid resins were added into 20 mL of the extractant. The tubes were shaken on an end-over shaker at 30 rpm for 16 hr. This extraction procedure was tested and found to provide ~100% P recovery from the hybrid resins. Aliquots were passed through 0.45 μm PVDF filters and

the P concentration in the filtrate was colorimetrically determined (He et al., 1998). The concentration of P retained in each mesh bag was converted to the time-weighted average concentration of P at the sampling site according to the field calibration coefficient described below.

To evaluate the passive detection method, the average DRP concentration calculated from the passive-sampled P in the hybrid resins was compared with the DRP concentrations of water samples from the Agridrain system.

4.2.8. Calibration of the passive sampling device

To estimate the DRP concentration in tile water from the extracted P values in the field-deployed hybrid resins, the amount of P adsorbed should be linearly correlated with the amount of P exposed to the hybrid resins, which is determined by the P concentration in water and the adsorption period. Calibration experiments were conducted to verify this linear relationship and to obtain the conversion coefficient (i.e., sampling rate) of the passive sampling device (i.e., mesh bags with hybrid resins).

In the laboratory, a flow-through device was used to simulate the adsorption of DRP by hybrid resins in tile water (Penn and Bowen, 2017). A 2 mg/L P stock solution was prepared in 0.01 M NaCl. The P concentration was set higher than common DRP concentrations in tile waters, which was necessary for obtaining a detectable P adsorption in resins within a relatively short time (up to 8 hr). Approximately 2.0 g of resins were put into the reaction chamber of the calibration apparatus. A peristaltic pump was used to pump the phosphate solution flowing through the reaction chamber at 9 mL/min. After a different running time (1, 2, 4, 6, and 8 hrs.), the resins were transferred to a 50 mL centrifugation tube for P recovery. A 20 mL extraction solution (0.5 M NaOH and 0.5 M Na_2SO_4) was added to the tube and shaken at an end-over shaker at 30 rpm for 16 h. The suspension was then passed through a 0.45 μm PVDF filter, and P concentration in the samples was determined colorimetrically (He et al., 1998). Since the P concentration exposed to the hybrid resins were constant at 2 mg/L, the amount of P adsorbed should be linearly related to the adsorption time; and the sampling rate was calculated accordingly.

Because the peristaltic pump used could not provide a flow rate higher than 9 mL/min, the extrapolation of DRP concentration using the sampling rate obtained from the laboratory calibration experiment may be affected by the actual flow rates in tiles, which can be greater than 9 mL/min. Therefore, another calibration experiment was conducted based on the field condition. To be specific, a sampling period with a stable flow rate at several liters/min and DRP concentrations of ~0.001-0.01 mg/L as determined from the monitoring data of the Agridrain auto-sampling system. The DRP concentrations of the three tiles water during the period were assumed to be constant at the auto-monitored values. Since the sampling time was the same for the three tile lines, the amount of P adsorbed should be linearly related to their DRP concentrations. The sampling rate was calculated accordingly and applied in the extrapolation of DRP concentration to other sampling periods.

4.2.9. Stability of the iron coating of hybrid resins

To verify that the field-deployed hybrid resins would not release iron into the drainage water, the stability of Fe coatings of the hybrid resin was tested. A mesh bag containing ~1 g of the hybrid resin was added into triplicate 125-mL polypropylene bottles containing 100 mL of 10 mM NaCl solution at pH 7. This experiment was done in triplicate. The bottles were shaken on an orbital shaker at 80 rpm. After 7 days, the hybrid resins were removed from the mesh bag and were air-dried. Approximately 0.1 g of the hybrid resin was placed in a clean polypropylene bottle to react with 100 mL of extractant solution containing 5% hydroxylamine and 5 M HCl (Sager, 1992; Upping et al., 1986). The bottle was placed in an ultrasonic bath (Bransoic, CPX2800) for 5 min and then shaken on an orbital shaker at 80 rpm for 48 hrs. The mixture was filtered with Whatman No. 2 filter papers to screen the pure resin beads, and the total Fe concentration in the filtrate was measured using the spectrophotometric method using 1, 10-phenanthroline (Sigma-Aldrich, St. Louis, MO) (Tamura et al., 1974). The total Fe concentration in these hybrid resins was compared with that of the material before the desorption experiments.

4.2.10. Statistical analysis

4.2.10.1. Calculation of the sampling rate

In the calibration experiment, the amount of P accumulated in the hybrid resin per unit time should be linearly correlated with the P concentration in the solution:

$$\frac{m_t}{t} = R_s \cdot c$$

where m_t is the amount of P adsorbed during the time (t) in the phosphate solution with constant concentration (c). Since the three parameters were either set constant or could be measured in the calibration experiment, the coefficient R_s of the hybrid resins was obtained as the slope by plotting $\frac{m_t}{t}$ vs c (Knutsson et al., 2013; Roll and Halden, 2016).

4.2.10.2. Average DRP concentration in monitored tile drainage water

The average concentrations of DRP in monitored tile drainage water were obtained from the field deployment experiments and the record from the autosamplers. From the field deployment of hybrid resin, the average concentration could be estimated using the equation

$$c = \frac{m_t}{R_s \cdot t}$$

where m_t is the amount of P adsorbed during the deployment time (t) and R_s is the sampling rate from the calibration experiment.

Based on the DRP concentration of each sampling period, the time-weighted and flow-weighted average concentrations of DRP were calculated respectively (Rozemeijer et al., 2010) as:

$$c_t = \frac{c_1 * t_1 + c_2 * t_2 + \cdots + c_n * t_n}{t}$$

$$c_Q = \frac{c_1 * Q_1 + c_2 * Q_2 + \cdots + c_n * Q_n}{Q_t}$$

where c_t is from the time-weighted average concentrations of DRP; c_n is the DRP concentration and t_n is the duration of n_{th} sampling period. c_Q is the flow-weighted

average concentration of DRP; Q_n is the daily discharge at the day and Q_t is the total discharge.

4.2.10.3. Load estimation

The load of P loss from a tile line in a certain time was estimated using the equation:

$$L_t = \frac{\sum c_n \cdot Q_n \cdot t_n}{t}$$

where L_t is the load of P loss; n is the number of the sampling period; and c_n and Q_n are the DRP concentration and the water flow volume of each deployment period for sampling time, t (Müller et al., 2007).

The Student's t-test analysis was conducted using IBM SPSS statistics for Windows, v.26 (IBM Corp., Armonk, NY, USA). The significance level was set at 0.05.

4.3. Results and Discussion

4.3.1. Material characterization

The physicochemical properties of the hybrid resins are summarized in Table 4.1. HR1 is an iron oxide coated strong-base polystyrene-DVB resin with total iron content of ~196 mg/g. HR2 is an iron oxide coated weak-base polyacrylic resin with total iron content of ~13.4 mg/g. The two hybrid resins have similar mean particle size, but total surface area of HR1 (~810 m^2/g) was much lower than that of HR2 (~3,515 m^2/g). The LC fitting of XAS spectra analysis showed that mineralogy in the two hybrid resins was predominantly goethite (Fig. 4.2). In the stability test of the iron oxide coating of the hybrid resins, total iron content was not significantly affected by shaking in a 10 mM NaCl solution for 7 days, suggesting that the goethite coating on the resin surface is stable during deployment (Table 4.1).

Iron oxide coated resins have been widely studied for the removal of anionic pollutants from wastewaters (e.g., Takeshita et al., 1979; Acelas et al., 2015; Pan et al., 2009b). The iron (oxyhydr)oxides in these hybrid resins were amorphous and nano-sized, which make them highly reactive (Pan et al., 2009b; Ren et al., 2012; Sengupta and

Cumbal, 2007; You et al., 2016). Goethite is a crystalline iron (oxyhydr)oxide and more stable than amorphous phases, which is important for the purpose of passive detection. The P adsorption capacity of goethite is less than that of amorphous iron hydroxides (Parfitt, 1989; Parfitt et al., 1975), but it is acceptable as long as it does not exceed the maximum P adsorption capacity during the resin bag deployment periods. To evaluate P adsorption capacity of the hybrid resins, batch isotherm experiments were conducted.

4.3.2. Batch P adsorption in the hybrid resins

4.3.2.1. Phosphate adsorption isotherm in the hybrid resins

The P adsorption isotherms for the hybrid resins are shown in Fig. 4.3a. The HR2 adsorbed more phosphate than HR1 at each initial P concentration. The isotherm curves were fitted well ($R^2 > 0.98$) to both the Freundlich (Fig. 4.3b) and the Langmuir (Fig. 4.3c) models. The P adsorption capacity of HR1 calculated from the Langmuir model was 7.69 mg/g, while that of HR2 was 19.84 mg/g for HR2 (Table 4.2).

The higher P adsorption capacity of HR2 could be due to the functional group property of the polyacrylic resin matrix. Since acrylic ester groups are polar and hydrophilic, polyacrylic resins are more reactive to water-soluble compounds like phosphate than polystyrene-DVB resins (Boari et al., 1976; Pan et al., 2009a; Zagorodni, 2006). The higher total surface area of HR2 (Table 4.1) also indicates that it has more reactive sites for phosphate.

4.3.2.2. Phosphate adsorption kinetics in the hybrid resins

To further understand P adsorption in the hybrid resins, P adsorption kinetic experiments were conducted. The P adsorption process was found to be biphasic (Fig. 4.4a) which suggested that the P adsorption in the hybrid resins was very quick and not limited by diffusion processes. Similar results were reported by several researchers. Ding et al. (2012) conducted P adsorption experiments with an iron oxide-coated polyacrylic resin. They reported a sharp increase of P adsorption in the first 10 minutes and then slightly increased after 30 minutes, which was similar to the kinetic data in this study.

To compare the adsorption kinetics in two hybrid resins, the data were fitted with the pseudo-first-order model (Ho and McKay, 1999) and the pseudo-second-order model (Ho and McKay, 2000) (Figs. 4.4b and Fig 4.4c). The parameters of these kinetic models in linear fitting plots (Figs. 4.4b and 4.4c) are summarized in Table 4.3. The pseudo-first-order model is the most widely used rate equation for the sorption of a solute from a liquid solution (Ho et al., 2000). The model describes non-reversible sorption processes governed by the first-order rate equation while the pseudo-second-order model describes sorption processes governed by the second-order rate equation. The pseudo-first-order model did not fit well to describe the adsorption process (R^2 = 0.726 for HR1 and R^2 = 0.487 for HR2) (Table 4.3). However, the pseudo-second-order model described the kinetic data well (R^2 > 0.999 for both two hybrid resins). The second-order rate constant $k_2$of the P adsorption in HR1 was 0.080 g/(mg min), which was slightly lower than that of HR2. In addition, the initial sorption rate, $k_2 {q_e}^2$ (Lalley et al., 2016) was calculated for both hybrid resins. The $k_2 {q_e}^2$ of P adsorption in HR1 was also lower than that of HR2. Sendrowski and Boyer (2013) also reported a rapid initial P adsorption and the best fitting of the pseudo-second-order kinetic model in the study of phosphate removal from urine using a hybrid anion exchange resin.

Overall, hybrid anion exchange resin is highly reactive for dissolved P. This property makes them ideal adsorbents for the passive detection method.

4.3.3. Field test of passive sampling of P in tile drainage water using hybrid resins

4.3.3.1. Recovery of passive-sampled P in the hybrid resins

Two different hybrid resins in mesh bags were deployed in three tile lines from March 12th to April 22nd, 2020. A total of 144 hybrid resin samples were collected. The adsorbed P in these hybrid resins were extracted and the results are shown in Fig. 4.5.

Comparing TP recovered in the hybrid resins from the three tiles, the recovery of P was lowest in Tile 7. Statistical analysis showed that hybrid resins collected from both Tiles 4 and 46 had a significantly higher TP content than that of Tile 7 (Table 4.4, p < 0.05). However, the amount of P adsorbed from Tiles 4 and 46 did not significantly differ (p = 0.073 for HR1 and p = 0.356 for HR2).

Comparing Figs. 4.5a and 4.5b, the recovery of TP in HR1 and HR2 is similar although the amount of extracted P fluctuated among different sampling periods. Total P in HR1 and HR2 remained at ~0.04-0.08 mg/g and 0.05-0.15 mg/g, respectively (Figs. 4.5a and 4.5b). The highest peaks (i.e., ~0.16 mg/g for HR1 and ~0.37 mg/g for HR2) are observed on March 19th. The highest recovery of TP in both resins coincides with a storm event (Fig. 4.7a) that occurred on March 19th with rainfall depth equal to 33.3 mm. A relatively small peak was identified on March 26th that also coincides with a rainfall event (Fig. 4.7a). The gradual rising trend in the last few sampling periods was also observed in both resins (Fig. 4.5). However, HR1 recovered less P than HR2 for each tile during the same sampling period ($p < 0.05$) (Table 4.5). A greater TP in the HR2 is explained by the results in the P isotherm and kinetic experiments. The relatively higher sorption rate of HR2 led to more phosphate adsorbed than HR1. It is important to note that the amount of P adsorbed by these hybrid resins was far below the maximum adsorption capacities (i.e., 7.69 mg/g for HR1 and 19.84 mg/g for HR2), suggesting that the hybrid resins are suited for the resin bag based passive detection method of P in tile water.

4.3.3.2. Calibration of the hybrid resin passive sampler

To calculate the DRP concentration in tile water from the amount of P extracted from the field-deployed hybrid resins, a functional relationship must be evaluated between the amount of P adsorbed in a certain time and the average P concentration in water. A linear relationship would be ideal for this application. The results of the laboratory calibration experiment are shown in Figs. 4.6a and 4.6b. The P content in the resins proportionally increased with increasing time. The amount of P adsorbed by the hybrid resins was linearly correlated to the amount of P exposed ($R^2 > 0.99$ for both hybrid resins) (Figs. 4.6a and 4.6b). The calculated sampling rate (R_L) was 0.1992 and 0.0156 L/h for HR1 and HR2, respectively. It should be noted that HR2 adsorbed less P than HR1 under the same conditions in the laboratory calibration experiment, which was different from the result of extracted P from field-deployed resin samples. However, the less adsorbed P is possibly due to the repulsion of hydroxyl ions in HR2. During the iron oxide coating of HR2, high concentrations of NaOH were used to precipitate ferric ions

and exchanged into the anion exchange resin. Although the resin was washed with a $NaHCO_3$ solution, residual hydroxyl ions could still have remained and imposed negatively influences on the adsorption of phosphate ions. But in the field application, hydroxyl ions on the resin surface were continually to be washed in flowing tile water during the 3-4 days of deployment, and its influence on P adsorption is less significant. Therefore, the P adsorption of HR2 was less affected in the field-deployed samples. Another factor that could influence the P adsorption is the flow rates. The flow rate of the laboratory calibration experiment is much lower than the actual flow rate in tiles as mentioned in the method section. Therefore, a field calibration is necessary to obtain a more reliable sampling rate for the calculation of average DRP concentration.

The sampling period from April 2nd to 5th was selected for the calibration because the concentration of DRP and tile water temperature were relatively stable during the period (see Figs. 4.7 and 4.8). There was no precipitation during this period and the water flow rate was stable at ~0.1 L/s. Based on the data from the Agridrain auto-sampling system, the DRP concentration of tile #4, #7 and #46 were considered to be constant at 0.0059, 0.0029 and 0.0109 mg/L, respectively. During the three days, HR1 adsorbed P at 0.0050, 0.0027, 0.0065 mg/g in the three tiles. The three pairs of DRP concentration and P content in HR1 was plotted in Fig. 4.6c and the linearly fitted (R^2 = 0.9058). The field sampling rate (R_F) of HR1 was 0.0763 L/h. Similarly, the DPR concentration and the P content in HR2 were linearly correlated (R^2 = 0.9145) (Fig. 4.6d) and the R_F of HR2 was 0.1351 L/h.

4.3.3.3. Estimation of DRP concentration of tile water using hybrid resin sampler

According to the result of calibration experiments, the passive-sampled P in the hybrid resins was converted into the average concentration of DRP in tile water using on the laboratory-sampling rate and the field-sampling rate. The line segments in Fig. 4.9 showed the average DRP concentration calculated from R_L in each sampling period. The DPR concentrations from HR1-sampling, HR2-sampling and auto-sampling were compared and the statistical analysis was conducted using paired Student's t-test (Table 4.5). For all three tile-lines, the DRP concentrations of auto-sampled tile water were significantly different from the DRP concentration calculated from the hybrid resin-

sampling based on the laboratory calibration data ($p < 0.05$). The results from HR1-sampling and HR2-sampling were also significantly different ($p < 0.05$). It suggests that the sampling rate from the laboratory calibration was not effective.

In contrast, the DRP concentrations calculated from R_F generally fall in the same range as the auto-sampling DRP data (Fig. 4.10). Statistical analysis showed no significant difference between the result of auto-sampling and passive-sampling, or between the passive sampling based on the field calibration data ($p > 0.05$) (Table 4.6). Similar trends of DRP data are shown in the data from the three sampling methods (i.e., hybrid resins and auto-sampler) (Fig. 4.10). For example, a peak was observed on March 19th in Fig. 4.10 except for the auto-sampled data of Tile 7. It corresponds to a heavy precipitation and a subsequent flood event (Figs. 4.7 and 4.8). The calculated DRP from hybrid resin-sampling were not always similar to the values from the auto-sampling. However, the auto-sampling data from the Agridrain system was single-point. It should be noted that the DRP data from the auto-sampler are discrete and may not capture quick changes in concentration due to increased flow. DPR concentrations in drainage waters could change even by an order of magnitude within a day (K. W. King et al., 2015; Müller et al., 2007; Smith et al., 2015). It is possible that the calculated DRP from hybrid resin-passive sampling might reflect the actual DRP values since the hybrid resins during the passive sampling were continuously exposed to DRP in tile waters. In addition, a larger response of DRP increase during the flooding event on March 19th was shown by the data from hybrid resin-sampling, especially HR2, than by the data from auto-sampling. This overestimation is attributed to the following two reasons. First, this might be influenced by the entry of particulate P during the storm event. During the storm event, a substantial quantity of particulate P including colloidal P is released in tile water (Y. Arai, personal communication, 15 June 2020). It could also be effected by stagnant (non-flowing tile water) during peak flooding (L. Gentry. Personal communication, 25 June 2020).

Although PP was not observed in the recovered resins, the possibility cannot be excluded that colloidal P adhesion occurred on the hybrid resins, which could lead to the overestimated values during the storm events. Second, the high volume of water during the storm event could have a dilution effect on the increase of total P discharge, which

may explain lower DRP values of auto-sampling DRP data to the flooding event than the hybrid resin-sampling data.

Throughout the entire monitoring period, the fluctuations of DRP concentrations of tile water were mainly influenced by precipitation events. Air temperature fluctuated but the water temperature was relatively stable (Fig. 4.7). The average DRP concentration of the entire monitoring period was calculated from the DRP data with R_F, and weighted averaged in two ways: time-weighted and flow-weighted (Table 4.7). Because of the positive relationship between the flow rate and DRP concentration, all the flow-weighted average DRP concentrations were significantly higher than their corresponding time-weighted average DRP concentrations ($p < 0.05$). Among the three tile lines, the highest flow-weighted average DRP concentration was 0.0198 ± 0.0003 mg/L from the flow-weighted HR2-sampling data of Tile 4, and the average DRP concentration of Tile 46 (0.0166 ± 0.0003 mg/L) was significantly higher than that of Tile 7 (0.0078 ± 0.0003 mg/L) ($p < 0.05$). These DRP concentrations are consistent with these reported for agricultural drainage water in the Midwest U.S., and are all lower than the critical eutrophication inducible level (0.02~0.03 mg/L) (Baker et al., 1975; Gentry et al., 2007b; K. W. King et al., 2015; Xue et al., 1998).

4.3.3.4. Evaluation of P loads in tile drainage water

Based on the DRP concentrations that were calculated with R_F and volumes of water flow, TP load in each sampling period was calculated (Table 4.8). Different P loads were observed from three tile lines ($p < 0.05$). According to the HR1-sampling data, tile 4, tile 7, and tile 46 released P at the rate of 0.53 ± 0.01, 0.18 ± 0.00, and 0.39 ± 0.01 g/day, respectively. Since tile 4, tile 7, and tile 46 cover 1.95, 1.86 and 1.63 hectares of drainage area, respectively, they discharged 0.27 ± 0.01, 0.10 ± 0.00 and 0.24 ± 0.01 grams of P per hectare per day, respectively. The data from HR2-sampling were slightly higher. They were 0.33 ± 0.00, 0.11 ± 0.01 and 0.25 ± 0.01 g/ha/d from tile 4, tile 7 and tile 46, respectively. In addition, the P discharge during the flooding event (March 19^{th} – 21^{st}) released 44.8-64.8 % of TP load in the three tiles during the six-week monitoring period. It showed the importance of high flow events on the loss of P from agricultural drainages,

which is in accordance with previous studies (Algoazany et al., 2007; Heathwaite and Dils, 2000; K. King et al., 2015; Smil, 2000).

4.4. Conclusion

This study showed that a passive detection technique using hybrid resin bags is a promising technique to monitor DRP in tile drainage water. The iron oxide coated-polyacrylic resin and -polystyrene resin were excellent adsorbents for P with the maximum P adsorption capacity of 7.69 and 19.84 mg/g, respectively. The P adsorption kinetic experiments showed that P adsorption in the hybrid polyacrylic and polystyrene resin was rapid with the second-order rate constant of 0.080 and 0.108 g/(mg min), respectively.

The field test of hybrid resin-samplers showed that the hybrid polyacrylic resin adsorbed more P than the hybrid polystyrene resin. The average DRP concentrations estimated from the passive sampling were 0.006-0.020 mg/L, which corresponded to loads of P loss at 0.10-0.33 g/ha/day. The passive samplings with the hybrid polyacrylic resin and the hybrid polystyrene resin predicted DRP concentrations of tile waters that have no significant difference (Paired Student's t-test, $p > 0.05$) with the auto-sampling data. High DRP concentrations and high flow rates were both observed during precipitation and subsequent flooding events. While both laboratory and in-field calibration experiments showed a linear correlation with the amount of P adsorbed in the hybrid resins (i.e., P concentration in water × adsorption time), sampling rate (R_f) calculated from the in-field calibration was necessary to improve the prediction of DRP concentrations in tile water.

Overall, iron oxide coated hybrid resins in the passive sampling method are proven to be suitable, reactive adsorbents to measure DRP in tile drainage waters. The passive detection technique for monitoring DRP flux in relatively high P concentrations and/or for longer sampling periods is theoretically possible but needs field verification. It should be further studied whether the predicted DRP in the passive sampling was affected by particulate P, since a considerable amount of particulate P in tiles is released during storm events (Kleinman et al., 2015; Saadat et al., 2018; Vaithiyanathan and Correll, 1992). The

development of more reactive hybrid resin that can be adapted to a wide range of temperature and flow rate is needed to expand the use of passive detection technique to different water bodies like rivers. The selection of mesh bags that are not greatly impacted by biofouling should be tested if the technique is adapted for a long-term deployment. Nevertheless, the passive detection method using iron oxide coated hybrid resins is recommended as an easy and economical tool to monitor seasonally fluctuating DRP flux in tile drainage waters as long as the hybrid resins are well calibrated for specific field conditions (e.g., flow rate and concentration range). The technique might be of interest to a large-scale monitoring project to understand and manage P loss in watersheds and or a river basin.

4.5. Figures

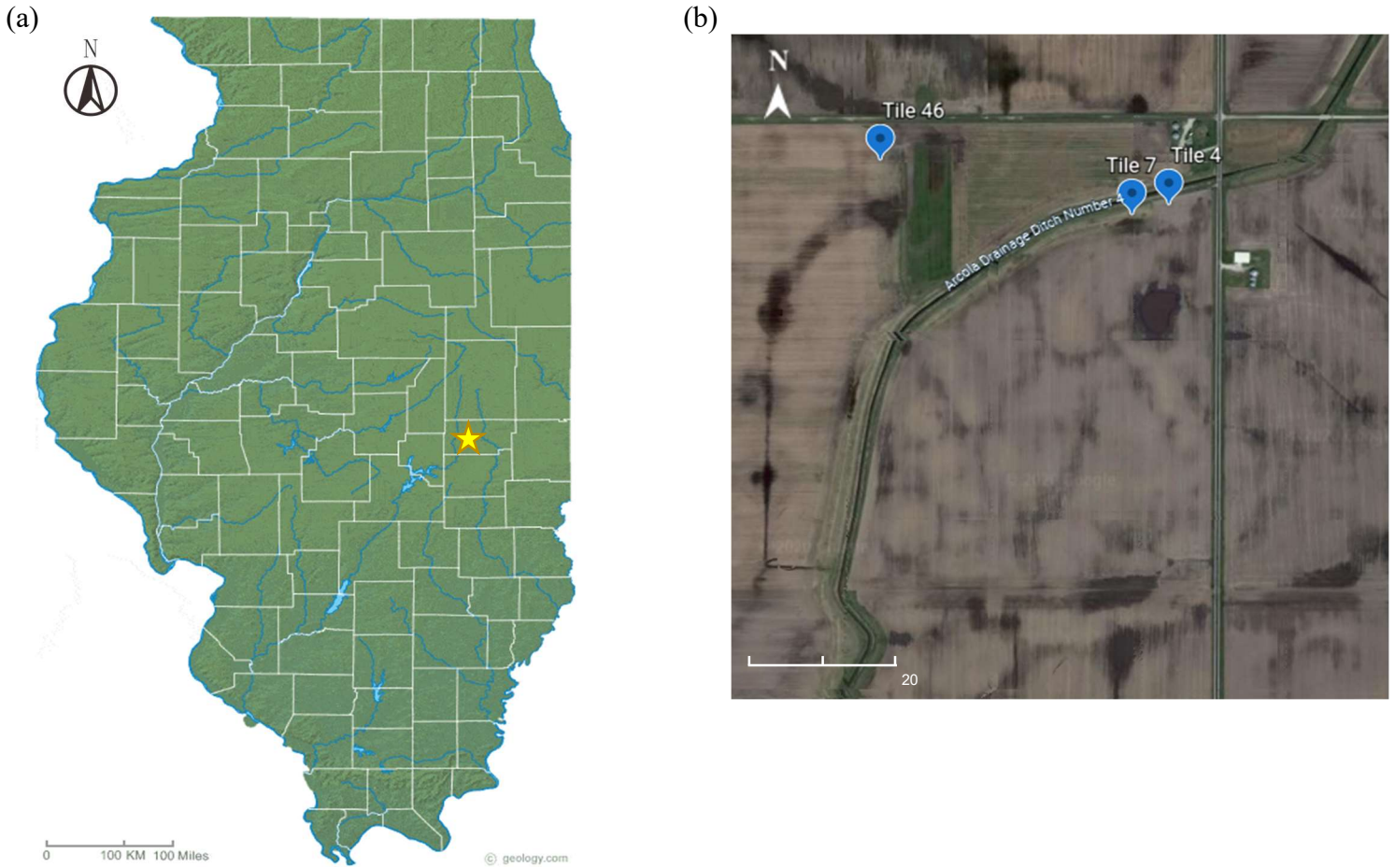

Fig. 4.1. (a) Location of the study site in Douglas County, Illinois. Cited from https://geology.com/topographic-physical-map/illinois.shtml. (b) A satellite image of the DRP monitoring site (39°43′27.5″N 88°13′56.8″W) obtained from Google Earth.

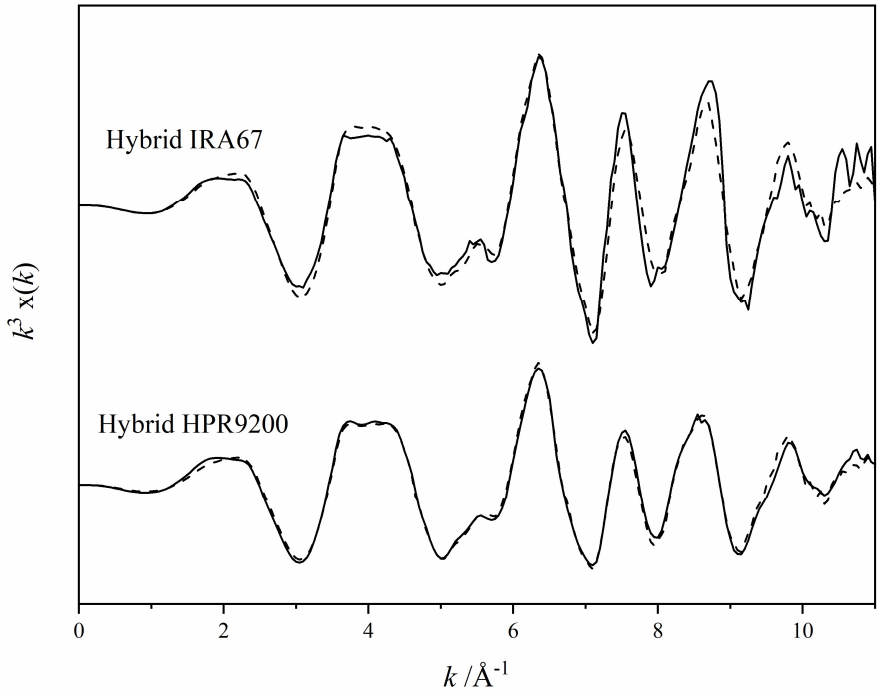

Fig. 4.2. Results to linear combination fitting of X-ray absorption spectroscopy (XAS) spectra of reference compounds on the spectra of hybrid HPR9200 (HR1) and hybrid IRA67 (HR2). Black solid line and dashed line represent the normalized k^3 weighted XAS spectra and fit, respectively. HR1 is 100 % goethite (R-factor: 0.01) and HR2 is 82±4% goethite and 18±2% hematite (R-factor: 0.06).

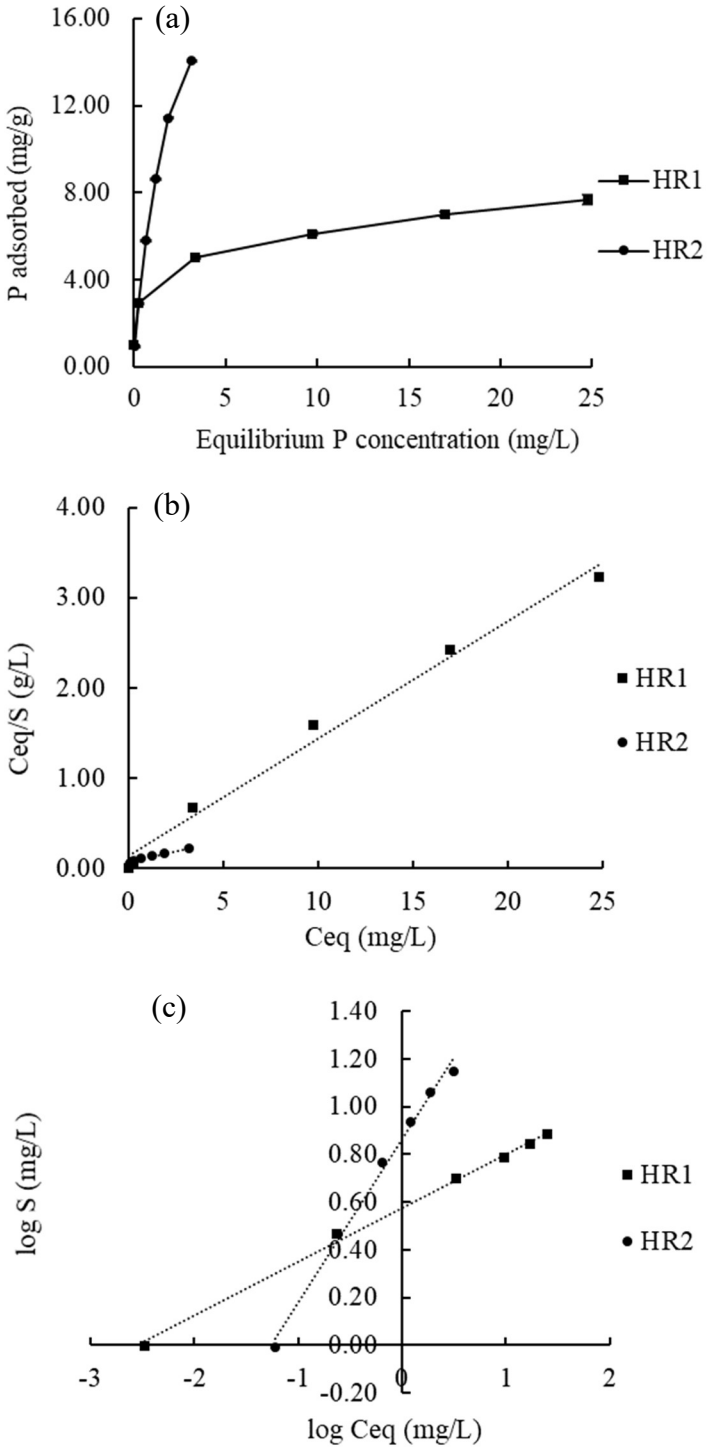

Fig. 4.3. (a) Phosphate adsorption isotherm at pH 7.5 in FerrIX™A33E (HR1), and Hybrid IRA67 (HR2). (b) and (c) show the linear fitting of the isotherm data in Langmuir model and Freundlich model, respectively.

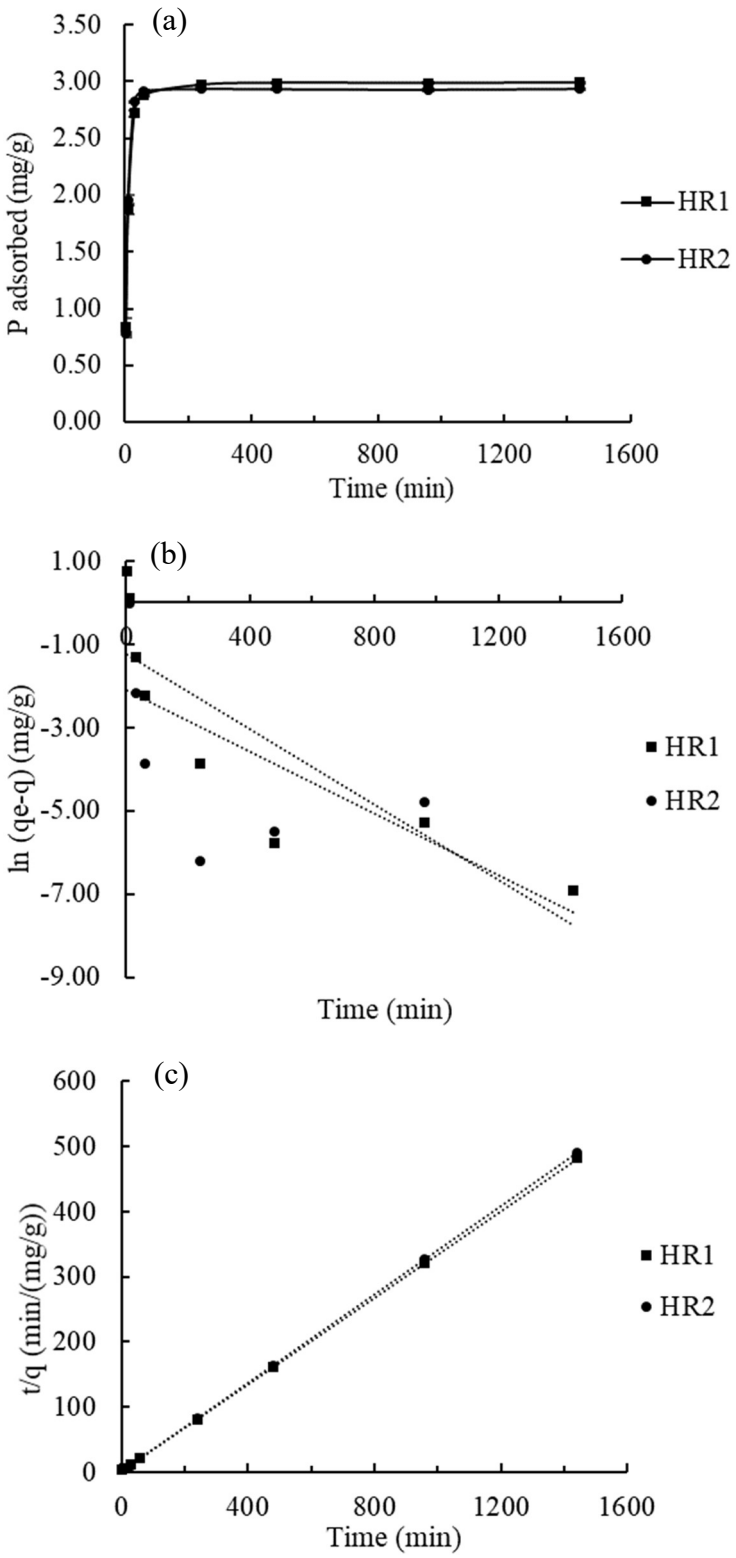

Fig. 4.4. (a) Phosphate adsorption kinetics in the hybrid resins. (b) and (c) show the linear fitting in the Pseudo-first-order model and the Pseudo-second-order model, respectively.

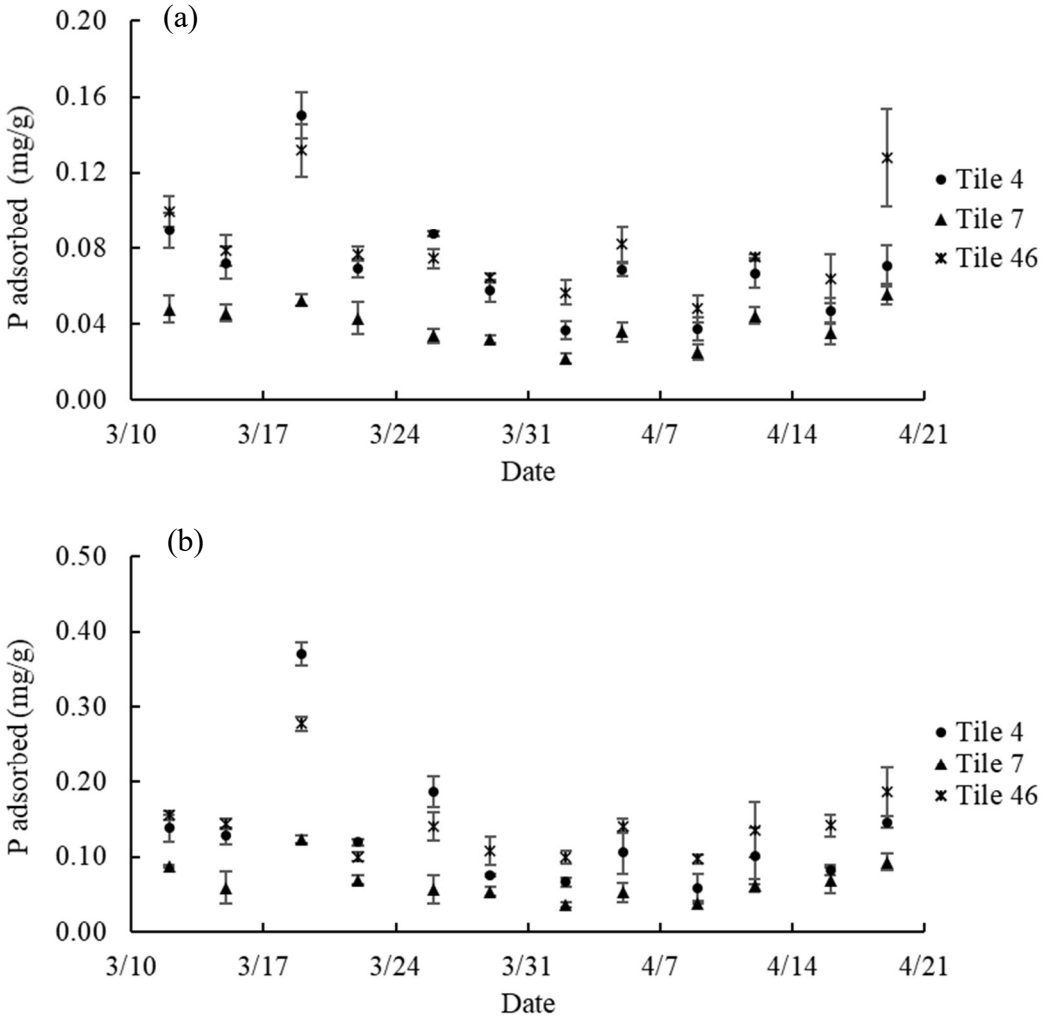

Fig. 4.5. Phosphate adsorption in the hybrid resin (a) HR1 and (b) HR2 from the three tile lines in each sampling period.

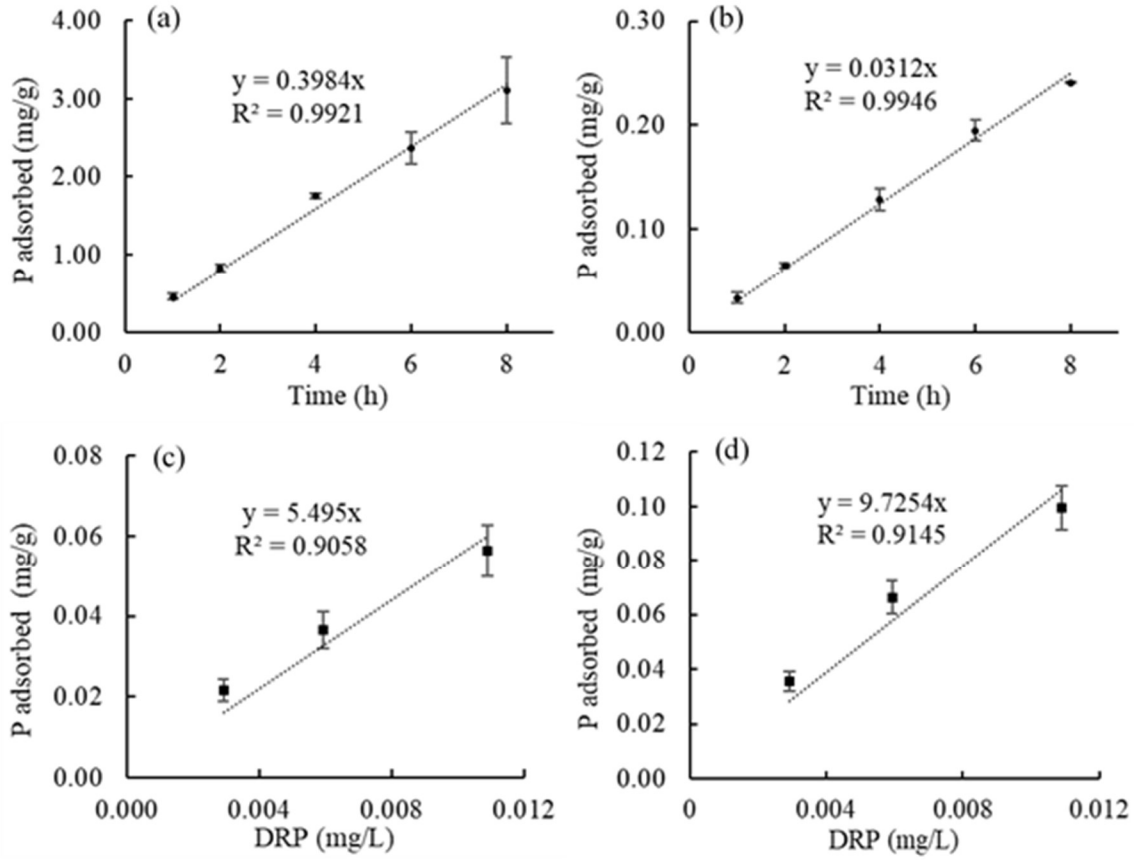

Fig. 4.6. Laboratory calibration experiments using (a) HR1 and (b) HR2. The dashed lines show the linear fitting of the amount of P adsorbed with different adsorption time. Laboratory sampling rate, R_L, for HR1 and HR2 is calculated to be 0.1992 and 0.0156 L/h, accordingly. (c) and (d) shows the result of field calibration experiments using HR1 and HR2, respectively. The dashed lines show the linear fitting of the amount of P adsorbed with the DRP concentration of the tile water. Field sampling rate, R_F, for HR1 and HR2, is 0.0763 and 0.1351 L/h, respectively.

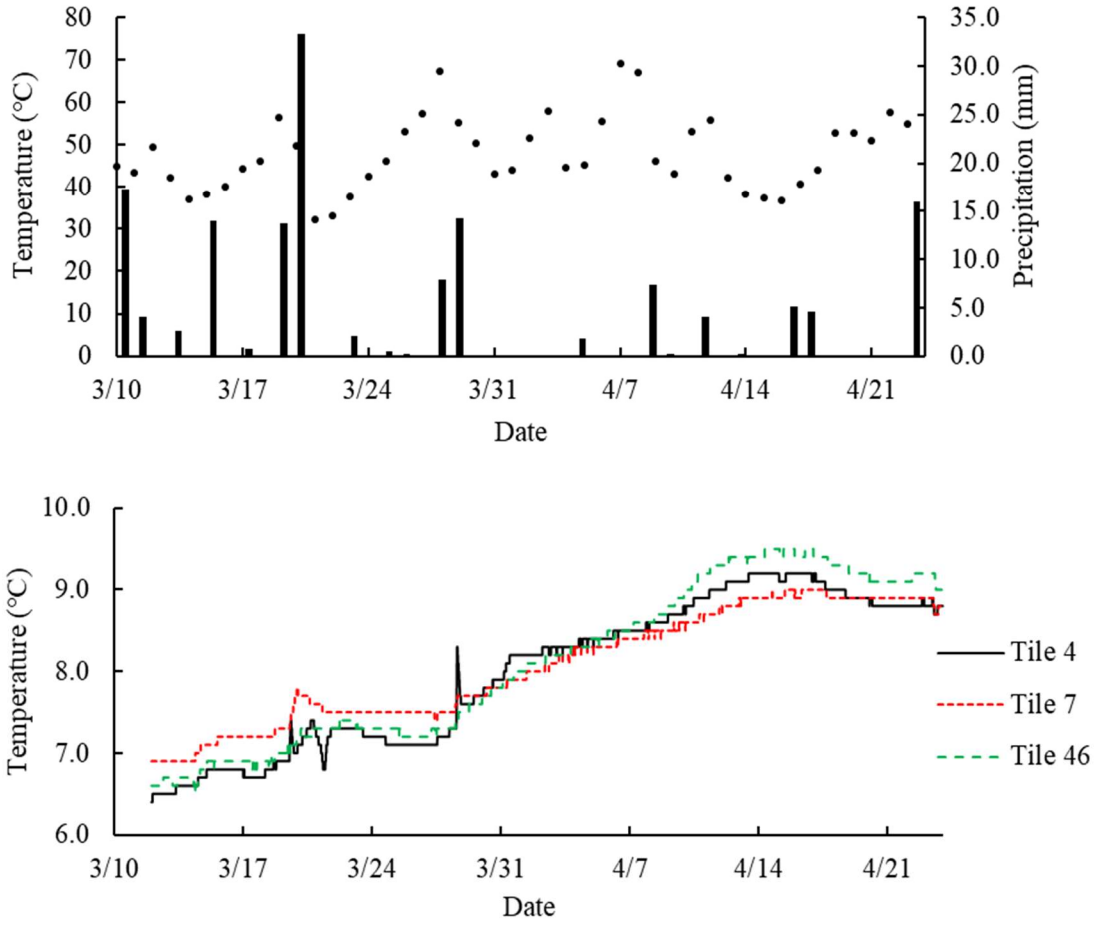

Fig. 4.7. Weather conditions in spring 2020 at the study site in East-Central Illinois, USA. (a) daily air temperature shown in dots and daily precipitation shown in columns; (b) tile water temperature.

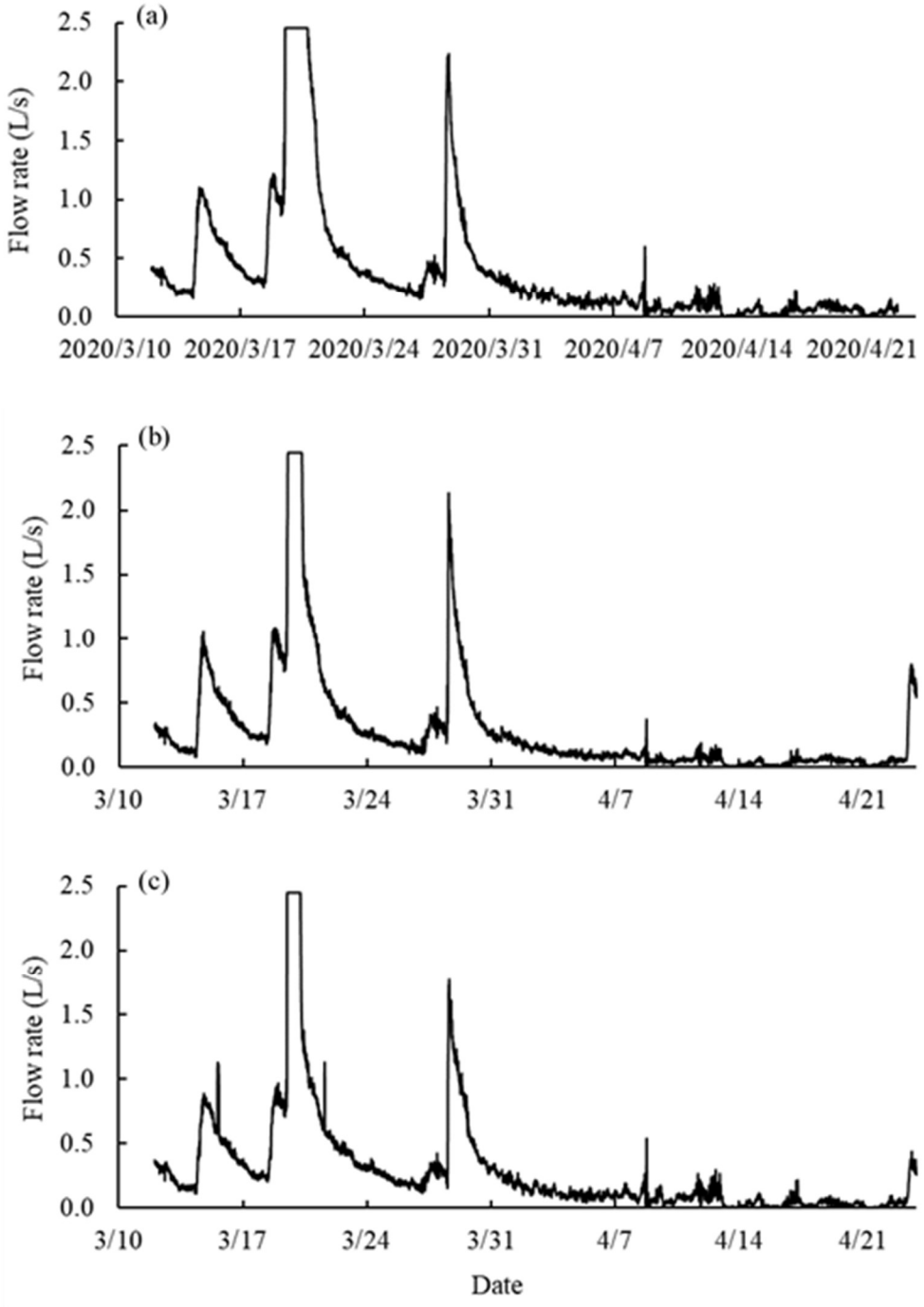

Fig. 4.8. Water flow rate in (a) tile line #4, (b) tile line #7 and (c) tile line #46 recorded by the Agridrain system. Please note that the flows between March 19th-20th exceeded 2.47 L/s, which is the detection limit of the Agridrain structure. This period is considered to be in flooding condition and is represented by horizontal straight lines.

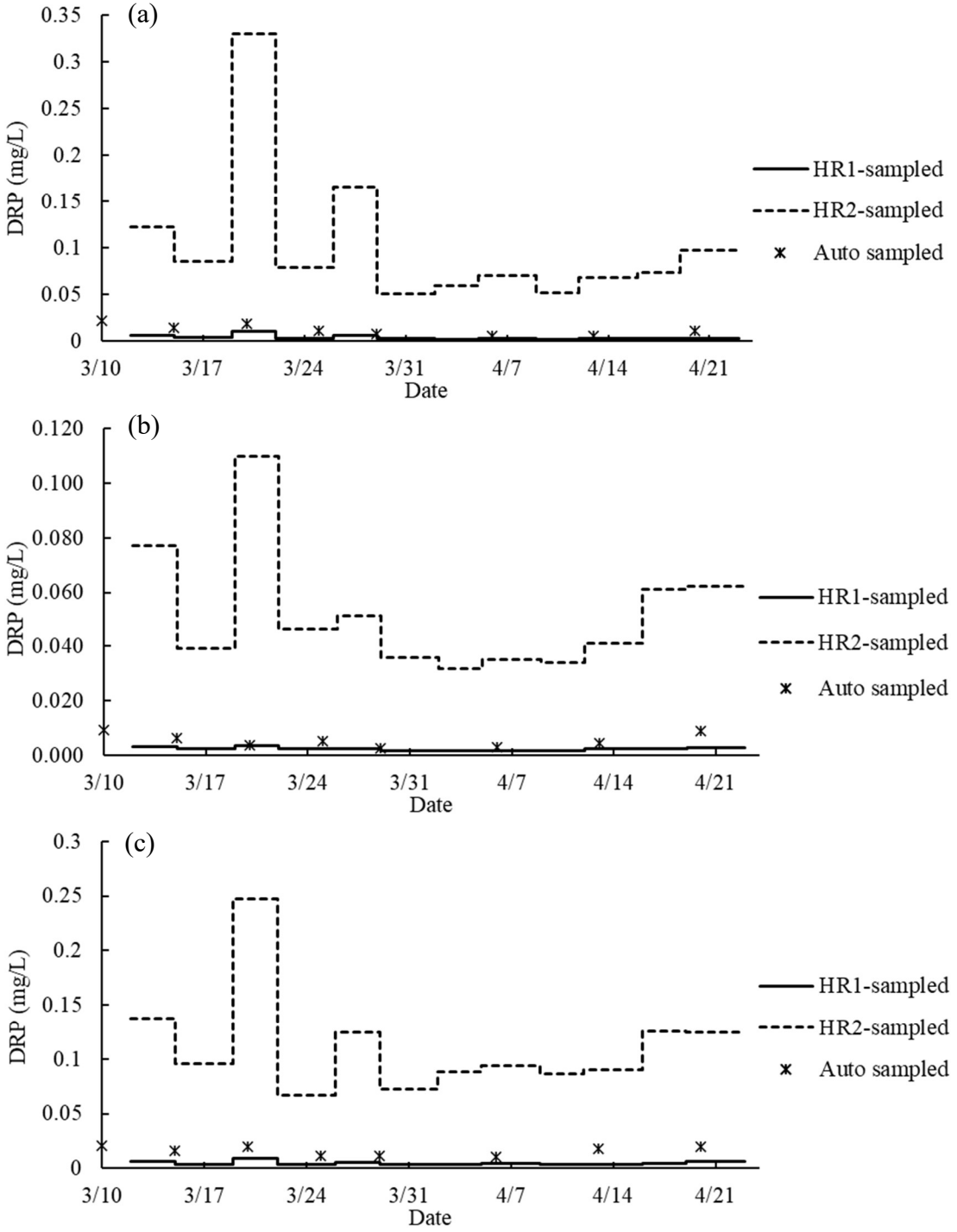

Fig. 4.9. Phosphate concentration of tile water from (a) tile #4, (b) tile #7 and (c) tile #46. The line segments represent the average DRP concentration in each sampling period calculated based on the lab sampling rates, R_L. The scattered dots show the DRP concentration of tile water weekly sampled by the Agridrain system.

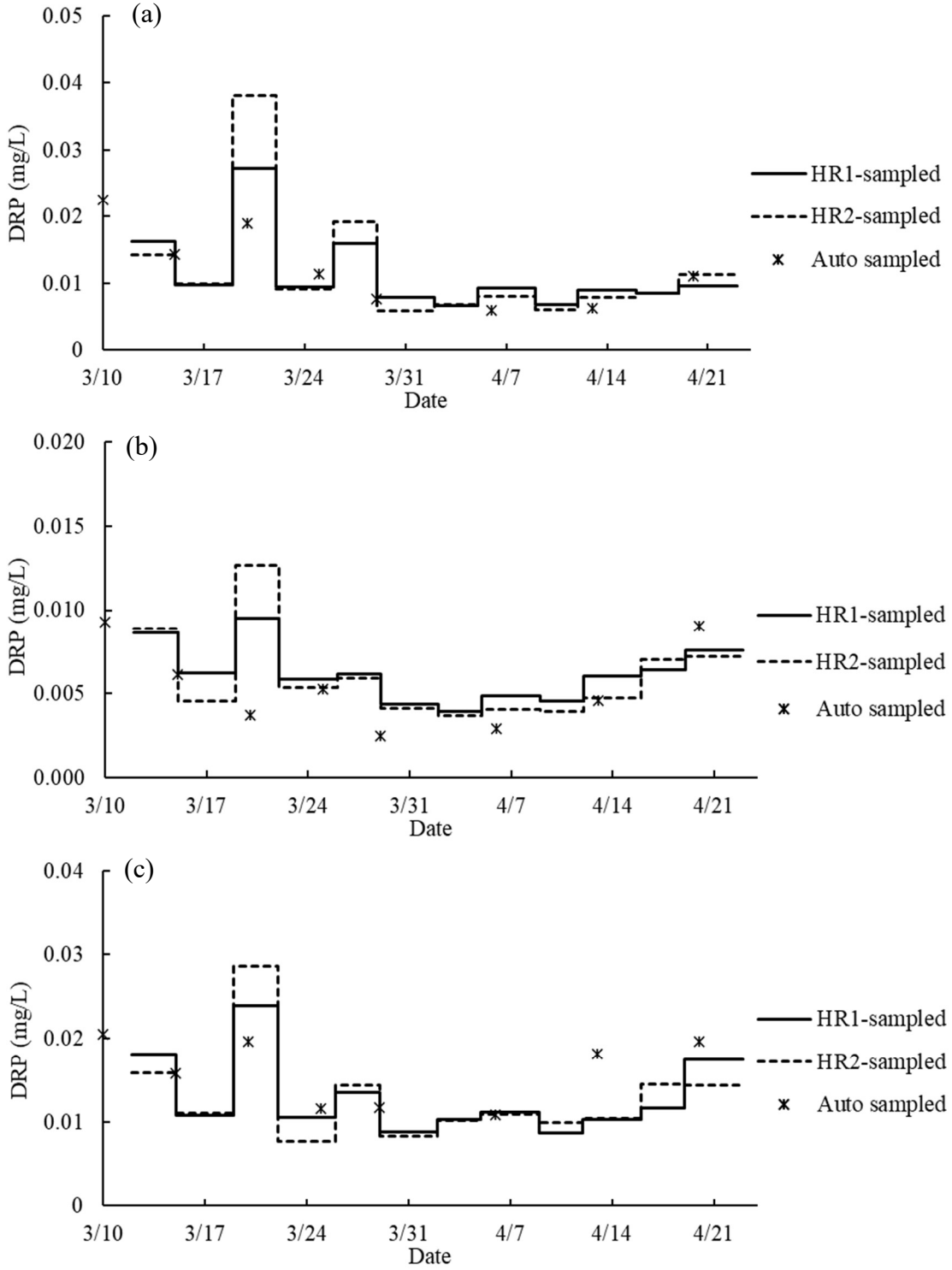

Fig. 4.10. Phosphate concentration of tile water from (a) tile #4, (b) tile #7 and (c) tile #46. The line segments represent the average DRP concentration in each sampling period calculated based on the field sampling rates, R_F. The scattered dots show the DRP concentration of tile water weekly sampled by the Agridrain system.

4.6. Tables

Table 4.1. Physical and chemical properties of hybrid anion exchange resins used in this study.

Resin	Matrix	Structure type	Type of functional groups	Physical form	Particle size (μm)	Total surface area (m^2/g)	Iron content before shaking (mg/g)	Iron content after shaking (mg/g)
FerrIX™A33E (HR1)	Polystyrene-DVB	Macroporous	Strong-base	Brown, opaque, spherical beads	750 ± 450	810 ± 38	196.0 ± 3.0	194.3 ± 2.5
Hybrid IRA67 (HR2)	Polyacrylic	Gel	Weak-base	Reddish brown, spherical beads	625 ± 125	3515 ± 21	13.4 ± 0.8	13.5 ± 0.5

Table 4.2. Parameters of isotherm models in phosphate adsorption by hybrid resins. Q_m and K_m represent the maximum adsorption (mg/g) and a parameter related to the bonding strength (L/mg) in the Langmuir model, respectively. K_f and n are a parameter related to the adsorption capacity and a parameter related to the intensity of adsorption in the Freundlich model, respectively.

Resin	Langmuir model			Freundlich model		
	Q_m (mg/g)	K_m (L/mg)	R^2	n	K_f ($mg^{1-1/n}\ L^{1/n}/g$)	R^2
FerrIX™A33E (HR1)	7.686	0.948	0.983	4.435	3.759	0.983
Hybrid IRA67 (HR2)	19.841	0.719	0.983	1.467	7.263	0.993

Table 4.3. Parameters of kinetic equations to model the P adsorption kinetic data in hybrid resins. q_e is the adsorption capacity of adsorbents (mg/g) at equilibrium. k_1 (g/mg/hr) is the first order rate constant. k_2 (g/mg/hr) is the second order rate constant.

Resin	Pseudo-first order model			Pseudo-second order model			
	k_1 (1/min)	q_e (mg/g)	R^2	k_2 (g/(mg min))	q_e (mg/g)	$k_2 q_e^2$ (mg/(g min))	R^2
FerrIX™A33E (HR1)	0.045	0.291	0.726	0.080	3.000	0.719	1.000
Hybrid IRA67 (HR2)	0.004	0.124	0.487	0.108	2.943	0.934	1.000

Table 4.4 Results of paired t-test for comparing the P content (mg/kg) in the hybrid resins deployed in three tile lines. The data are shown in Fig. 4.5.

Data sets	Pairs	Paired Differences					t	df	*p* (2-tailed)
		Mean	Std. Deviation	Std. Error Mean	95% Confidence Interval of the Difference				
					Lower	Upper			
HR1_sampled	Tile_4 - Tile_7	0.032	0.024	0.007	0.016	0.047	4.497	11	0.001
	Tile_7 - Tile_46	-0.042	0.018	0.005	-0.053	-0.031	-8.317	11	0.000
	Tile_4 - Tile_46	-0.011	0.019	0.005	-0.022	0.001	-1.978	11	0.073
HR2_sampled	Tile_4 - Tile_7	0.065	0.065	0.019	0.024	0.106	3.470	11	0.005
	Tile_7 - Tile_46	-0.077	0.030	0.009	-0.096	-0.058	-8.950	11	0.000
	Tile_4 - Tile_46	-0.012	0.044	0.013	-0.040	0.016	-0.964	11	0.356

Table 4.5. Results of paired t-test for comparing the DRP concentrations obtained by the hybrid resin-sampling method and the auto-sampling method. The passive-sampling data were calculated based on the laboratory calibration data. DPR concentrations of each auto-sampled tile water were compared with the calculated DPR concentration in corresponding passive-sampling periods. The data are shown in Fig. 4.9.

Data sets	Pairs	Paired Differences					t	df	*p* (2-tailed)
		Mean	Std. Deviation	Std. Error Mean	95% Confidence Interval of the Difference				
					Lower	Upper			
Tile_4	HR1_sampled - HR2_sampled	-0.112	0.094	0.036	-0.199	-0.025	-3.149	6	0.020
	HR1_sampled - Auto_sampled	-0.006	0.003	0.001	-0.008	-0.003	-5.953	6	0.001
	HR2_sampled - Auto_sampled	0.106	0.093	0.035	0.020	0.192	3.029	6	0.023
Tile_7	HR1_sampled - HR2_sampled	-0.056	0.027	0.010	-0.081	-0.031	-5.499	6	0.002
	HR1_sampled - Auto_sampled	-0.002	0.002	0.001	-0.004	0.000	-3.038	6	0.023
	HR2_sampled - Auto_sampled	0.053	0.027	0.010	0.028	0.078	5.212	6	0.002
Tile_46	HR1_sampled - HR2_sampled	-0.114	0.060	0.023	-0.169	-0.058	-4.980	6	0.003
	HR1_sampled - Auto_sampled	-0.010	0.003	0.001	-0.013	-0.007	-9.143	6	0.000
	HR2_sampled - Auto_sampled	0.104	0.060	0.023	0.048	0.159	4.585	6	0.004

Table 4.6. Results of paired t-test for comparing the DRP concentrations obtained by the hybrid resin-sampling method and the auto-sampling method. The passive-sampling data was calculated based on the field calibration data. DPR concentrations of each auto-sampled tile water were compared with the calculated DPR concentration in corresponding passive-sampling periods. The data are shown in Fig. 4.10.

Data sets	Pairs	Paired Differences					t	df	*p* (2-tailed)
		Mean	Std. Deviation	Std. Error Mean	95% Confidence Interval of the Difference				
					Lower	Upper			
Tile_4	HR1_sampled - HR2_sampled	-0.001	0.005	0.002	-0.005	0.003	-0.470	6	0.655
	HR1_sampled - Auto_sampled	0.002	0.004	0.001	-0.001	0.005	1.402	6	0.210
	HR2_sampled - Auto_sampled	0.003	0.007	0.003	-0.004	0.010	0.953	6	0.377
Tile_7	HR1_sampled - HR2_sampled	-0.007	0.003	0.001	-0.010	-0.004	-5.579	6	0.001
	HR1_sampled - Auto_sampled	-0.005	0.002	0.001	-0.007	-0.003	-5.724	6	0.001
	HR2_sampled - Auto_sampled	0.002	0.003	0.001	-0.001	0.005	1.379	6	0.217
Tile_46	HR1_sampled - HR2_sampled	0.014	0.006	0.002	0.009	0.020	6.760	6	0.001
	HR1_sampled - Auto_sampled	-0.001	0.004	0.001	-0.005	0.003	-0.677	6	0.524
	HR2_sampled - Auto_sampled	-0.015	0.004	0.001	-0.019	-0.012	-10.348	6	0.000

Table 4.7. Average DRP concentrations in tile water throughout the six-week monitoring period. The DRP concentrations were calculated from the field-calibrated passive sampling method, and averaged with the time and flow volume of each sampling period, respectively. Standard deviations are shown in parentheses.

Sampling site	Sampling material	Time-weighted average DPR (mg/L)	Flow-weighted average DPR (mg/L)
Tile 4	HR1	0.0111 (0.0002)	0.0163 (0.0005)
	HR2	0.0116 (0.0002)	0.0198 (0.0003)
Tile 7	HR1	0.0061 (0.0000)	0.0071 (0.0000)
	HR2	0.0059 (0.0000)	0.0078 (0.0003)
Tile 46	HR1	0.0127 (0.0008)	0.0155 (0.0004)
	HR2	0.0127 (0.0001)	0.0166 (0.0003)

Table 4.8. Load of P (unit: g/period) discharged through each tile line in each sampling period calculated from flow volumes and DRP concentrations based on HR1- and HR2-sampling. The period refers to 3-4 days of deployment period of the resin bags. Standard deviations are shown in parentheses.

Sampling site	Sampling material	Sampling period (shown as the initial date)												Total P load (g)	Average P load (g/day)
		12-Mar	15-Mar	19-Mar	22-Mar	26-Mar	29-Mar	2-Apr	5-Apr	9-Apr	12-Apr	16-Apr	19-Apr		
Tile 4	HR1	1.7 (0.18)	1.95 (0.23)	12.49 (1.02)	1.29 (0.09)	2.11 (0.03)	1.28 (0.13)	0.29 (0.04)	0.4 (0.02)	0.14 (0.02)	0.17 (0.02)	0.13 (0.02)	0.19 (0.03)	22.16 (0.61)	0.53 (0.01)
	HR2	1.49 (0.19)	1.95 (0.17)	17.42 (0.72)	1.26 (0.05)	2.54 (0.28)	0.96 (0.02)	0.3 (0.03)	0.35 (0.09)	0.13 (0.04)	0.15 (0.05)	0.13 (0.01)	0.23 (0.01)	26.89 (0.46)	0.64 (0.01)
Tile 7	HR1	0.69 (0.11)	0.99 (0.10)	3.36 (0.20)	0.58 (0.11)	0.68 (0.08)	0.58 (0.04)	0.13 (0.02)	0.15 (0.02)	0.07 (0.01)	0.08 (0.01)	0.08 (0.01)	0.11 (0.01)	7.51 (0.01)	0.18 (0.00)
	HR2	0.71 (0.02)	0.73 (0.27)	4.49 (0.17)	0.53 (0.05)	0.65 (0.21)	0.55 (0.06)	0.12 (0.01)	0.13 (0.03)	0.06 (0.00)	0.06 (0.01)	0.08 (0.02)	0.11 (0.01)	8.22 (0.35)	0.20 (0.01)
Tile 46	HR1	1.47 (0.12)	1.72 (0.18)	7.91 (0.83)	1.19 (0.06)	1.39 (0.09)	1.23 (0.04)	0.32 (0.04)	0.37 (0.04)	0.17 (0.03)	0.16 (0.00)	0.11 (0.02)	0.16 (0.03)	16.2 (0.45)	0.39 (0.01)
	HR2	1.3 (0.05)	1.77 (0.08)	9.44 (0.31)	0.87 (0.05)	1.47 (0.20)	1.17 (0.20)	0.32 (0.03)	0.36 (0.02)	0.2 (0.01)	0.17 (0.04)	0.13 (0.01)	0.13 (0.02)	17.33 (0.35)	0.41 (0.01)

4.7. References

Acelas, N.Y., B.D. Martin, D. López, and B. Jefferson. 2015. Selective removal of phosphate from wastewater using hydrated metal oxides dispersed within anionic exchange media. Chemosphere 119: 1353–1360.

Ahrens, L., A. Daneshvar, A.E. Lau, and J. Kreuger. 2015. Characterization of five passive sampling devices for monitoring of pesticides in water. J. Chromatogr. A 1405: 1–11.

Algoazany, A.S., P.K. Kalita, G.F. Czapar, and J.K. Mitchell. 2007. Phosphorus transport through subsurface drainage and surface runoff from a flat watershed in east central Illinois, USA. J. Environ. Qual. 36(3): 681–693.

Almeida, M.I.G.S., B.M. Jayawardane, S.D. Kolev, and I.D. McKelvie. 2018. Developments of microfluidic paper-based analytical devices (μPADs) for water analysis: A review. Talanta 177(2017): 176–190.

Baker, L., K.L. Campbell, H.P. Johnson, and J. Hanway. 1975. Nitrate, Phosphorus, and Sulfate in Subsurface Drainage Wate. J. Environ. Qual. 4(3): 406–412.

Boari, G., L. Liberti, and R. Passino. 1976. Selective Renovation of Eutrophic Wastes Phosphate Removal. Water Res. 10(5): 421–428.

Carpenter, S.R., N.F. Caraco, D.L. Correll, R. W.Howarth, A.N. Sharpley, et al. 1998. Nonpoint pollution of surface waters with phosphorus and nitrogen. Ecol. Appl. 8(1998): 559–568.

Chitrakar, R., S. Tezuka, A. Sonoda, K. Sakane, K. Ooi, et al. 2006. Phosphate adsorption on synthetic goethite and akaganeite. J. Colloid Interface Sci. 298(2): 602–608.

Chun, J.A., and R.A. Cooke. 2008. Calibrating agridrain water level control structures using generalized weir and orifice equations. Appl. Eng. Agric. 24(5): 595–602.

Ding, L., C. Wu, H. Deng, and X. Zhang. 2012. Adsorptive characteristics of perchlorate from aqueous solutions by MIEX resin. J. Colloid Interface Sci. 376(1): 224–232.

Edenborn, H.M., B.H. Howard, J.I. Sams, D.J. Vesper, and S.L. Edenborn. 2017. Passive detection of Pb in water using rock phosphate agarose beads. J. Hazard. Mater. 336: 240–248.

Funes, A., F.J. Martínez, I. Álvarez-Manzaneda, J.M. Conde-Porcuna, J. de Vicente, et al. 2018. Determining major factors controlling phosphorus removal by promising adsorbents used for lake restoration: A linear mixed model approach. Water Res. 141: 377–386.

Gentry, L.E., M.B. David, T. V. Royer, C.A. Mitchell, and K.M. Starks. 2007a. Phosphorus Transport Pathways to Streams in Tile-Drained Agricultural Watersheds. J. Environ. Qual. 36: 408–415.

Gentry, L.E., M.B. David, T. V. Royer, C.A. Mitchell, and K.M. Starks. 2007b. Phosphorus Transport Pathways to Streams in Tile-Drained Agricultural Watersheds. J. Environ. Qual. 36: 408–415.

Gong, X., K. Li, C. Wu, L. Wang, and H. Sun. 2018. Passive sampling for monitoring polar organic pollutants in water by three typical samplers. Trends Environ. Anal. Chem. 17(January): 23–33.

Gunold, R., R.B. Schäfer, A. Paschke, G. Schüürmann, and M. Liess. 2008. Calibration of the Chemcatcher®passive sampler for monitoring selected polar and semi-polar pesticides in surface water. Environ. Pollut. 155(1): 52–60.

He, Z., V. Baligar, K. Ritchey, and D. Martens. 1998. Determination of Soluble Phosphorus in the Presence of Organic Ligands or Fluoride. Soil Sci. Soc. Am. J. 62(6): 1538–1541.

Heathwaite, A.L., and R.M. Dils. 2000. Characterising phosphorus loss in surface and subsurface hydrological pathways. Sci. Total Environ. 251–252: 523–538.

Ho, Y.S., and G. McKay. 1999. The sorption of lead(II) ions on peat. Water Res. 33(2): 578–584.

Ho, Y.S., and G. McKay. 2000. The kinetics of sorption of divalent metal ions onto sphagnum moss peat. Water Res. 34(3): 735–742.

Ho, Y.S., J.C.Y. Ng, and G. McKay. 2000. Kinetics of pollutant sorption by biosorbents: Review. Sep. Purif. Methods 29(2): 189–232.

Jayawardane, B.M., I.D. McKelvie, and S.D. Kolev. 2012. A paper-based device for measurement of reactive phosphate in water. Talanta 100: 454–460.

De Jonge, H., and G. Rothenberg. 2005. New device and method for flux-proportional sampling of mobile solutes in soil and groundwater. Environ. Sci. Technol. 39(1): 274–282.

King, K., M. Williams, and N. Fausey. 2015a. Contributions of Systematic Tile Drainage to Watershed-Scale Phosphorus Transport. J. Environ. Qual. 44(2): 486–494.

King, K.W., M.R. Williams, M.L. Macrae, N.R. Fausey, J. Frankenberger, et al. 2015b. Phosphorus Transport in Agricultural Subsurface Drainage: A Review. J. Environ. Qual. 44(2): 467–485.

Kingston, J.K., R. Greenwood, G.A. Mills, G.M. Morrison, and L.B. Persson. 2000. Development of a novel passive sampling system for the time-averaged measurement of a range of organic pollutants in aquatic environments. J. Environ. Monit. 2(5): 487–495.

Kleinman, P.J.A., D.R. Smith, C.H. Bolster, and Z.M. Easton. 2015. Phosphorus Fate, Management, and Modeling in Artificially Drained Systems. J. Environ. Qual. 44(2): 460–466.

Klute, A., D.L. Carter, M.M. Mortland, and W.D. Kemper. 1986. Specific Surface. John Wiley & Sons, Ltd. p. 413–423

Knutsson, J., S. Rauch, and G.M. Morrison. 2013. Performance of a passive sampler for the determination of time averaged concentrations of nitrate and phosphate in water. Environ. Sci. Process. Impacts 15(5): 955–962.

Lalley, J., C. Han, X. Li, D.D. Dionysiou, and M.N. Nadagouda. 2016. Phosphate adsorption using modified iron oxide-based sorbents in lake water: Kinetics, equilibrium, and column tests. Chem. Eng. J. 284: 1386–1396.

Luengo, C., M. Brigante, J. Antelo, and M. Avena. 2006. Kinetics of phosphate adsorption on goethite: Comparing batch adsorption and ATR-IR measurements. J. Colloid Interface Sci. 300(2): 511–518.

Müller, B., A. Stöckli, R. Stierli, E. Butscher, and R. Gächter. 2007. A low cost method to estimate dissolved reactive phosphorus loads of rivers and streams. J. Environ. Monit. 9(1): 82–86.

O'Brien, D.S., B. Chiswell, and J.F. Mueller. 2009. A novel method for the in situ calibration of flow effects on a phosphate passive sampler. J. Environ. Monit. 11(1): 212–219.

O'Neal, J.A., and T.H. Boyer. 2013. Phosphate recovery using hybrid anion exchange: Applications to source-separated urine and combined wastewater streams. Water Res. 47(14): 5003–5017.

Pan, B., B. Pan, W. Zhang, L. Lv, Q. Zhang, et al. 2009a. Development of polymeric and polymer-based hybrid adsorbents for pollutants removal from waters. Chem. Eng. J. 151(1–3): 19–29.

Pan, B., J. Wu, B. Pan, L. Lv, W. Zhang, et al. 2009b. Development of polymer-based nanosized hydrated ferric oxides (HFOs) for enhanced phosphate removal from waste effluents. Water Res. 43(17): 4421–4429.

Parfitt, R.L. 1989. Phosphate reactions with natural allophane, ferrihydrite and goethite. J. Soil Sci. 40(2): 359–369.

Parfitt, R.L., R.J. Atkinson, and R.S.C. Smart. 1975. The Mechanism of Phosphate Fixation by Iron Oxides1. Soil Sci. Soc. Am. J. 39(5): 837–841.

Penn, C., and J. Bowen. 2017. Characterization of PSMs. Design and Construction of Phosphorus Removal Structures for Improving Water Quality. Fisrt edit. Springer. p. 105

Ravel, B., and M. Newville. 2005. ATHENA, ARTEMIS, HEPHAESTUS: Data analysis for X-ray absorption spectroscopy using IFEFFIT. J. Synchrotron Radiat. 12(4): 537–541.

Ren, J., N. Li, and L. Zhao. 2012. Adsorptive Removal of Cr (VI) from Water by Anion Exchanger Based Nanosized Ferric Oxyhydroxide Hybrid Adsorbent. Chem. Biochem. Eng. Q. 26(2): 111–118.

Roll, I.B., and R.U. Halden. 2016. Critical review of factors governing data quality of integrative samplers employed in environmental water monitoring. Water Res. 94: 200–207.

Rozemeijer, J., Y. van der Velde, H. de Jonge, F. van Geer, H.P. Broers, et al. 2010. Application and Evaluation of a New Passive Sampler for Measuring Average Solute

Concentrations in a Catchment Scale Water Quality Monitoring Study. Environ. Sci. Technol. 44(4): 1353–1359.

Saadat, S., L. Bowling, J. Frankenberger, and E. Kladivko. 2018. Nitrate and phosphorus transport through subsurface drains under free and controlled drainage. Water Res. 142: 196–207.

Sager, M. 1992. Chemical speciation and environmental mobility of heavy metals in sediments and soils. Tech. Instrum. Anal. Chem. 12(C): 133–175.

Schäfer, R.B., A. Paschke, B. Vrana, R. Mueller, and M. Liess. 2008. Performance of the Chemcatcher® passive sampler when used to monitor 10 polar and semi-polar pesticides in 16 Central European streams, and comparison with two other sampling methods. Water Res. 42(10–11): 2707–2717.

Sendrowski, A., and T.H. Boyer. 2013. Phosphate removal from urine using hybrid anion exchange resin. Desalination 322: 104–112.

Sengupta, A.K., and L.H. Cumbal. 2007. Hybrid anion exchanger for selective removal of contaminating ligands from fluids and method of manufacture thereof. : U.S. Patent 7,291,578.

Sengupta, S., and A. Pandit. 2011. Selective removal of phosphorus from wastewater combined with its recovery as a solid-phase fertilizer. Water Res. 45(11): 3318–3330.

Sharpley, A.N., S.C. Chapra, R. Wedepohl, J.T. Sims, T.C. Daniel, et al. 1994. Managing Agricultural Phosphorus for Protection of Surface Waters: Issues and Options. J. Environ. Qual. 23: 437–451.

Smil, V. 2000. Phosphorus in the environment: natural flows and human interferences. Annu. Rev. energy Environ. 25(1): 53–88.

Smith, D.R., K.W. King, L. Johnson, W. Francesconi, P. Richards, et al. 2015. Surface Runoff and Tile Drainage Transport of Phosphorus in the Midwestern United States. J. Environ. Qual. 44(2): 495.

Takeshita, R., I. Yoshida, and K. Ueno. 1979. Adsorption behaviour of phosphate ion on the iron (III) compleks of a chelating Resin. Bul. Chem. Soc. Japan 52(9): 2577–2580.

Tamura, H., K. Goto, T. Yotsuyanagi, and M. Nagayama. 1974. Spectrophotometric determination of iron(II) with 1,10-phenanthroline in the presence of large amounts of iron(III). Talanta 21(4): 314–318.

Upping, E., D.W. Thompson, M. Ohnstad, and N.B. Hetherington. 1986. Effects of ph on the release of metals from naturally-occurring oxides of mn and fe. Environ. Technol. Lett. 7(1–12): 109–114.

USDA Soil Survey. 2006. Soil Survey of Douglas County, Illinois.

Vaithiyanathan, P., and D.L. Correll. 1992. The Rhode River Watershed: Phosphorus Distribution and Export in Forest and Agricultural Soils. J. Environ. Qual. 21(2): 280–288.

Vrana, B., I.J. Allan, R. Greenwood, G.A. Mills, E. Dominiak, et al. 2005. Passive sampling techniques for monitoring pollutants in water. TrAC - Trends Anal. Chem. 24(10): 845–868.

Worsfold, P., I. McKelvie, and P. Monbet. 2016. Determination of phosphorus in natural waters: A historical review. Anal. Chim. Acta 918: 8–20.

Xue, Y., M.B. David, L.E. Gentry, and D.A. Kovacic. 1998. Kinetics and modeling of dissolved phosphorus export from a tile- drained agricultural watershed. J. Environ. Qual. 27(4): 917–922.

You, X., D. Guaya, A. Farran, C. Valderrama, and J.L. Cortina. 2016. Phosphate removal from aqueous solution using a hybrid impregnated polymeric sorbent containing hydrated ferric oxide (HFO). J. Chem. Technol. Biotechnol. 91(3): 693–704.

Zagorodni, A.A. 2006. Ion exchange materials: properties and applications. First edit. Elsevier.

CONCLUSIONS

In this study, a series of laboratory and field experiments has been conducted to evaluate a passive detection technique using well-characterized hybrid (i.e., iron oxide-coated) anion exchange resins for the monitoring of P in agricultural tile waters. The following conclusions are drawn from the results of the study.

Anion exchange resins are one of the best adsorbents for P, and its performance of P removal from water is highly influenced by resin matrix, resin functional groups, and surface modification. Accordingly, three anion exchange resins with different 1) polymer matrices (polystyrene and polyacrylic), 2) resin functional groups (strong-base and weak-base), and 3) surface modification with iron oxide were evaluated for their P adsorption capacity and kinetics.

Phosphate adsorption capacity at near-neutral pH was in the following order of the strong-base polystyrene resin, the weak-base polystyrene resin, and the weak-base polyacrylic resin (13.16, 5.17 and 21.19 mg/g, respectively). The P adsorption capacity of iron oxide coated resins (i.e., hybrid resins) followed the same order, indicating that the properties of parent resin itself had a greater influence on the P adsorption than the surface modification with iron oxide. The P adsorption kinetics were fast in all adsorbents. The initial sorption rate was ranging from ~0.1 to 3.63 mg/(g min). Phosphate adsorption in the hybrid resins was not strongly interfere by co-existing nitrate and sulfate compared to that in the pure resins, suggesting that the hybrid resins were selective toward phosphate. Furthermore, adsorbed P in the hybrid resins was more irreversibly adsorbed P than the pure resins. These characteristics make the hybrid resins an ideal P adsorbent in the passive detection technique. Accordingly, commercially available polystyrene hybrid resin and a laboratory synthesized polyacrylic hybrid resin were tested for the adsorbent used in the passive detection technology.

The passive sampling using a mesh bag contraption containing hybrid resins was proven to be a successful method in monitoring DRP in tile drainage water. While both the hybrid resins are suitable adsorbents in the passive sampling because of the high P adsorption performance, the field test showed that the hybrid polyacrylic resin removed more P from tile water than the hybrid polystyrene resin. When the adsorbents were calibrated in the field, the passive detection technique predicted DRP concentrations

reasonably well. The passive samplings with hybrid resins produced DRP concentrations of tile waters with no significant difference (Paired Student's t-test, $p > 0.05$) with the auto-sampling data. High DRP concentrations during precipitation and subsequent flooding events were also predicted well. Overall, the passive detection method with iron oxide coated hybrid resins has potential for the monitoring of concentrations and loads of DRP from a large number of agricultural waterways because of its simplicity and economical feature.